

Loughborough University Institutional Repository

A study of the filtration of fibre/particle mixtures

This item was submitted to Loughborough University's Institutional Repository by the/an author.

Additional Information:

- A Doctoral Thesis. Submitted in partial fulfillment of the requirements for the award of Doctor of Philosophy of Loughborough University.

Metadata Record: <https://dspace.lboro.ac.uk/2134/6323>

Publisher: © Kuhan Chellappah

Please cite the published version.

This item was submitted to Loughborough's Institutional Repository (<https://dspace.lboro.ac.uk/>) by the author and is made available under the following Creative Commons Licence conditions.



CC creative commons
COMMONS DEED

Attribution-NonCommercial-NoDerivs 2.5

You are free:

- to copy, distribute, display, and perform the work

Under the following conditions:

BY: **Attribution.** You must attribute the work in the manner specified by the author or licensor.

Noncommercial. You may not use this work for commercial purposes.

No Derivative Works. You may not alter, transform, or build upon this work.

- For any reuse or distribution, you must make clear to others the license terms of this work.
- Any of these conditions can be waived if you get permission from the copyright holder.

Your fair use and other rights are in no way affected by the above.

This is a human-readable summary of the [Legal Code \(the full license\)](#).

[Disclaimer](#) 

For the full text of this licence, please go to:
<http://creativecommons.org/licenses/by-nc-nd/2.5/>

A STUDY OF THE FILTRATION OF FIBRE/PARTICLE MIXTURES

by

KUHAN CHELLAPPAH

A Doctoral Thesis submitted in partial fulfilment of the requirements for
the award of Doctor of Philosophy degree of Loughborough University

June 2010

Advanced Separation Technologies Group,
Department of Chemical Engineering,
Loughborough University,
Loughborough,
Leics. LE11 3TU

ABSTRACT

This thesis investigates the constant pressure cake filtration of interacting cellulose fibre/TiO₂ (rutile) mixtures, and involved experimental studies using an automated pressure filtration apparatus. The influence of suspension composition, filtration pressure and solution environment on filtration has been discussed in relation to cake properties such as average cake porosity and specific resistance. To help interpret the filtration results, sedimentation data were also obtained.

The average porosities of filter cakes formed from pure rutile and fibre suspensions in deionised water were approximately 0.6 and 0.75, respectively, and a steady and progressive increase in porosity with fibre fraction was generally observed. With filtrations at 450 kPa, the average specific cake resistances for pure fibre and rutile in deionised water were approximately 9.4×10^{13} and 4.2×10^{12} m kg⁻¹ respectively, with the variation of specific resistance with solids composition showing a minimum. Similar trends were observed at other tested filtration pressures with suspensions in deionised water but not with filtrations of suspensions in 0.2 M NaCl and 0.1 M CaCl₂ solutions. The minima in average specific cake resistance with solids composition for feeds in deionised water was attributed to rutile-fibre interactions. Abrupt transitions in cake structure were evident part way through some filtrations, and resulted in unexpected filtrate flow behaviour. This is an interesting phenomenon, and not only were the changes in cake structure relatively reproducible, but also the nature of the change could be altered by changes in filtration pressure, solids composition and/or solution environment.

The study of fibre/particle binary filtration behaviour, in particular the porosity and specific cake resistance trends, were substantiated by relevant theoretical treatment and modelling analysis. With the porosity trends, an additive porosity concept seemed to represent the data better than interparticle penetration models. With the specific cake resistance trends, a semi-empirical equation was proposed which appeared to represent a wide range of binary mixture filtration data. A mathematical framework was also developed in an attempt to understand the underlying physical mechanisms which led to filter cake restructuring, and possible explanations were postulated.

Keywords: Cake filtration, Sedimentation, Porosity, Packing, Permeability, Fibres.

ACKNOWLEDGEMENTS

I would like to thank my supervisors, Professor R.J. Wakeman and Dr E.S. Tarleton, for their expert guidance and support throughout my time at Loughborough. They have always been there for me and it has been a privilege to work under their guidance. I would also like to take this opportunity to express my gratitude to some of the technical and academic related staff of the Department of Chemical Engineering at Loughborough University for their assistance with regards to various matters. Last but not least, I would like to thank my parents and some friends for their ceaseless support in many aspects during the progression of this work.

TABLE OF CONTENTS

ABSTRACT	I
ACKNOWLEDGEMENTS	II
TABLE OF CONTENTS	III
LIST OF FIGURES	VII
LIST OF TABLES	XIV
CHAPTER 1: INTRODUCTION	1
1.1. MOTIVATION FOR RESEARCH	1
1.2. AIMS AND OBJECTIVES	2
1.3. THESIS STRUCTURE	3
REFERENCES	3
CHAPTER 2: LITERATURE REVIEW	4
2.1. INTRODUCTION	4
2.2. FILTRATION AND MODES OF OPERATION	4
2.3. CAKE FILTRATION FUNDAMENTALS	7
2.4. COMPRESSIBLE CAKE FILTRATION	12
2.4.1. Deviations from ‘incompressible’ cake behaviour	12
2.4.2. Importance of physico-chemical properties	15
2.4.3. Rigorous analysis of compressible cake filtration	19
2.5. ANOMALOUS FILTRATION BEHAVIOUR	21
2.6. FILTRATION OF BINARY MIXTURES	23
2.7. PREVIOUS EXPERIMENTAL TECHNIQUES	30
2.8. CLOSURE	35

REFERENCES	37
CHAPTER 3: EXPERIMENTAL MATERIALS AND METHODS	47
3.1. INTRODUCTION	47
3.2. CONSTANT PRESSURE FILTRATION APPARATUS	48
3.2.1. Apparatus description	48
3.2.2. Typical operating procedure	52
3.2.3. Cleaning and calibration	55
3.3. SEDIMENTATION APPARATUS AND METHODS	55
3.4. VALIDATION FILTRATION EXPERIMENTS	57
3.5. MATERIALS AND METHODS	61
3.5.1. Titania (rutile) characterisation	61
3.5.2. Tissue paper (fibre) characterisation	66
3.5.3. Membrane characterisation	72
3.5.4. Suspension preparation methods	74
3.6. SUMMARY	75
REFERENCES	75
CHAPTER 4: SEDIMENTATION AND FILTRATION RESULTS	77
4.1. INTRODUCTION	77
4.2. SEDIMENTATION RESULTS AND DISCUSSION	77
4.2.1. Single component sedimentation	78
4.2.2. Binary suspension sedimentation	80
4.3. FILTRATION RESULTS AND DISCUSSION	85
4.3.1. Basic data treatment and calculations	85
4.3.2. General filtration behaviour of single component suspensions	87
4.3.3. General filtration behaviour of binary suspensions	92
4.3.4. Effects of solids composition	100
4.3.4.1. Effects of solids composition on porosity	100
4.3.4.2. Effects of solids composition on specific resistance	106
4.3.5. Effects of filtration pressure	108
4.3.6. Effects of solution environment	108
4.4. CONCLUSIONS	110
REFERENCES	111
CHAPTER 5: FURTHER DISCUSSION AND MODELLING	113

5.1. INTRODUCTION	113
5.2. MODEL DERIVATION	114
5.3. ANALYSIS OF THE MODEL CHARACTERISTICS	117
5.3.1. Analysis assuming constant porosity and effective specific surface	117
5.3.2. Analysis assuming constant effective specific surface	118
5.3.3. Analysis of the role of effective specific surface in the model	121
5.3.3.1. Analysis assuming a constant value of S_B	124
5.3.3.2. Analysis assuming two values of S_B	129
5.3.3.3. Significance of S_B	131
5.4. APPLICATION OF MODEL TO EXPERIMENTAL DATA	133
5.5. CONCLUSIONS	146
REFERENCES	147
CHAPTER 6: ANOMALOUS FILTRATION BEHAVIOUR	148
6.1. INTRODUCTION	148
6.2. PREVIOUS RESEARCH	148
6.3. GENERAL EXPERIMENTAL OBSERVATIONS	150
6.4. ANALYSIS OF CAKE STRUCTURE CHANGES	161
6.4.1. Changing channel radius and number of channels	163
6.4.2. Changing channel radius and cake porosity	171
6.5. DISCUSSION AND IMPLICATIONS	173
6.6. CONCLUSIONS	178
REFERENCES	178
CHAPTER 7: OVERALL CONCLUSIONS AND FUTURE WORK	180
7.1. OVERALL CONCLUSIONS	180
7.2. FUTURE WORK	183
REFERENCES	186
LIST OF NOTATION	187
APPENDIX A: SELECTED FILTRATION DATASHEETS	190

Table of Contents

APPENDIX B: RECORDED LIQUID PRESSURE PROFILES	215
APPENDIX C: FURTHER DISCUSSION ON THE PACKING MODELS	217
APPENDIX D: ADDITIONAL DETAILS OF PERMEABILITY MODEL	224
APPENDIX E: SUPPLEMENT TO PERMEABILITY MODEL FITTING	233
APPENDIX F: SUPPLEMENT TO SECTION 6.4	239
APPENDIX G: PAPERS ARISING FROM THE RESEARCH	245

LIST OF FIGURES

Figure 2.1: Schematic showing the two filtration modes, dead-end and crossflow.	5
Figure 2.2: Mechanisms of filtration. Depth filtration occurs by the standard blocking law whilst most cake filtrations occur by a combination of blocking and bridging. The ‘intermediate blocking mechanism’ (not shown here) allows for the particles to cause both pore blocking and cake formation (Wakeman and Tarleton, 1999).	6
Figure 2.3: Schematic of growing filter cake (Wakeman, 1978).	8
Figure 2.4: Variation of hydraulic pressure and solid compressive pressure within a filter cake (Tiller and Leu, 1980).	10
Figure 2.5: Effect of pressure on ‘filtration plot’ of anatase experimental data (mean particle size = 0.3 μm , pH = 4 (isoelectric point)) (adapted from Wakeman <i>et al.</i> , 1991).	12
Figure 2.6: Variation of solid volume fraction through the cake thickness during an expression process (Wakeman, 2007b).	16
Figure 2.7: Schematic of the potential energy barrier generated between two approaching particles (Wakeman and Tarleton, 1999).	18
Figure 2.8: Forces on a portion of a filter cake.	20
Figure 2.9: Anomalous ‘filtration plot’ of a zinc sulphide suspension filtration (Tarleton and Willmer 1997).	24
Figure 2.10: Changes in measured solids concentration with time for the zinc sulphide filtration. The corresponding ‘filtration plot’ is shown in Figure 2.9 (Tarleton and Willmer 1997).	24
Figure 2.11: Regular packing structures of equal spheres. The coordination numbers and corresponding porosities are shown (Suzuki, 2006).	25
Figure 2.12: Effect of particle shape on specific surface (Wakeman and Tarleton, 2005).	26
Figure 2.13: Dependence of the binary mixture porosity, ε_{av} , on volume fraction of large particles, X_D , for a glass beads size ratio of 3.33. The boxes illustrate the packing, (a) mixture enriched with small particles; (b) mixture close to the maximum packing density (minimum porosity); (c) mixture enriched with large particles (Dias <i>et al.</i> , 2004b).	29
Figure 2.14: Schematic diagram of filter (Shirato <i>et al.</i> , 1980).	33
Figure 2.15: Apparatus used by Fathi-Najafi and Theliander (1995).	34
Figure 2.16: Schematic representation of the mechatronic based filtration apparatus (Tarleton, 1999b).	36

Figure 2.17: Hydraulic pressure history of a 400 kPa constant pressure filtration of a talc suspension (Tarleton and Hadley, 2003). Legend represents the height that a pressure probe is above the filter medium	36
Figure 3.1: Photograph of the experimental apparatus.	48
Figure 3.2: Schematic of pressure filtration apparatus without the compressed air circuitry.	49
Figure 3.3: Schematic of the pressure filtration apparatus compressed air circuitry.	50
Figure 3.4: Micro-pressure transducer arrangement of the mechatronic pressure filtration apparatus (Tarleton, 2008)	53
Figure 3.5: The main (upstream) pressure transducer (PT1 in Figure 2.3) calibration. The gradient and intercept were inserted into the computer program.	56
Figure 3.6: Example of typical micro-pressure transducer (the transducer closest to the medium is used here as an example) calibration. The gradient and intercept were inserted into the computer program.	56
Figure 3.7: Photograph of suspensions settled in their measuring cylinders.	57
Figure 3.8: Plot of cumulative volume of filtrate vs. time for filtrations of 10% w/w calcite suspensions at a constant pressure of 300 kPa. The error bars are based on three repeat filtrations.	59
Figure 3.9: Liquid pressure history 0.5 mm above the filter medium as obtained from three repeat 300 kPa filtrations of 10% w/w calcite suspensions.	59
Figure 3.10: Hydraulic pressure history in a forming calcite cake/suspension at a constant filtration pressure of 300 kPa.	60
Figure 3.11: Hydraulic pressure profiles through the filter cake at various times during the 300 kPa filtration of a 20% w/w calcite suspension.	60
Figure 3.12: Scanning Electron Micrograph image of the rutile used.	62
Figure 3.13: Rutile cumulative size distribution as measured using the Zetasizer. A median size of $\sim 0.45 \mu\text{m}$ was obtained.	64
Figure 3.14: Zeta potential values of rutile in deionised (DI) water as well as 0.2 M NaCl and 0.1 M CaCl ₂ solutions. Error bars shown are based on three repeat measurements.	64
Figure 3.15: Size distributions of rutile in deionised (DI) water, 0.2 M NaCl and 0.1 M CaCl ₂ solutions.	66
Figure 3.16: Scanning Electron Micrograph image of the tissue paper used.	67
Figure 3.17: EDX plot (frequency against energy levels) of a sample of tissue paper.	68
Figure 3.18: Cumulative size (width) distributions of the fibres in the tissue paper, as obtained by measuring more than one hundred fibres from SEM images at various magnifications.	69

Figure 3.19: Zeta potential values of fibres (with fillers) in deionised (DI) water as well as 0.2 M NaCl and 0.1 M CaCl ₂ solutions.	71
Figure 3.20: Pore size distribution of the Versapor membrane (taken from Willmer, 1997).	73
Figure 3.21: Scanning Electron Micrograph of the topographic view of a Versapor membrane (taken from Willmer, 1997).	73
Figure 4.1: Sedimentation curves for pure rutile in deionised (DI) water and 0.1 M CaCl ₂ .	79
Figure 4.2: Sedimentation curves for pure fibres in deionised (DI) water and 0.1 M CaCl ₂ solution. The total solids concentration for these two experiments was 0.16% v/v; pure fibres did not settle appreciably in either solution environments at 1.1% v/v.	79
Figure 4.3: Initial settling rate vs. total solids (fibre) concentration for pure fibre suspensions.	80
Figure 4.4: Example batch settling curves for binary suspensions in deionised water.	81
Figure 4.5: Example batch settling curves for binary suspensions in 0.1 M CaCl ₂ solution.	81
Figure 4.6: Effect of fibre fraction (X_D) on the initial settling rate for suspensions in deionised (DI) water and 0.1 M CaCl ₂ solution.	83
Figure 4.7: Effects of fibre fraction (X_D) on the proportion of sludge for suspensions in deionised (DI) water and 0.1 M CaCl ₂ solution.	83
Figure 4.8: Plots of cumulative filtrate volume vs. filtration time for 1.1% v/v fibre and rutile suspensions in deionised water at a constant filtration pressure of 450 kPa.	88
Figure 4.9: The initial (linear) portion of the plots of reciprocal filtrate flow rate vs. cumulative filtrate volume for 1.1% v/v fibre and rutile suspensions in deionised water at a constant filtration pressure of 450 kPa.	89
Figure 4.10: Cumulative filtrate volume vs. filtration time for 1.1% v/v fibre suspensions in deionised water at various filtration pressures.	90
Figure 4.11: Reciprocal filtrate flow rate vs. cumulative filtrate volume for 1.1% v/v fibre suspensions in deionised water at various filtration pressures.	91
Figure 4.12: Cumulative filtrate volume vs. filtration time for 1.1% v/v rutile suspensions in deionised water at various filtration pressures.	91
Figure 4.13: Effect of filtration pressure on average specific cake resistance for 1.1% v/v fibre and rutile suspensions in deionised water.	92
Figure 4.14: Cumulative filtrate volume vs. filtration time for 150 kPa filtrations of 1.1% v/v binary suspensions in deionised water at various solids compositions. The solids compositions are quantified in terms of the X_D values.	93

Figure 4.15: Reciprocal filtrate flow rate vs. cumulative filtrate volume for 150 kPa filtrations of binary suspensions in deionised water at various solids compositions.	93
Figure 4.16: Cumulative filtrate volume vs. filtration time for 450 kPa filtrations of binary suspensions in deionised water at various solids compositions.	94
Figure 4.17: Cumulative filtrate volume vs. filtration time for 450 kPa filtrations of binary suspensions in 0.1 M CaCl ₂ at various solids compositions.	95
Figure 4.18: Cumulative filtrate volume vs. filtration time for 450 kPa filtrations of binary suspensions in 0.2 M NaCl at various solids compositions.	95
Figure 4.19: Cumulative filtrate volumes 10 s into the 450 kPa filtrations at various solids compositions and solution environments.	96
Figure 4.20: Effects of solids composition and filtration pressure on filter cake average porosity for filtrations from deionised water.	97
Figure 4.21: Effects of solids composition and filtration pressure on filter cake average specific resistance for filtrations from deionised water.	98
Figure 4.22: Effects of solids composition and solution environment on filter cake average porosity for 450 kPa filtrations.	99
Figure 4.23: Effects of solids composition and solution environment on filter cake average specific resistance for 450 kPa filtrations.	100
Figure 4.24: Effects of solids composition on ϵ_{av} for filtrations from deionised water at constant pressures of 150, 450 and 600 kPa. The prediction given by equations (4.20) and (4.21), Tokumitsu model, is included for the 450 kPa data and predictions given by equation (4.24), Shirato model, are included for all pressures.	102
Figure 4.25: Schematic representation of the rutile particles coating the fibre surfaces. The schematic is not to scale and the rutile particles have been represented by spheres.	105
Figure 4.26: Effects of solids composition on α_{av} for filtrations from deionised water at constant pressures of 150, 450 and 600 kPa.	106
Figure 5.1: Family of curves obtained using equation (5.19), varying S_1/ϕ_1 and keeping S_2/ϕ_2 constant. Experimental data from 450 kPa filtrations with deionised water is included. The parameters used for the curves are summarised in Table 5.1.	122
Figure 5.2: Family of curves obtained using equation (5.19), varying S_2/ϕ_2 and keeping S_1/ϕ_1 constant. Experimental data from 450 kPa filtrations with deionised water is included. The parameters used for the curves are summarised in Table 5.2.	123
Figure 5.3: Variation in fibre (S_1/ϕ_1) and rutile (S_2/ϕ_2) specific surface area in contact with the permeating fluid (deionised water) as determined from equations (5.27) and (5.28) assuming S_B remains constant with solids	

composition. The corresponding experimental data for cake average specific resistance is shown in Figure 4.21.	127
Figure 5.4: Family of curves produced by increasing S_B , keeping the fibre effective specific surface constant. Experimental data from 450 kPa filtrations with deionised water is included. The parameters used for the curves are summarised in Table 5.3.	130
Figure 5.5: Values of S_B calculated from equation (4.40) for the filtrations from deionised water as well as 0.2 M NaCl and 0.1 M CaCl ₂ solutions.	132
Figure 5.6: Plot of S_0 vs. solids composition, the experimental representations were calculated from equation (5.35) and data from 450 kPa filtrations with deionised water. The pure component specific surface values (S_1/ϕ_1 and S_2/ϕ_2) were calculated from equation (5.11).	134
Figure 5.7: Experimental filtration data at 450 kPa with deionised water and the model fit using equations (5.39) and (5.40) as well as equation (5.41).	137
Figure 5.8: Experimental filtration data at 150 kPa and 600 kPa with deionised water and the model fits using equation (5.41).	138
Figure 5.9: Experimental filtration data at 450 kPa with 0.2 M NaCl and 0.1 M CaCl ₂ solutions, and the model fits using equation (5.41).	139
Figure 5.10: Experimental filtration data at 196 kPa with deionised water at pH 4.5 (where rutile-silica aggregation occurred) and pH 9.6 (where no aggregation occurred), and the model fits using equation (5.41). In this figure, an X_D of 0 refers to pure rutile and an X_D of 1 to pure silica. The experimental data points were recalculated from Iritani <i>et al.</i> (2002).	140
Figure 5.11: A schematic representation of a hypothetical case where equation (5.9) may be used to describe the variation of effective solids specific surface with solids composition. Here no changes in either component's packing (due to the presence of the other component) or interactions between the two components take place.	142
Figure 5.12: Values of b_1 and b_2 (equation (5.41)) for rutile/fibre binary suspension filtrations with deionised water at the different filtration pressures. Corresponding values of b_{1a} and b_{2a} (equations (5.39) and (5.40)) are included for comparison.	144
Figure 6.1: Filtration plots for pure fibre suspensions (1.1% v/v) in deionised water at three filtration pressures.	151
Figure 6.2: Filtration plots for pure fibre suspensions in deionised water at 550 kPa; a repeat experiment is shown to indicate reproducibility.	152
Figure 6.3: Filtrate flow rate profile for pure fibre suspensions (1.1% v/v) in deionised water at three filtration pressures.	152
Figure 6.4: Filtration plots for binary suspensions of various solids compositions (fibre rich suspensions of total solids concentration of 1.1% v/v) in deionised water at 450 kPa.	153

Figure 6.5: Filtrate flow rate profile for binary suspensions of various solids compositions (total solids concentration of 1.1% v/v) in deionised water at 450 kPa.	154
Figure 6.6: Filtration plots for binary suspensions of various solids compositions (from fibre rich to intermediate solids compositions, with total solids concentration of 1.1% v/v) in deionised water at 450 kPa.	155
Figure 6.7: Filtrate flow rate profile for an $X_D = 0.859$ suspension in deionised water. The data, and points A and B, correspond with those in Figure 6.6 at $X_D = 0.859$.	155
Figure 6.8: Filtration plots for binary suspensions of various solids compositions in 0.1 M CaCl_2 solution at 450 kPa.	157
Figure 6.9: Filtrate flow rate just prior to the transition vs. solids composition for experiments performed with deionised water and 0.1 M CaCl_2 solution.	160
Figure 6.10: Average channel radius vs. filtration time for filtrations of pure fibre suspensions from deionised water at three filtration pressures when $a = 1$. The corresponding flow rate profiles are given in Figure 6.3.	165
Figure 6.11: Number of channels vs. filtration time for filtrations of pure fibre suspensions from deionised water at three filtration pressures when $a = 1$. The corresponding flow rate profiles are given in Figure 6.3.	165
Figure 6.12: Effect of varying a on the increase in R_a during the period of increased filtration rate for the filtration of pure fibre suspension from deionised water at 450 kPa.	166
Figure 6.13: Effect of varying a on the number of channels during the period of increased filtration rate for the filtration of pure fibre suspension from deionised water at 450 kPa.	167
Figure 6.14: R_a profile for filtrations of pure fibre suspensions from deionised water at three filtration pressures when $a = 0.05$.	168
Figure 6.15: Number of channels vs. filtration time for filtrations of pure fibre suspensions from deionised water at three filtration pressures when $a = 0.05$.	169
Figure 6.16: R_a profile for filtrations of binary suspensions of various solids composition from deionised water at 450 kPa when $a = 0.05$. The corresponding flow rate profiles are given in Figure 6.5.	170
Figure 6.17: Number of channels vs. filtration time for filtrations of binary suspensions of various solids composition from deionised water at 450 kPa when $a = 0.05$. The corresponding flow rate profiles are given in Figure 6.5.	170
Figure 6.18: Variation of the model representation of filter cake average porosity with filtration time for a 550 kPa filtration of a pure fibre suspension in deionised water.	172
Figure 6.19: Liquid pressure profile at various heights (from the medium) within a cake forming during the 450 kPa filtration of a $X_D = 0.154$ suspension from 0.1 M CaCl_2 solution. The corresponding filtration plot is shown in Figure 6.20.	175

Figure 6.20: Filtration plot for a $X_D = 0.154$ suspension in 0.1 M CaCl_2 solution at a filtration pressure of 450 kPa. The corresponding liquid pressure profile is given as Figure 6.19.	176
Figure 6.21: Liquid pressure profile at various heights (from the medium) within a cake forming during the 600 kPa filtration of a $X_D = 0.391$ suspension from deionised water. The corresponding filtration plot is shown in Figure 6.22.	176
Figure 6.22: Filtration plot for a $X_D = 0.391$ suspension in deionised water at a filtration pressure of 600 kPa. The corresponding liquid pressure profile is given as Figure 6.21.	177

LIST OF TABLES

Table 2.1: Summary of the methods for assessing cake structure in filtration processes (Tarleton, 1999a).	32
Table 4.1: Batch gravity settling experimental observations for suspensions of various fibre fractions in deionised water.	84
Table 4.2: A breakdown of the Shirato additive law (equation (4.24)).	104
Table 5.1: Parameters for the curves plotted in Figure 5.1 at the various S_B .	122
Table 5.2: Parameters for the curves plotted in Figure 5.2 at the various S_B .	123
Table 5.3: Parameters for the curves plotted in Figure 5.4 at the various S_B .	131
Table 5.4: Summary of parameters relevant to Figures 5.7 – 5.10.	145
Table 6.1: Some parameters of interest during the abrupt transition in cake structure for selected filtrations. The values reported here are representative of the datasets obtained.	158

CHAPTER 1: INTRODUCTION

1.1. MOTIVATION FOR RESEARCH

Cake filtration is an important and widely used separation process in many areas in which the objectives may be to either recover a clear filtrate, or to recover the suspended solids, or both. The aforementioned areas include the chemical and petrochemical, mineral, food, pharmaceutical and water treatment industries. In the process industries, separation and purification of the product stream is probably the stage where most value is added. Also, increasing environmental awareness has resulted in ever more stringent legislations to control liquid discharge compositions. These two factors have led to separation science and technology playing a pivotal role in the relationship between product quality, competitiveness and the environment. The resurgence of interest in separation technology in recent years has led to a revival of cake filtration studies. However, the improvement of this technology relies on understanding with greater insight and better information of the various aspects of the filtration process (Tien, 2002).

Fibrous solids are known to induce complexities in filtration due to their irregular shapes, high aspect ratios and wide size distributions. A significant proportion of process/waste streams that require dewatering contain fibrous or similarly elongated solids, and are usually complex mixtures containing various solids of differing sizes, shapes and surface properties. Examples of industries where such suspensions may be commonplace include water and wastewater treatment, paper and pulp, and pharmaceutical (where needle shaped particles are often encountered). The study of binary suspensions containing particles and fibres are therefore of significant industrial and academic interest as such systems are representative of process/waste streams involving one particulate component, which can be colloidal in nature, and another which is much larger and of a high aspect ratio. Despite its importance, there appears to be a sparsity of research on the cake filtration of fibrous suspensions, and particularly for binary suspensions containing particles and fibres. Moreover, in the study of binary

suspension filtration, a further level of complexity is introduced when the two constituent solid components interact with one another (e.g. aggregate).

Designing and scaling-up pressure filtration systems depend largely on the availability and accuracy of relevant experimental data as well as the interpretation of this data which can be hindered by difficulties such as theoretical limitations. Certain mechanisms that can lead to non-linear and anomalous ‘filtration plots’ are currently not well understood and this gives rise to an inherent problem because the assumption of (almost) linear filtration plots is an indispensable component of traditional filtration analysis, with the slope of these filtration plots being an important parameter in many practical scale up and optimum cycle calculations. Elucidating the mechanisms that lead to unusual filtration plots is therefore of both practical and academic interest.

1.2. AIMS AND OBJECTIVES

The main aim of this research is to understand the constant pressure cake filtration behaviour of interacting cellulose fibre/TiO₂ (rutile) mixtures. The research involves experimental studies using a computer controlled pressure filtration apparatus capable of automated data acquisition. The influence of suspension composition, filtration pressure and solution environment on filtration is discussed in relation to cake properties such as average cake porosity (ϵ_{av}) and average specific cake resistance (α_{av}). To help interpret the filtration results, sedimentation data is also obtained.

The stages involved in achieving the desired aims were as follows:

1. Characterising the materials and filter medium, in terms of the relevant properties;
2. Understanding the apparatus to be used, along with producing a detailed operating procedure;
3. Carrying out pressure filtration experiments systematically, according to an outlined experimental matrix formulated to isolate the effects of specific variables such as solids composition, filtration pressure and solution environment;
4. Carrying out sedimentation experiments to assist with the interpretation of filtration results;

5. Undertaking further theoretical analysis, particularly on the effects of aggregation of the constituent solids at the various solids compositions, filtration pressures and solution environments.

A secondary aim of this research was to attempt to elucidate the mechanisms that lead to anomalous filtration plots. The effects of solids composition and filtration pressure on the abrupt changes that occur during a filtration are briefly investigated. In some cases, hydraulic pressure profiles through the filter cake were obtained for the duration of the formation stage.

1.3. THESIS STRUCTURE

This thesis consists of six chapters. Chapter 1 is intended to put the thesis into general context in terms of the research performed and where it fits into the present field of knowledge. Chapter 2 critically reviews relevant literature, including the experimental techniques used by selected previous researchers. Chapter 3 outlines the experimental apparatus and presents some initial results obtained to validate the apparatus and the operating procedure. Chapter 3 also discusses relevant properties of the materials used in the current investigation. Chapters 4 to 6 discuss the important findings of the research. Chapter 4 discusses the overall filtration results; sedimentation data was used to aid in the filtration data interpretation. In Chapter 5, a modelling approach for binary suspension filtration is presented and discussed in relation to the assumptions and limitations. A curve fitting approach is taken to fit the model to the experimental data and this is discussed towards the end of Chapter 5. Chapter 6 discusses some interesting observations during selected individual experiments, in particular anomalous filtration plots. Chapter 7 concludes the thesis by providing overall conclusions and suggesting potential future investigations.

REFERENCES

Tien, C. (2002) Cake filtration research- a personal view. *Powder Technology* **127**, 1-8.

CHAPTER 2: LITERATURE REVIEW

2.1. INTRODUCTION

This chapter critically reviews previously published literature relevant to the present work. An introduction to filtration and modes of operation is followed by a review of cake filtration fundamentals, where relevant design equations are presented. Discussions of compressible cake filtration begin with an explanation of why ‘conventional filtration theory’ can fail, especially with highly compressible cakes. The importance of physico-chemical properties on filtration are presented and discussed. Some previous works that attempt a more rigorous analysis of compressible cake filtration are also reviewed, with shortcomings highlighted. Taking the review into further depth, deviations from traditional compressible cake filtration behaviour that have been previously observed are presented; these unusual occurrences take the form of abrupt changes to cake structure part way through a filtration. Researchers have attributed the transitions in cake structure to various causes and these are discussed, but as yet the exact mechanism(s) that lead to this phenomenon is not well understood. After a discussion on some advances in binary suspension filtrations, a review of previous relevant experimental investigations is given, highlighting techniques, advances and limitations.

2.2. FILTRATION AND MODES OF OPERATION

Filtration can be classified according to the mode of operation, namely deadend or crossflow (Wakeman and Tarleton, 1999). In dead-end filtration, the feed flow is perpendicular to the filter surface whereas in crossflow filtration the feed flow is tangential to the filter surface; these two processes are shown schematically in Figure 2.1. The process involved in this study is the dead-end filtration of solid/liquid mixtures. The filter medium, denoted by the dotted lines in Figure 2.1, is that critical component which determines whether or not a filter will perform adequately and can be defined as

any permeable material upon or within which particles are deposited by the process of filtration (Purchas, 1996).

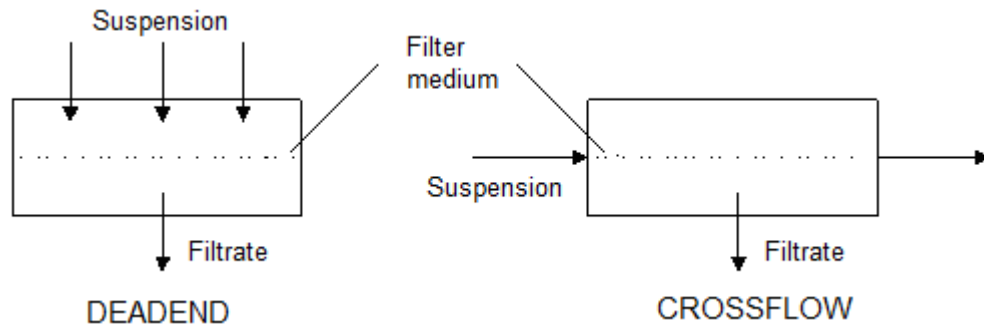


Figure 2.1: Schematic showing the two filtration modes, dead-end and crossflow.

Dead-end filtration can be further sub-divided to cake filtration and depth filtration. With depth filtration, the particles are generally smaller than the filter pores and particle deposition is predominantly inside the filter medium. The particles either get trapped or lodged in the tortuous filter pores or are adsorbed onto active sites within the depth of the filter medium. The adsorption of these particles depends to a large extent on the electrostatic interaction between the particles and the surface, which in turn depends on the pore surface and particle's repulsive electrical double layer forces and attractive van der Waals forces. Cake filtration occurs when the solids concentration is sufficiently high and the particles are more similar in size or larger than the filter pores, so that the particles bridge over the entrance of the filter medium pores to form a deposit on the filter surface known as the 'filter cake'. This filter cake brings about an additional resistance to flow and acts as a 'secondary filter', through which subsequent filtration occurs.

The so-called 'laws' of filtration inferred by the mechanisms described by Figure 2.2 have been studied by Grace (1956) and Hermia (1982) amongst others. Their origins stem from the stochastic modelling of filtration and the behaviour of a particle

arriving at the surface of a filter medium. The characteristic form of the filtration laws is:

$$\frac{d^2t}{dV^2} = k_1 \left(\frac{dt}{dV} \right)^{k_2} \quad (2.1)$$

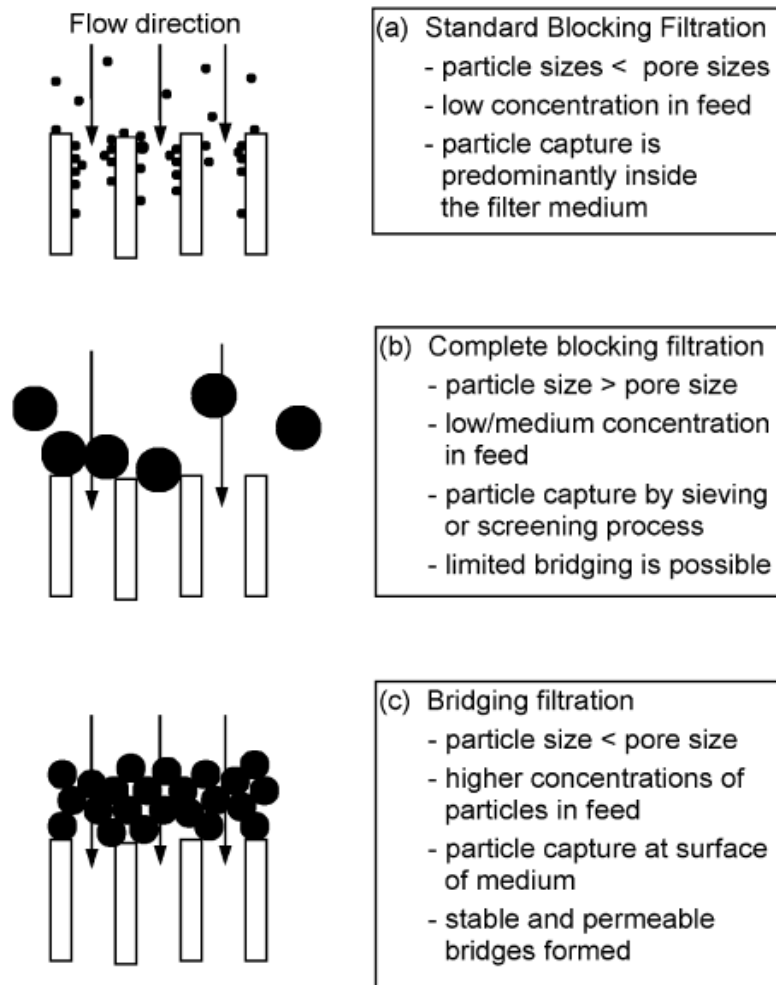


Figure 2.2: Mechanisms of filtration. Depth filtration occurs by the standard blocking law whilst most cake filtrations occur by a combination of blocking and bridging. The ‘intermediate blocking mechanism’ (not shown here) allows for the particles to cause both pore blocking and cake formation (Wakeman and Tarleton, 1999).

for constant pressure filtration, where k_1 and k_2 are constant. k_1 is dependent on the initial flow rate of slurry reaching the medium, and $k_2 = 2, 1.5, 1$ and 0 for complete blocking, standard blocking, intermediate blocking and cake filtration respectively. These ‘laws’ are convenient for visualising and giving an understanding to the microscopic phenomena that may take place at the filter medium surface, but they do not describe the physics of particle deposition beyond the initial few moments of filtration (Wakeman and Tarleton, 1999).

A filter may be operated under a variety of conditions depending on how the driving pressure for the process is developed. When the suspension is fed to the filter from a feed vessel where the space above the suspension is subjected to a source of compressed gas, or when the volume downstream of the filter is subjected to vacuum conditions, filtration is accomplished at a constant pressure differential and in this case the rate of filtration decreases with time. When the suspension is fed using a positive displacement pump, filtration is performed under constant flow rate conditions; in this case the pressure drop increases with time.

2.3. CAKE FILTRATION FUNDAMENTALS

Figure 2.3 shows a schematic of a growing filter cake (Wakeman, 1978). When all the solids are part of the filter cake (i.e. no more solids are in the slurry phase), filtration ends and deliquoring begins. Classical cake filtration theory was initially developed from Darcy’s equation for fluid flow through a porous medium. The equation relates the flow rate (q) of a filtrate of dynamic viscosity μ to the driving pressure gradient and can be written in one dimensional spatial coordinates as:

$$\frac{dp_L}{dx} = -\frac{\mu q}{k} \quad (2.2)$$

where p_L is the hydraulic pressure at a distance of x through the cake and k is the local permeability.

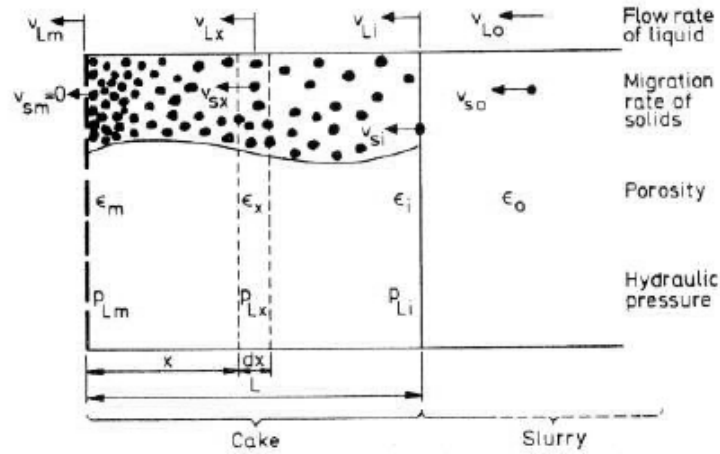


Figure 2.3: Schematic of growing filter cake (Wakeman, 1978).

Ruth (1946) modified Darcy's equation to material coordinates, given as:

$$\frac{dp_L}{dw} = \mu\alpha q \quad (2.3)$$

where α is the local specific cake resistance and w is the mass of dry solids deposited per unit area up to height x . The specific cake resistance is defined by

$$\alpha = \frac{1}{\rho_s(1-\varepsilon)k} \quad (2.4)$$

and the mass of dry solids is related to thickness by

$$dw = \rho_s(1-\varepsilon)dx \quad (2.5)$$

where ρ_s is the true density of the solid and ε the local porosity. Ruth showed that the resistance of a cake formed during filtration is proportional to the amount of cake deposited provided the cake porosity (and hence the specific cake resistance) is constant for a fixed filtration pressure. Therefore, the proportionality is only valid for essentially incompressible cakes.

As the solids deposit on the surface of, or within, a one dimensional cake, the liquid flows through the interstices of the porous cake and filter medium, exiting at the other side. The hydraulic pressure drops throughout the cake due to friction as the liquid

flows over the surfaces of the individual particles. The drag imparted to the particles results in a compression process which causes a decrease in porosity and an increase in resistance. Heertjes (1964) correctly pointed out that this factor should ideally be recognized in filtration theory. The total force experienced by a particle is the sum of all the surface and body forces. The particles transmit stresses throughout the filter cake, and for this to happen it is commonly assumed that the particles are in point contact. The total drag force divided by the cross-sectional area is termed the effective pressure, p_s (Tiller and Green, 1973); for a more detailed description of the parameter p_s , see Wakeman (1985). The effective pressure has also been denoted as the solids compressive pressure (Teoh *et al.*, 2002), solid stress (Landman *et al.*, 1995), drag pressure (Theliander and Fathi-Najafi, 1996) and particle pressure (Landman and White, 1994).

Neglecting gravity forces, wall friction and inertial forces, a force balance on a one dimensional filter cake results in:

$$p_s + p_L = P_{app} \quad (2.6)$$

where P_{app} is the applied pressure (Tiller and Leu, 1980). Typical curves illustrating variations of hydraulic and effective pressures within a filter cake are presented in Figure 2.4. At a constant applied pressure, differentiating equation (2.6) with respect to material coordinates yields:

$$\left(\frac{dp_s}{dw}\right)_t + \left(\frac{dp_L}{dw}\right)_t = 0 \quad (2.7)$$

Although equations (2.6) and (2.7) are the most commonly used relationships linking the hydraulic and effective pressures, it is noted that various other relationships between effective and hydraulic pressures have also been obtained by applying multiphase flow theory and carrying out volume averaging of the momentum equations of the liquid and solid phases; the differences between these relationships are due to the assumptions and volume averaging procedures used (e.g. Willis *et al.*, 1974; Rietema, 1982; Tien *et al.*, 2001).

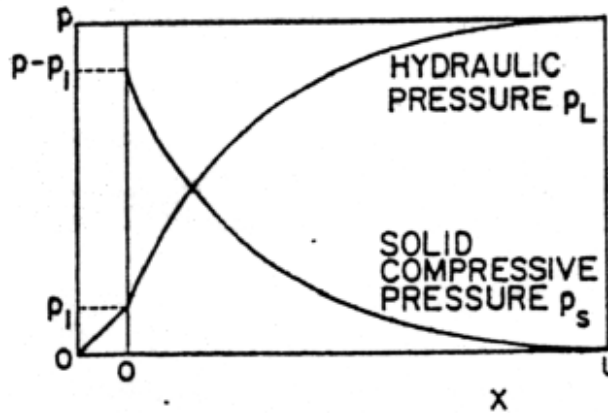


Figure 2.4: Variation of hydraulic pressure and solid compressive pressure within a filter cake (Tiller and Leu, 1980).

Substituting equation (2.7) into equation (2.3) and integrating over the entire cake depth and total filtration time with respect to $p_s(0, \Delta p - \Delta p_m)$ and $w(w_c, 0)$ gives

$$\mu q w_c = \frac{\Delta P - \Delta p_m}{\alpha_{av}} = \frac{\Delta P - \mu q R_m}{\alpha_{av}} = \frac{\Delta P_c}{\alpha_{av}} \quad (2.8)$$

where $\mu q R_m$ represents the pressure (p_m) required to overcome the resistance of the filter medium ($R_m = L_m/k_m$), ΔP is the applied pressure and ΔP_c is the pressure drop across the cake. As integration over the entire cake depth has been performed, the specific cake resistance is no longer the local value as in equation (2.3) but is now an average value (α_{av}). Equation (2.8) can be rearranged to give:

$$q = \frac{1}{A} \frac{dV}{dt} = \frac{\Delta P}{\mu(\alpha_{av} w_c + R_m)} \quad (2.9)$$

where V is the volume of filtrate collected in time t through a filter of area A . From a mass balance on the filtration system:

$$w_c = \frac{s\rho}{A(1-ms)} V = c \frac{V}{A} \quad (2.10)$$

where c is the effective feed concentration, s the mass fraction of solids in the feed and m the ratio of mass of wet cake to mass of dry cake. m can be related to average cake porosity using equation (2.11) and c can be related to m using equation (2.12).

$$m = 1 + \frac{\varepsilon_{av}\rho}{(1 - \varepsilon_{av})\rho_s} \quad (2.11)$$

$$c = \frac{s\rho}{1 - ms} \quad (2.12)$$

where ρ is the liquid density. Substituting equation (2.10) into equation (2.9) gives:

$$q = \frac{1}{A} \frac{dV}{dt} = \frac{A\Delta P}{\mu\alpha cV + A\mu R_m} \quad (2.13)$$

Equation (2.13) is generally called the classical filtration equation. For constant pressure operations, integrating equation (2.13) at constant ΔP gives

$$\frac{t}{V} = \frac{\alpha c \mu}{2A^2 \Delta p} V + \frac{\mu R_m}{A \Delta p} \quad (2.14)$$

Equation (2.14) implies that a plot of t against V will yield a parabolic profile. In order to simplify the extraction of desired information, t/V is commonly plotted against V , generally giving a straight line whose slope is an indication of the specific resistance provided the fluid viscosity and filtration area remain constant throughout filtration. Plots of dt/dV against V generally also give straight lines, in accordance with equation (2.13). Plots in the form of t/V against V or dt/dV against V are commonly known as ‘filtration plots’ and an example is shown in Figure 2.5 (taken from Wakeman *et al.*, 1991). In accordance with equation (2.14), the gradient on the initial portion of these plots is proportional to the average specific cake resistance; it is noted that the gradient decreases less rapidly for progressive increases in applied pressure, resulting in an increase of specific resistance with applied pressure due to cake compressibility.

It is important to keep in mind the assumptions made in deriving equations (2.13) and (2.14). Besides the aforementioned assumptions (such as constant specific cake resistance), it is also assumed that the filter medium characteristics remain

unaltered during filtration, streamline flow occurs through the whole filter cake so the only pressure loss across the cake is due to frictional drag, the filtration area is constant, permeability is time independent and the rate of fluid flow into one face of the cake is equal to the discharge from the opposite face. The classical filtration equation, equation (2.13), also does not explicitly take into account forces arising from physico-chemical interactions, which can be a significant factor when filtering finer particles. The average specific cake resistance and cake porosity effectively ‘lump’ all difficult to account for parameters into measurable/characteristic values.

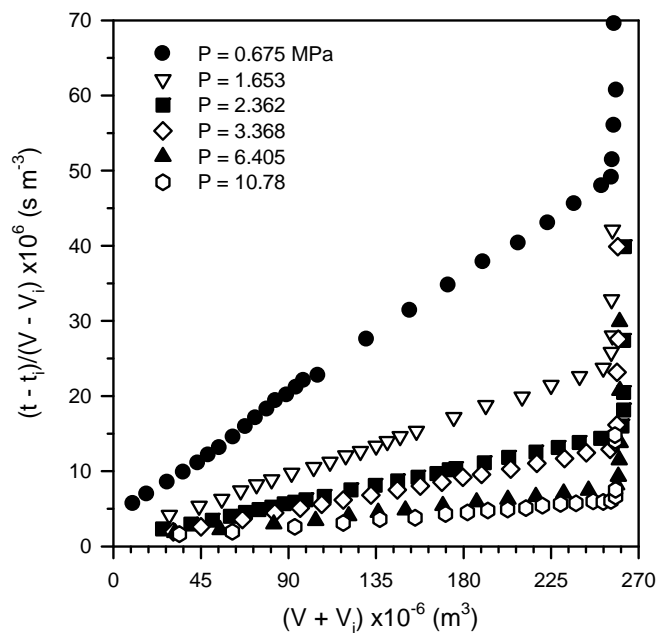


Figure 2.5: Effect of pressure on ‘filtration plot’ of anatase experimental data (mean particle size = 0.3 μm , pH = 4 (isoelectric point)) (adapted from Wakeman *et al.*, 1991).

2.4. COMPRESSIBLE CAKE FILTRATION

2.4.1. Deviations from ‘incompressible’ cake behaviour

In reality, almost all cakes are compressible to a certain extent. From the 1950s to the 1970s, filtration analysis using Equations (2.8-2.14) have almost completely

dominated the literature. Some of the factors which complicate the filtration of some materials (Tiller *et al.*, 1979) are:

1. Cake compression involving re-alignment of particles with a subsequent decrease in porosity;
2. Deformation of fragile particles under high pressures and break up of particles under shearing;
3. Increase in filter medium resistance due to blinding;
4. Variation of cake resistance as a result of smaller particles blinding the filter cake;
5. The fact that solid velocities cannot be neglected for more concentrated suspensions at short filtration times.

The specific cake resistance is perhaps the most important term in equation (2.13) because it determines the filtrate flow rate and pressure drop across the cake. For compressible filter cakes, the specific cake resistance in equations (2.8), (2.9), (2.13) and (2.14) becomes an average value (α_{av}), following Ruth's concept (Ruth, 1946). It has been found that ε_{av} , α_{av} and c can be functions of applied pressure, time of filtration (Tiller, 1953; Bakker *et al.*, 1959; Hameed, 1970; Christensen, 2006), suspension concentration (Bakker *et al.*, 1959; Wakeman, 1979; Rushton *et al.*, 1980), particle size distribution (Grace, 1953; Wakeman *et al.*, 1991; Wakeman, 2007a), particle shape and morphology (Grace, 1953; Bakker *et al.*, 1959; Wakeman, 2007a), particle surface charge (Wakeman *et al.*, 1989; 1991) and blinding of the filter cake and/or the filter medium (Sørensen *et al.*, 1995).

Average specific resistance has been analysed from a basic viewpoint in the study of viscous flow through packed beds of particulate materials by several workers such as Carman (1937; 1938), Fair (1951), Fair and Hatch (1933) and Coulson (1949). Perhaps the most significant outcome of this collection of work was the development of the Kozeny-Carman equation which was derived for viscous flow in granular beds by the assumption of perfectly random packing of discrete particles and through the use of a mean hydraulic pore diameter expressed in terms of the void fraction and particle specific surface. Comparing the Kozeny-Carman equation to Darcy's equation yields an

expression for specific resistance in terms of the porosity, specific surface, solid density and permeability. The Kozeny-Carman model is a useful tool for correlating resistance data for fluid flow through porous media and for determining the specific surface of powder samples from permeability data. The Kozeny-Carman equation has received much criticism, largely undeserved since it correlates bed resistance data for a wider range of porous media types than any other permeability theory (Spielman, 1973). Instead of viewing a packed bed as a bundle of tortuous channels as the Kozeny-Carman theory does, the Happel cell model (Happel and Brenner, 1965) views the bed grains as an assemblage of interacting, but essentially individual spheres, with the flow field around an average sphere being described more realistically and in more detail. For spherical particles, the expression for the permeability derived from the cell model is:

$$k = \frac{x^2}{36} \frac{6 - 9(1 - \varepsilon)^{\frac{1}{3}} + 9(1 - \varepsilon)^{\frac{5}{3}} - 6(1 - \varepsilon)^2}{(1 - \varepsilon) \left(3 + 2(1 - \varepsilon)^{\frac{5}{3}} \right)} \quad (2.15)$$

The Kozeny-Carman and Happel cell model have generally been applied macroscopically, giving estimates of the average permeability and specific cake resistance. Shirato and Aragaki (1972) argue that the determination of an average specific resistance will not shed any light on the internal mechanism of cake filtration operations nor on some particular problems which are encountered in industry. Kelsey (1965) found that the specific cake resistance decreased with higher suspension concentrations and attributed this to a reduction in the time available for particles to orientate themselves. The arrival rate of the particles at the filter medium is also thought to influence cake properties as has been reported by Rushton (1973; 1976) and Wakeman (1979). Particle size distribution is known to affect cake resistance as the fine particles may pass through the cake along with the suspending liquid and lodge themselves at various locations within the cake depth, producing a non-homogenous cake (Tien, 1991). Wakeman (2007a) discusses the influence of particle properties on filtration. He pointed out that the particle properties with the most profound effects on the specific resistance are the particle size, size distribution, shape and interaction with the surrounding fluid. Furthermore, if the particle properties could be specified for a

filtration, the target properties would be for the particles to have as large a size as possible, be as near to spherical as possible, and have a monosize distribution.

Tiller and Crump (1977) acknowledged the fact that, generally, the porosity is minimum at the filter medium surface and a maximum at the cake-suspension interface (refer to Figure 2.3, for example). This is due to the nature of the drag exerted by the fluid. Tiller and Crump went on to experimentally show that the porosity of a latex cake remained almost constant over 80 % of the cake, and that a resistant ‘skin’ developed in the 20 % of the cake closest to the medium. Tiller and Green (1973) had suggested in a previous paper that when compressible materials experience rapid changes of flow resistance at low pressures, a thin ‘skin’ of dry, resistant material may form next to the filter media and that most of the hydraulic pressure drop is located within this narrow region. Tiller and Green (1973) showed that porosity was unaffected by pressure through 90 % of the cake, even at applied pressures as high as 1000 kPa, suggesting that the thin ‘skin’ effectively absorbs most of the pressure and contributes the most to resistance. Wakeman (2007b) recalculated data from Sørensen’s (1992) work on biological sludge and noted a steep gradient of the solids concentration profile close to the filter media (Figure 2.6). Wakeman acknowledged that this ‘skin’ formation occurs only with extremely compressible cakes and causes a low permeability (and hence a high localised pressure loss) close to the filter medium. Wakeman (2007b) went on to point out that although ‘skin’ formation is a property of a cake, it results from consolidation of the cake by constituents of the material packing more closely due to a wide size distribution or deformation of components in the feed. However, although various researchers (Sørensen, 1992; Bierck and Dick, 1990) have noted the occurrence of ‘skin’ formation, the phenomenon is still not currently well understood from a fundamental point of view.

2.4.2. Importance of physico-chemical properties

Belfort *et al.* (1994) claimed that many experimental works show that productivity and efficiency during filtration depend on the physico-chemical properties of the suspension being filtered, such as pH or salinity. Wakeman *et al.* (1989) also

highlighted the importance of colloid science in cake filtration, especially with fine colloidal particles. In general, the lower the repulsive force between particles so the greater is the extent of aggregation. Hence a greater effective particle size makes separation easier. The extent of aggregation of interacting particles may be assessed by sedimentation experiments whereby particles of a greater effective size should generally settle more quickly.

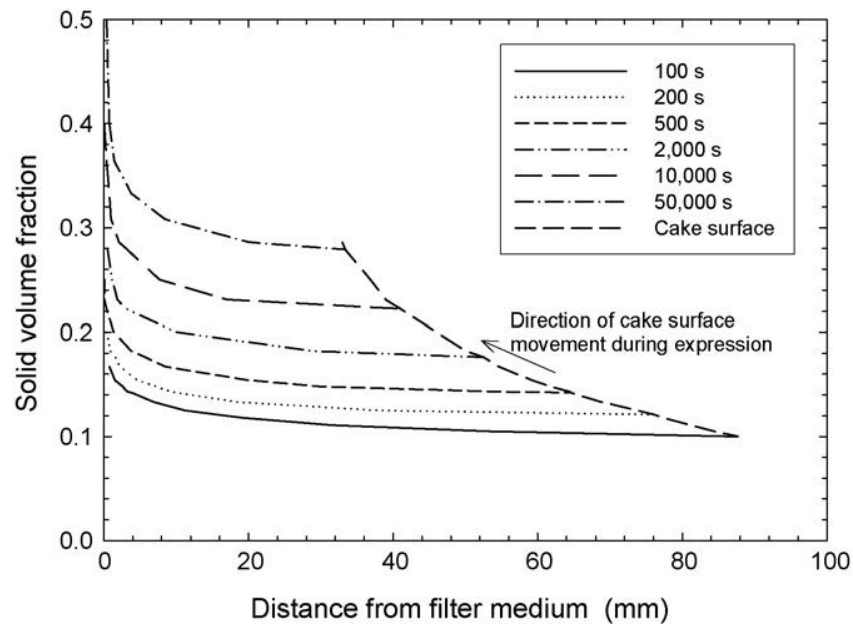


Figure 2.6: Variation of solid volume fraction through the cake thickness during an expression process (Wakeman, 2007b).

It has been stated in the literature that only models taking into account physico-chemical properties of the suspension can accurately and thoroughly describe experimental filtration performance (Cohen and Probstein, 1986). Rietema (1953) had previously shown how introducing ions into the suspension to be filtered changed its stability and hence cake structure, but he was unable to correlate the results for this effect at that time. It was later shown that surface interaction variations induce changes in the cake permeability (McDonogh *et al.*, 1984; 1992). Hlavacek and Remy (1995) established a link between the specific resistance of a filter cake, the zeta potential of

the feed suspension and the particle size distribution. The surface interaction between a filter medium and solute has also been shown to affect solute retention (Bacchin *et al.*, 1996). Detailed discussions of physico-chemical influences on filtration is not attempted here, instead an introduction to the fundamental nature of these influences is presented. Interested readers are referred to the authoritative text by Hunter (2001).

The interplay of forces between particles in lyophobic sols may be interpreted noting that the potential energy of interaction between a pair of particles consists of two components (Derjaguin and Landau, 1941):

1. A repulsive component, V_R , arising from the overlap of the electrical double layers (assuming ion adsorption equilibrium is maintained), and
2. A component, V_A , due to van der Waals attraction arising from electromagnetic effects.

A sol is defined as a suspension of colloidal particles in a liquid and the term lyophobic is indicative of the repulsion that the solid material has for the liquid in which it is dispersed. The total potential energy of interaction is given by (Wakeman and Tarleton, 1999):

$$V_T = V_R + V_A \quad (2.16)$$

$$V_R = \frac{\pi \varepsilon_p a_1 a_2 (\psi_1^2 + \psi_2^2)}{a_1 + a_2} \left(\frac{2\psi_1 \psi_2}{\psi_1^2 + \psi_2^2} \ln \left(\frac{1 + \exp(-\kappa H)}{1 - \exp(\kappa H)} \right) + \ln(1 - \exp(-2\kappa H)) \right) \quad (2.17)$$

$$V_A = -\frac{A}{12} \left(\frac{y}{x^2 + xy + x} + \frac{y}{x^2 + xy + x + y} + 2 \ln \left(\frac{x^2 + xy + x}{x^2 + xy + x + y} \right) \right) \quad (2.18)$$

where ε_p is the permittivity of the fluid, a_1 and a_2 the particle radii, ψ_1 and ψ_2 the potentials measured at the outer boundary of the Stern layer, κ the reciprocal electrical double layer thickness, H the interparticle distance, A the Hamaker constant, $x = H/(a_1 + a_2)$ and $y = a_1/a_2$.

A schematic diagram of the potential energy barrier generated between two approaching particles is shown in Figure 2.7 (Wakeman and Tarleton, 1999). If particles

are brought sufficiently close to either the primary or secondary minima, the potential energy is either partially or fully breached and the particles are considered to aggregate. At very small distances of separation Born repulsion is predominant due to overlapping electron clouds. A primary minimum potential energy exists where $V_R + V_A$ is significantly negative, limiting the distance of closest approach, $H_{S\ min}$. At intermediate distances of separation, the electrical repulsion term is dominant at low ionic strength and high surface potentials, giving rise to a primary maximum, V_m . If V_m is large compared with the thermal energy of the particles, KT ($\sim 4.2 \times 10^{-20}$ J), the system should be stable, otherwise particles will aggregate. The height of the energy barrier to aggregation depends on the magnitude of the Stern and zeta potentials and on the range of repulsive forces. At larger distances of separation V_R decreases more rapidly than V_A and a secondary minimum may appear.

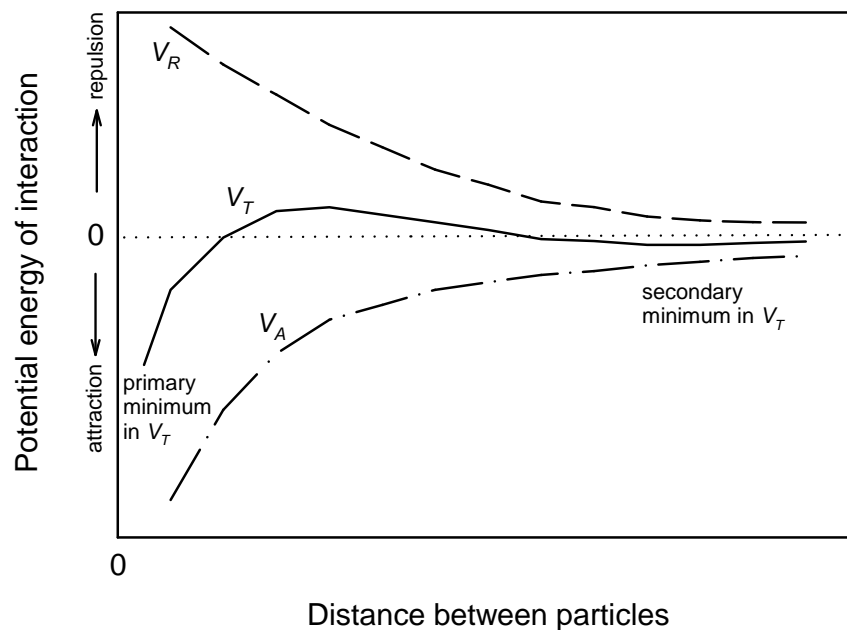


Figure 2.7: Schematic of the potential energy barrier generated between two approaching particles (Wakeman and Tarleton, 1999).

2.4.3. Rigorous analysis of compressible cake filtration

In attempting to improve the fundamental understanding of compressible cake filtration, more rigorous models have been developed without some of the assumptions used in the conventional theory. Smiles (1970) was one of the first to come up with a model based on the differential equations of continuity and momentum using a Lagrangian coordinate system. Atsumi and Akiyama (1975) and Tosun (1986) criticized Smiles' boundary condition at the cake-suspension interface as it indicated no flux at this interface; Atsumi and Akiyama went on to use a moving boundary condition at the growing cake surface in their work. Numerous other workers (Willis and Tosun, 1980; Tosun, 1986; Stamatakis and Tien, 1991; Chase and Willis, 1992; Tosun *et al.*, 1995; Burger *et al.*, 2001) have carried out theoretical studies on cake filtration based on volume averaged continuum theory for multiphase flow. The fundamental basis of the different models proposed by these various workers is similar; discrepancies arise due to differing assumptions, constitutive equations, boundary/initial conditions and solution procedures. As pointed out by Olivier *et al.* (2007), the fundamental basis for these various works are the material and momentum balance equations for both the liquid and solid phases and material property parameters (compressibility and permeability). An illustration of some of the typical forces acting on a portion of a filter cake is shown in Figure 2.8.

A typical form of the basic partial integro-differential equation describing liquid movement and cake volume change is given by Wakeman (1978) as:

$$\int_0^x \frac{d\varepsilon_x}{dt} dx = (1 - \varepsilon_x) \left[\frac{k_x}{\mu} \frac{dp_L}{dx} - \left(\frac{k_x}{\mu} \frac{dp_L}{dx} \right)_{x=0} \right] \quad (2.19)$$

As Koenders and Wakeman (1997a) pointed out, another common feature of these models is that they do not recognise any interparticle interactions and if they have any validity it is only for systems of large particles. The models developed by Auzerais *et al.* (1988), Buscall and White (1987) and Landman *et al.* (1991, 1993, 1995) have attempted to overcome the theoretical deficiencies of previous models by using the concept of the particles being networked and defining a gel point at which the

suspension becomes fully networked (Auzerais *et al.* used the volume packing at close packing rather than the gel point).

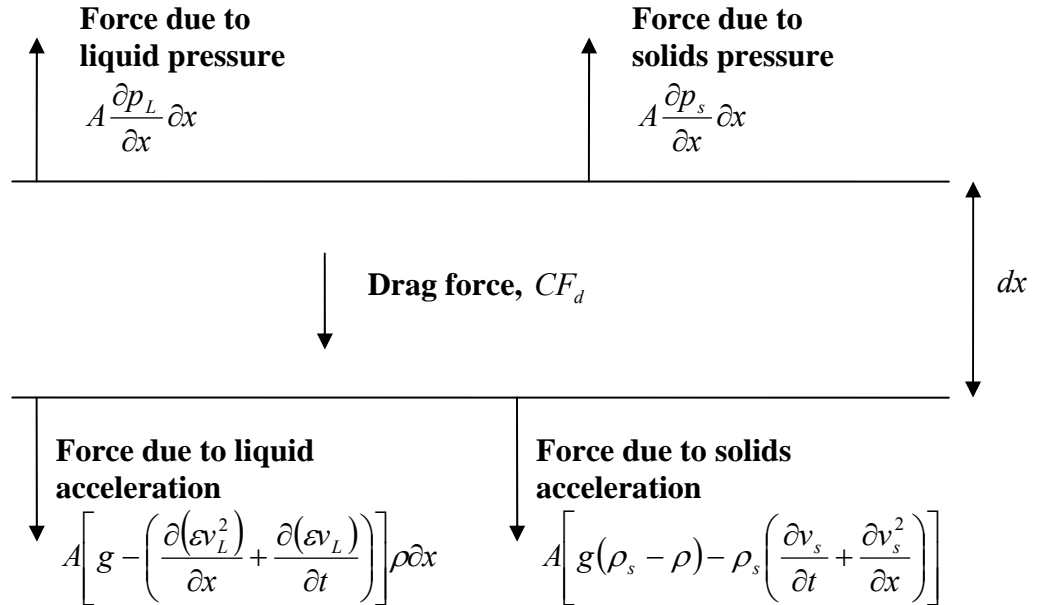


Figure 2.8: Forces on a portion of a filter cake.

Koenders and Wakeman (1997a; 1997b) analysed the initial stages of cake formation by developing semi-empirical expressions for filter cakes consisting of charged, inorganic, colloidal interacting particles. Expressions for the two-particle interactive potential, which is a function of particle size, zeta potential, electrical double layer thickness and the distance between particle surfaces, were obtained from the DLVO theory (Hunter, 2001). Although the work of Koenders and Wakeman give a more fundamental understanding of how pH, particle size, zeta potential and ionic strength influence the compressibility of filter cakes, Teoh *et al.* (2006) argue that the expressions developed by Koenders and Wakeman do not give a good fit to their experimental data. Teoh *et al.* pointed out that the expressions developed by Koenders

and Wakeman suggest that a plot of v/t against $t^{1/2}$ for data during the initial period of filtration should yield a straight line. Meeten (2000) claimed that this linearity at the initial period of filtration only holds for relatively incompressible cakes. In their work, Koenders and Wakeman assumed that compressive stress is only due to the double layer force. On the other hand, previous work by Bowen and Jenner (1995) assumed the compressive stress (or the disjoining pressure) to be the sum of the double layer force, van der Waals force and the hydration force. However, Bowen and Jenner's work involved micromechanics that did not allow for structure formation and as a consequence the theory is inadequate for low zeta potential or low solidosity.

2.5. ANOMALOUS FILTRATION BEHAVIOUR

'Cake collapse', where abrupt changes in cake structure occur partway through a filtration, was first observed by Rietema (1953) and subsequently by Baird and Perry (1967). Rietema hypothesised a concept of 'flow stabilised cakes' for constant pressure and constant rate filtrations. Rietema proposed that when a random packing of rather loose structure, non-deformable particles is compressed vertically then it is necessary that each particle should move not only in a vertical, but also in a horizontal, direction. Rietema acknowledged the fact that the compressive force originates from the cake solids pressure which increases from the cake-suspension interface to the cake-medium interface. If the component of this compressive force which tries to move the particle in a direction other than the axial is counterbalanced by a second force of other origin, compression will be prevented and the cake structure will retain its packing density and porosity. Rietema suggested that such a stabilising force should be the same throughout the cake and should originate from the interstitial liquid flow. Therefore, when the filtration rate decreases below a critical value, or when the cake reaches a critical thickness, a layer of denser packing and increasing thickness is formed at the bottom of the cake (the cake rapidly collapses to a new pseudo-equilibrium state) while the upper layer retains its original packing and porosity. Rietema called this phenomenon 'retarded packing compressibility' and claimed that it can greatly affect the average filtration rate. Shirato and co-workers (1971, 1972) disagree with the concept of retarded packing compressibility and pointed to Rietema's experimental set up and

conditions as being a contributing factor, not allowing normal compression to occur. However, various other works (Fathi-Najafi and Theliander, 1995; Sørensen *et al.*, 1995; Tarleton and Willmer, 1997) have also reported the ‘retarded packing compressibility’. Furthermore, some of the aforementioned works did not use an intrusive experimental set up similar to Rietema’s,

One observation made with retarded packing compressibility is that the cake gives a minimum porosity not at the cake-medium interface but at a position further into the cake. Wakeman (1981a) deduced that cake collapse indicates the assumption of point contact of particles is invalid and so the force balance is incomplete. Banda and Forssberg (1988) claimed that particles are not always in point contact after examining micrographs of particulate filter cakes showing contact between particles across finite areas. Antelmi *et al.* (2001) used small-angle neutron scattering as well as void volume fraction and permeate flux measurements to analyse latex filter cakes and concluded that at all tested filtration pressures (20-400 kPa), the cakes were extensively collapsed. They claimed that the mechanisms that produced this collapse only required very small relative motions of the particles, which leave the local coordination of the latex particles unchanged but allow large voids to be reduced. Antelmi *et al.* also claimed that these motions can be inhibited by using particles with non-spherical shapes and by increasing the friction forces that act between particle surfaces.

Sørensen *et al.* (1995) found dramatic deviations from their expected filtration behaviour, in terms of an abrupt increase in filtrate flux part way through a filtration. They initially listed possible reasons to account for this abrupt change including: penetration of air through the filter cake, channelling, wall effects, sedimentation, and compression/blinding interactions. Sørensen *et al.* subsequently went on to eliminate all of the above possibilities (in the context of their work) apart from the compression/blinding interaction. They suggested the most likely reason to be deposition of small scale solids within the cake structure increasing the flow resistance and consequently the local effective pressure. The local effective pressure then causes a decrease in porosity due to the compressible behaviour. Sørensen *et al.* suggested that in some parts of the cake the hydraulic pressure gradient may increase due to this compression/blinding interaction, leading to a detaching shear force on the walls of the

channels forming the filter cake structure. This gives rise to the possibility of a situation where locally increasing hydraulic pressure gradients in some sections of the cake cause an erosion of previously deposited small-scale solids resulting in a temporary reduction in the flow resistance, as well as an increase in filtrate turbidity (as evidenced by their experimental measurements).

Tarleton and Willmer (1997) noted abrupt changes during the filtration of zinc sulphide suspensions. Figures 2.9 and 2.10 illustrate the effects of the abrupt change in terms of the macroscopic effect on the filtrate flow through the cake as well as the corresponding measurements of solids volume fraction within the cake. It is seen that large deviations from the expected linear behaviour occur after approximately 9000 s into filtration. The filtrate flow rate seen at point B increased to three times the rate experienced at point A and then reduced again to a value close to the original flow rate at point C.

Tarleton and Willmer (1997) point out that the corresponding solids concentration given by the electrode pairs 10, 15 and 20 mm above the membrane show that between points B and C the measured solids concentrations either remained essentially constant or reduced and then increased more sharply at the point C. They then go on to point out that the gradient of the t/V against V plot after point C appears to be similar to that recorded up to the point A, indicating that suspension was still present above the cake and thus essentially eliminating the notion that sedimentation resulted in supernatant permeating through a formed cake after point B. In their paper, Tarleton and Willmer discuss the complexities of analysing such forms of cake restructuring or 'collapse' and the confusion it has brought about.

2.6. FILTRATION OF BINARY MIXTURES

The properties of a filter cake at any given time during a filtration depend, to a large extent, on the packing behaviour of its constituent particles. Many researchers have investigated the packing of assemblies of equal spheres because of its simplicity and its convenience in theoretical work. Six typical unit cells are shown in Figure 2.11 (Suzuki, 2006). Regular packings of equal spheres are seldom encountered in filtration.

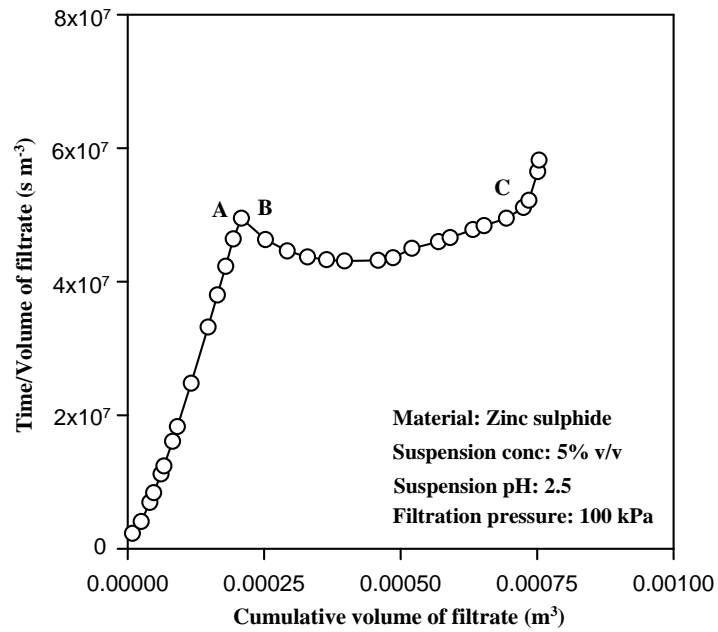


Figure 2.9: Anomalous ‘filtration plot’ of a zinc sulphide suspension filtration (Tarleton and Willmer 1997).

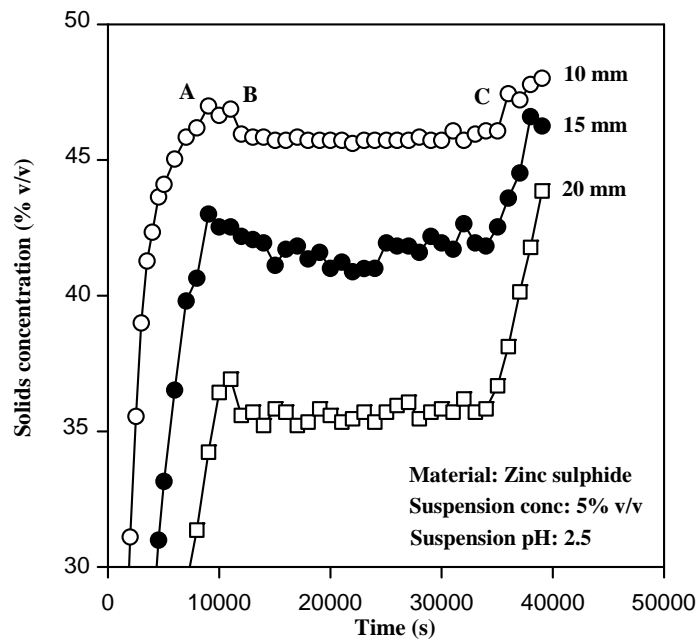


Figure 2.10: Changes in measured solids concentration with time for the zinc sulphide filtration. The corresponding ‘filtration plot’ is shown in Figure 2.9 (Tarleton and Willmer 1997).

Irregular shaped particles of wide size distributions often add to the complexity of random packing structures where porosities and coordination numbers vary with filtration time and spatially within a filter cake. Figure 2.12 (Wakeman and Tarleton, 2005) illustrate the typical effects of some common, regular, particle shapes on the specific surface.

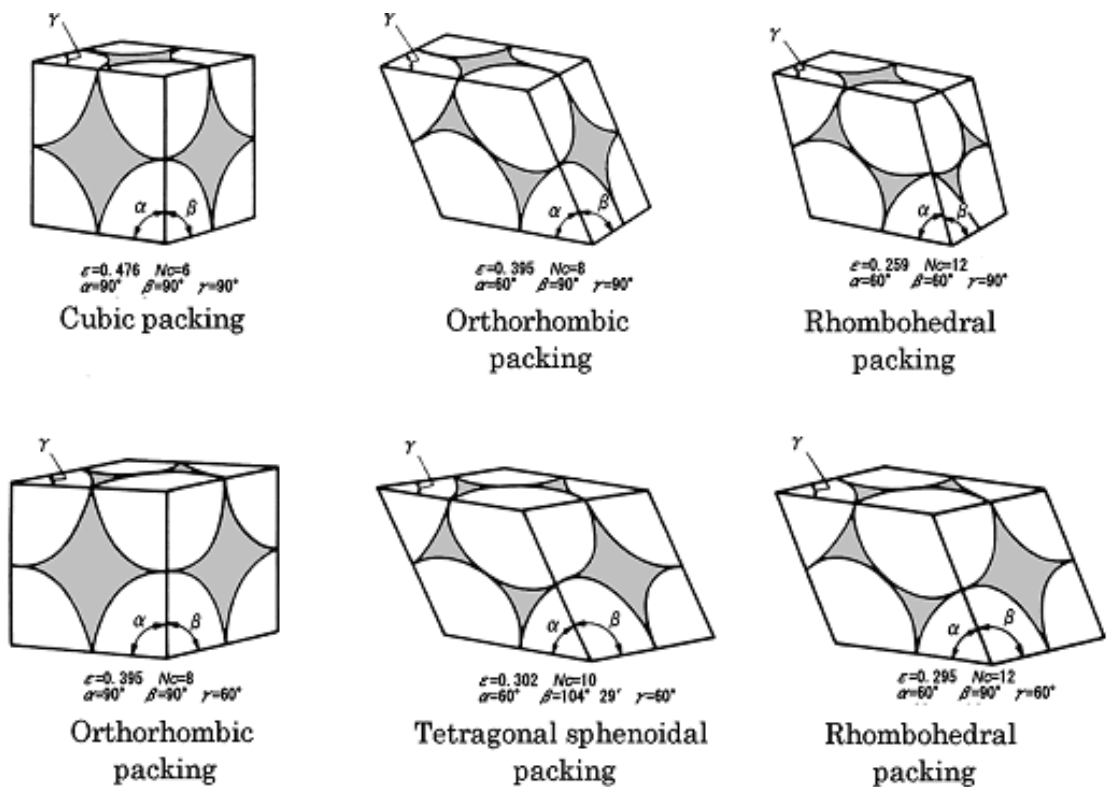


Figure 2.11: Regular packing structures of equal spheres. The coordination numbers and corresponding porosities are shown (Suzuki, 2006).

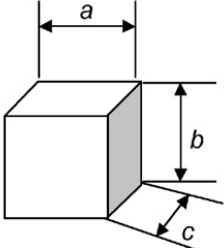
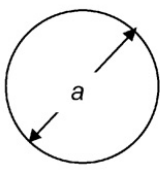
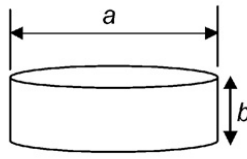
		
Cubic $b = c = a$ Rectangular $b = a; c = 10a$ (say)	Spherical	Fibrous $b = 10000a$ (say) Cylindrical $b = 10a$ (say) Flakey $b = 0.01a$ (say)
Surface $2(ab + ac + bc)$	πa^2	$\frac{\pi}{4} a^2 + \pi ab$
Volume abc	$\frac{\pi}{6} a^3$	$\frac{\pi}{4} a^2 b$
Specific surface $\frac{2(ab + ac + bc)}{abc}$	$\frac{6}{a}$	$\frac{1}{b} + \frac{4}{a}$

Figure 2.12: Effect of particle shape on specific surface (Wakeman and Tarleton, 2005).

Shirato *et al.* (1963) proposed a simple additive law for predictions of porosities of filter cakes resulting from filtrations of binary suspensions. Say the two solids components are denoted 1 and 2, and that the cake porosity produced from the filtration of the pure component 1 is $\varepsilon_{av,1}$ and its volume fraction of solids in the mixture is X_D . The corresponding values for pure component 2 are $\varepsilon_{av,2}$ and $(1-X_D)$. Then the associated void volume for component 1 will be $\varepsilon_{av,1}X_D/(1-\varepsilon_{av,1})$ and $\varepsilon_{av,2}(1-X_D)/(1-\varepsilon_{av,2})$ for component 2. The additive porosity at a fixed X_D is given by the sum of the void volumes divided by the sum of the total volumes due to each solids component¹:

$$\varepsilon_{av} = \frac{\frac{\varepsilon_{av,1}X_D}{1-\varepsilon_{av,1}} + \frac{\varepsilon_{av,2}(1-X_D)}{1-\varepsilon_{av,2}}}{\frac{X_D}{1-\varepsilon_{av,1}} + \frac{1-X_D}{1-\varepsilon_{av,2}}} \quad (2.20)$$

Shirato *et al.* tested this additive law on different mixtures of clay slurries and claimed that, when filtering mixtures whose particle size distributions are similar, the equilibrium porosity of the resultant filter cake will be close to that predicted by his proposed additive law. He went on to suggest that when the particle size distributions

¹ Shirato's equation (equation (2.20)) is discussed further and used in Chapter 4 (as equation (4.24)).

are considerably different, the equilibrium porosity will be less than the additive value, owing to the fact that the smaller solids will fill in the voids created by the larger solids. As discussed by Heertjes and Zuideveld (1978), a drawback of the Shirato additive law is that the filling of a pore volume generated by one component by another (finer) component cannot be described.

Tokumitsu² (1964) proposed an equation for porosity prediction for a packed bed rich in small particles:

$$\varepsilon_{av} = 1 - \frac{1 - \varepsilon_{av,2}}{(1 - X_D) + AX_D(1 - \varepsilon_{av,2})} \quad (2.21)$$

and another for a packed bed rich in large particles:

$$\varepsilon_{av} = 1 - \frac{1 - \varepsilon_{av,1}}{X_D(1 + \beta_s\beta_c)^3} \quad (2.22)$$

where β_s and β_c are given by:

$$\beta_s = \left(\frac{x_2}{x_1} \right)^n \quad (2.23)$$

$$\beta_c = \left(1 + \frac{1 - X_D}{X_D} \right)^{\frac{1}{3}} - 1 \quad (2.24)$$

x_1 is the size of large particles and x_2 the size of small particles. Correspondingly, $\varepsilon_{av,1}$ and $\varepsilon_{av,2}$ are the average porosities of the pure large and small component cakes, respectively. The physical significance of the parameters used in equations (2.21) to (2.24) is briefly discussed as follows (Abe and Hirose, 1982). When large particles are added to a packed bed of small particles, the large particles need excess space beyond their own true volume. These large particles penetrate into the packed bed of fines taking up a volume A times their own true volume, where A is given by:

$$A = 1 + f_c \left(\frac{x_2}{x_1} \right) \quad (2.25)$$

² The appropriate forms of Tokumitsu's equations are used in Chapter 4.

where f_c takes the value of 1 for $x_2/x_1 \sim 0.5$, 1.2 for $x_2/x_1 \sim 0.25$, and 1.4 for $x_2/x_1 < 0.125$, respectively. On the other hand, when fines are added to a packed bed of large particles they tend to not only fill up inter-particle voids but also eventually force the large particles apart. The two main factors that influence the altered packing due to the addition of fines are the particle size ratio (as described by β_s in equation (2.23)) and solids composition (as described by β_c in equation (2.24)). n in equation (2.23) depends on the particle shape and takes the value of 1/2 for rounded particles and 1/3 for angular ones. The combined use of Tokumitsu's equations is an example of an interparticle penetration model and generally predicts a minimum in porosity at some intermediate solids composition.

Much of the published work on the packing of binary mixtures of solids suggests that a minimum porosity occurs at some intermediate solids composition (McGeary, 1961; Gray, 1968; Sohn and Moreland, 1968; Haughey and Beveridge, 1969; Leclerc, 1975; Harr, 1977; Abe and Hirose, 1982). Some more recent theoretical (Yu and Standish 1988, Yu *et al.*, 1996; Mota *et al.*, 2001; Dias *et al.*, 2004a) and experimental (Suzuki *et al.*, 1986; Mota *et al.*, 2001; Dias *et al.*, 2004a) works suggest that the larger the difference in size between the coarse and fine particles in a mixture so the more pronounced is the non-linearity in the porosity versus solids composition relationship. Some packing characteristics of a binary mixture of spheres showing a minimum porosity is illustrated in Figure 2.13 (Dias *et al.*, 2004b). More pertinent to the deadend filtration of binary suspensions, in particular with regards to specific cake resistance, are the works of Shirato *et al.* (1963), Abe and Hirose (1982), Wakeman (1996) and Iritani *et al.* (2002).

In terms of specific resistance, Shirato *et al.* (1963) pointed out that if one follows the concepts by Grace (1953) and Tiller (1953), and defines S as the average effective specific surface area, the following equation will result:

$$(kS^2)^{0.5} = \left(\frac{\alpha \rho_s \int_0^P \frac{\varepsilon_x^3}{1 - \varepsilon_x} dp_L}{\Delta P} \right)^{0.5} \quad (2.26)$$

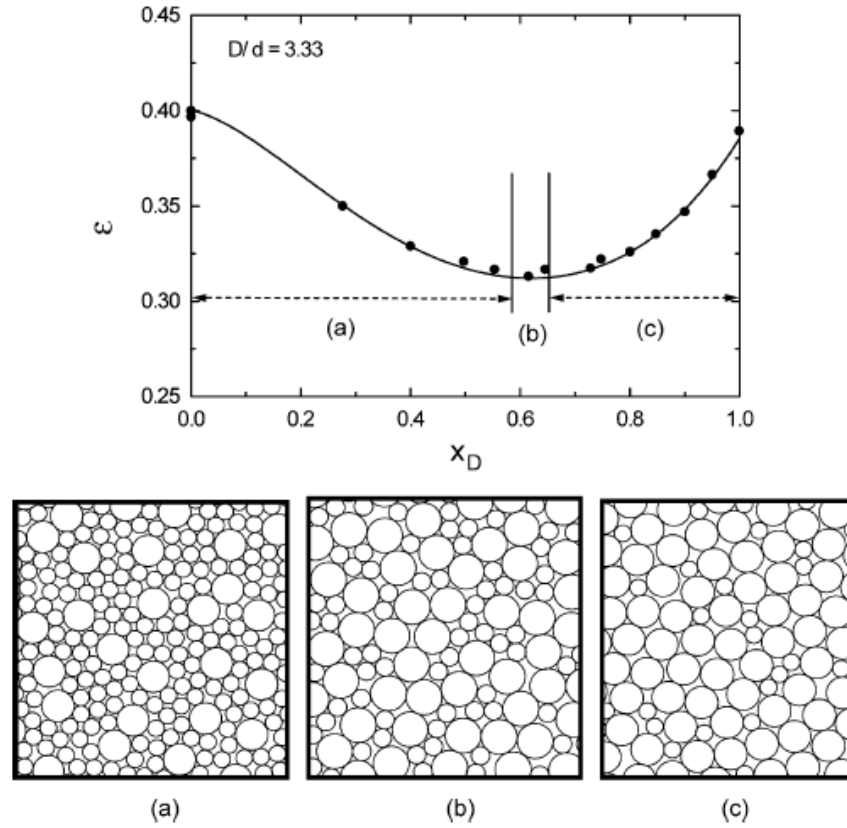


Figure 2.13: Dependence of the binary mixture porosity, ϵ_{av} , on volume fraction of large particles, X_D , for a glass beads size ratio of 3.33. The boxes illustrate the packing, (a) mixture enriched with small particles; (b) mixture close to the maximum packing density (minimum porosity); (c) mixture enriched with large particles (Dias *et al.*, 2004b).

where k is the Kozeny constant, ϵ_x the local porosity and ΔP the filtration pressure. Abe and co-workers (1979, 1993) claimed that the specific resistance of cakes formed from binary mixtures can be described by³:

$$\alpha_{av} = \frac{180(1 - \epsilon_{av})}{\epsilon_{av}^3 (X_D \rho_L + (1 - X_D) \rho_S)} \left(\frac{X_D}{\phi_L x_1} + \frac{1 - X_D}{\phi_S x_2} \right)^2 \quad (2.27)$$

³ Equation (2.27) is further discussed and developed in Chapter 5.

where subscripts 1 and 2 refer to the large and small solids component, respectively, X_D refers to the volume fraction of the larger particles, x refers to particle size and ϕ refers to a surface factor. The surface factor for each component at an arbitrary pressure is determined by using the experimental data (α_{av} and ε_{av}) from the filtration of a single component suspension.

Wakeman (1996) came up with an empirical relationship between the single component values of specific resistance and the mixture value at a given pressure, this relationship may be expressed as:

$$\alpha_{av} = \alpha_{2,av} - (2\alpha_{2,av} - \alpha_{1,av})X_D + \alpha_{2,av}X_D^2 \quad (2.28)$$

where again subscripts 1 and 2 refer to the large and small solids components, respectively. It is noted that when $X_D = 0$, $\alpha_{av} = \alpha_{2,av}$ and when $X_D = 1$, $\alpha_{av} = \alpha_{1,av}$. Wakeman developed this empirical equation to estimate the filtration characteristics in the absence of a fundamental model that is able to predict the specific resistance of the cake formed from binary mixtures. Although the equation gave a good fit to Wakeman's experimental data (calcite/anatase mixtures), in his paper Wakeman explicitly mentioned that it is not claimed that the equation is a general one for use with any mixture of solids.

2.7. PREVIOUS EXPERIMENTAL TECHNIQUES

Generally speaking, for any physically meaningful analysis of filtration data to be made, reliable filtration apparatus and a skilled operator are necessary for good quality data acquisition. Basic filtration data are commonly obtained in laboratories with relatively elementary equipment such as the single leaf filter operating at either constant under- or over-pressure, with data manually recorded. Performing these experiments manually can introduce significant errors unless great care is taken.

The importance of local filter cake properties have been established and to enable analysis of these local properties, it is common practice to perform sequences of constant pressure and/or vacuum experiments and analyse the resultant data with the aid

of cake samples. The difficulties of taking representative cake samples and the desire to assess *in situ* cake formations has lead researchers to the development, though not widespread adoption, of alternative techniques which in some cases facilitate the near continuous determination of cake structure throughout an experiment (Tarleton, 1999a). Some of these experimental techniques include the use of intrusive electrodes (Rietema, 1953; Baird and Perry, 1967; Dobson, 1970; Wakeman, 1981b; Holdich, 1990; Tarleton and Hancock, 1996; 1997) or intrusive pressure probes (Shirato *et al.*, 1980; Willis *et al.*, 1983; Murase *et al.*, 1989; Wu, 1994; Fathi-Najafi and Theliander, 1995; Sedin *et al.* 2003; Johansson and Theliander, 2007), flush mounted electrodes (Shirato *et al.*, 1971; Shirato and Aragaki, 1972) or flush mounted pressure probes (Harvey *et al.*, 1988) and spectroscopy methods such as X-rays and NMR (Bierck *et al.*, 1988; Bierck and Dick, 1990; Tiller *et al.*, 1995; La Heij *et al.*, 1996; Erk *et al.*, 2006). Tarleton (1999a) pointed out that although the measurement techniques employed in filtration differ in detail, the generic arrangements are similar and the advantages and disadvantages can be summarised as shown in Table 2.1 (Tarleton, 1999a)

Shirato *et al.* (1971) and Murase *et al.* (1989) claim that horizontal electrodes that intrude the filter cake (like the one used by Rietema, 1953) will tend to interfere with cake formation such that the probes artificially support a growing filter cake. However, these researchers had not quantified the erroneous effects of intrusive electrode probes. Tarleton (1999a) attempted to quantify the influence of intrusive electrodes on cake formation with respect to filtration parameters by conducting a series of experiments on calcite and talc using a 102 mm diameter filter cell and varying electrode lengths (0-50 mm) and diameters (0-3.5 mm). Tarleton found that macroscopic cake formation and properties are significantly altered only over more extreme ranges of electrode length and diameter, whereby further increase in length and/or diameter decreased the measured cake porosity of the more compressible talc filtration but had relatively little influence for the nearly incompressible calcite filtration.

Table 2.1: Summary of the methods for assessing cake structure in filtration processes (Tarleton, 1999a).

	Electrodes (electrical resistance)	Pressure transducers	X-rays etc.
Type of field	soft (electric field lines can distort)	n/a	hard (passage of radiation is not distorted)
(Potential) accuracy	moderate-good	can be good (depending on the transducer quality)	good
Speed of measurement	fast	fast	can be slow
Ease of use	good	good	poor
Ability to measure a range of cake properties	good	poor	poor
Cost	relatively low	can be high	can be high

Although electrode design and arrangements can be made in a non-intrusive manner, a fundamental problem with this technique is that measurements close to the filter medium, which is the region of greatest interest, cannot be made due to unwanted distortion of the electric field lines close to the filter medium. For example, in Tarleton's work (1999a), the closest electrode is 10 mm above the filter medium. Shirato *et al.* (1971) illustrate one advantage of using pressure probes by simultaneously measuring the cake's electrical resistance (using electrodes) and hydraulic pressure profiles (using pressure probes). In their work, the electrode closest to the medium is positioned at a height of 10.5 mm above the medium and the probe closest to the medium is at a height of only 1.8 mm.

Shirato *et al.* (1980) conducted experiments to investigate variations of hydraulic pressure throughout the filter cake using six pressure probes protruding from

the top of the filter cell (Figure 2.14). These pressure transducers are connected to pressure probes made of brass tubes of 3 mm inner diameter. The lower ends of the probes were located at different (by several millimetres) heights above the filter medium. Shirato *et al.* completely filled each probe with deionised water; otherwise the measurements led to significant errors.

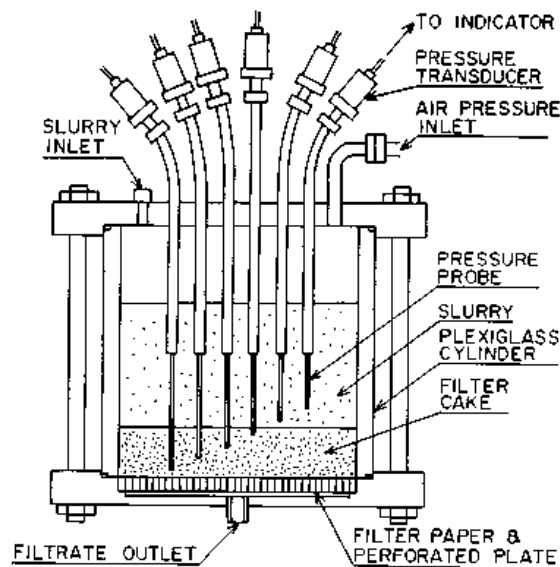


Figure 2.14: Schematic diagram of filter (Shirato *et al.*, 1980).

Wu (1994) used an apparatus similar to Shirato *et al.* (1980). After an experiment, Wu sliced the cake into six pieces and each piece was weighed and dried to assess the porosity at various heights. Fathi-Najafi and Theliander (1995) tried to alleviate the problem of particle sedimentation during filtration by separating the filter cake into two and recirculating some of the suspension from the upper part of the chamber (Figure 2.15). However, the problem of intrusive probes influencing the filter cake formation was still not solved. Many of the filtrations performed by Fathi-Najafi and Theliander using this apparatus resulted in ‘cake collapse’ (see Section 2.5 for some

discussion on such anomalous filtration behaviour) and was attributed to the formation of channels within the cake.

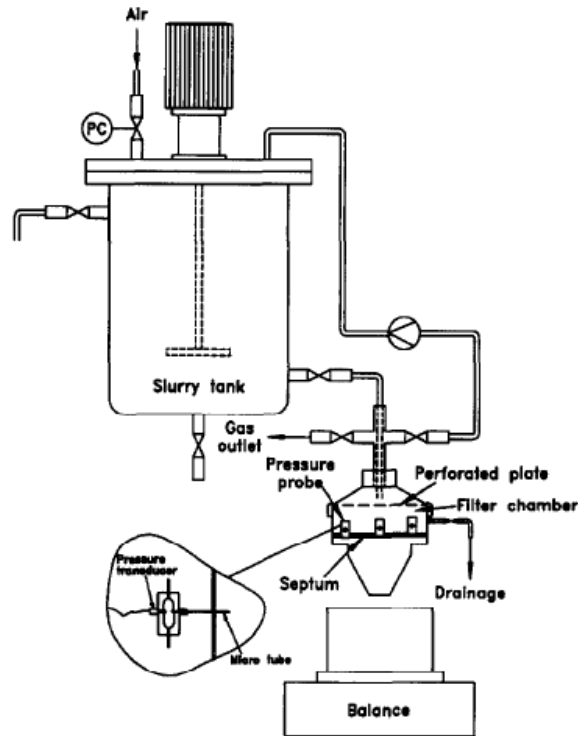


Figure 2.15: Apparatus used by Fathi-Najafi and Theliander (1995).

Tarleton and Hancock (1997) recognised a lack of consistency in test methods and analysis procedures for filtration experiments and investigated a technology to try to rectify this. Tarleton and co-workers (1997; 1998; 1999b) proposed the use of mechatronic principles, which integrates electronics, computers, process control and mechanical systems, to investigate the local properties of filter cakes during filtration. A schematic representation of the mechatronic based filtration apparatus is shown in Figure 2.16 (Tarleton, 1999b). Ten micro-pressure transducers (for hydraulic pressure measurements) were fixed in a spiral arrangement around the inner circumference of the filter cell and ranged from heights of 0.5 mm to 15.3 mm from the filter medium and protrude ~2 mm into the cell. This essentially allows non intrusive measurements of

cake properties to be made close to the filter medium. Moreover, the pneumatic valves are computer controlled and the relevant filtration data semi-continuously transmitted and displayed on the personal computer. Tarleton (1999b) pointed out that this allows filtration data to be acquired in a repeatable and reliable manner with a minimum of operator interference for either constant or variable pressure conditions. The on-line measurement of experimental parameters also allowed a real time display of results on the computer screen as an experiment proceeded. Examples of hydraulic pressure profile results from test talc filtration experiments by Tarleton and Hadley (2003) using the aforementioned apparatus are shown in Figure 2.17.

2.8. CLOSURE

Many of the complications that arise during filter cake formation have been highlighted in this chapter. Some of these complications can lead to unusual filtration behaviour, and hence subsequent complexities in design procedures and calculations for solid/liquid separation equipment. Filtrations of binary suspensions add a level of complexity to single component suspension filtrations. Investigations into binary suspension filtrations and anomalous filtration plots require an appropriate apparatus, enabling reliable determination of data, and systematically planned filtration experiments. An apparatus similar to that used by Tarleton (1999b) has been identified as being suitable for this work and a description of this apparatus and its operational procedures are given in the next chapter.

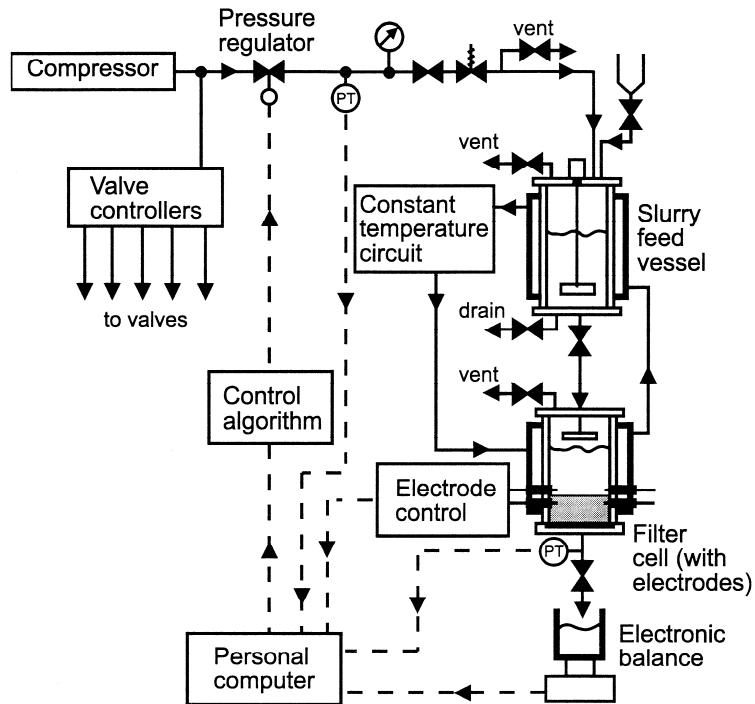


Figure 2.16: Schematic representation of the mechatronic based filtration apparatus (Tarleton, 1999b).

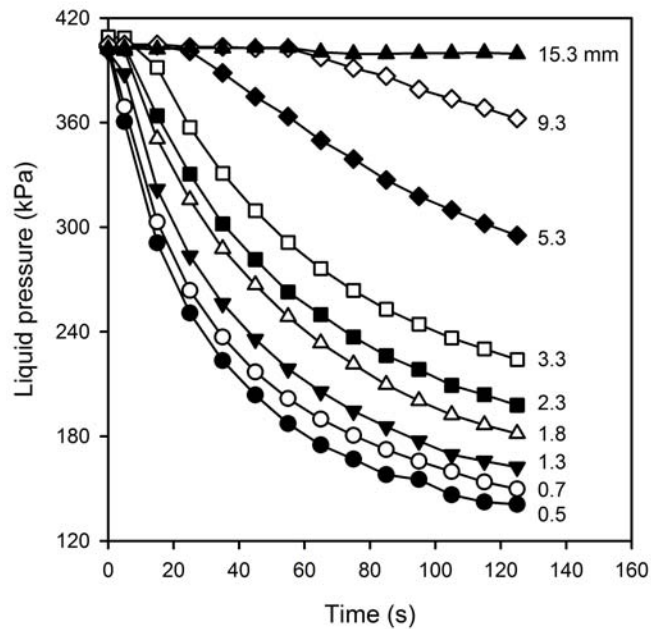


Figure 2.17: Hydraulic pressure history of a 400 kPa constant pressure filtration of a talc suspension (Tarleton and Hadley, 2003). Legend represents the height that a pressure probe is above the filter medium

REFERENCES

- Abe E., Hirosue H. and Yokota K. (1979) Pressure drop through a packed bed of binary mixture. *J. Chemical Engineering Japan* **12**, 302-306.
- Abe E. and Hirosue H. (1982) Porosity estimation of a mixed cake in body filtration. *J. Chemical Engineering Japan* **15**, 490-493.
- Abe E., Hirosue H. and Yamada N. (1993) Prediction of the filtration characteristic in body filtration. *Proc. 6th World Filtration Congress*, pp.137-140, Nagoya.
- Antelmi D., Cabane B., Meireles M. and Aimar P. (2001) Cake collapse in pressure filtration. *Langmuir* **17**, 7137-7144.
- Atsumi K. and Akiyama T. (1975) A study of cake filtration- formulation as a Stefan problem. *J. Chemical Engineering Japan* **8**, 487-492.
- Auzerais F.M., Jackson R., and Russel W.B. (1988) The resolution of shocks and the effects of compressible sediments in transient settling. *J. Fluid Mechanics* **195**, 437-462.
- Bacchin P., Aimar P. and Sanchez V. (1996) Influence of surface interaction on transfer during colloid ultrafiltration. *J. Membrane Science* **115**, 49-63.
- Baird R.L. and Perry M.G. (1967) The distribution of porosity in filter cakes. *Filtration and Separation* **4**, 471-476.
- Bakker P.J., Heertjes P.M. and Hibou J.L. (1959) The influence of the initial filtration velocity and of vibration on the resistance of a polystyrene filter cake. *Chemical Engineering Science* **10**, 139-149.
- Banda S.M.H. and Forssberg K.S. (1988) Variation of filter cake permeability with mean pore diameter of the cake. *Scandinavian J. Metallurgy* **17**, 67-72.
- Belfort G., Davies R.H. and Zydney A.L. (1994) The behaviour of suspensions and macromolecular solutions in crossflow microfiltration, *J. Membrane Science* **96**, 1-58.
- Bierck B.R., Wells S.A. and Dick R.I. (1988) Compressible cake filtration: monitoring cake formation and shrinkage using synchrotron X-rays. *J. Water Pollution Control* **60**, 645-650.

- Bierck B.R. and Dick R.I. (1990) In situ examination of effects of the pressure differential on compressible cake filtration. *International Association on Water Pollution Research and Control*. Sludge Management Conference, Los Angeles.
- Bowen W.R. and Jenner F. (1995) Dynamic ultrafiltration model for charged colloidal dispersions: A Wigner-Seitz cell approach. *Chemical Engineering Science* **50**, 1707-1736.
- Burger R., Concha F. and Karlseu, K.H. (2001) Phenomenological model of filtration process: 1. cake formation and expression. *Chemical Engineering Science* **56**, 4537-4553.
- Buscall R. and White L.R. (1987) The consolidation of concentrated suspensions- the theory of sedimentation. *J. Chemical Society, Faraday Transactions* **1**, 873-891.
- Carman P.C. (1937) Fluid flow through granular beds. *Transactions Institution of Chemical Engineers* **15**, 150-166.
- Carman P.C. (1938) The determination of the specific surface of powders. *J. Society of Chemical Industry* **57**, 225-234.
- Chase G.G. and Willis M.S. (1992) Compressive cake filtration. *Chemical Engineering Science* **47**, 1373-1381.
- Christensen M.L. (2006) *The Effect of Filter Cake Viscoelasticity on Filtration- A study of activated sludge dewatering*. PhD Thesis, Aalborg University.
- Cohen R.D. and Probstein R.F. (1986) Colloidal fouling of reverse osmosis membranes. *J. Colloid and Interface Science* **114**, 194-207.
- Coulson J.M. (1949) The flow of fluids through granular beds: effect of particle shape and voids in streamline flow. *Transactions Institution of Chemical Engineers* **27**, 237-257.
- Derjaguin B.V. and Landau L. (1941) Theory of the stability of strongly charged lyophobic solutions and of the adhesion of strongly charged particles in solution of electrolytes. *Acta Physicochim* **14**, 663.

- Dias R., Teixeira J.A., Mota M. and Yelshin, A. (2004a) Particulate binary mixtures: dependence of packing porosity on particle size ratio. *Industrial and Engineering Chemistry Research* **43**, 7912-7919.
- Dias R., Teixeira J.A., Mota M. and Yelshin A. (2004b) Preparation of controlled particulate mixtures with glass beads of different sizes. *Separation and Purification Technology* **51**, 180-184.
- Dobson B. (1970) *Continuous Rotary Vacuum Filtration*. PhD Thesis, University of Sheffield.
- Erk A., Hardy E.H., Althaus T. and Stahl, W. (2006) Filtration of colloidal suspensions- MRI investigation and numerical simulation. *Chemical Engineering Technology* **29**, 828-831.
- Fair G.M. (1951) The hydraulics of rapid sand filters. *J. Institution of Water Engineers* **5**, 171-213.
- Fair G.M. and Hatch L.P. (1933) Fundamental factors governing the streamline flow of water through sand. *J. American Water Works Association* **25**, 1551-1565.
- Fathi-Najafi M. and Theliander H. (1995) Determination of local filtration properties at constant pressure. *Separation Technology* **5**, 165-178.
- Grace H.P. (1953) Resistance and compressibility of filter cakes. *Chemical Engineering Progress* **49**, 303-318.
- Grace H.P. (1956) Structure and performance of filter media. *American Institute of Chemical Engineers J.* **2**, 307-336.
- Gray W.A. (1968) *The Packing of Solid Particles*. Chapman and Hall, London.
- Hameed M.S. (1970) *General Studies on the Rotary Vacuum Filter*. PhD Thesis, Manchester University.
- Happel J. and Brenner H. (1965) *Low Reynolds Number Hydrodynamics*. Prentice-Hall, Englewood Cliffs, N.J.
- Harr M.E. (1977) *Mechanics of Particulate Media*. McGraw-Hill, New York.
- Harvey M.A., Bridger K. and Tiller F.M. (1988) Apparatus for studying incompressible and moderately compressible cake filtration. *Filtration and Separation* **23**(1), 28-36.

Haughey D.P. and Beveridge G.S.G. (1969) Structural properties of packed beds- a review. *Canadian J. Chemical Engineering* **47**, 130-140.

Heertjes P.M. (1964) Filtration. *Transactions Institution of Chemical Engineers* **42**, T266-T274.

Heertjes P.M. and Zuideveld P.L. (1978) Clarification of liquids using filter aids, Part III: Cake resistance in surface filtration. *Powder Technology* **19**, 45-64.

Hermia J. (1982) Constant pressure blocking filtration laws- application to power law non-Newtonian fluids. *Transactions Institution of Chemical Engineers* **60**, 183-187.

Hlavacek M. and Remy J.F. (1995) Simple relationships among zeta potential, particle size distribution and specific resistance for colloid suspensions coagulated with ferric chloride. *Separation Science and Technology* **30**, 549-563.

Holdich R.G. (1990) Solids concentration and pressure profiles during compressible cake filtration. *Chemical Engineering Communications* **91**, 255-268.

Hunter R.J. (2001) *Foundations of Colloid Science* (2nd Edn.) Oxford University Press, Oxford.

Kelsey G.D. (1965) The practical aspects of continuous rotary vacuum filters. *Transactions Institution of Chemical Engineers* **43**, 248-255.

Koenders M.A. and Wakeman R.J. (1997a) Filter cake formation from structured suspensions. *Transactions Institution of Chemical Engineers* **75**, 309-320.

Koenders M.A. and Wakeman R.J. (1997b) Initial deposition of interacting particles by filtration of dilute suspensions. *American Institute of Chemical Engineers J.* **43**, 946-958.

La Heij E.J., Kerkhof P.J.A.M., Kopinga K. and Pel, L. (1996) Determining porosity profiles during filtration and expression of sewage sludge by NMR imaging. *American Institute of Chemical Engineers J.* **42**, 953-959.

Landman K.A., Sirakoff C. and White L.R. (1991) Dewatering of flocculated suspensions by pressure filtration. *Physics of Fluids A* **3**, 1495-1509.

Landman K.A. and Russel W.B. (1993) Filtration in large pressures for strongly flocculated suspensions. *Physics of Fluids A* **5**, 550-560.

- Landman K.A. and White L.R. (1994) Solid/liquid separation of flocculated suspensions. *Advances in Colloid and Interface Science* **51**, 175-246.
- Landman K.A., White L.R. and Eberl M. (1995) Pressure filtration of flocculated suspensions. *American Institute of Chemical Engineers J.* **41**, 1687-1700.
- Leclerc D. (1975) Characteristics of unconsolidated filter media. In: *The Scientific Basis of Filtration*. Ives K.J. (Ed.) Nato Advanced Study Institute Series, Noordhoff-Leyden, Cambridge.
- McDonogh R.M., Fell C.J.D. and Fane A.G. (1984) Surface charges and permeability in the ultrafiltration of non-flocculating colloids. *J. Membrane Science* **21**, 285-294.
- McDonogh R.M., Welsch K., Fane A.G. and Fell C.J.D. (1992) Incorporation of the cake pressure profiles in the calculation of the effect of particle charge on the permeability of filter cakes obtained in the filtration of colloids and particulates. *J. Membrane Science* **72**, 197-204.
- McGeary R.K. (1961) Mechanical packing of spherical particles. *J. American Ceramic Society* **44**, 513-522.
- Meeten G.H. (2000) Septum and filtration properties of rigid and deformable particle suspensions. *Chemical Engineering Science* **55**, 1755-1767.
- Mota M., Teixeira J.A. and Yelshin A. (2001) Binary spherical particle mixed beds: porosity and permeability relationship measurement. *Filtration* **1**(4), 101-106.
- Murase T., Iritani E., Cho J.H. and Shirato M. (1989) Determination of filtration characteristics based upon filtration tests under step-up pressure conditions. *J. Chemical Engineering of Japan* **22**, 373-378.
- Olivier J., Vaxelaire J. and Vorobiev E. (2007) Modelling of cake filtration: an overview. *Separation Science and Technology* **42**, 1667-1700.
- Purchas D.B. (1996) *Handbook of Filter Media*. Elsevier, Oxford.
- Rietema K. (1953) Stabilizing effects in compressible filter cakes. *Chemical Engineering Science* **2**, 88-94.
- Rietema K. (1982) Science and technology of dispersed two-phase systems I and II. *Chemical Engineering Science* **37**, 1125-1150.

- Rushton A., (1973) Sedimentation effects in filtration. *Filtration and Separation* **10**, 267-272.
- Rushton A. (1976) Liquid-solid separation, recent research evaluated. *Filtration and Separation* **13**, 573-578.
- Rushton A., Hosseini M. and Hassan I. (1980) The effects of velocity and concentration on filter cake resistance. *J. Separation Process Technology* **1**, 35-41.
- Ruth B.F. (1946) Correlating filtration theory with industrial practice. *Industrial and Engineering Chemistry* **38**, 564-571.
- Sedin P., Johansson C. and Theliander H. (2003) On the measurement and evaluation of pressure and solidosity in filtration. *Chemical Engineering Research and Design* **81**, 1393-1405.
- Shirato M., Sambuichi M. and Okamura S. (1963) Filtration behaviour of a mixture of two slurries. *American Institute of Chemical Engineers J.* **9**, 599-605.
- Shirato M., Aragaki T., Ichimura K. and Ootsuti N. (1971) Porosity variation in filter cakes under constant pressure filtration. *J. Chemical Engineering Japan* **2**, 172-177.
- Shirato M. and Aragaki T. (1972) Verification of internal flow mechanism theory of cake filtration. *Filtration and Separation* **5**, 290-297.
- Shirato M., Aragaki T. and Iritani E. (1980) Analysis of constant pressure filtration of power-law non-Newtonian fluids. *J. Chemical Engineering Japan* **13**, 61-66.
- Smiles D. (1970) A theory of constant pressure filtration. *Chemical Engineering Science* **25**, 985-996.
- Sohn H.Y. and Moreland C. (1968) The effect of particle size distribution on packing density. *Canadian J. Chemical Engineering* **46**, 162-167.
- Sørensen P.B. (1992) *Unified Modelling of Filtration and Expression of Biological Sludge*. PhD Thesis, Aalborg University.
- Sørensen P.B., Christensen J.R. and Bruus J.H. (1995) Effect of small scale solids migration in filter cakes during filtration of waste water solids suspension. *Water Environmental Research* **67**, 25-32.

Spielman L.A. (1975) Flow through porous media and fluid-particle hydrodynamics, in *The Scientific Basis of Filtration*. Ives K.J. (Ed.) Nato Advanced Study Institute Series, Noordhoff-Leyden.

Stamatakis K. and Tien C. (1991) Cake formation and growth in cake filtration. *Chemical Engineering Science* **46**, 1917-1933.

Suzuki M. (2006) Packing properties, in *Powder Technology Handbook* (3rd Edn.). Masuda H., Higashitani K. and Yoshida, H. (Eds.) Taylor and Francis; Boca Raton, USA.

Tarleton E.S. and Hancock D.L. (1996) The imaging of filter cakes through electrical impedance tomography. *Filtration and Separation* **33**, 491-494.

Tarleton E.S. and Hancock D.L. (1997) Using mechatronics for the interpretation and modelling of the pressure filter cycle. *Chemical Engineering Research and Design* **75**, 298-308.

Tarleton E.S. and Willmer S.A. (1997) The effects of scale and process parameters in cake filtration. *Chemical Engineering Research and Design* **75**(A), 497-507.

Tarleton E.S. (1999a) The use of electrode probes in determinations of filter cake formation and batch filter scale-up. *Mineral Engineering* **12**, 1263-1274.

Tarleton E.S. (1999b) Using mechatronics technology to assess pressure filtration. *Powder Technology* **104**, 121-129.

Tarleton E.S. and Hadley R.C. (2003) The application of mechatronic principles in pressure filtration and its impact on filter simulation. *Filtration* **3**(1) 40-47.

Teoh S.K., Tan R.B.H. and Tien C. (2002) Correlation of C-P cell and filtration test data using a new test cell. *Separation and Purification Technology* **29**, 131-139.

Teoh S.K., Tan R.H.B. and Tien C. (2006) Analysis of cake filtration data- A critical assessment of conventional filtration theory. *American Institute of Chemical Engineers J.* **52**, 3427-3442.

Theliander H. and Fathi-Najafi M. (1996) Simulation of the build up of a filter cake. *Filtration and Separation* **33**, 417-420.

- Tien C. (1991) Penetration of fine particles within filter cakes in cake filtration. *J. Chinese Institute of Chemical Engineers* **22**, 385-391.
- Tien C., Teoh S.K. and Tan R.B.H. (2001) Cake filtration analysis- The effect of the relationship between the pore liquid pressure and the cake compressive stress. *Chemical Engineering Science* **56**, 5361-5369.
- Tiller F.M. (1953) The role of porosity in filtration I: numerical methods. *Chemical Engineering Progress* **49**, 467-479.
- Tiller F.M. and Green T.C. (1973) Role of porosity in filtration IX: skin effect with highly compressible materials. *American Institute of Chemical Engineers J.* **19**, 1266-1269.
- Tiller F.M. and Crump J.R. (1977) Solid-liquid separation: An overview. *Chemical Engineering Progress* **73**, 65-75.
- Tiller F.M., Crump J.R. and Ville F. (1979) Filtration theory in its historical perspective, a revised approach with surprises. *Proc. 2nd World Filtration Congress*, London, 1-13.
- Tiller F.M. and Leu W.F. (1980) Basic data fitting in filtration. *J. Chinese Institute of Chemical Engineers* **11**, 61-70.
- Tiller F.M. and Yeh C.S. (1987) The role of porosity in filtration. Part XI: Filtration followed by expression. *American Institute of Chemical Engineers J.* **33**, 1241-1255.
- Tiller F.M., Hsyung N.B. and Cong D.Z. (1995) The role of porosity in filtration: Part XII. Filtration with sedimentation. *American Institute of Chemical Engineers J.* **41**, 1153-1164.
- Tokumitsu Z. (1964) *J. Materials Science of Japan* **13**, 152.
- Tosun I. (1986) Formulation of cake filtration. *Chemical Engineering Science* **41**, 2563-2568.
- Tosun I., Willis M.S., Desai F. and Chase G.G. (1995) Analysis of drag and particulate stress in porous media flows. *Chemical Engineering Science* **50**, 1961-1969.

- Wakeman R.J. (1978) A numerical integration of the differential equations describing the formation of and flow in compressible filter cakes. *Transactions Institution of Chemical Engineers* **56**, 258-265.
- Wakeman R.J. (1979) On the use of compressibility coefficients to model cake filtration process. *Proc. 2nd World Filtration Congress*, London, 57-65.
- Wakeman R.J. (1981a) Thickening and filtration: a review and evaluation of recent research. *Transactions Institution of Chemical Engineers* **59**, 147-160.
- Wakeman R.J. (1981b) The formation and properties of apparently incompressible filter cakes under vacuum on downward facing surfaces. *Transactions Institution of Chemical Engineers* **59**, 260-270.
- Wakeman R.J. (1985) Filtration theory: formation and structure of compressible filter cakes, in *Mathematical Models and Design Methods in Solid-Liquid Separation*. A. Rushton. (Ed.) Martinus Nijhoff, Dordrecht.
- Wakeman R.J., Thuraisingham S.T. and Tarleton E.S. (1989) Colloid science in solid-liquid separation technology. Is it important? *Filtration and Separation* **26**, 277-283.
- Wakeman R.J., Sabri M.N. and Tarleton E.S. (1991) Factors affecting the formation and properties of wet compacts. *Powder Technology* **65**, 283-292.
- Wakeman R.J. (1996) Characteristics of filtration using solids added to the suspension as a body aid. *Proc. 7th World Filtration Congress* **1**, Budapest, 234-238.
- Wakeman R.J. and Tarleton E.S. (1999) *Filtration: Equipment Selection, Modelling and Process Simulation*. Elsevier, Oxford.
- Wakeman R.J. and Tarleton E.S. (2005) *Solid/Liquid Separation: Principles of Industrial Filtration*. Elsevier, Oxford.
- Wakeman R.J. (2007a) The influence of particle properties on filtration. *Separation and Purification Technology* **58**, 234-241.
- Wakeman R.J. (2007b) Separation technologies for sludge dewatering. *J. Hazardous Material* **144**, 614-619.

Willis M.S., Shen M. and Gray K.J. (1974) Investigations of the fundamental assumptions relating compression-permeability data with filtration. *Canadian J. Chemical Engineering* **52**, 331-337.

Willis M.S. and Tosun I. (1980) A rigorous cake filtration theory. *Chemical Engineering Science* **35**, 2427-2438.

Wu Y. (1994) An analysis of constant-pressure filtration. *Chemical Engineering Science* **49**, 831-836.

Yu A.B. and Standish N. (1988) An analytical-parametric theory of the random packing of particles. *Powder Technology* **55**, 171-186.

Yu A.B., Zou R.P. and Standish N. (1996) Modifying the linear packing model for predicting the porosity of non-spherical particle mixtures. *Industrial and Engineering Chemistry Research* **35**, 3730-374.

CHAPTER 3: EXPERIMENTAL MATERIALS AND METHODS

3.1. INTRODUCTION

This chapter covers the preparatory elements for the main experimental study (the results of which are presented and discussed in Chapters 4 to 6). The mechatronic filtration apparatus used for the constant pressure filtration experiments is described with the aid of relevant, labelled schematics. The operating procedure for the apparatus is outlined with reference to the schematics and the safety precautions to be taken are highlighted. The cleaning and calibration procedures are also shown. As discussed in more detail in Chapter 4, sedimentation data was obtained to help interpret the filtration results. The apparatus used for sedimentation experiments is shown in this chapter and the method for carrying out a sedimentation experiment discussed.

Calcium carbonate (calcite) suspensions were filtered to attain familiarity with the filtration apparatus and check its correct operation. Another important reason for the calcite filtrations (validation experiments) was to obtain and subsequently carry out checks on the filtrate flow data and hydraulic pressure profiles within the forming cake/suspension. The checks were in relation to trends and reproducibility, and were useful assurance that any trends and characteristics observed with the fibrous and binary suspensions were not just artefacts of the apparatus or operating procedure.

The final part of this chapter presents the work done on characterising the materials used for the filtration and sedimentation experiments discussed in Chapter 4. Titania (rutile) and tissue paper (predominantly cellulose fibres) were characterised in terms of their size, size distribution, shape and surface charge. The filter medium used was characterised in relation to its thickness, permeability and structure.

3.2. CONSTANT PRESSURE FILTRATION APPARATUS

3.2.1. Apparatus description

Figure 3.1 shows a photograph of the experimental apparatus, Figure 3.2 shows a schematic of the pressure filtration apparatus without the compressed air system and Figure 3.3 gives a schematic of the compressed air circuit. A stainless steel suspension feed vessel of 2 L capacity was connected to a stainless steel filter cell (Figure 3.2). Although both vessels were built to withstand 1000 kPa pressures, the maximum operating pressure was 600 kPa. The feed was manually fed into a funnel located above the feed vessel inlet; the flow into the feed vessel was controlled by a manual valve (V16). A stainless steel stirrer was employed in the feed vessel to keep the suspension well mixed and to help prevent particle settling. The stirrer, driven by a Parvalux motor, was operated by a switch on the main control box and rotated at a fixed speed of 330 rpm. Suspension flowed from the feed vessel to the filter cell through an automated ball valve (CV2) which was sequenced by means of a personal computer.



Figure 3.1: Photograph of the experimental apparatus.

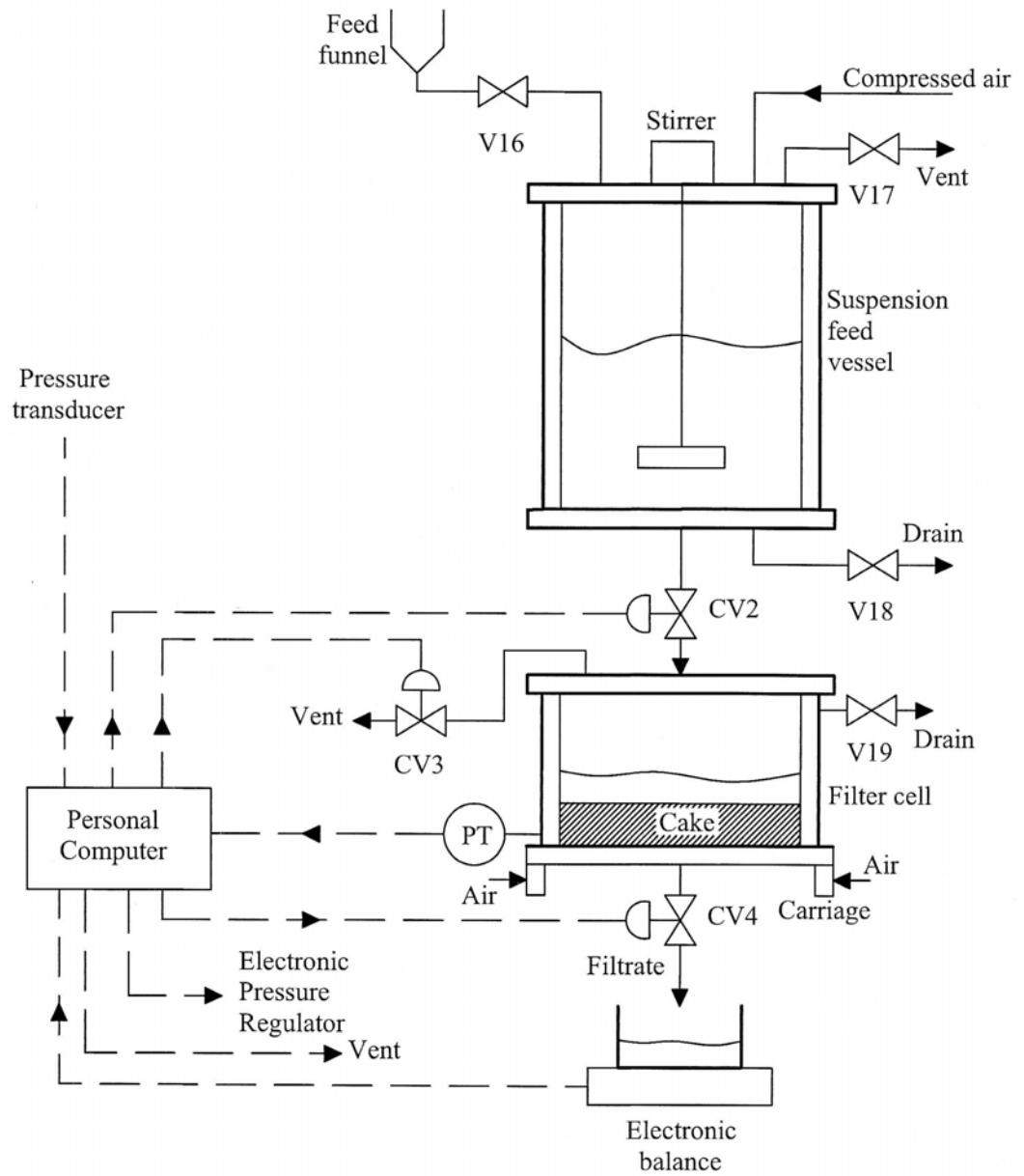


Figure 3.2: Schematic of pressure filtration apparatus without the compressed air circuitry.

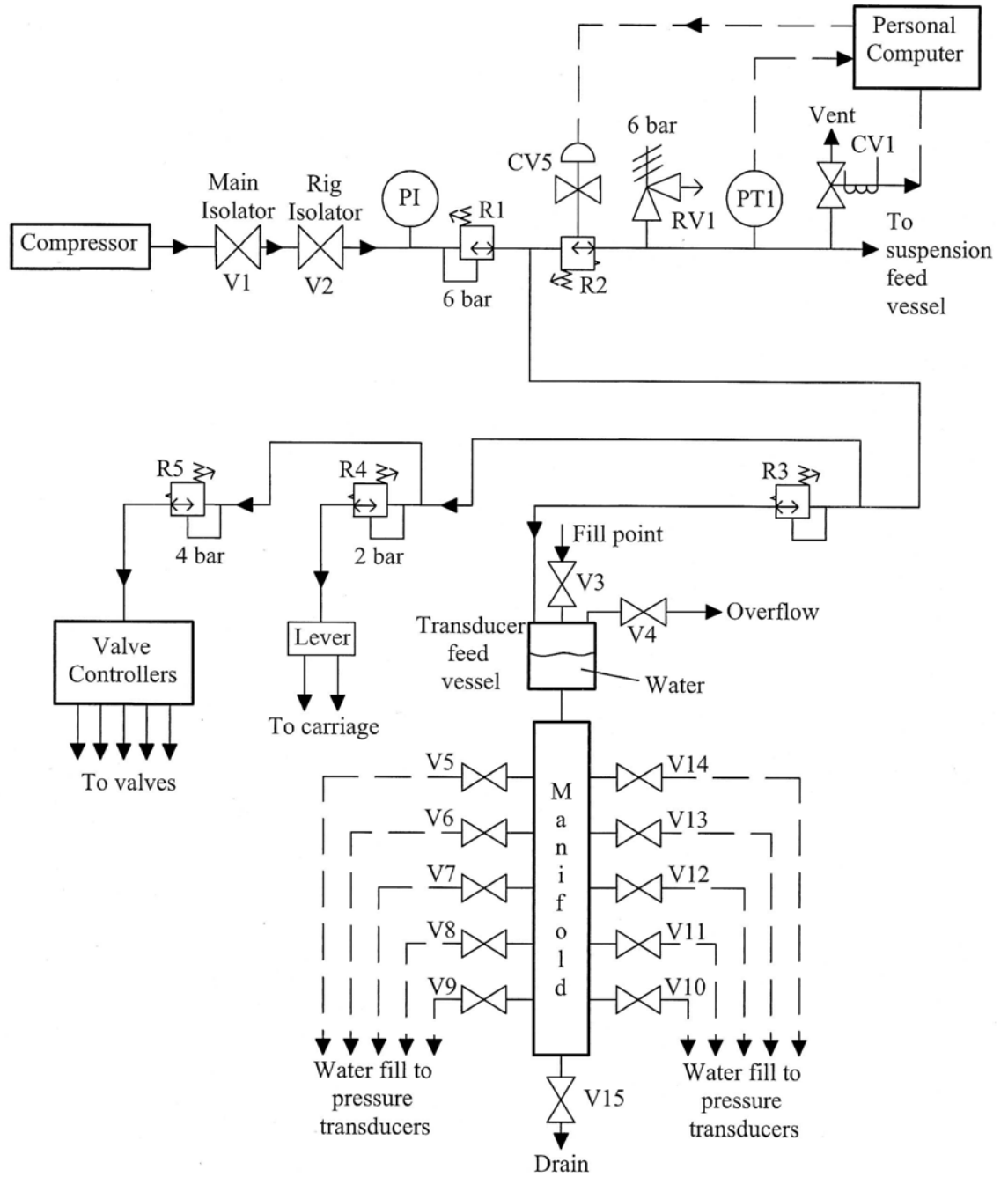


Figure 3.3: Schematic of the pressure filtration apparatus compressed air circuitry.

The filter cell base rested on a detachable platform whose position could be adjusted by means of a pneumatic system to enable cleaning, insertion and removal of the filter medium as well as filter cake removal. The air pressure controlling the platform height was maintained at 200 kPa by means of a Norgren manual pressure regulator (R4) which prevented the carriage from rising or falling too quickly. The filter medium (120 cm² area) rested upon a sintered support, which in turn rested on a star shaped support to maintain the sinter's shape on a sloping filter cell base. The filter cell base was sloped to angle the filtrate flow directly to an electronic balance with minimal hold up. Both the feed vessel and filter cell had tubing attached for drainage and venting. The drainage and venting for the suspension feed vessel were manually controlled by the drain valve V18 and the vent valve V17. For the filter cell, draining was manually controlled by the drain valve V19 and the venting was automatically controlled by ball valve CV3. All the drain valves in the apparatus were connected to the same outlet and closed during feeding and filtration.

The personal computer attached to the filter and ancillaries utilised a QuickBasic computer program to control the automated pneumatic ball valves via solenoid valves situated in the main control box. The program enabled the user to control the valve sequencing and also to carry out experiments at constant flow, constant pressure and stepped pressure. The user specifies the parameters for each experiment. Although this apparatus allows for experimentation under constant pressure, constant flow and variable pressure/flow conditions, this thesis features only constant pressure filtrations. For a constant pressure filtration experiment, the sample time (time between each data sample) and the filtration pressure are specified.

The filtration pressure was pneumatically generated and transmitted to the personal computer by a pressure transducer (PT1); the personal computer sent a signal to the electronic pressure regulator (CV5) which set the desired filtration pressure (Figure 3.3). A Norgren pressure relief valve (RV1) prevented the filter cell and suspension vessel from experiencing pressures higher than 600 kPa. The filtrate was collected and weighed by an Ohaus electronic balance which sent its readings to the personal computer. The balance was capable of weighing up to 4000 g accurate to 2 decimal places and could take up to 10 readings per second. Values of filtration

pressure, filtrate volume, hydraulic pressure and time were saved at set intervals on the personal computer for further analysis.

In an attempt to determine the transient liquid pressure variations within the filter cake, titanium micro-pressure transducers were fixed in a spiral arrangement around the circumference of the wall of the filter cell. These transducers sent electrical signals to the personal computer, enabling liquid pressure profiles to be measured, which in turn allowed further analysis of cake characteristics and filtration behaviour. The transducers were attached to custom made stainless steel holders and micro-bore tubes (0.5 mm I.D.). As illustrated in Figure 3.4, the ten transducers ranged from 0.5 mm to 15.3 mm in height above the filter medium (0.5, 0.8, 1.0, 1.3, 1.8, 2.3, 3.3, 5.3, 9.3 and 15.3 mm) and protruded ~2 mm into the cell. A liquid bridge was created between the cake and the tip of a transducer by injecting deionised water from a separate reservoir into each holder. This water was delivered through nylon piping from the transducer feed vessel reservoir and valves V5-V14. The transducer feed vessel was filled with deionised water through its filling point with the flow being controlled by valve V3.

3.2.2. Typical operating procedure

Prior to using the rig, all electrical equipment was safety tested and a COSHH form completed. Appropriate personal protective equipment (PPE) such as a lab coat and safety glasses were worn throughout experimentation and the laboratory environment was maintained in a clean and tidy state. A typical experiment utilised the following procedure:

- With preliminary safety preconditions satisfied, the compressor was switched on to allow the build up of air pressure. Meanwhile the computer was booted up and the software opened, and a new results file created and named for data storage. The required inputs such as the filtration pressure and sample times were specified. The drain valves were closed and an empty beaker was placed under the drain outlet.

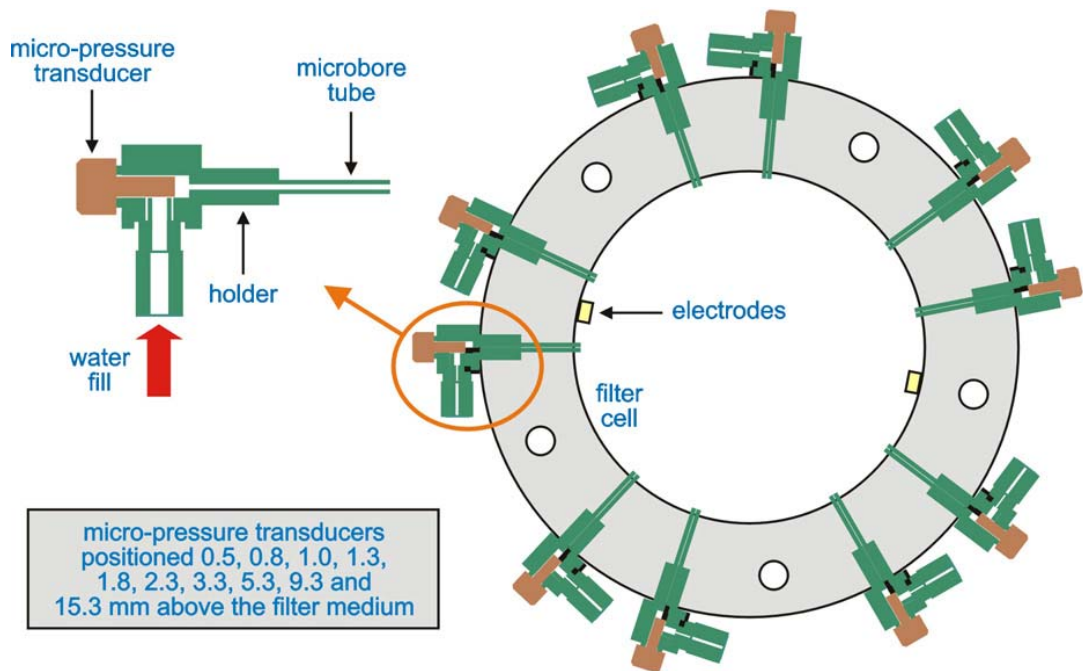


Figure 3.4: Micro-pressure transducer arrangement of the mechatronic pressure filtration apparatus (Tarleton, 2008)

- The manual pressure regulator, R1, was set to 600 kPa. Once the compressor had built up sufficient air pressure (approximately 5 minutes after the compressor was switched on), the airline valve V2 was opened. The transducer feed vessel was then filled with deionised water through its fill point. Valves V5–V14 were subsequently opened and closed to allow sufficient liquid to flow between the tip of each transducer and the end of the corresponding microbore tube; a jet of water from the tube tip indicated that the required liquid bridge was in place.
- Next the filter cell base was placed correctly upon its carriage; a spirit level was periodically used to ensure that the surface was horizontal. The star shaped sintered support for the sinter plate was fitted into the base, followed by the sinter plate and the chosen filter medium. The filter cell base was carefully raised (pneumatically) via a lever and fastened to the filter cell and the securing nuts tightened to the required torque with a torque wrench. The Ohaus balance was placed beneath the filter cell with a container placed upon the pan in order to collect the filtrate.

- A known volume of suspension was made up in a beaker to the required solids composition and solution environment (see Section 3.5.4 for more detail); the constituents were carefully weighed. A suspension was made immediately prior to its introduction into the suspension feed vessel (and subsequently the filter cell) to prevent alterations of its characteristics due to ageing. Care was taken to ensure that the suspension was well mixed, with the solids homogeneously distributed throughout the suspension. With the aid of a ladder, the vent valve (V17) and the suspension inlet valve (V16) on the feed vessel were opened, and the suspension gradually poured into the feed funnel. With all the suspension poured (and the stirrer on), both the vent and inlet valves (V17 and V16) were closed. The experiment was then started via the personal computer which sequenced the appropriate valves and recorded all relevant filtration data.
- Once the experiment was complete and the data recorded and saved, the filtration pressure was automatically relieved. The stirrer was stopped after draining the feed vessel of remaining suspension. The electronic balance and container were removed from beneath the filter cell. The carriage was raised via the lever to support the base of the filter cell which was then unfastened from the filter cell and carefully lowered. Any excess slurry on top of the cake was removed using a pipette and the height of the cake recorded before as much of the cake as possible was separated from the filter medium and weighed. This cake was then placed in an oven and allowed to dry overnight at a moderate temperature of $\sim 60^{\circ}\text{C}$ after which the cake was re-weighed and the ratio of wet cake to dry cake determined.
- Following an experiment the suspension feed vessel, filter cell, base and sinter were cleaned with distilled water and a brush, and then wiped clean. The manual pressure regulator, R1, was set to 0 kPa and the air to the rig isolated using V2. The compressor was switched off and the drain valves (V4, V17, V18 and V19) opened. The main power to the apparatus and personal computer were turned off as necessary.
- In the event of an emergency during an experiment, the emergency stop button (red button on the control box) was pressed, shutting off all electrical power to the rig.

The air pressure was subsequently isolated using V2 and the manual vent and drain valves (V4, V17, V18 and V19) opened.

3.2.3. Cleaning and calibration

Before the commencement of experiments, the apparatus was dismantled and cleaned with deionised water and a clean brush. After thorough cleaning, the apparatus was flushed with deionised water by allowing water to permeate through the sinter plate; this process was repeated several times. Any blockages in the micro-pressure transducers were unclogged by means of a suitable fine wire.

The main (upstream) pressure transducer (PT1 in Figure 3.3) was calibrated by recording the transducer voltage output at various known applied pressures. The voltage outputs, given in terms of analogue-digital (AD) readings, were then plotted against the applied pressures. As seen in Figure 3.5, the relationship between the AD readings and the applied pressures was linear. The calculated gradient and intercept were subsequently inserted into the computer program used to drive the rig. The micro-pressure transducers within the filter cell were similarly calibrated, but in this case, the filter cell base was filled with water prior to calibration. The micro-pressure transducer voltage outputs were plotted against the applied pressures (the relationship between them was again linear), and calculated gradients and intercepts were again inserted into the computer program. Typical micro-pressure transducer calibration curves are shown in Figure 3.6. Although it was necessary to calibrate the main pressure transducer once, the micro-pressure transducers were recalibrated every few experiments because of potential blockages in the micro-bore tubes.

3.3. SEDIMENTATION APPARATUS AND METHODS

For a sedimentation experiment, a well mixed suspension (990 ± 10 ml) was poured into a plastic 1 litre graduated measuring cylinder (of 360 mm length and 59.5 mm inner diameter). The suspension-supernatant interface height and corresponding elapsed time were recorded at suitable intervals. The corresponding time was measured

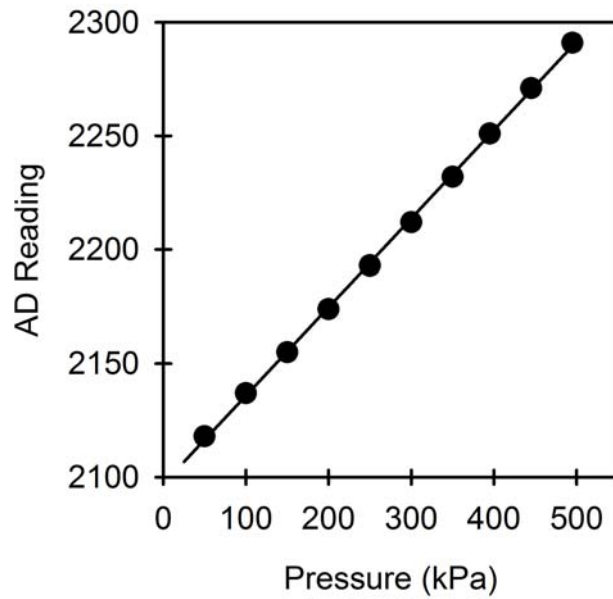


Figure 3.5: The main (upstream) pressure transducer (PT1 in Figure 2.3) calibration. The gradient and intercept were inserted into the computer program.

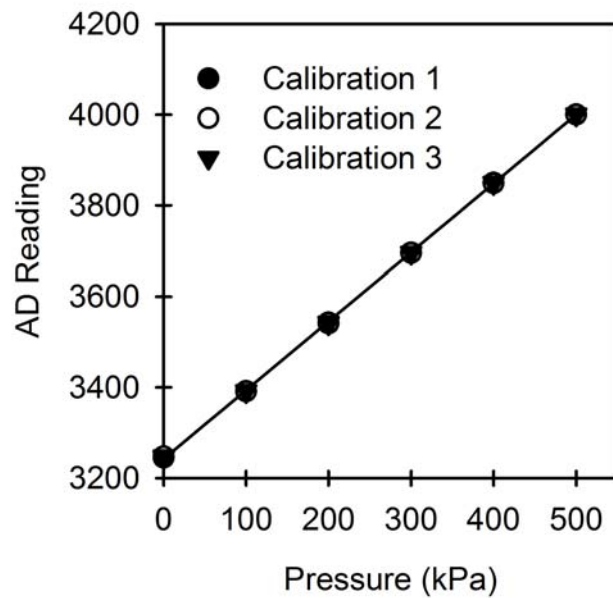


Figure 3.6: Example of typical micro-pressure transducer (the transducer closest to the medium is used here as an example) calibration. The gradient and intercept were inserted into the computer program.

using a stopwatch. Initial settling rate was determined from a graph of suspension-supernatant interface height vs. time, where the initial points fall on a straight line whose gradient can be calculated. Another parameter of interest was the proportion of sludge, which was taken as the final sediment height (after 24 h settling) expressed as a percentage of the initial suspension height. Figure 3.7 shows a photograph of completed sedimentation experiments. After a sedimentation experiment, the measuring cylinder was emptied and then washed thoroughly with deionised water and a brush.



Figure 3.7: Photograph of suspensions settled in their measuring cylinders.

3.4. VALIDATION FILTRATION EXPERIMENTS

Constant pressure validation filtration experiments were carried out with calcium carbonate (calcite) suspensions as these filtrations are relatively well studied. The 10% w/w calcite suspensions were prepared by stirring 100 g calcite in 900 g deionised water at approximately 700 rpm for an hour prior to filtration. Approximately 700 g of suspension was used for each filtration.

A typical plot of cumulative volume of filtrate vs. filtration time for filtrations at 300 kPa is shown in Figure 3.8; the error bars are based on three repeat experiments.

Relative to the filtrate flow data, the hydraulic pressure profiles within the forming filter cake generally had lower, but still acceptable, reproducibility. As an example, Figure 3.9 illustrates the hydraulic pressure history as recorded by the micro-pressure transducer 0.5 mm above the filter medium (closest to the septum) during three repeat filtrations. An example of the hydraulic pressure profile within the growing filter cake is illustrated in Figures 3.10 and 3.11. Figure 3.10 shows the hydraulic pressure history during a 300 kPa filtration at various depths within the forming cake/suspension and Figure 3.11 shows the corresponding hydraulic pressure profile at various times. At the start of filtration ($t = 0$ s) the calcite suspension was in its original homogeneously mixed state. At $t = 0$ s the particles in suspension were sufficiently far apart to carry zero compressive solids pressure and the liquid pressure was equal to the filtration pressure. Once the solids phase became sufficiently concentrated (i.e. 'a cake formed'), the liquid pressure typically began to fall. The cake thickness increased as time progressed in the filtration, causing reductions in liquid pressure at heights further away from the medium surface (Figures 3.10 and 3.11). Simultaneously, regions of cake closest to the medium became more compact due to the drag imparted by the continual flow of liquid through the cake interstices as well as the increasing weight of particles above those already constituting the cake. As a direct result of this compaction, the liquid pressure at any given height tended to decrease with time and the lowest measured liquid pressures were at the two transducers closest to the medium (0.5 and 0.7 mm from the medium surface).

From Figure 3.10, an unusual pattern is seen at a height of 3.3 mm above the medium where the liquid pressure appears to persistently rise abruptly back to the filtration pressure following steep decreases. In repeat experiments, a similar pattern was shown by between one and three transducers at heights between 1.8 and 5.3 mm above the medium. This behaviour may be due to a thickening/settling moving interface, particles intermittently blocking the transducers, or a combination of both. The general pressure profile trends within the forming cakes obtained from repeat experiments were similar. The transducers of greatest interest are the ones closest to the filter medium (0.5, 0.7 and 1.0 mm from the medium), and these transducers all showed similar and consistent trends.

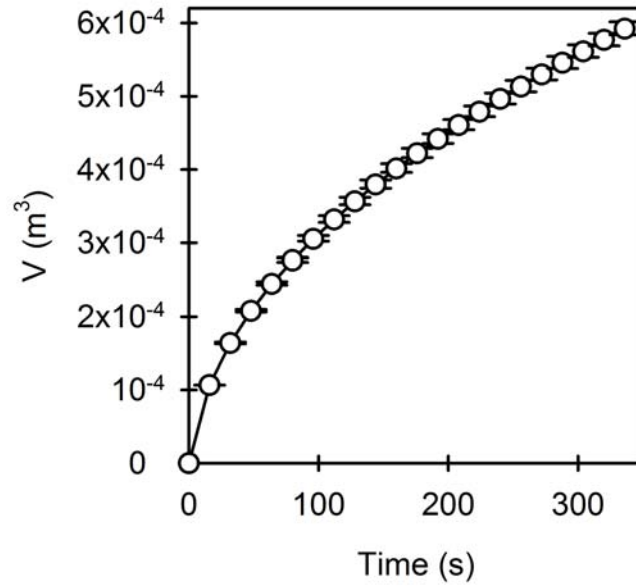


Figure 3.8: Plot of cumulative volume of filtrate vs. time for filtrations of 10% w/w calcite suspensions at a constant pressure of 300 kPa. The error bars are based on three repeat filtrations.

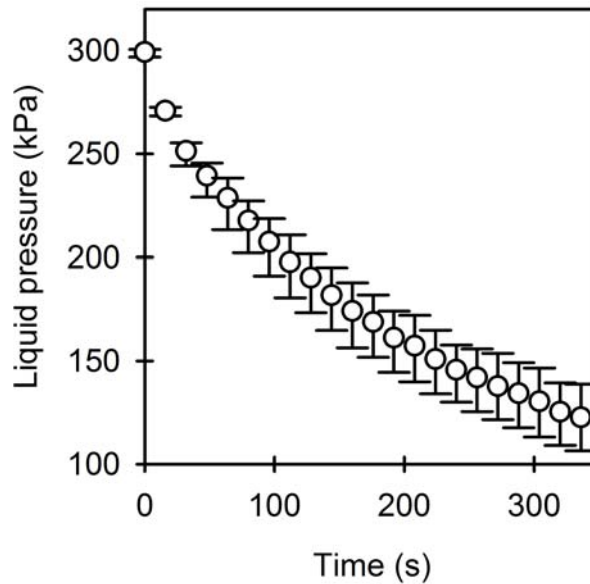


Figure 3.9: Liquid pressure history 0.5 mm above the filter medium as obtained from three repeat 300 kPa filtrations of 10% w/w calcite suspensions.

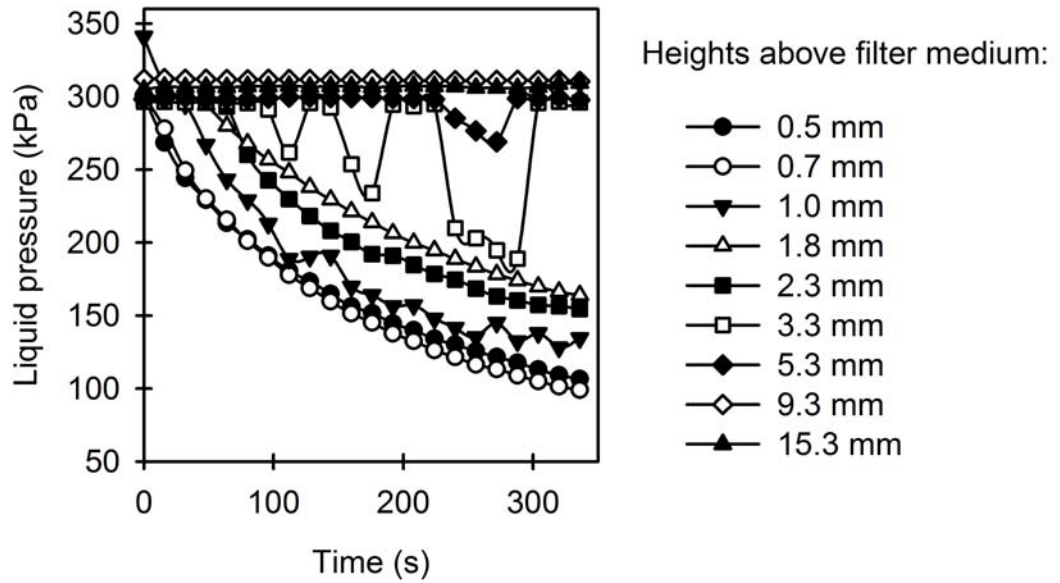


Figure 3.10: Hydraulic pressure history in a forming calcite cake/suspension at a constant filtration pressure of 300 kPa.

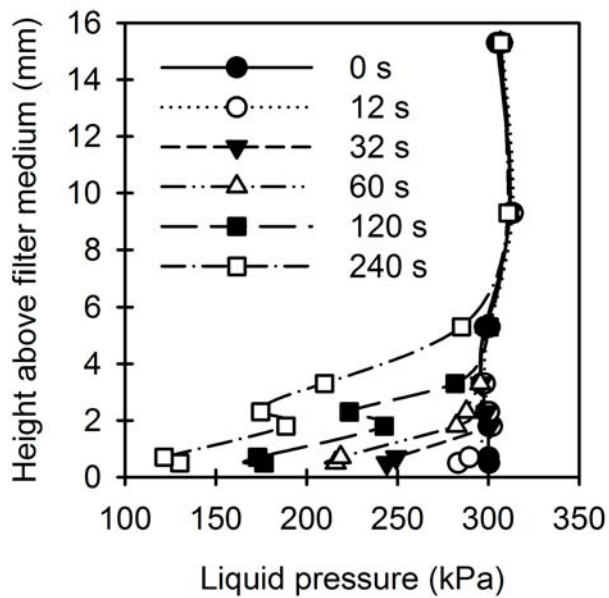


Figure 3.11: Hydraulic pressure profiles through the filter cake at various times during the 300 kPa filtration of a 20% w/w calcite suspension.

In general, the expected trends were observed. The filtrate flow data was reproducible. It was noted that the micro-pressure transducers can be prone to some fluctuations and/or blockages, resulting in a slightly more, but still generally acceptable, variation in liquid pressure profiles.

3.5. MATERIALS AND METHODS

After acknowledging the fact that an accurate determination of solids properties would greatly enhance the state of knowledge or fundamental understanding of solid/liquid separation theory, Beddow (1986) described particle characterisation as being the term generally used to indicate a measured property or properties of the solids. Wakeman (2007) claimed that three parameter types may be identified to fully describe a solid/liquid system: the primary properties, the state of the system and the macroscopic properties. The primary properties are those which can be measured independently of the other components of the system, and are the solid and liquid physical properties such as the size, size distribution and shape of the particles, and the surface properties of the particles in their solution environment. The description of the state of a system includes parameters such as concentration and extent of dispersion of the solid phase. This description combines with the primary properties to control the macroscopic properties that are measured to investigate a particular separation method. Such measurements may include the bulk settling rate of solids in a suspension and the specific resistance of a filter cake. When considering a particular solid/liquid separation, the filter medium is that critical component which can be defined as any permeable material upon or within which particles are deposited by the process of filtration (Purchas, 1996). Consequently, the relevant filter medium properties are generally also of interest.

3.5.1. Titania (rutile) characterisation

Titania is commonly found in two crystal forms, rutile and anatase. Rutile is the polymorph used in this work and is also the most common. The rutile (RSM-2) used in

this work was obtained from Tioxide Plc. (now Huntsman) and Figure 3.12 shows a typical Scanning Electron Micrograph image. The tendency of primary particles to form clusters is noted. Rutile particle size distributions in deionised water were measured using a Malvern Zetasizer 3000 HS, and a Malvern Mastersizer was used for rutile particle size distributions in 0.2 M NaCl and 0.1 M CaCl₂ solutions. The Zetasizer employs photon correlation spectroscopy using a single detector at a 90° angle with the collimated laser light scattered by each particle to produce a diffraction pattern which is subsequently analysed by a computer algorithm.

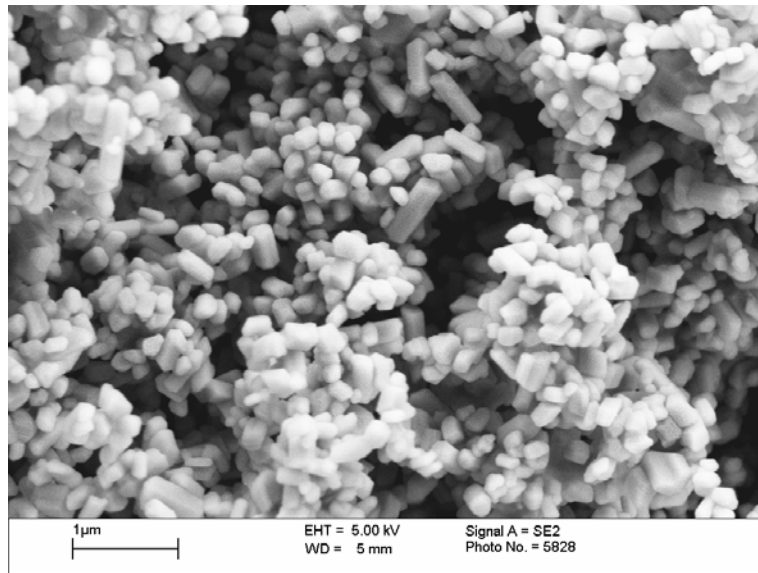


Figure 3.12: Scanning Electron Micrograph image of the rutile used.

Electrophoretic mobility (particle velocity/electric field strength) measurements of rutile were also made at various pH values using the Malvern Zetasizer 3000 HS. pH values were decreased by dropwise addition of a 0.1 M HCl solution and increased by dropwise addition of a 0.1 M NaOH solution. According to Henry's formula (Hunter, 2001):

$$U_E = \left(\frac{2\varepsilon\zeta}{3\eta} \right) f(\kappa a) \quad (3.1)$$

where ζ is the zeta (ζ) potential, U_E the electrophoretic mobility, η the viscosity, ε the dielectric constant, and $f(\kappa a)$ is a monotonically varying function which increases from 1.0 at $\kappa a = 0$ to 1.5 at $\kappa a = \infty$. κ has the dimensions of $(L)^{-1}$ and is called the Debye-Huckel parameter. The reciprocal of the Debye-Huckel parameter is taken as the thickness of the electrical double layer. The parameter a refers to the radius of the particle and therefore κa measures the ratio of the particle radius to the electrical double layer thickness. In the context of this work, where relatively large particles are used in aqueous media, this ratio can be taken to approach ∞ , because the double layer thickness is negligible compared to the particle size. When dealing with particles of this size range, the force on the particle is almost solely due to the electrophoretic retardation whereby the ions in the double layer drag the fluid with them and the particle moves in the opposite direction (Hunter, 2001). Therefore, the Smoluchowski limit was used to convert the mobility measurements to ζ -potential values, taking $f(\kappa a)$ as 1.5 which results in:

$$\zeta = \frac{U_E \eta}{\varepsilon} \quad (3.2)$$

Figure 3.13 shows the cumulative size distribution for rutile in deionised water. It is well known that complexities arise in particle size analysis due to several factors such as aggregate formation (states of dispersion), particle geometry (deviations from sphericity), and measuring techniques/measurement device algorithm. However, the median particle size of approximately 0.45 μm (as obtained from the Zetasizer) is considered to be a reasonable representation. This value also corresponds with the Scanning Electron Micrograph images taken (Figure 3.12 for example) and with the measurements of previous researchers studying the filtration characteristics of rutile (Mikulášek *et al.*, 1998; Iritani *et al.*, 2002; Tarleton *et al.*, 2003). It is also noted from Figure 3.12 that rutile is not exactly spherical but rather elliptical and slightly elongated with an aspect ratio of 2-4.

Figure 3.14 shows the variation of rutile ζ -potential with pH. It is common for particles in aqueous media to exhibit a negative charge due to cations being more readily hydrated than anions (Shaw, 1992). The hydrated cation generally has a greater

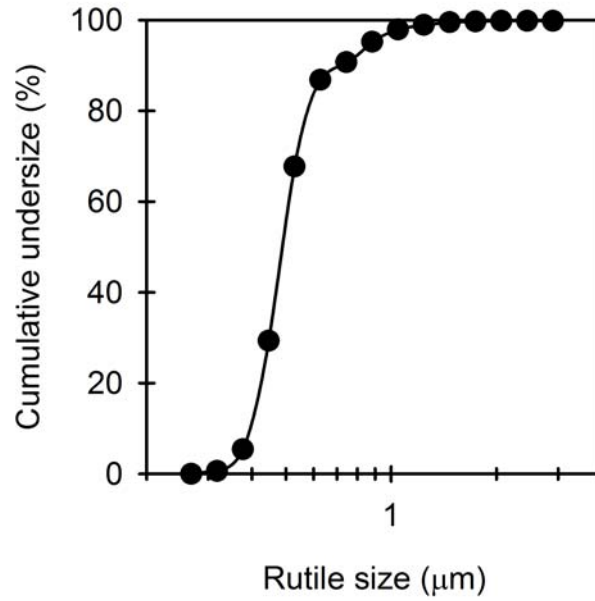


Figure 3.13: Rutile cumulative size distribution as measured using the Zetasizer. A median size of $\sim 0.45 \mu\text{m}$ was obtained.

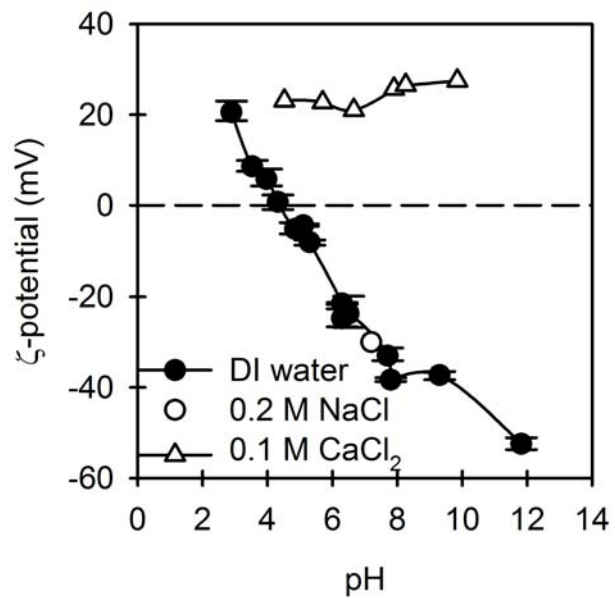


Figure 3.14: Zeta potential values of rutile in deionised (DI) water as well as 0.2 M NaCl and 0.1 M CaCl₂ solutions. Error bars shown are based on three repeat measurements.

tendency to remain in the aqueous medium whereas the less hydrated and more polarising anions are more likely to be specifically adsorbed at the particle-fluid interface. When a surface has become negatively charged it preferentially attracts positive charges and so a charge reversal can result. The point at which charge reversal takes place (ζ -potential = 0) is commonly known as the isoelectric point and at this point there is generally minimal long range repulsions between primary particles and hence a greater tendency for aggregate formation. It is seen that the isoelectric point of rutile in deionised water is at a pH of approximately 4.3; similar results for rutile suspensions have been shown in previous works (Marchant, 1999; Mikulášek *et al.*, 1998). Ca^{2+} ions appear to adsorb onto rutile surfaces, leading to charge reversal. In the presence of 0.1 M CaCl_2 solution, rutile surface charge appears to be almost invariant with pH over the range tested. Na^+ ions appear to be an indifferent electrolyte, not significantly altering rutile surface charge. The natural pH of rutile suspensions were 8.4 in deionised water, 7.5 in 0.2 M NaCl solution, and 6.9 in 0.1 M CaCl_2 solution. Over this experimental pH range of interest, the ζ -potential values for rutile were approximately -35 mV in deionised water, -30 mV in 0.2 M NaCl solution, and +21 mV in 0.1 M CaCl_2 solution.

Figure 3.15 illustrates the size distributions of rutile in deionised water as well as in 0.2 M NaCl and 0.1 M CaCl_2 solutions. It is seen that the addition of NaCl and CaCl_2 resulted in a wider distribution and larger size; the median size of rutile particles in 0.2 M NaCl and 0.1 M CaCl_2 solutions were approximately 4.2 and 15 μm respectively. These values do not refer to rutile's primary particle size but instead are indications of the degrees of aggregation that occur in the NaCl and CaCl_2 solution environments. The aggregation is attributed to suppression of the rutile electrical double layer. It can be seen that the extent of aggregation is greater in 0.1 M CaCl_2 and this could be due to: (1) Ca^{2+} ions physically adsorbing onto the solids surfaces whereas Na^+ ions behaved as an indifferent electrolyte, and/or (2) the 0.1 M CaCl_2 solution being of a greater ionic strength than the 0.2 M NaCl solution. The ionic strength (I) of 0.2 M NaCl and 0.1 M CaCl_2 solutions were 0.2 and 0.6 respectively, as calculated using the Debye-Hückel theory (Atkins, 1998):

$$I = \frac{1}{2} \sum_j z_j^2 b_j \quad (3.3)$$

where z_j is the charge number of an ion j and b_j its concentration. Aggregate breakage (and possibly re-agglomeration) may perhaps occur during a filtration, making the rutile effective size in these solution environments a dynamic parameter.

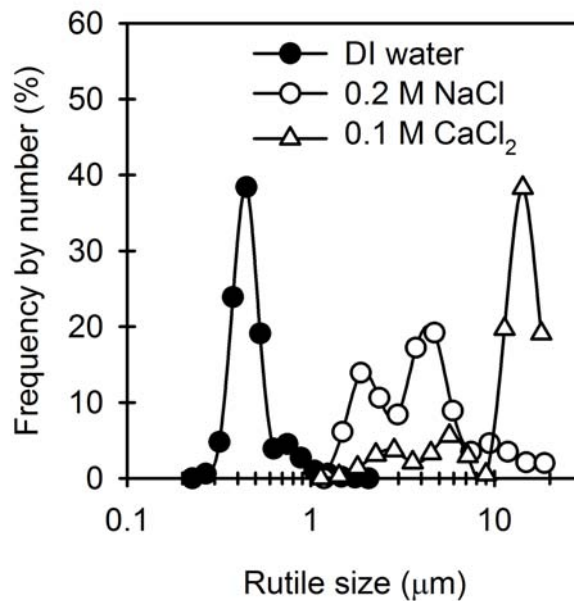


Figure 3.15: Size distributions of rutile in deionised (DI) water, 0.2 M NaCl and 0.1 M CaCl₂ solutions.

3.5.2. Tissue paper (fibre) characterisation

The fibres used were in the form of tissue paper (Merton Cleaning Supplies (Leicester) Ltd). When the tissue paper was dispersed into deionised water two types of suspended solids were produced, cellulose fibres and the fillers associated with the tissue. Such suspensions are notoriously difficult to characterise. The true density of the tissue paper (including the fillers) was 1300 kg m^{-3} , as measured using a pycnometer. Figure 3.16 shows a Scanning Electron Micrograph (SEM) image of a section of tissue paper.

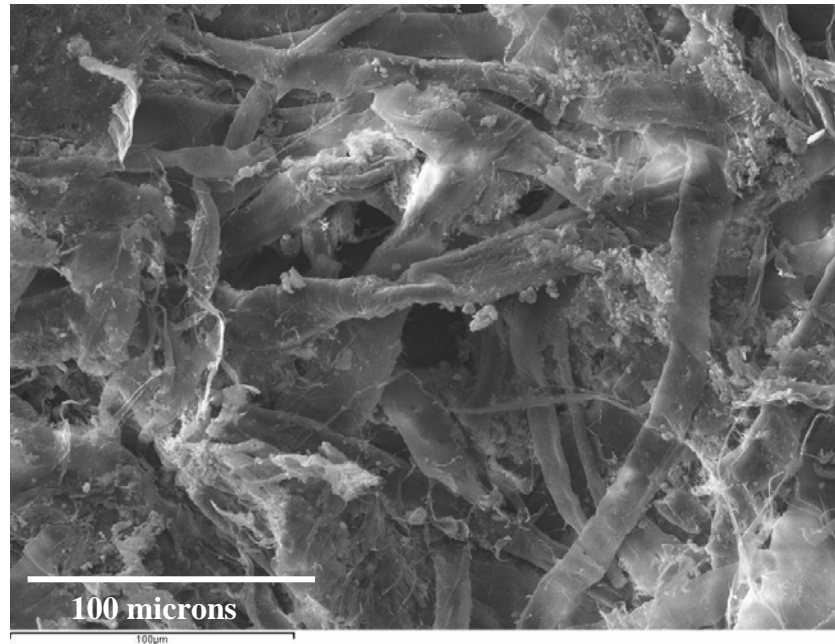


Figure 3.16: Scanning Electron Micrograph image of the tissue paper used.

Energy dispersive X-ray spectroscopy (EDX) was used to determine the type of fillers in the tissue paper (see Figure 3.17). The carbon and oxygen peaks (the carbon peak overlaps with calcium peaks) are due to the presence of cellulose fibres. Cellulose fibres (organic compounds with the chemical formula $(C_6H_{10}O_5)_n$) are polysaccharides consisting of a linear chain of several hundred to over ten thousand linked glucose units (Crawford, 1981). It may be inferred from the calcium, carbon and oxygen peaks in Figure 3.17 that the main filler used in the tissue paper is calcium carbonate ($CaCO_3$). The presence of $CaCO_3$ was also confirmed by placing the cursor over the individual filler particles on the monitor interfaced with the EDX instrument. Calcite is the most stable polymorph of $CaCO_3$ and is a common filler in many paper making industries. The presence of the gold peak is due to the gold coating of the sample prior to analysis and the presence of the other peaks are most likely due to the impurities in the water used by the paper making process.

Wakeman (2007) explained that if the solid properties could be specified for a filtration, the target properties would be for the solids to have as large a size as possible,

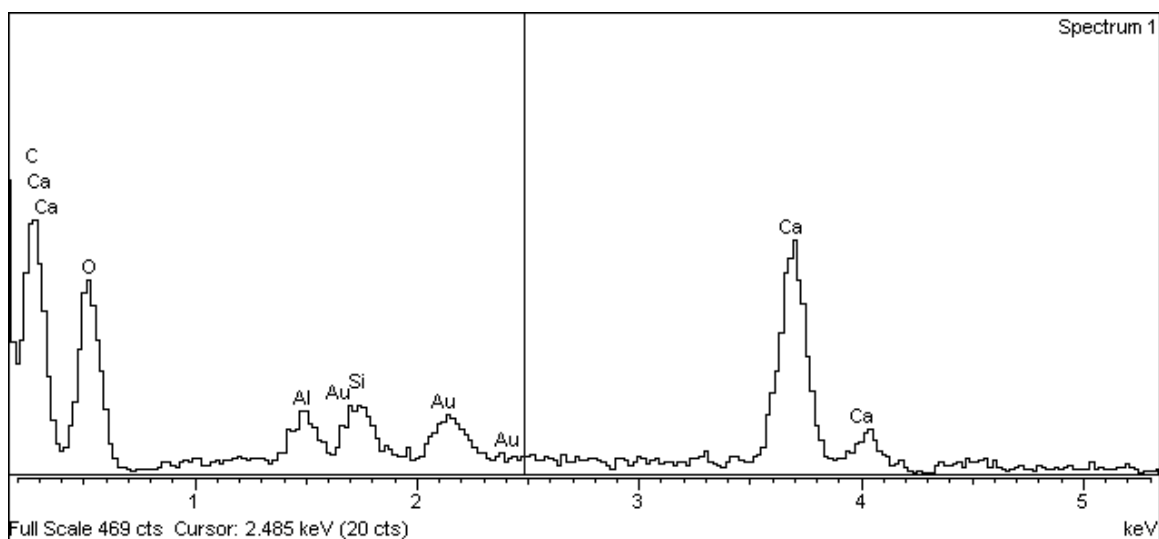


Figure 3.17: EDX plot (frequency against energy levels) of a sample of tissue paper.

be as near to spherical as possible, and have a monosize distribution. However, in Figure 3.16, the highly irregular nature of the fibre shapes and sizes are illustrated. The fibres are seen to be non-cylindrical and upon closer inspection appear to have angular edges. Due to the high aspect ratio and non-uniform shape of the fibres, neither light scattering nor photon correlation spectroscopy could be used for reliable fibre size distribution measurements. The size (width) distributions of the fibres were therefore obtained by measuring more than a hundred fibres at various magnifications of SEM image. Care was taken to ensure each fibre was only measured once. SEM images of different, strategically selected magnifications were used to avoid partiality in the measurements and measurement artifacts due to the choice of scale. The large numbers of fibres carefully measured at the selected magnifications approximately ensure that a representative distribution was obtained. The fibres were generally non-cylindrical with aspect ratios more than 10, and more likely in the region of 100. Although determinations were difficult, estimates were obtained by examining images of individual fibres ‘rubbed-off’ from samples of the tissue paper.

The median and mean diameters are a measure of the central tendency of the distribution, and the standard deviation is a measure of the spread of the data. The

median fibre diameter (x_{50}) is seen to be approximately 15 μm (Figure 3.18), the mean fibre diameter is 17.1 μm and the standard deviation is 10.8 μm .

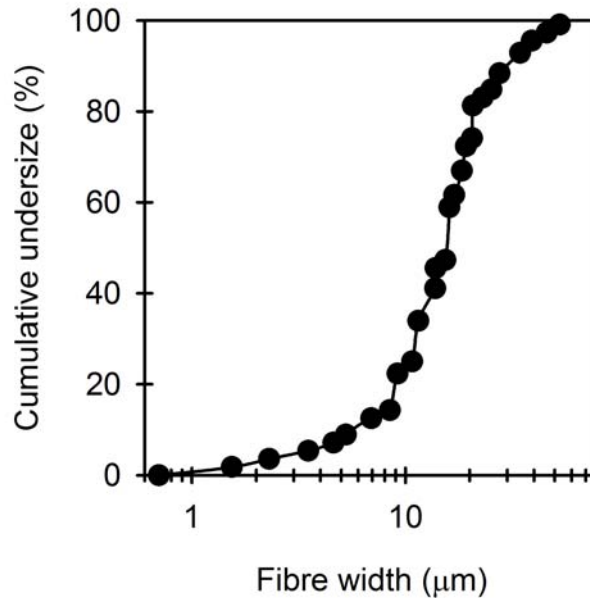


Figure 3.18: Cumulative size (width) distributions of the fibres in the tissue paper, as obtained by measuring more than one hundred fibres from SEM images at various magnifications.

The formulae used to calculate the mean diameter, \bar{x} , and the standard deviation, σ , are given in equations (3.4) and (3.5), respectively:

$$\bar{x} = \frac{\sum n_i x_i}{\sum n_i} = \sum f_i x_i \quad (3.4)$$

$$\sigma = \left[\frac{\sum n_i (x_i - \bar{x})^2}{\sum n_i} \right]^{\frac{1}{2}} = \left[\sum f_i (x_i - \bar{x})^2 \right]^{\frac{1}{2}} \quad (3.5)$$

where x_i is the midpoint of a size class range, n_i the number of fibres with diameters in that class range and f_i the fraction of total fibres with diameters in that class range. The

standard deviation of 10.8 μm is quite large (much wider distribution than rutile) but this is not surprising as fibre diameters as small as 0.8 μm and as large as 69 μm were observed.

The CaCO_3 fillers were removed by acid treatment for the purpose of characterisation. Torn pieces of toilet paper were dried (to remove moisture) and subsequently weighed. 5 g of dry paper were sheared in a weak acid (HCl) solution (500 g) of pH 2.5 at a relatively high rotational stirrer speed of 900 rpm for 3 hours. In order to further enhance the dislodgement of CaCO_3 from the fibrous network, the suspension was sonicated using a Branson Digital Sonifier for 5 minutes at an amplitude setting of 50% 2 hours into the stirring. The suspension was then poured into a graduated cylinder with a permeable sintered stainless steel support at the bottom in order to allow the acid solution to drain under gravity. The sintered support was expected to contain the fibres. During gravity drainage, more acid solution was gradually poured into the cylinder to efficiently wash the fibres while the suspension was stirred gently with a metal rod. A total of 2.3 L of acid solution was used, and it was expected that the vast majority of CaCO_3 would be removed from the fibrous network by this method. The fibres deposited on the sintered support were then dried and reweighed. It was noted that these fibres were far less 'white' compared to the initial toilet paper, due to the removal of CaCO_3 . From a mass balance, it was determined that 10% w/w of the tissue paper consisted of CaCO_3 fillers. Using this knowledge, and considering that the density of the tissue paper is 1300 kg m^{-3} , it was calculated that the tissue paper contains approximately 4.8% v/v CaCO_3 and that the density of the cellulose fibre alone was 1230 kg m^{-3} . In the calculation it was assumed that the density of CaCO_3 is 2700 kg m^{-3} , which is a typical value for calcite.

It should be noted that some of the values presented above may not be absolutely accurate (due to the inherent difficulties in characterising such complex suspensions), but they serve as adequate approximations for the purpose of this work. It should also be noted that attempts were made to remove fillers by vacuum filtration in a sequential stage-wise manner (a fairly common method), initially starting with a 10 μm rated track-etched membrane, with the idea of using finer membranes for subsequent stages. However, filtrations using the 10 μm membrane (also using a 4 μm filter cloth)

were extremely slow as hardly any filtration occurred in the first few hours, presumably due to medium blinding. Therefore, this line of filler removal was not pursued.

Figure 3.19 shows ζ -potential values of fibres in deionised water as well as 0.2 M NaCl and 0.1 M CaCl₂ solutions. There were no limitations in using the Zetasizer for measuring the fibre ζ -potential as the Smoluchowski equation can be applied to particles of arbitrary shape provided the particle dimensions are much greater than the electrical double layer thickness (Hunter, 2001). Although Figure 3.19 shows the surface charge of fibres including the fillers, the presence of fillers did not appear to significantly influence the measurements and this maybe due to the low concentration of fillers and/or similarly charged fibres and fillers. For example, the measured ζ -potential for cellulose fibres alone (after the removal of CaCO₃ fillers via acid washing), in deionised water, was approximately -15 mV at a pH of 7.5 (not shown in Figure 3.19).

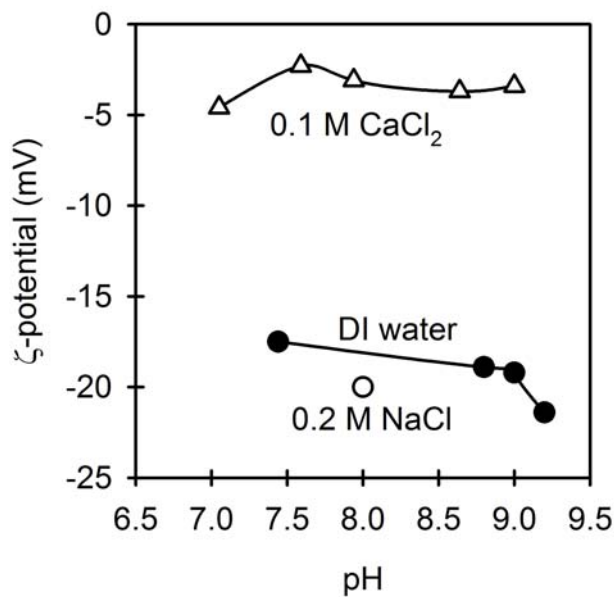


Figure 3.19: Zeta potential values of fibres (with fillers) in deionised (DI) water as well as 0.2 M NaCl and 0.1 M CaCl₂ solutions.

As with rutile, it is again likely that Ca^{2+} ions adsorb onto the fibre surfaces while Na^+ ions behave as an indifferent electrolyte. In the 0.1 M CaCl_2 solution environment the fibre ζ -potential is close to its isoelectric point and almost invariant with pH. The 0.2 M NaCl solution environment did not significantly alter the fibre ζ -potential. The natural pH of fibre suspensions were 7.6 in deionised water, 8.2 in 0.2 M NaCl solution, and 7.3 in 0.1 M CaCl_2 solution. Over this experimental pH range of interest, the ζ -potential values for fibres were approximately -18 mV in deionised water, -20 mV in 0.2 M NaCl solution, and -5 mV in 0.1 M CaCl_2 solution.

For this thesis, a pure fibre suspension refers to the toilet paper suspended in a given solution environment, prepared as outlined in Section 3.5.4. The fillers were not removed prior to a filtration or sedimentation experiment as they were low in concentration (tissue paper contains ~4.8% v/v of fillers), and it was unsure how acid washing would alter the cellulose fibre properties and hence filtration and sedimentation performance. The fillers, along with the cellulose fibres and fibre fines, were taken to represent one entity, referred to in the rest of this thesis simply as ‘fibres’.

3.5.3. Membrane characterisation

A microporous, hydrophilic Versapor membrane, manufactured by Pall Corporation was used as the filter medium, as it was in the work of Willmer (1997). The membrane comprised an acrylic copolymer cast on a nonwoven nylon substrate. The membrane was rated at 0.2 μm and had a thickness of 185 μm . The manufacturer quoted membrane permeability was $7.9 \times 10^{-15} \text{ m}^2$ and the membrane permeability as measured by Wakeman and Tarleton (1992) was $7.0 \times 10^{-15} \text{ m}^2$. Figures 3.20 and 3.21 are reproduced from Willmer’s thesis and show the membrane pore size distribution and a Scanning Electron Micrograph image of the topographic view of the membrane, respectively. A Coulter Porometer was used to determine the pore size distribution of the membrane which appears to be relatively narrow, peaking at approximately 0.2 μm .

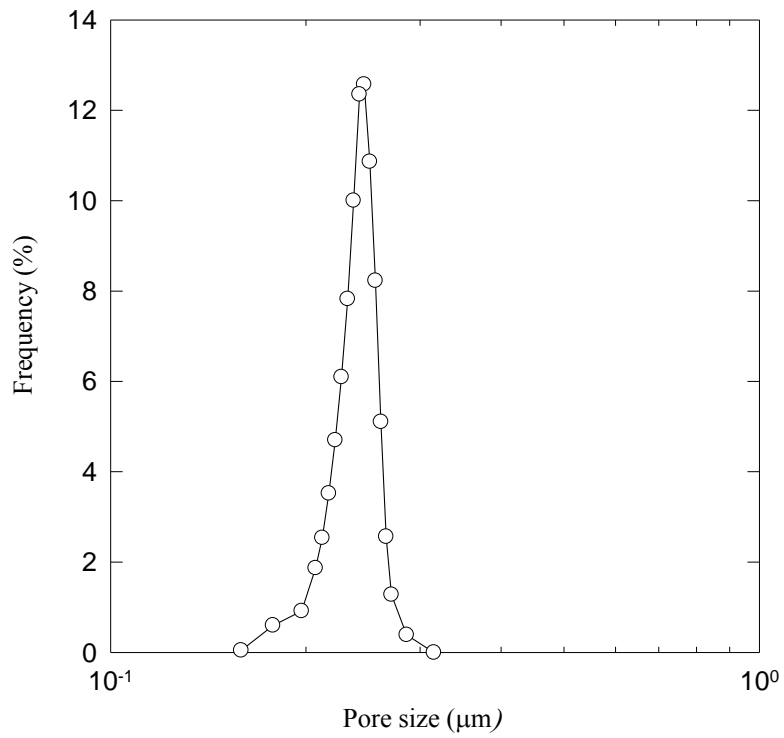


Figure 3.20: Pore size distribution of the Versapor membrane (taken from Willmer, 1997).

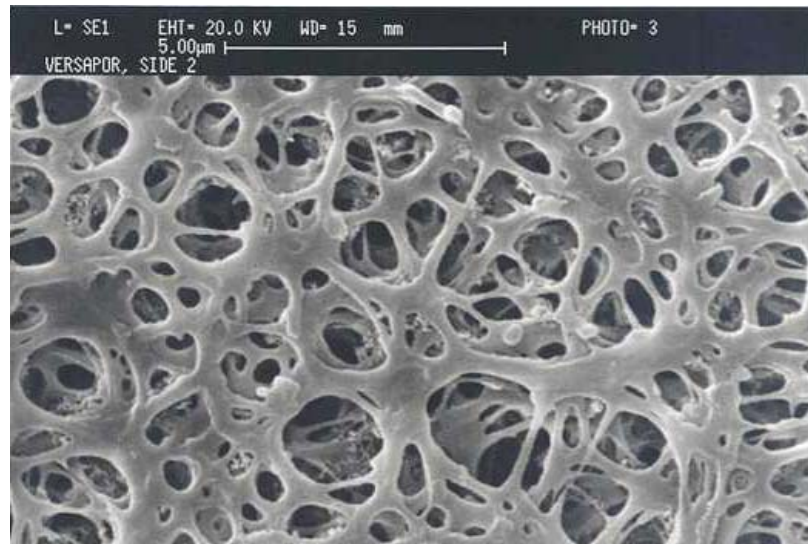


Figure 3.21: Scanning Electron Micrograph of the topographic view of a Versapor membrane (taken from Willmer, 1997).

3.5.4. Suspension preparation methods

Suspensions consisting of either pure fibres, or rutile, or binary mixtures of the two, in double distilled deionised water, 0.2 M NaCl or 0.1 M CaCl₂ solutions were used in experiments. With sedimentation experiments, the suspension total solids concentration was maintained at 1.1% v/v. With filtration experiments, the total solids concentration was maintained at $1.1 \pm 0.2\%$ v/v as calculated after an experiment using the dry solids true volume, as well as the final filtrate volume and cake moisture content. Although ~80% of filtration experiments were with suspensions of $1.1 \pm 0.1\%$ v/v solids concentration, a greater variance was evident relative to the sedimentation experiments due to inherent handling and flow issues using the described filtration apparatus with such complex suspensions (in particular due to the fibre component). This variance in suspension total solids concentration is not expected to significantly influence the filtration results, as illustrated by repeat experiments which gave an acceptable degree of reproducibility (discussed in Chapter 4). All suspensions were prepared in 1 L quantities, but only ~500 ml were used for each filtration.

In an experiment involving NaCl or CaCl₂, homogeneous solutions were prepared prior to any solids addition. In an experiment involving fibres, small pieces of torn up tissue paper were continually introduced into the aqueous phase (deionised water, 0.2 M NaCl or 0.1 M CaCl₂ solutions). In an experiment involving a binary mixture, rutile was added into the suspending medium and mixed for 30 minutes at 600 rpm prior to fibre addition in an attempt to reduce problems relating to dispersion. The final suspension was stirred for approximately 3 h at 800 rpm with a flat blade stirrer prior to a filtration or sedimentation experiment. Care was taken to ensure that suspensions were well mixed so as to minimise batch to batch variations (especially in parameters such as fibre length). Experiments were carried out at a constant temperature of $21 \pm 2^\circ\text{C}$ and over a narrow pH range. The pH of suspensions in deionised water ranged from approximately 8.4 (pure rutile) to 7.6 (pure fibres), in 0.2 M NaCl solution from 7.5 (pure rutile) to 8.2 (pure fibres) and in 0.1 M CaCl₂ solution from 6.9 (pure rutile) to 7.3 (pure fibres).

3.6. SUMMARY

The mechatronic filtration apparatus has been discussed in detail, mainly with regard to its arrangement and operating procedure. Validation experiments enabled familiarity with the apparatus and some of its intricacies. The resulting trends were as expected and consistent, thus validating the apparatus and operating procedure. The relevant properties of the materials used in subsequent filtration experiments (tissue paper, titania and Versapor membranes) have been characterised. The type of filler used in the tissue paper was determined along with the approximate amount of filler per unit weight or volume of tissue paper. Although the characterisations carried out have some limitations, as would almost any attempt at characterising such complex particle and fibre systems, the results are considered to be sufficiently accurate and representative for the purpose of this work. The method of preparing suspensions for subsequent experiments has also been outlined.

REFERENCES

- Atkins P.W. (1998) *Physical Chemistry* (6th Edn.). Oxford University Press. Oxford.
- Beddow J.K. (1986) Size, shape, and texture analysis applied to solid-liquid systems, in *Advances in Solid-Liquid Separation*. Muralidhara H.S. (Ed.) Batelle Press. Ohio.
- Crawford R.L. (1981). *Lignin Biodegradation and Transformation*. John Wiley, New York.
- Hunter R.J. (2001) *Foundations of Colloid Science* (2nd Edn.). Oxford University Press. Oxford.
- Iritani E., Mukai Y. and Toyoda Y. (2002) Properties of a filter cake formed in dead-end microfiltration of binary particulate mixtures. *J. Chemical Engineering Japan* **35**, 226-233.
- Marchant J.Q. (1999) *The Crossflow Microfiltration of Concentrated Titania Dispersions*. PhD Thesis, Loughborough University.

Mikulášek P., Wakeman R.J. and Marchant J.Q. (1998) Crossflow microfiltration of shear-thinning aqueous titanium dioxide dispersions. *Chemical Engineering J.* **69**, 53-61.

Purchas D.B. (1996) *Handbook of Filter Media*. Elsevier, Oxford.

Shaw D.J. (1992) *Introduction to Colloid and Surface Chemistry* (4th Edn.). Butterworth-Heinemann. Oxford.

Tarleton E.S., Wakeman R.J. and Liang Y. (2003) Electrically enhanced washing of ionic species from fine particle filter cakes. *Chemical Engineering Research and Design* **81**, 201-210.

Wakeman R.J. and Tarleton E.S. (1992) Membrane characterisation: the need for a standard. *Process Industry J.* **July**, 16-19.

Wakeman R.J. (2007) The influence of particle properties on filtration. *Separation and Purification Technology* **58**, 234-241.

Willmer S.A. (1997) *A Study of Compressibility and Scale and Their Influence in Dead-End Pressure Filtration*. PhD Thesis, Loughborough University.

CHAPTER 4: SEDIMENTATION AND FILTRATION RESULTS

4.1. INTRODUCTION

This chapter presents relevant experimental results and discusses the constant pressure cake filtration performance of fibrous as well as interacting binary (fibre and rutile) suspensions. The influence of suspension composition, filtration pressure and solution environment on filtration is discussed in relation to cake properties such as average cake porosity (ϵ_{av}) and average specific cake resistance (α_{av}). Interpretation of the filtration data is aided by the analysis of sedimentation behaviour for identical suspensions.

The experimental data presented are representative of the dataset obtained during the investigation. Error bars shown for some datasets indicate the level of reproducibility. The effects of solids composition on binary suspension filtration are presented in terms of the variable X_D which is defined as the ratio of the volume of fibres to the total volume of solids in the suspension; $X_D = 0$ indicates a pure rutile suspension (i.e. no fibres) whereas $X_D = 1$ indicates a pure fibre suspension (i.e. no rutile). The filtration pressures investigated ranged from 50 kPa to 600 kPa. The solution environments investigated were deionised water as well as 0.2 M NaCl and 0.1 M CaCl₂ solutions. For all experiments, the total solids concentration was kept constant at 1.1% v/v (unless stated), as discussed in Section 3.5.4. More detailed descriptions of the apparatus, materials and method of suspension preparation have been given in Chapter 3.

4.2. SEDIMENTATION RESULTS AND DISCUSSION

For a sedimentation experiment, a well mixed suspension (990 ± 10 ml) was poured into a plastic 1 litre graduated measuring cylinder (of 360 mm length and 59.5 mm inner diameter). The suspension-supernatant interface height and corresponding

elapsed time were recorded at suitable intervals and the experimental parameters of interest, for aiding in the interpretation of the filtration results, were the initial settling rate and proportion of sludge; the determination of these two parameters were discussed in Section 3.3.

The initial settling rate gives an indication of the extent of aggregation (or the effective particle size in terms of settling) and the proportion of sludge gives some indication of the sediment packing tendencies. The results below are presented in the form of initial settling rate and proportion of sludge vs. X_D to assist in: (1) qualitative assessments of the degree of physico-chemical interactions (state of aggregation); and (2) determination of packing characteristics at different solids compositions and solution environments.

4.2.1. Single component sedimentation

Pure fibres (1.1% v/v suspensions) did not settle appreciably in any of the solution environments investigated (deionised water, 0.2 M NaCl or 0.1 M CaCl₂ solutions) as the constituent fibres appeared to be networked in the settling cylinder. Pure rutile did not settle appreciably in deionised water (initial settling rate = 1.1×10^{-5} m s⁻¹). However, as shown in Figure 4.1, pure rutile settled more readily in 0.1 M CaCl₂ solution (initial settling rate = 3.2×10^{-2} m s⁻¹) and this is attributed to suppression of the rutile electrical double layer which promoted aggregation. Figure 4.2 shows that pure fibre suspensions of lower total solids concentrations (0.16% v/v) settled more readily and the initial settling rate was greater for fibre suspensions in 0.1 M CaCl₂ solution (1.4×10^{-1} m s⁻¹) than in deionised water (3.9×10^{-2} m s⁻¹). Further, the supernatant of a settled fibre suspension in deionised water was significantly more turbid than the supernatant of a corresponding suspension in 0.1 M CaCl₂ solution. It is noted that the fibres were close to their isoelectric point in 0.1 M CaCl₂ solution (see Figure 3.19). As illustrated by Figure 4.3, the improved settling performance of fibre suspensions in 0.1 M CaCl₂ was only evident at lower concentrations, because at higher concentrations the constituent fibres started to network.

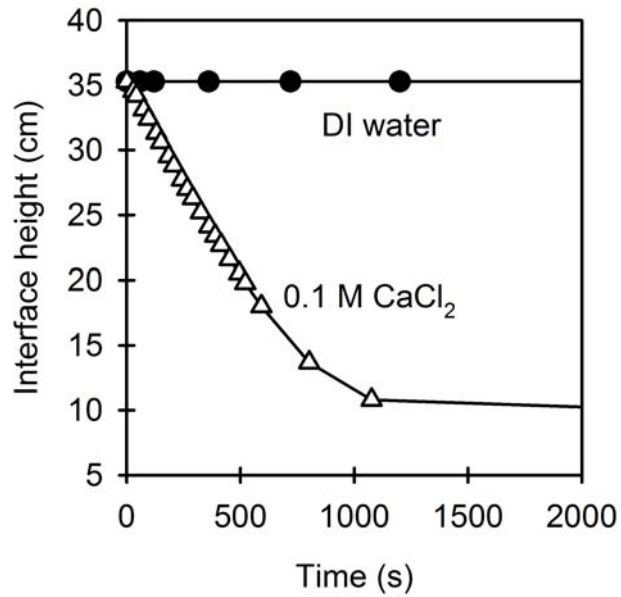


Figure 4.1: Sedimentation curves for pure rutile in deionised (DI) water and 0.1 M CaCl₂.

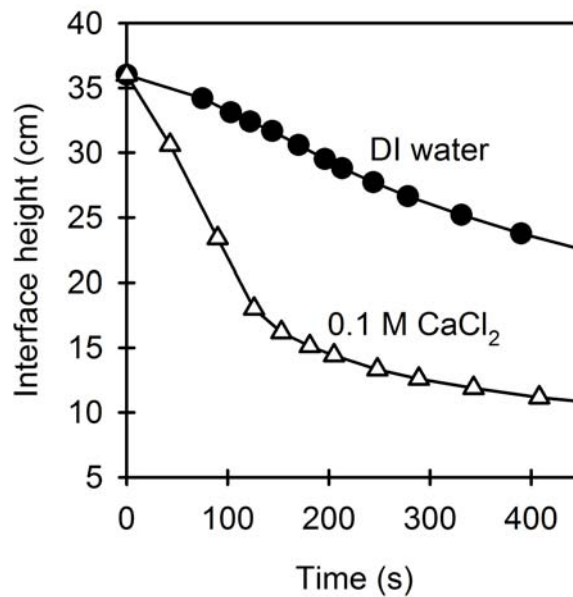


Figure 4.2: Sedimentation curves for pure fibres in deionised (DI) water and 0.1 M CaCl₂ solution. The total solids concentration for these two experiments was 0.16% v/v; pure fibres did not settle appreciably in either solution environments at 1.1% v/v.

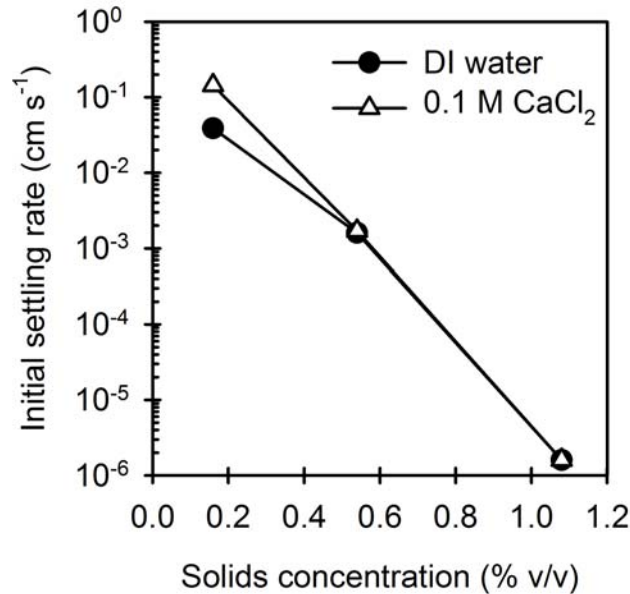


Figure 4.3: Initial settling rate vs. total solids (fibre) concentration for pure fibre suspensions.

4.2.2. Binary suspension sedimentation

Example batch settling curves for binary suspensions in deionised water and 0.1 M CaCl₂ solution are shown in Figures 4.4 and 4.5. It is seen that the equilibrium packing and times taken to reach equilibrium conditions varied with solids composition. In general, the approximate time taken to reach pseudo-equilibrium conditions (t_e) decreased with increasing fibre fraction until ~50% by volume of solids consisted of fibres. The time taken to reach pseudo-equilibrium conditions increased with further increase in fibre fraction (above 50%). For instance, with suspensions in deionised water, $t_e \sim 10,000$ s at an X_D of 0.067; ~ 2000 s at an X_D of 0.391; and $\sim 14,000$ at an X_D of 0.856. With fibre rich suspensions, even after this pseudo-equilibrium state is reached, a slow and gradual compression of the deposit was observed.

It is seen that pure rutile and fibre suspensions in deionised water and pure fibre suspensions in 0.1 M CaCl₂ solutions do not readily settle. For suspensions in deionised water, mixtures of rutile and fibres were observed to settle more readily than pure component suspensions. This is perhaps more clearly illustrated in Figure 4.6 where it is

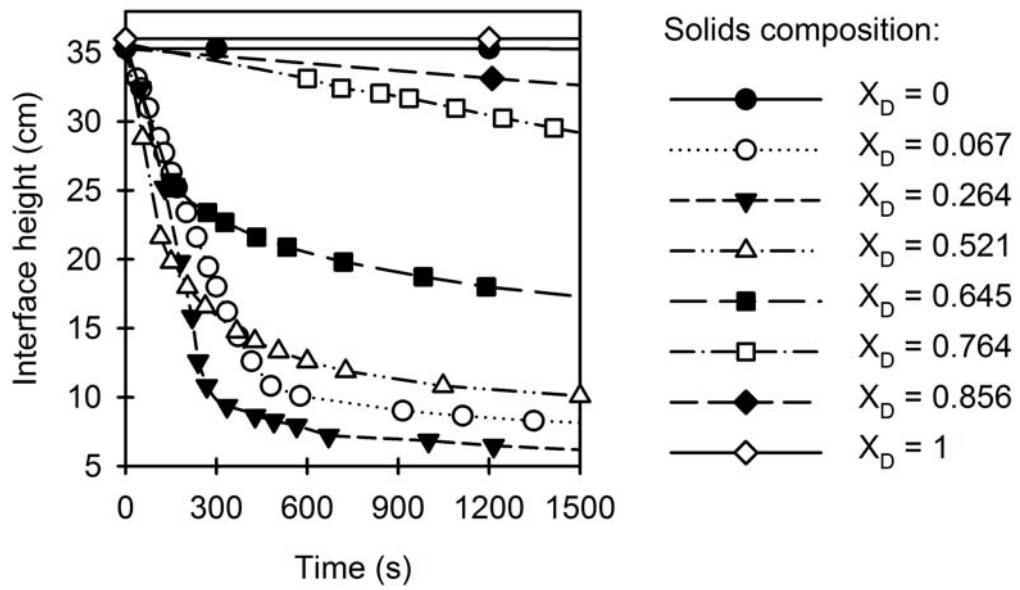


Figure 4.4: Example batch settling curves for binary suspensions in deionised water.

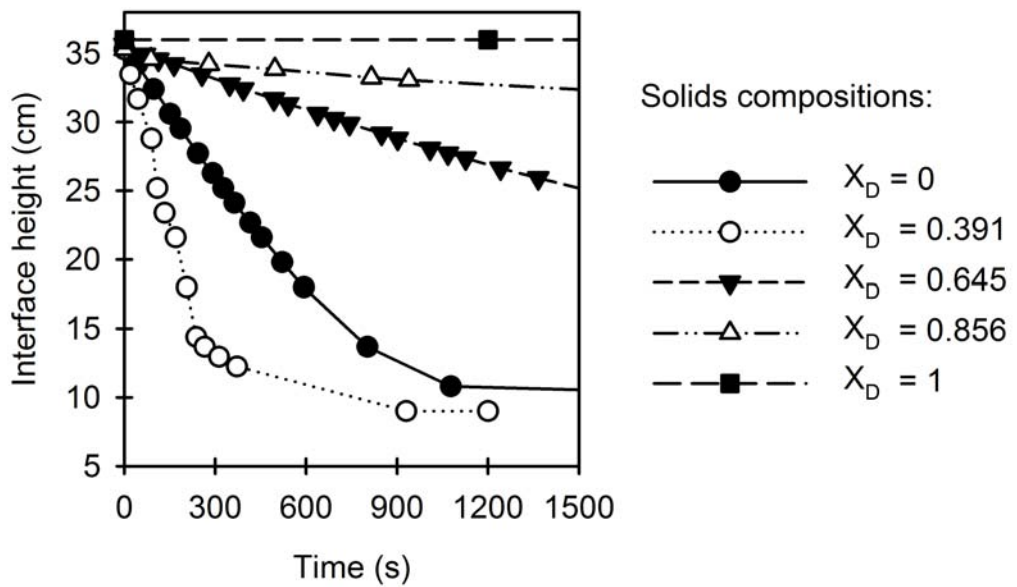


Figure 4.5: Example batch settling curves for binary suspensions in 0.1 M CaCl_2 solution.

seen that pure rutile and pure fibre in deionised water appear to be stable suspensions. With only small amounts of fibres added to a pure rutile suspension, rutile-fibre interactions take place and the suspension de-stabilises. The initial settling rate continues to increase with X_D up to the point where ~50% by volume of the solids consists of rutile, presumably due to the increasing surface area available for interaction. Further increases in X_D caused a sharp reduction in initial settling rate until approximately 75% by volume of the solids consisted of fibres, and subsequent increases in X_D rendered the suspension essentially stable once again. It is interesting that $X_D = 0.5$ is also the approximate threshold where the proportion of sludge begins to undergo a more marked increase (Figure 4.7). The reduction in initial settling rate and increase in proportion of sludge when more than 50% of the solids consist of fibres may be an indication of the constituent fibres becoming networked, resulting in more structured suspensions. The general sedimentation trends for suspensions in deionised water and 0.1 M CaCl_2 solution appear to be similar. Initial settling rates in the range $0.1 < X_D < 0.8$ were lower for suspensions in CaCl_2 solution, presumably due to the formation of low density, loosely networked aggregates. The presence of more loosely networked aggregates in CaCl_2 solution was evidenced by the greater proportions of sludge at a given X_D (Figure 4.7).

The effect of increasing fibre fraction on the resultant deposit packing appears to become more pronounced as X_D increases. The proportion of sludge progressively increases with fibre fraction; from a minimum obtained for pure rutile suspensions⁴ to a maximum for pure fibre suspensions ($X_D = 1$), where the deposit bed porosity was close to that present before settling commenced. The progressive increase in proportion of sludge is an interesting result considering the rutile/fibre size ratio since if the rutile was free to migrate within interfibre voids then this would lead to a minimum proportion of sludge at an intermediate solids composition. Typical theoretical predictions for binary mixtures almost always show a minimum porosity (maximum packing density) at some intermediate mixture fraction, generally attributed to interparticle penetration (see, for example, Mota *et al.*, 2001; Dias *et al.*, 2004). Theoretical works have been backed up by experimental findings (McGeary, 1961; Leclerc, 1975), which suggest that the greater the difference in size between the coarse and fine particles in a mixture so the

⁴ an exception being pure rutile in DI water which did not readily settle (proportion of sludge ~100%)

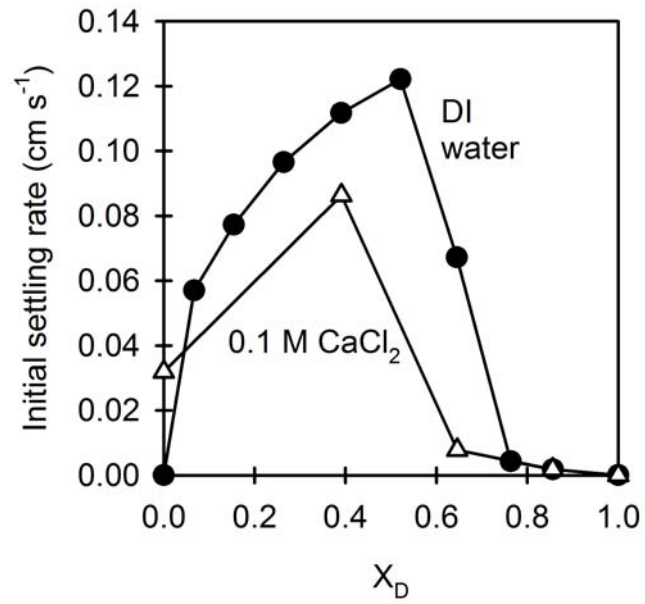


Figure 4.6: Effect of fibre fraction (X_D) on the initial settling rate for suspensions in deionised (DI) water and 0.1 M CaCl₂ solution.

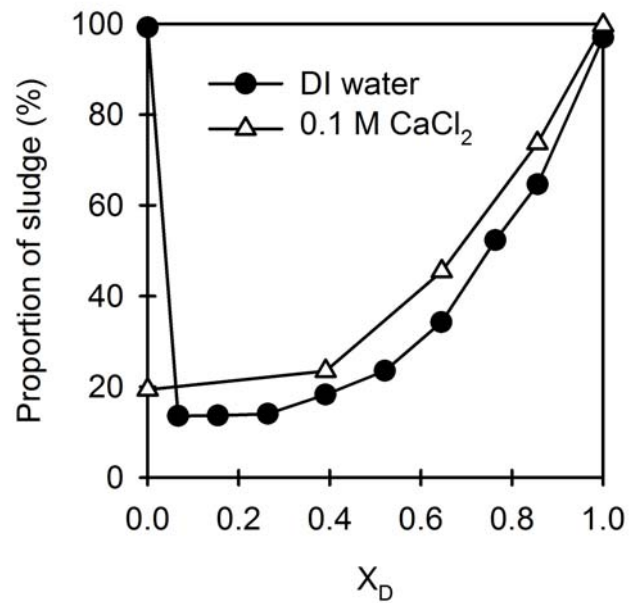


Figure 4.7: Effects of fibre fraction (X_D) on the proportion of sludge for suspensions in deionised (DI) water and 0.1 M CaCl₂ solution.

more pronounced is the non-linearity in the porosity versus solids composition relationship.

It is noted that the batch settling tests resulted in some amounts of foam at the top of the cylinder (~1.5-3 cm thick) at certain mixture compositions. In some cases, this foam appeared to have entrained some solids; this was however not expected to be a significant issue that affected the results. The mud line clarity was primarily affected by the supernatant turbidity where a turbid supernatant resulted in a mud line of low visibility. Table 4.1 summarises some observations made during batch settling tests.

Table 4.1: Batch gravity settling experimental observations for suspensions of various fibre fractions in deionised water.

X_D	Presence of foam	Solids apparently entrained in the foam	Visibility of mud line
0	No	No	No appreciable settling
0.067	Yes	Not apparent	High
0.154	Yes	Possibly small amounts	High
0.264	Yes	Possibly small amounts	Initially moderate
0.391	Yes	Yes	Initially moderate
0.521	Yes	Yes	Initially low, turbid supernatant
0.645	Yes	Yes	Initially low, turbid supernatant
0.764	No	No	Initially low, very turbid supernatant
0.856	No	No	Initially low, very turbid supernatant
1	No	No	No appreciable settling

4.3. FILTRATION RESULTS AND DISCUSSION

4.3.1. Basic data treatment and calculations

The filtrate flow data from each filtration test were saved on the interfacing computer, copied onto floppy disk and stored as Unicode files. Selected datasheets for the filtration experiments discussed in this chapter are presented in Appendix A. Although liquid pressure profiles were recorded by the micro-pressure transducers in the validation experiments, the majority of pressure profiles in this investigation could not be reliably measured due to the nature of the binary cakes, particularly the fibre rich ones. As an example, the recorded liquid pressure profiles for an $X_D = 0.859$ suspension in deionised water at three filtration pressures are given in Appendix B, where it is seen that the measured liquid pressure at various heights within the cake unexpectedly (and perhaps erroneously) remained almost constant at the applied filtration pressure throughout. However, with a few filtration experiments, the liquid pressure profiles do show some variation with time, and were analysed (where appropriate) to provide some insight into specific filtration behaviour as discussed in Chapter 6. Although these values may not be absolute in their accuracy, they were useful for the purpose of comparing the behaviour at one cake height relative to another. No further reference to recorded liquid pressure profiles is made in this chapter.

To maintain consistency in parameters such as the total solids concentration, so that comparisons could be made between different solids fractions, it was important to establish appropriate relationships and systematically calculate relevant parameters each time. The need to regularly check mass and volume balances were made more significant due to the complex nature of the binary mixtures in this investigation, in particular the fibre component (in terms of handling and flow characteristics). It was mentioned in Section 3.5.4 that checks were made on the solids concentration after a filtration experiment. In order to allow for checks and calculation of parameters of interest, besides the filtrate flow data, other information recorded included the mass of fibres (M_1) and rutile (M_2) in the feed and the mass of wet (M_{wc}) and dry (M_{dc}) cake after a filtration. Other relevant constants include the filtration area ($A = 0.012 \text{ m}^2$), fibre

density ($\rho_l = 1300 \text{ kg m}^{-3}$), rutile density ($\rho_2 = 4200 \text{ kg m}^{-3}$) and liquid density ($\rho_l = 1000 \text{ kg m}^{-3}$). From the aforementioned constants and recorded information, relevant checks on the mass and volume balance can be made and other parameters of interest can be calculated using the following relationships:

$$X_M = \frac{M_1}{M_1 + M_2} \quad (4.1)$$

$$M_1 = X_M M_{dc} \quad (4.2)$$

$$M_2 = (1 - X_M) M_{dc} \quad (4.3)$$

$$V_1 = \frac{M_1}{\rho_1} \quad (4.4)$$

$$V_2 = \frac{M_2}{\rho_2} \quad (4.5)$$

$$V_{feed} = V_1 + V_2 + V_{fin} + \frac{M_{wc} - M_{dc}}{\rho_l} \quad (4.6)$$

$$X_D = \frac{V_1}{V_1 + V_2} \quad (4.7)$$

$$C_{V1} = \frac{V_1}{V_{feed}} \times 100\% \quad (4.8)$$

$$C_{V2} = \frac{V_2}{V_{feed}} \times 100\% \quad (4.9)$$

$$C_{VTS} = C_{V1} + C_{V2} \quad (4.10)$$

$$\rho_s = \frac{M_{dc}}{V_1 + V_2} \quad (4.11)$$

$$\rho_s = X_D \rho_1 + (1 - X_D) \rho_2 \quad (4.12)$$

$$s = \frac{M_1 + M_2}{V_{fin}\rho_l + M_{wc}} \quad (4.13)$$

$$m = \frac{M_{wc}}{M_{dc}} \quad (4.14)$$

$$c = \frac{\rho_l s}{1 - ms} \quad (4.15)$$

$$w = \frac{M_1 + M_2}{A} \quad (4.16)$$

$$L = \frac{V_{fin}}{A} \frac{s(\rho_s(m-1) + \rho_l)}{\rho_s(1 - ms)} \quad (4.17)$$

where ρ_s is the effective solids density, s the mass fraction of total solids in the feed, c the mass of solids per unit volume of feed liquid, m the ratio of mass of wet cake to mass of dry cake, w the mass of dry solids deposited per unit filtration area, L the final cake thickness, and V_{feed} the total feed volume. The two key cake properties investigated were the average specific cake resistance (α_{av}) and average cake porosity (ε_{av}), and were calculated using equations (4.18) and (4.19):

$$\alpha_{av} = \frac{m_{dt/dV} A^2 \Delta P}{\mu c} \quad (4.18)$$

$$\varepsilon_{av} = 1 - \frac{w}{\rho_s L} \quad (4.19)$$

where $m_{dt/dV}$ is the gradient of a dt/dV vs. V 'filtration plot'.

4.3.2. General filtration behaviour of single component suspensions

Before looking at binary suspension filtration behaviour, it is pertinent to get a feel for the filtration behaviour of the two single component suspensions; especially with pure fibre suspensions, since there is a seeming lack of published data in this area. Filtrations of fibre suspensions were carried out at various pressures between 50 and

600 kPa. Figure 4.8 shows a typical plot of cumulative filtrate volume vs. filtration time at a pressure of 450 kPa and Figure 4.9 shows the initial (linear) portion of the reciprocal filtrate flow rate vs. cumulative filtrate volume plot; data for a rutile suspension filtration at the same pressure is included in these two figures for comparison purposes.

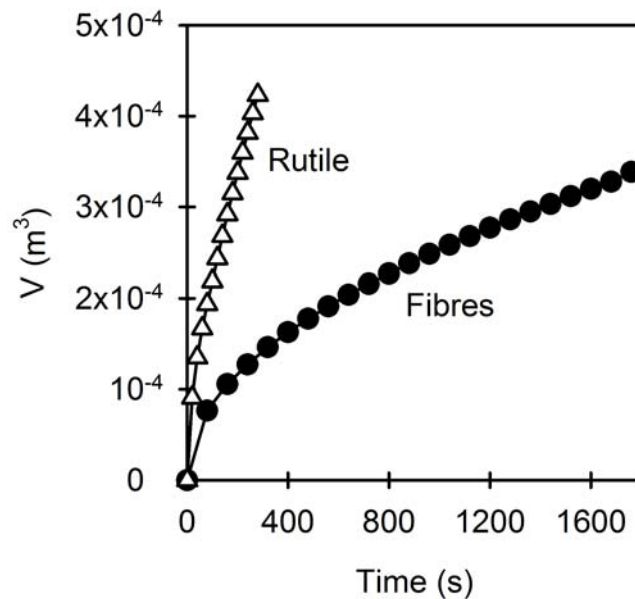


Figure 4.8: Plots of cumulative filtrate volume vs. filtration time for 1.1% v/v fibre and rutile suspensions in deionised water at a constant filtration pressure of 450 kPa.

Rutile, and particularly fibre, suspensions in deionised water were generally difficult to filter and formed cakes of relatively high resistance. Filtration of pure fibre and rutile suspensions from deionised water at various pressures resulted in cakes displaying average specific resistance values between 10^{13} and 10^{14} m kg^{-1} for pure fibre cakes and between 10^{12} and 10^{13} m kg^{-1} for pure rutile cakes. Wakeman and Tarleton (2005) classified the relative ease of filtration using the magnitude of the specific resistance and claimed separation becomes ‘difficult’ when $\alpha_{av} \sim 10^{12}$ m kg^{-1} and ‘very difficult’ when $\alpha_{av} > 10^{13}$ m kg^{-1} . Filtration of fibre suspensions at various pressures and with other filter media (a 4 μm rated filter cloth was also trialled) were unexpectedly

slow. Moreover, with pure fibre suspensions the 4 μm rated filter cloth gave much slower filtration rates than with the 0.2 μm rated membrane, and this was attributed to fibre fine fractions blinding the filter cloth. The presence of fibre fine fractions were visually observed and evidenced by the turbid supernatant obtained from a settled 0.16% v/v fibre suspension.

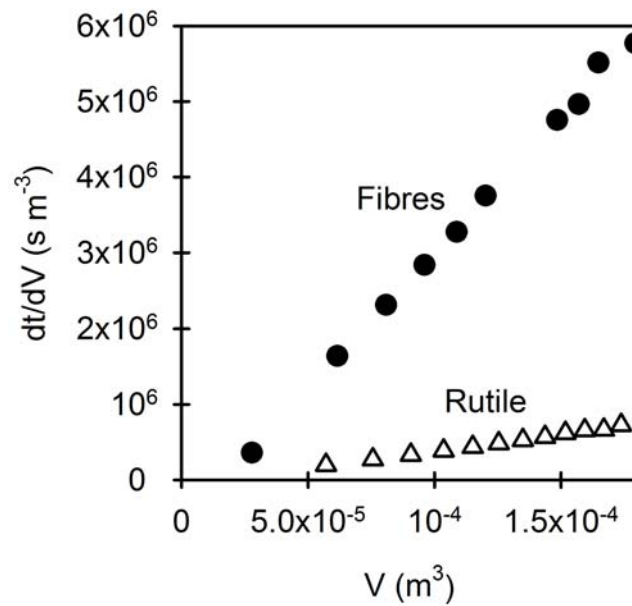


Figure 4.9: The initial (linear) portion of the plots of reciprocal filtrate flow rate vs. cumulative filtrate volume for 1.1% v/v fibre and rutile suspensions in deionised water at a constant filtration pressure of 450 kPa.

Figures 4.10 and Figure 4.11 show example plots of cumulative filtrate volume vs. filtration time and reciprocal flow rate vs. cumulative filtrate volume for pure fibre suspensions at various filtration pressures. Figure 4.12 shows plots of cumulative filtrate volume vs. filtration time for pure rutile suspensions at various filtration pressures. Figures 4.10 – 4.12 show expected trends. In Figures 4.10 and 4.12, it is seen that at a given time, the cumulative filtrate volume for a pure fibre or rutile suspension is greater for raised filtration pressure. The instantaneous filtrate flow rate can be determined from the gradient of the V vs. t plot at a given time, and from Figures 4.10 and 4.12 it is seen

that this behaviour follows a consistent sequence with flow rate generally increasing with pressure. This trend is also manifested in Figure 4.11, where the gradient of the dt/dV vs. V plot decreases as the filtration pressure increases. Consistent with ‘established’ filtration theory, the decrease in gradient is most evident at the lower filtration pressures. The average specific resistance values were calculated from such plots of reciprocal flow rate vs. cumulative filtrate volume according to equation (4.18).

A regression analysis determined the compressibility index values (n value in the relationship $\alpha_{av} = \alpha_0(1-n)\Delta P^n$) to be approximately 0.6 for pure fibre cakes and 0.3 for pure rutile cakes (refer to Figure 4.13). These values indicate moderate compressibility, with the pure fibre cakes having a greater compressibility. α_0 is the specific resistance at unit applied pressure. Values of α_0 for pure fibres and rutile were determined to be $1.23 \times 10^{11} \text{ m kg}^{-1} \text{ Pa}^{-n}$ and $6.12 \times 10^{10} \text{ m kg}^{-1} \text{ Pa}^{-n}$, respectively.

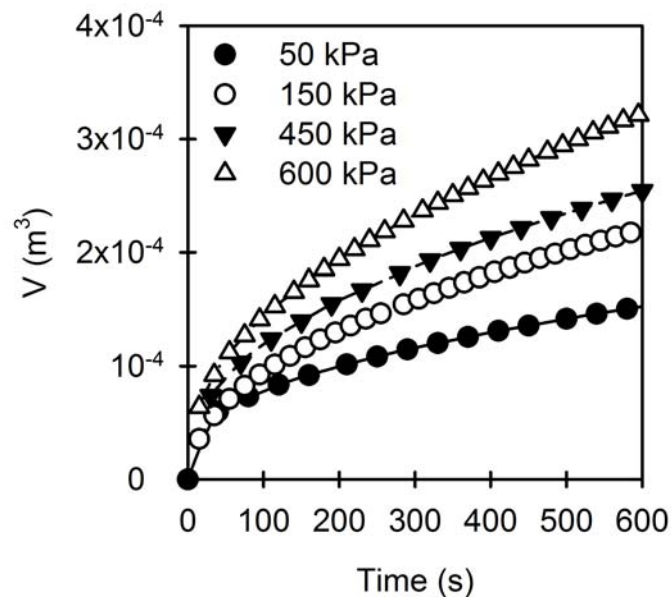


Figure 4.10: Cumulative filtrate volume vs. filtration time for 1.1% v/v fibre suspensions in deionised water at various filtration pressures.

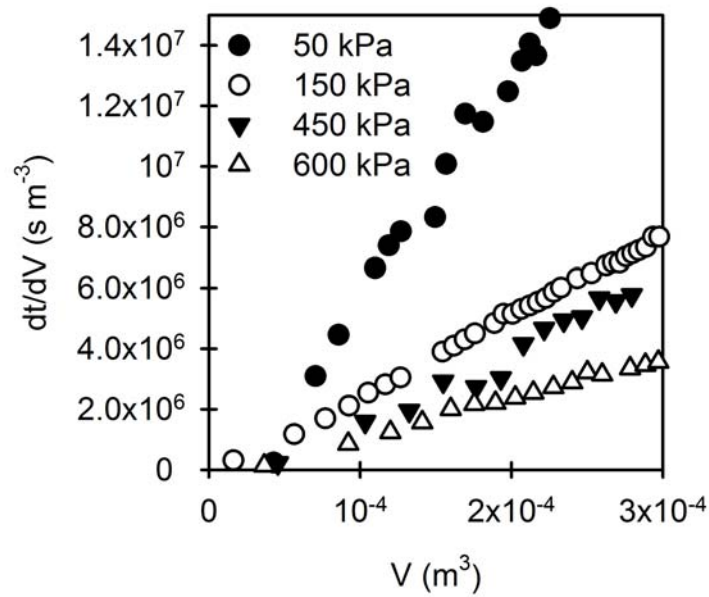


Figure 4.11: Reciprocal filtrate flow rate vs. cumulative filtrate volume for 1.1% v/v fibre suspensions in deionised water at various filtration pressures.

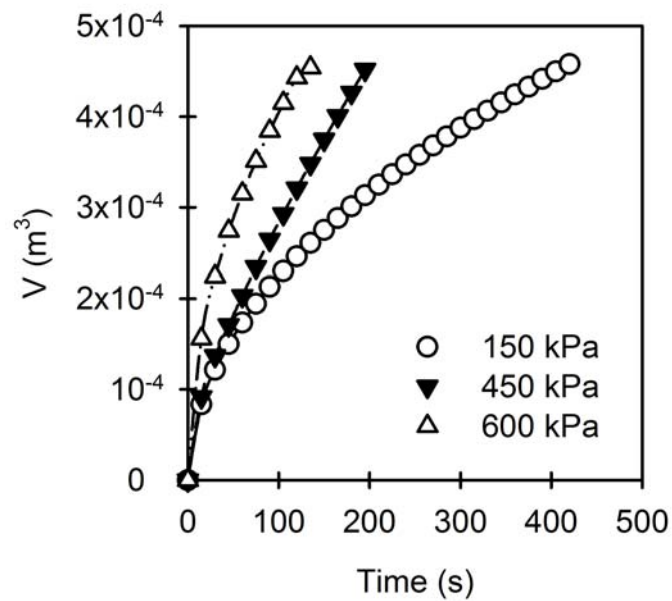


Figure 4.12: Cumulative filtrate volume vs. filtration time for 1.1% v/v rutile suspensions in deionised water at various filtration pressures.

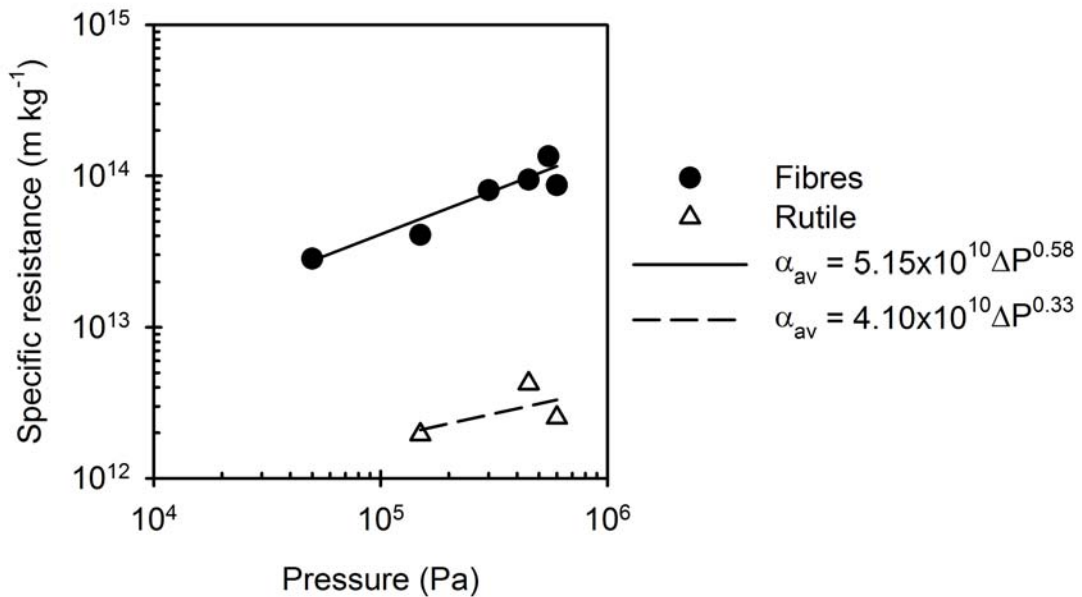


Figure 4.13: Effect of filtration pressure on average specific cake resistance for 1.1% v/v fibre and rutile suspensions in deionised water.

4.3.3. General filtration behaviour of binary suspensions

Examples of typical data obtained by the filtration of binary suspensions from deionised water, as well as 0.2 M NaCl and 0.1 M CaCl₂ solutions are shown in Figures 4.14 to 4.18. Figures 4.14 and 4.15 give examples of typical filtration plots for 150 kPa filtrations with deionised water. It is seen that a variation in solids composition results in relatively large variations in filtration behaviour. It is apparent that the filtration rates are greatest with the filtration of suspensions consisting of 39.1% and 64.6% by volume fibres (Figure 4.14) in the solids phase. Figure 4.15 shows the gradient of the initial (linear) portion of the dt/dV vs. V plots is smallest at $X_D = 0.391$ and 0.646 . However, it should be noted that the average specific resistance is not exclusively a function of this gradient as c (mass of solids per unit volume of feed liquid) in equation (4.18) changes with solids composition even though the total solids concentration was kept constant. Filtration of a pure fibre suspension proceeded at the slowest rate, followed by filtration of a pure rutile suspension.

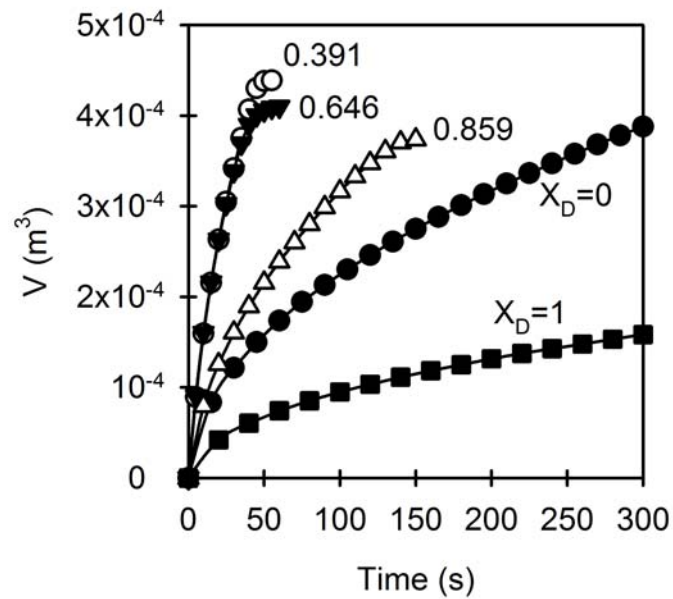


Figure 4.14: Cumulative filtrate volume vs. filtration time for 150 kPa filtrations of 1.1% v/v binary suspensions in deionised water at various solids compositions. The solids compositions are quantified in terms of the X_D values.

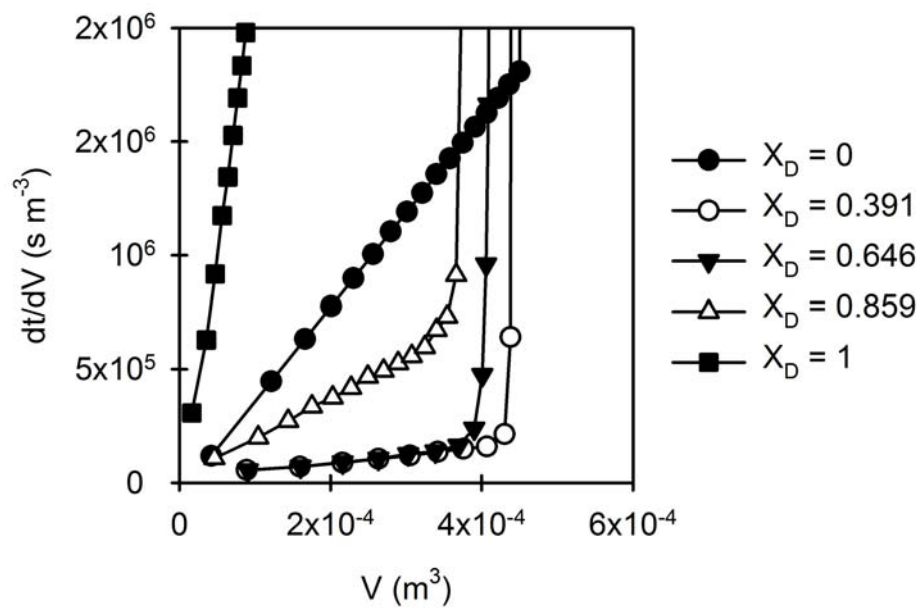


Figure 4.15: Reciprocal filtrate flow rate vs. cumulative filtrate volume for 150 kPa filtrations of binary suspensions in deionised water at various solids compositions.

Figure 4.16 shows typical filtration plots for 450 kPa filtrations from deionised water and similar general trends are observed. Once again filtration with $X_D = 0.646$ was quickest. It should also be noted that, under certain conditions, unusual filtration plots were observed; this anomalous behaviour has not been illustrated in the figures in the current chapter but is discussed further in Chapter 6.

Figure 4.17 shows an example of typical filtration plots for 450 kPa filtrations from 0.1 M CaCl_2 solution. In comparison to Figure 4.16, it is seen that a greater variation in filtration behaviour due to variation in solids composition is observed with suspensions made up in deionised water. Figure 4.18 shows typical filtration plots for 450 kPa filtrations from 0.2 M NaCl solution. It is again seen that, relative to filtrations from deionised water, variations in solids composition had less of an effect on the filtration behaviour although the same general trends were observed.

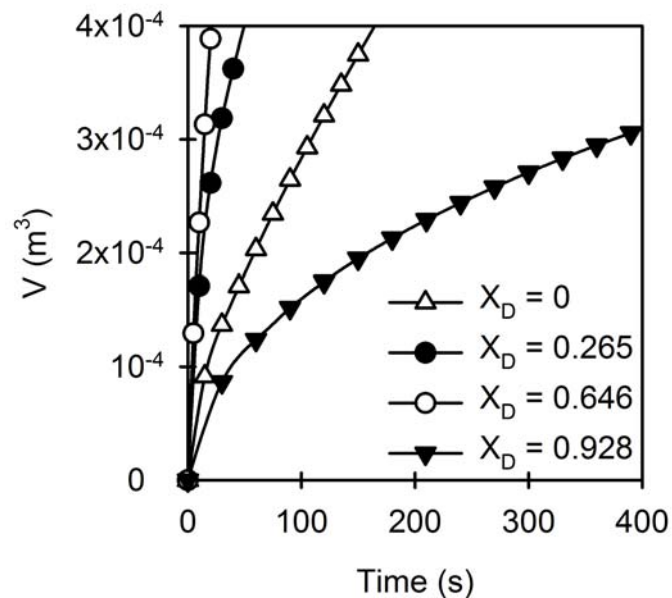


Figure 4.16: Cumulative filtrate volume vs. filtration time for 450 kPa filtrations of binary suspensions in deionised water at various solids compositions.

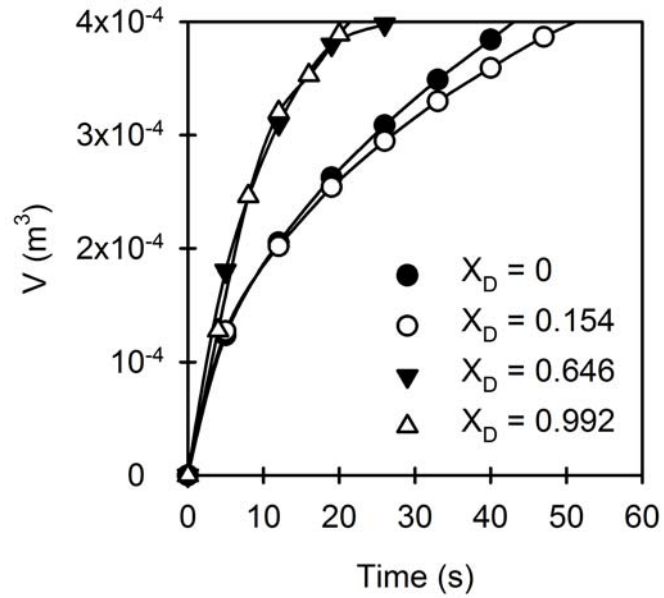


Figure 4.17: Cumulative filtrate volume vs. filtration time for 450 kPa filtrations of binary suspensions in 0.1 M CaCl_2 at various solids compositions.

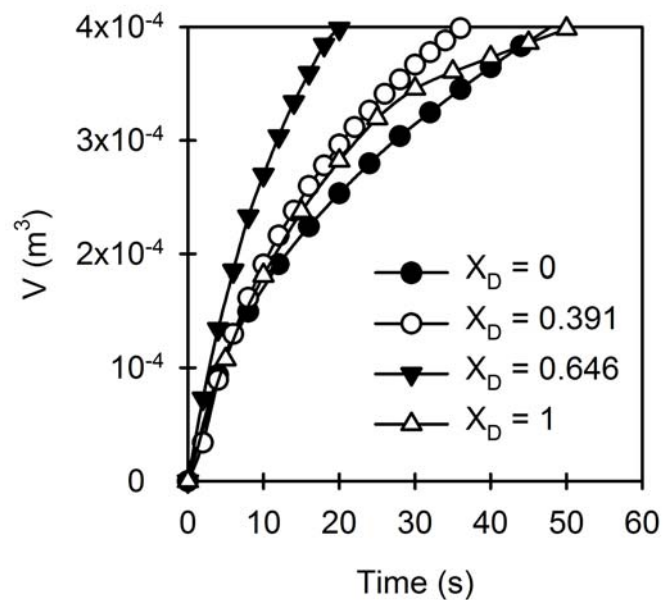


Figure 4.18: Cumulative filtrate volume vs. filtration time for 450 kPa filtrations of binary suspensions in 0.2 M NaCl at various solids compositions.

Figure 4.19 indicates the effects of rutile/fibre composition and solution environment on the filtration rate during the initial stage of the 450 kPa filtrations. As inferred from Figures 4.16 – 4.18, the effects of solids composition were less evident on the filtration performance for suspensions in 0.2 M NaCl and 0.1 M CaCl₂ solution environments relative to suspensions made with deionised water. With the suspensions in deionised water, the filtration rate generally increased from pure rutile up to a maximum at $X_D \sim 0.5$. A further increase in fibre fraction reduced the filtration rate down to a minimum for a pure fibre suspension ($X_D = 1$). This behaviour is also evident in Figure 4.16. The filtration rates with a pure fibre suspension were lower than with a pure rutile suspension. Filtration rates with suspensions in 0.1 M CaCl₂ were marginally greater than with suspensions in 0.2 M NaCl. Over the range $0.3 < X_D < 0.7$, the influence of solution environment seemed less significant than with rutile rich suspensions ($X_D < 0.3$), where the 0.2 M NaCl and 0.1 M CaCl₂ solutions seemed to increase the filtration rates. The effects of solution environment were seen to be most significant for fibre rich suspensions ($0.7 < X_D$), where the 0.2 M NaCl and particularly the 0.1 M CaCl₂ solutions seemed to cause a pronounced increase in the filtration rates.

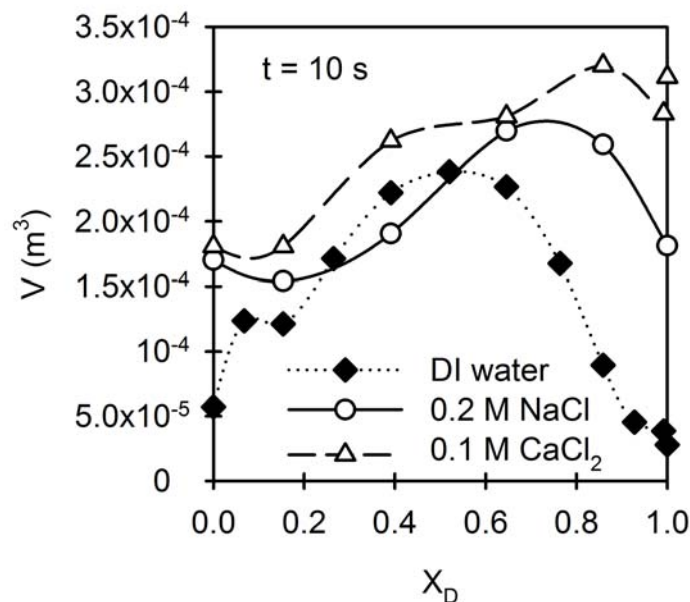


Figure 4.19: Cumulative filtrate volumes 10 s into the 450 kPa filtrations at various solids compositions and solution environments.

Figures 4.20 and 4.21 summarise the effects of rutile/fibre composition and filtration pressure on the filter cake average porosity and specific resistance for filtrations from deionised water. It is clearly evident that solids composition had a greater effect on filtration performance compared to applied pressure. With filtrations at 450 kPa, the average specific cake resistances for pure fibre and rutile in deionised water were approximately 9.4×10^{13} and 4.2×10^{12} m kg^{-1} respectively, with the variation of α_{av} with fibre fraction showing a minimum. The minimum in α_{av} was in the region of 2.7×10^{11} m kg^{-1} and observed at an X_D of 0.646. Filtrations with deionised water at the other trialled pressures showed similar trends. The average porosities of filter cakes formed from pure rutile and fibre suspensions in deionised water were approximately 0.6 and 0.75, respectively. In general, a steady and progressive increase in ϵ_{av} with fibre fraction was observed.

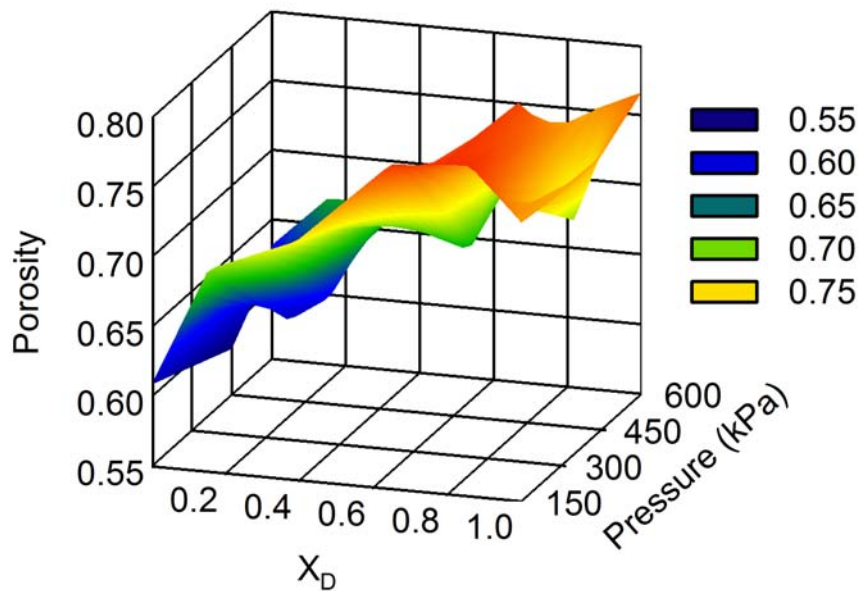


Figure 4.20: Effects of solids composition and filtration pressure on filter cake average porosity for filtrations from deionised water.

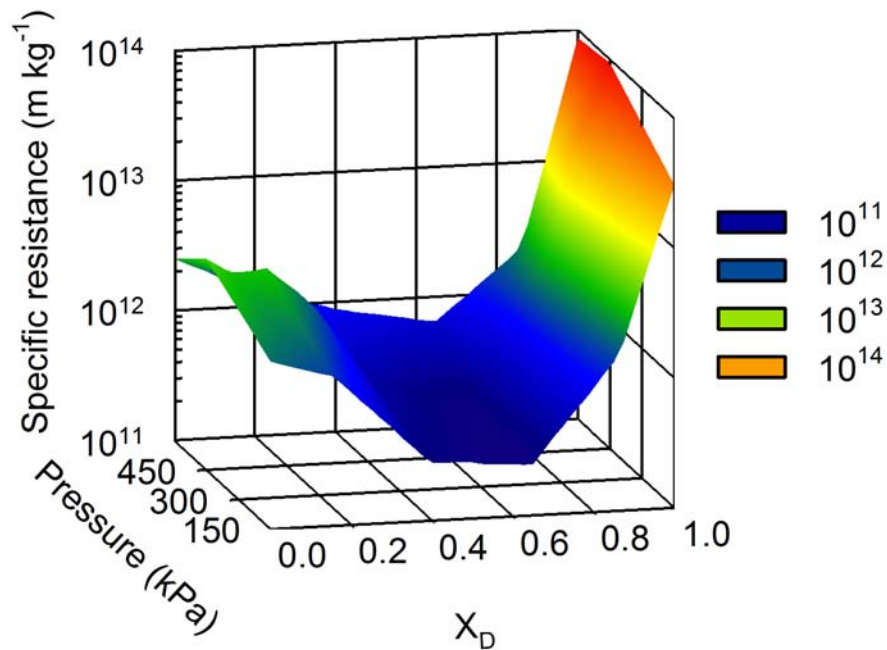


Figure 4.21: Effects of solids composition and filtration pressure on filter cake average specific resistance for filtrations from deionised water.

Considering the relationships between the parameters α_{av} and ε_{av} with fibre fraction gives rise to an apparent anomaly. As suggested by the Kozeny-Carman (Wakeman and Tarleton, 2005) and Happel cell (Happel and Brenner, 1965) models, an increase in porosity generally results in a decrease in specific resistance (see Section 2.4.1). However, it should be recognised that these models only provide reasonable approximations and the correlation of resistance data obtained from these models could be used for comparison purposes if the solids form remains similar. The fibres and rutile are of very different forms (see Figures 3.12 and 3.16 for example), and this may result in varying packing mechanisms when moving from pure rutile to pure fibre cakes. Also, possible fibre-rutile interactions may further influence the specific surface exposed to fluid flow (and hence the total drag force experienced at the solid/liquid interface) at the various solids compositions, which in turn will affect the specific resistance. Due to the

change in solids form and possible interactions, the Kozeny-Carman and Happel cell models cannot be used with confidence across the range of solids composition.

Figures 4.22 and 4.23 show the effects of solids composition and solution environment on the filter cake average porosity and specific resistance for 450 kPa filtrations from deionised water as well as 0.2 M NaCl and 0.1 M CaCl₂ solutions. Error bars for some data were obtained from up to three repeat experiments and are included to illustrate the level of reproducibility. The results illustrated in Figure 4.23 are generally consistent with Figure 4.19, where the lowest filtration rates were due to a greater average specific resistance. It is seen that, to a certain extent, the NaCl and CaCl₂ solution environments produced similar trends in filtration behaviour; these solution environments resulted in a greater average porosity for rutile rich cakes and a lower average specific resistance for rutile and fibre rich cakes. The behaviour shown in Figures 4.20 to 4.23 is further described and interpreted in the following sections.

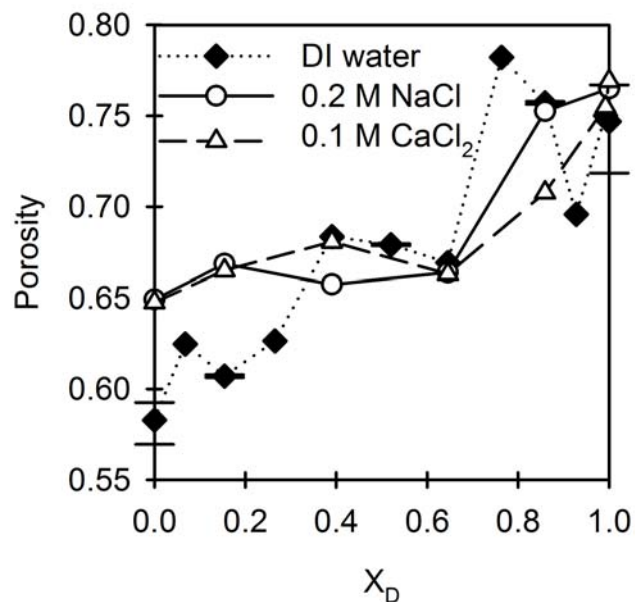


Figure 4.22: Effects of solids composition and solution environment on filter cake average porosity for 450 kPa filtrations.

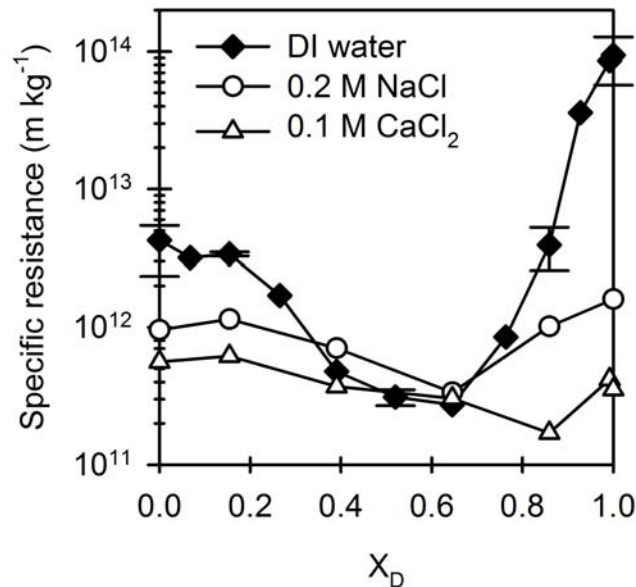


Figure 4.23: Effects of solids composition and solution environment on filter cake average specific resistance for 450 kPa filtrations.

4.3.4. Effects of solids composition

4.3.4.1. Effects of solids composition on porosity

Typical theoretical predictions for binary mixtures show a minimum in the variation of porosity with solids composition, and a larger difference in size between the coarse and fine solids generally yields a more pronounced non-linearity (see Section 2.6). However, in this study, the variation of porosity with volume fraction of fibres is shown to be relatively limited and in many cases almost linear despite the fibres being of wide size distribution and generally several orders of magnitude larger than the rutile particles. By way of example, two models are presented and compared to illustrate the fibre/rutile packing characteristics. These two models are taken to be representative of two approaches; the first attempts to describe the concept of interparticle penetration (Tokumitsu, 1964), and the second the concept of additive porosity (Shirato *et al.*, 1963). Although there are various interparticle penetration models (or variants) that have been previously developed for binary mixture packing (see Dias *et al.*, 2004 for

example, which gives further references), they all show similar general trends; the Tokumitsu model is used in this chapter as a representative example. Further discussion on this point, and justifications for the use of the Tokumitsu model to represent the interparticle penetration mechanism, are presented in Appendix C where another interparticle penetration model (from Dias *et al.*, 2004) is also presented for comparison purposes.

The following two equations have been proposed by Tokumitsu (1964) to predict the porosity of a packed bed formed from a binary mixture of particles. For a packed bed rich in small particles:

$$\varepsilon_{av} = 1 - \frac{1 - \varepsilon_{av,2}}{(1 - X_D) + X_D \left(1 + 1.4 \left(\frac{x_2}{x_1} \right) \right) (1 - \varepsilon_{av,2})} \quad (4.20)$$

and for a packed bed rich in large particles:

$$\varepsilon_{av} = 1 - \frac{1 - \varepsilon_{av,1}}{X_D \left(1 + \left(\frac{x_2}{x_1} \right)^{\frac{1}{3}} \left(\left(1 + \frac{1 - X_D}{X_D} \right)^{\frac{1}{3}} - 1 \right) \right)^3} \quad (4.21)$$

where x_1 is the size of large particles (fibres in this case) and x_2 the size of small particles (rutile in this case)⁵. Correspondingly, $\varepsilon_{av,1}$ and $\varepsilon_{av,2}$ are the average porosities of pure fibre and rutile filter cakes, respectively. Briefly, equation (4.20) attempts to describe the penetration of large particles into a packed bed of fines and equation (4.21) attempts to describe the penetration of fines into a packed bed of large particles. Plots of equations (4.20) and (4.21) vs. solids composition, with equation (4.20) emanating from the pure fine component and equation (4.21) emanating from the pure large component, will result in two curves which intersect at some intermediate solids composition. This point of intersection is generally taken to be representative of a minimum porosity and indicates a transition from one dominant mechanism to another. Discontinuation of these two curves beyond the intersection point results in one smooth curve which attempts to describe the variation of porosity with solids composition. Further details of

⁵ The original form of Tokumitsu's equations is presented in Section 2.6.

the physical meaning behind equations (4.20) and (4.21) are given in Section 2.6 and by Abe and Hirose (1982).

The difficulty in determining an appropriate value for fibre ‘size’ for input into equation (4.21) led to, in the first instance, the use of the fibre median width of $15\ \mu\text{m}$ to represent fibre ‘size’. Predictions of ε_{av} given by equations (4.20) and (4.21) for cakes formed from suspensions in deionised water at 450 kPa are plotted in Figure 4.24 along with the experimental data to illustrate a typical theoretical prediction assuming interparticle penetration.

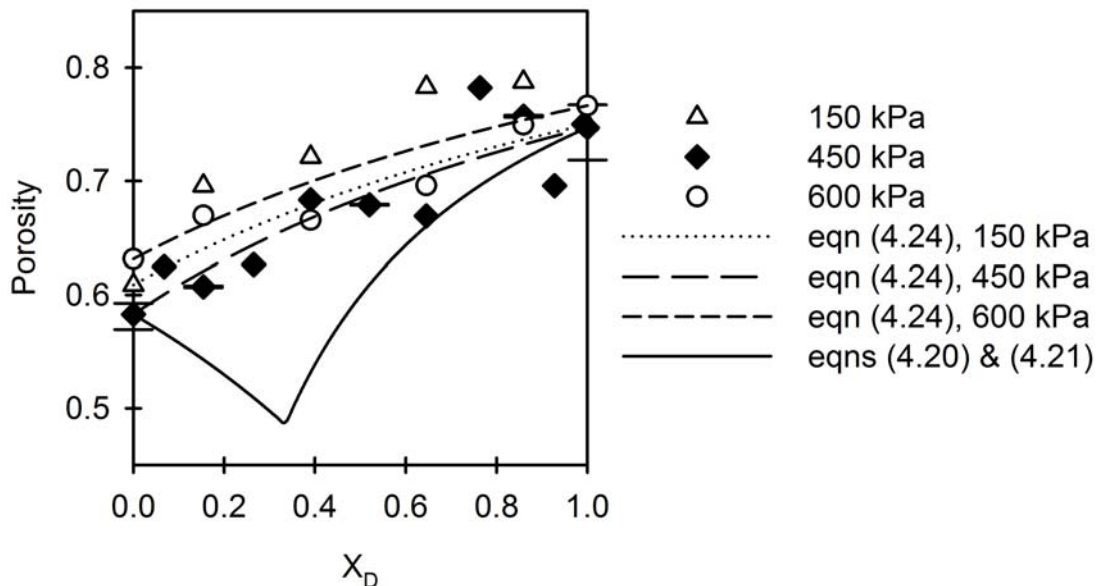


Figure 4.24: Effects of solids composition on ε_{av} for filtrations from deionised water at constant pressures of 150, 450 and 600 kPa. The prediction given by equations (4.20) and (4.21), Tokumitsu model, is included for the 450 kPa data and predictions given by equation (4.24), Shirato model, are included for all pressures.

Similar results were obtained using equations (4.20) and (4.21) on the 150 and 600 kPa data. In general, similar trends were also obtained when an ‘equivalent packing diameter’, x_{p1} , was used instead of x_1 (fibre width) in equations (4.20) and (4.21) (see

Appendix C). Previous researchers (Yu and Standish, 1993; Yu *et al.*, 1993) have claimed that the equivalent packing diameter is a useful concept in relating non-spherical packing to spherical packing. The equivalent packing diameter (x_{p1}) of a non-spherical solid is defined by Yu and Standish (1993) and Yu *et al.* (1993) as the diameter of a sphere having the same size-dependent packing behaviour as the solid and can be expressed for a cylindrical fibre as:

$$x_{p1} = \left(3.1781 - 3.6821 \frac{1}{\psi} + 1.5040 \frac{1}{\psi^2} \right) \left(1.145 \left(\frac{l_1}{x_1} \right)^{\frac{1}{3}} x_1 \right) \quad (4.22)$$

where ψ is the fibre sphericity and l_1 the fibre length. Fibre lengths were calculated assuming an aspect ratio of 100; see Section 3.5.2 for fibre characterisation. Assuming the fibre to be cylindrical, the fibre sphericity is given by:

$$\psi = 2.621 \frac{\left(\frac{l_1}{x_1} \right)^{\frac{2}{3}}}{1 + 2 \left(\frac{l_1}{x_1} \right)} \quad (4.23)$$

It should be noted that the fibres were shown to be non-cylindrical with more angular edges (Section 3.5.2). However, approximating the fibres to a cylindrical form appears to be a reasonable approach and comparisons with another interparticle penetration model (Dias *et al.*, 2004) seems to validate the claims made by Yu and co-workers that the equivalent packing diameter is a useful concept in relating non-spherical packing to spherical packing (again, see Appendix C).

Using the Shirato additive law, the additive porosity is given by the sum of the void volumes divided by the sum of the total volumes due to each component:

$$\varepsilon_{av} = \frac{\frac{\varepsilon_{av,1} X_D}{1 - \varepsilon_{av,1}} + \frac{\varepsilon_{av,2} (1 - X_D)}{1 - \varepsilon_{av,2}}}{\frac{X_D}{1 - \varepsilon_{av,1}} + \frac{1 - X_D}{1 - \varepsilon_{av,2}}} \quad (4.24)$$

Table 4.2 illustrates how Shirato *et al.* (1963) arrived at equation (4.24). Predictions of ε_{av} given by the Shirato additive law are also plotted in Figure 4.24.

Table 4.2: A breakdown of the Shirato additive law (equation (4.24)).

	First component	Second component
Volume fraction	X_D	$1 - X_D$
Porosity in pure state at a given pressure	$\varepsilon_{av,1}$	$\varepsilon_{av,2}$
Total bed volume in pure state due to component	$\frac{X_D}{1 - \varepsilon_{av,1}}$	$\frac{1 - X_D}{1 - \varepsilon_{av,2}}$
Associated void volume	$\frac{\varepsilon_{av,1} X_D}{1 - \varepsilon_{av,1}}$	$\frac{\varepsilon_{av,2} (1 - X_D)}{1 - \varepsilon_{av,2}}$

From Figure 4.24 it is seen that equation (4.24) represents the behaviour of the rutile/fibre system better than equations (4.20) and (4.21) and assuming the theoretical justifications of either model is correct, this brings about some physical implications. As discussed by Heertjes and Zuideveld (1978), a drawback of the Shirato additive law is that the filling of a pore volume generated by one component by another (finer) component cannot be described. This filling of pore volume can be expected to occur when the fines are free to migrate within the cake structure. However, it has previously been shown when discussing sedimentation results (Section 4.2.2) that rutile-fibre aggregation occurs, as observed visually and evidenced by the fact that mixtures settled far more readily than pure component suspensions. Considering the fibre and rutile shapes and the size distributions, the fibres may be coated by rutile to reduce the interfibre porosity to a small extent; the schematic representation in Figure 4.25 is an attempt to illustrate this.

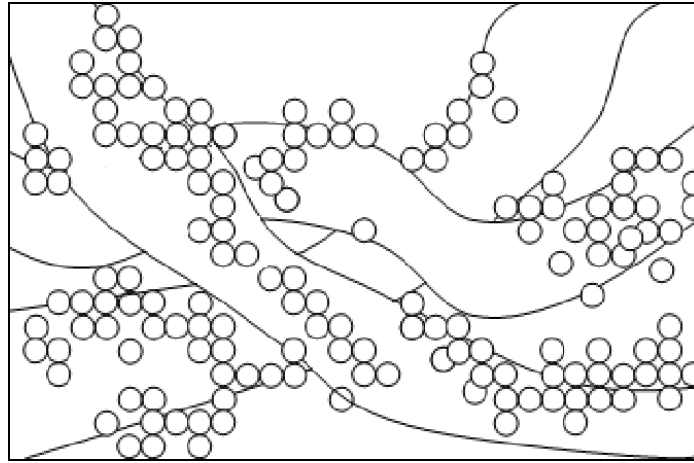


Figure 4.25: Schematic representation of the rutile particles coating the fibre surfaces. The schematic is not to scale and the rutile particles have been represented by spheres.

In Figure 4.25, it is suggested that the rutile particles deposit on fibre surfaces, where clusters of rutile form. Due to the significant size difference between rutile and fibres, these clusters result in a change in the fibre bed porosity towards the porosity of a pure rutile bed as the filter cake becomes richer in rutile. If the rutile was free to migrate within the fibrous bed instead of being held onto fibre surfaces, then one may have expected the trend as suggested by interparticle penetration models, where a maximum packing density (minimum porosity) would be evident at some intermediate solids composition. Figure 4.24 suggests that for the system investigated, the general concept of additive porosity seems to be better than interparticle penetration. Despite its simplicity and the criticism directed towards it, the Shirato additive law may still be useful in describing the packing of aggregating binary systems where adsorption of one solids component onto the surfaces of the other reduces the occurrence of fines freely migrating within the filter cake.

4.3.4.2. Effects of solids composition on specific resistance

The trend of α_{av} with solids composition for filtrations from deionised water passes through a minimum in the region $0.3 < X_D < 0.7$ (Figure 4.26). This minimum is an interesting result as in many cases specific resistance has previously been reported to decrease gradually and become lowest when $X_D = 1$ (for example, Shirato *et al.*, 1963; Wakeman, 1996). However, a similar minimum in α_{av} at an intermediate X_D value was more recently reported by Iritani *et al.* (2002) when aggregation occurred between the two solids (rutile and silica) being filtered from the binary mixture. Iritani *et al.* did not observe a minimum in α_{av} in the absence of such aggregation. Similarly, the most likely reason for the concave α_{av} vs. X_D trend observed in the present work is rutile-fibre aggregation. A contributing factor may be simultaneous sedimentation which leads to size classification within the cake where larger solids are more prevalent closer to the medium which promotes a reduced α_{av} .

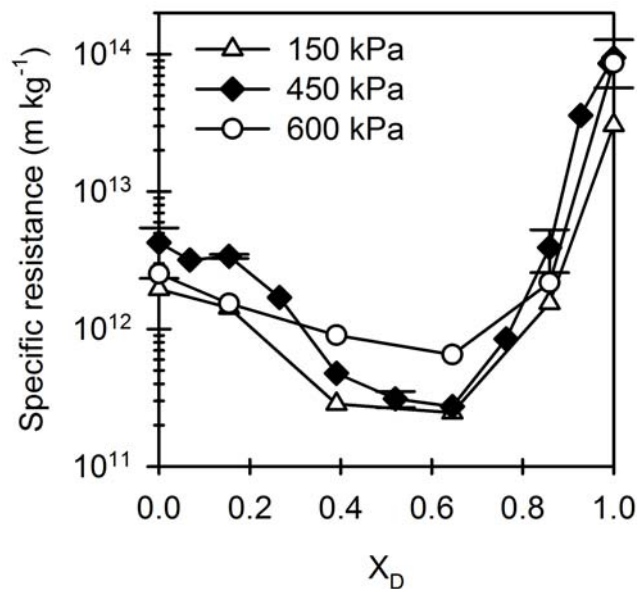


Figure 4.26: Effects of solids composition on α_{av} for filtrations from deionised water at constant pressures of 150, 450 and 600 kPa.

The α_{av} vs. X_D trend for suspensions in deionised water generally corresponds to the trend of initial settling rate vs. X_D (Figure 4.6) where the greatest initial settling rates were obtained in the region $0.3 < X_D < 0.6$; this is not surprising as the initial settling rates were largely influenced by the degree of aggregation. It is well known in flocculation/coagulation studies that a minimum specific resistance can coincide with a maximum settling rate. Further, the influence of simultaneous sedimentation with filtration is most significant for suspensions which give the greatest initial settling rates. However, a more explicit relationship between α_{av} and initial settling rate cannot be easily formulated because: (1) at higher fibre concentrations suspensions tend to become structured, thereby altering the settling behaviour; (2) settling rates will be reduced for loosely networked aggregates (lower effective density difference between the settling solids and suspending liquid); and (3) complications arise from simultaneous sedimentation during filtration.

An increase in fibre volume fraction (X_D) results in somewhat more porous cakes (larger ϵ_{av}) and also in a greater mean 'size'. Hence, increasing values of X_D may be expected to result in more permeable filter cakes (i.e. lower α_{av}). However, when fibres dominate the filtration further complexity is introduced by a fibre's ability to coil up and 'mat out' (Wakeman and Tarleton, 2005). Yet more complications arise due to the presence of solids of widely varying shapes and sizes in the fibrous suspension with fines potentially present under conditions conducive to blinding of the forming cake. Supporting evidence for the presence of fines is that filtrations of fibrous suspensions proceeded at an extremely slow rate using a 4 μm rated filter medium, and the turbidity of the supernatant of a fibrous suspension settled in deionised water was significantly greater than that of the corresponding supernatant in 0.1 M CaCl_2 (see Figure 4.2 for the corresponding settling curves).

Further theoretical and modelling analysis on the effects of interactions between the two solids in a binary mixture on the average specific resistance of a filter cake is discussed in Chapter 5. In Chapter 5, it is also discussed how aggregation may lead to a loss in effective specific surface, which in turn results in a decrease in specific resistance.

4.3.5. Effects of filtration pressure

The porosities of all binary mixture cakes were slightly greater at 150 kPa than at 450 and 600 kPa, presumably because the aggregates were able to maintain a more open structure at the lower pressure. However, in general the effects of filtration pressure on ε_{av} seemed to be limited. Also, the effects of filtration pressure on α_{av} are less evident relative to the effects of solids composition and solution environment. One noticeable effect on Figure 4.26 is the increase in α_{av} for filtrations of $0.3 < X_D < 0.7$ suspensions at the highest pressure of 600 kPa, which is perhaps not surprising as the extent of aggregation is seemingly greatest over this solids composition range and so the filter cake compressibility could reasonably be expected to be higher. A direct consequence of the increase in α_{av} is that the minimum observed in the α_{av} vs. X_D trend for filtrations at 600 kPa is less pronounced (Figure 4.26).

4.3.6. Effects of solution environment

With filtrations at 450 kPa, α_{av} values for rutile ($X_D < 0.3$) and fibre ($X_D > 0.7$) rich cakes were significantly lower for the suspensions in 0.2 M NaCl and in particular 0.1 M CaCl₂ solutions (Figure 4.23). The set of specific resistance data corresponding to filtrations with 0.1 M CaCl₂ were more in keeping with the rising ε_{av} vs. X_D trend. The CaCl₂ solution environment had a marginally greater effect on the filtration behaviour relative to the NaCl solution environment and this could be due to: (1) Ca²⁺ ions physically adsorbing onto the solids surfaces whereas Na⁺ ions behaved as an indifferent electrolyte (see Sections 3.5.1 and 3.5.2), and/or (2) the 0.1 M CaCl₂ solution being of a greater ionic strength. The ionic strength (I) of 0.2 M NaCl and 0.1 M CaCl₂ solutions were 0.2 and 0.6 respectively, as calculated using the Debye-Hückel theory (see Section 3.5.1). The larger ionic strength with 0.1 M CaCl₂ solution would tend to result in a greater reduction in the solids electrical double layer, and hence a lower specific resistance relative to the 0.2 M NaCl solution environment; this can be seen in Figure 4.23.

The reduction in α_{av} for feeds of pure rutile in CaCl_2 solution corresponded with increases in cake porosity and initial settling rate. The reduction in α_{av} for rutile rich cakes was therefore attributed to suppression of the rutile electrical double layer resulting in a larger effective particle size. The reduction in α_{av} for fibre rich cakes was more significant and more difficult to reconcile. A 0.1 M CaCl_2 solution environment reduced α_{av} values for pure fibre cakes by two orders of magnitude. Potential reasons include charge, packing and/or swelling effects.

Swelling of the fibres in CaCl_2 solution will result in a larger fibre size and hence tend to lower α_{av} . Although swelling may be a contributing factor, parameter proportionality shows that to solely account for the reduction in α_{av} the effective fibre 'size' will have to increase by more than ten times its original value in deionised water. This parameter proportionality was assessed using the Kozeny-Carman theory (Wakeman and Tarleton, 2005). An increase in fibre effective 'size' by an order of magnitude seems unlikely since it is difficult to imagine a cluster of ten fibres. Changes to fibre packing in the presence of CaCl_2 may alter the volume specific surface in contact with the fluid (S_v). To solely account for the reduction in α_{av} , S_v would need to decrease by approximately fifteen times its original value in deionised water (again assessed using the Kozeny-Carman theory). Due to the high aspect ratio of the fibres, such a reduction in S_v may be plausible via changes in fibre packing. Although charge effects on fibres may initially appear to be insignificant due to the relatively large fibre dimensions, it is perhaps the most likely reason for the reduction in α_{av} . The fines present in the fibre suspensions may have been removed (aggregated) in the presence of CaCl_2 . The fines, along with wide shape and size distributions, may be responsible for the large α_{av} value with feeds of pure fibre in deionised water in the first place. The presence of fines was previously suggested in Section 4.3.4.2 and is supported by the fact that filtrations of fibre suspensions proceeded at an extremely slow rate using a 4 μm rated filter medium. The fines aggregation hypothesis is further supported by the fact that: 1) at a lower solids concentration (0.16% v/v), the initial settling rate for pure fibres was greater in 0.1 M CaCl_2 solution than in deionised water; (2) the supernatant of a settled fibre suspension in deionised water was significantly more turbid than the supernatant of a corresponding suspension in 0.1 M CaCl_2 solution; and (3) the fibrous solids were close to their iso-electric point in 0.1 M CaCl_2 (see Figure 3.19).

Taking into account that the fibres and rutile were oppositely charged in 0.1 M CaCl_2 solution, the effect of CaCl_2 solution environment on rutile-fibre interactions could be expected to be greater than on rutile-rutile and fibre-fibre interactions as rutile-fibre electrostatic repulsions were not just reduced but altered to become attractive forces. Hence the 0.1 M CaCl_2 solution environment may have been expected to cause a greatest effect in the intermediate solids composition range (in the region $0.3 < X_D < 0.7$). However, although there is a significant difference in α_{av} with rutile rich ($X_D < 0.3$) and fibre rich ($0.7 < X_D$) cakes due to the three different solution environments, there was little variation in ε_{av} (Figure 4.25) and α_{av} (Figure 4.26) due to NaCl and CaCl_2 addition in the solids composition range $0.3 < X_D < 0.7$. This apparent discrepancy may be explained by the fact that α_{av} cannot be expected to continually decrease and ε_{av} to continually increase with increased states of aggregation as there will eventually be a lower limit to the packing fraction under a given applied pressure. This limit seems to have already been reached by filter cakes formed from suspensions in deionised water over the solids composition range $0.3 < X_D < 0.7$.

4.4. CONCLUSIONS

Filtration data presented in this chapter indicate the significance of physico-chemical interactions as the most likely cause of minima in the trend of α_{av} with solids composition for feeds in deionised water. In general, the relationship between α_{av} and solids composition corresponded with the sedimentation data. The influence of solids composition was most pronounced in the absence of NaCl and CaCl_2 and the influence of solution environment was most pronounced at the extremes of solids composition (i.e. rutile rich and fibre rich). For rutile rich cakes, the reduction in α_{av} due to 0.2 M NaCl and 0.1 M CaCl_2 solution environments were most likely via suppression of the rutile electrical double layer. For fibre rich cakes, although several hypotheses have been postulated, definitive reasons for the reduction in α_{av} due to NaCl and CaCl_2 addition were not apparent. Compared to the influence of solids composition and solution environment, the influence of filtration pressure on α_{av} was less significant. The general concept of additive porosity seems to be better than interparticle penetration

with the rutile/fibre system, and this was attributed to rutile coating fibre surfaces instead of more freely migrating within the filter cake.

REFERENCES

- Abe E. and Hirose H. (1982) Porosity estimation of a mixed cake in body filtration. *J. Chemical Engineering Japan* **13**, 490-493.
- Dias R., Teixeira J.A., Mota M. and Yelshin A. (2004) Particulate binary mixtures: Dependence of packing porosity on particle size ratio, *Industrial Engineering Chemistry Research* **43**, 7912-7919.
- Happel J. and Brenner H. (1965) *Low Reynolds Number Hydrodynamics*. Prentice-Hall, Englewood Cliffs, N.J.
- Heertjes P.M. and Zuideveld P.L. (1978) Clarification of liquids using filter aids, Part III: Cake resistance in surface filtration, *Powder Technology* **19**, 45-64.
- Iritani E., Mukai Y. and Toyoda Y. (2002) Properties of a filter cake formed in dead-end microfiltration of binary particulate mixtures, *J. Chemical Engineering Japan* **35**, 226-233.
- Leclerc D. (1975) Characteristics of unconsolidated filter media. In: *The Scientific Basis of Filtration*. Ives K.J. (Ed.) Nato Advanced Study Institute Series. Noordhoff-Leyden, Cambridge.
- McGeary R.K. (1961) Mechanical packing of spherical particles. *J. American Ceramic Society* **44**, 513-522.
- Mota M., Teixeira J.A., Bowen W.R. and Yelshin A. (2001) Binary spherical particle mixed beds: Porosity and permeability relationship measurement. *Filtration* **1**(4), 101-106.
- Shirato M., Sambuichi M. and Okamura S. (1963) Filtration behavior of a mixture of two slurries. *American Institute Chemical Engineers J.* **9**, 599-605.

Tokumitsu Y. (1964) On the packing of granular materials. *J. Material Science Japan* **13**, 752-758.

Yu A.B. and Standish N. (1993) Characterisation of non-spherical particles from their packing behaviour. *Powder Technology* **74**, 205-213.

Yu A.B., Standish N. and McLean A. (1993) Porosity calculation of binary mixtures of nonspherical particles. *J. American Ceramic Society* **76**, 2813-2816.

Wakeman R.J. (1996) Characteristics of filtration using solids added to the suspension as a body aid. *Proc. 7th World Filtration Congress*, pp.234-238, **1**, Budapest.

Wakeman R.J. and Tarleton E.S. (2005) *Solid/Liquid Separation: Principles of Industrial Filtration*. Elsevier, Oxford.

CHAPTER 5: FURTHER DISCUSSION AND MODELLING

5.1. INTRODUCTION

The permeability of a filter cake is the most important factor in cake filtration (in relation to filter design and scale-up) and is often interpreted through a measure of the cake's specific resistance. Models for flow through porous media are generally based on Darcy's law, which uses a single parameter (the permeability) to account for the characteristics of the porous medium in so far as they affect fluid flow. There have been many attempts to relate permeability to the geometric considerations of a porous medium. One of the most widely used of these theories is that due to Kozeny-Carman. In this theory, fluid flowing through a porous body loses energy where it is in contact with the internal surfaces of the body; these surfaces generally possess a very complex geometry which cannot be easily described mathematically, but for practical purposes can be interpreted through the body's porosity and specific surface (Wakeman and Tarleton, 2005). The Kozeny-Carman theory is based on the internal pores being represented by a bundle of capillary tubes whose orientation is at 45° to the fluid inflow face of the porous medium. The theory has received some criticism, which is largely undeserved since it correlates bed resistance data for a wider range of porous media types than any other permeability theory. Although the combination of the Kozeny-Carman equation and Darcy's law provide a relatively well established basis for determining the specific surface of particle samples from permeability data and correlating resistance data for fluid flow through a porous bed consisting of a single component solid, the situation is less obvious for binary mixtures.

A particular objective of this chapter is to assist in the interpretation of the filtration results presented in Section 4.3. In this chapter, the combined use of the Kozeny-Carman equation and Darcy's law is presented and discussed in relation to application in the filtration of binary mixtures. Upon close study, this approach is shown to have its limitations, particularly when significant aggregation takes place between the two solids phases. The difficulties in overcoming these limitations from a purely

fundamental basis are highlighted, and a semi-empirical model is presented and discussed.

5.2. MODEL DERIVATION

Abe *et al.* (1979) had previously derived a model to predict the average specific cake resistance of binary mixtures based on the Darcy and Kozeny-Carman equations. The model derivation is briefly presented here together with further development, starting from the Kozeny-Carman equation:

$$\Delta P = \frac{5S_0^2(1-\varepsilon_{av})^2}{\varepsilon_{av}^3} Lu\mu \quad (5.1)$$

The height of the packed bed is given by:

$$L = \frac{v}{1-\varepsilon_{av}} \quad (5.2)$$

and substituting (5.2) into (5.1) gives:

$$\Delta P = \frac{5S_0^2(1-\varepsilon_{av})}{\varepsilon_{av}^3} vu\mu \quad (5.3)$$

Pressure drop across the cake is also given by:

$$\Delta P = u\mu R_c \quad (5.4)$$

Replacing the resistance of the cake with the average specific cake resistance leads to:

$$\Delta P = u\mu\alpha_{av}w \quad (5.5)$$

Substituting (5.5) into (5.3) and rearranging gives:

$$\alpha_{av} = \frac{5(1-\varepsilon_{av})}{\varepsilon_{av}^3} S_0^2 \frac{v}{w} \quad (5.6)$$

But v/w is the inverse of the packed bed true density, expressed by equation (5.7):

$$\frac{v}{w} = \frac{1}{X_D \rho_1 + (1 - X_D) \rho_2} \quad (5.7)$$

Substituting equation (5.7) into equation (5.6) gives:

$$\alpha_{av} = \frac{5(1 - \varepsilon_{av})}{\varepsilon_{av}^3 (X_D \rho_1 + (1 - X_D) \rho_2)} S_0^2 \quad (5.8)$$

Assuming an ‘additive’ mechanism, the specific surface of the binary mixture at a given solids composition can be expressed in terms of the effective specific surface of the two solids components⁶:

$$S_0 = X_D \frac{S_1}{\phi_1} + (1 - X_D) \frac{S_2}{\phi_2} \quad (5.9)$$

Substituting (5.9) into (5.8) gives:

$$\alpha_{av} = \frac{5(1 - \varepsilon_{av})}{\varepsilon_{av}^3 (X_D \rho_1 + (1 - X_D) \rho_2)} \left(\frac{X_D S_1}{\phi_1} + \frac{(1 - X_D) S_2}{\phi_2} \right)^2 \quad (5.10)$$

Abe *et al.* (1979) related the specific surface to particle size (assuming spherical particles) and referred to ϕ_i (where $i = 1$ for solids component 1 and 2 for solids component 2) as a surface factor without providing a clear explanation of the parameter. In this thesis, no relationship between specific surface and particle size is assumed and ϕ_i is (perhaps more appropriately) termed a shape factor. Also, the term S_i/ϕ_i is kept as a ratio and not broken up since little is known about the exact relative magnitudes of either S_i or ϕ_i . ϕ_i can be thought of as a lumped parameter taking into account sphericity, surface roughness, as well as pure component size distribution and surface interactions. Hence, S_i can be considered to be the specific surface that corresponds to idealised spheres. As pointed out by Donohue and Wensrich (2009), although a shape factor can be used to account for irregular particles, it must be determined empirically. The effective specific surface (S_i/ϕ_i) for both components in equation (5.9) is determined using the specific resistance and porosity values of a cake formed from filtration of a single component solid as:

⁶ The significance of equation (5.9) is discussed later, an alternate form is presented as equation (5.43).

$$\frac{S_i}{\phi_i} = \sqrt{\frac{\alpha_{av,i} \varepsilon_{av,i}^3 \rho_{s,i}}{5(1 - \varepsilon_{av,i})}} \quad (5.11)$$

where $i = 1$ for the first pure solids component or 2 for the second; for the data in this thesis, 1 refers to fibres and 2 to rutile. Equation (5.11) was obtained from equation (5.10) by substituting for $X_D = 0$ or 1 for the two pure solids components, and rearranging.

The ratio of effective specific surfaces is a commonly recurring parameter and is defined by S_B according to equation (5.12):

$$S_B = \frac{S_1 / \phi_1}{S_2 / \phi_2} \quad (5.12)$$

Using equation (5.11) to determine the effective specific surfaces in equation (5.12) leads to:

$$S_B = \sqrt{\frac{\alpha_{av,1} \varepsilon_{av,1}^3 (1 - \varepsilon_{av,2}) \rho_1}{\alpha_{av,2} \varepsilon_{av,2}^3 (1 - \varepsilon_{av,1}) \rho_2}} \quad (5.13)$$

Substituting equation (5.12) into equation (5.10) and manipulating gives:

$$\alpha_{av} = \frac{5(1 - \varepsilon_{av})}{\varepsilon_{av}^3 (X_D \rho_1 + (1 - X_D) \rho_2)} \left(X_D + (1 - X_D) \frac{1}{S_B} \right)^2 \left(\frac{S_1}{\phi_1} \right)^2 \quad (5.14)$$

It should be noted that S_B as defined in equation (5.13) refers to the ratio of pure component specific surfaces, with a pure component's specific surface determined from equation (5.11). However, a pure component's effective specific surface may vary in the presence of another solids component due to physico-chemical effects and/or varying packing mechanisms. If the changes in S_1/ϕ_1 and S_2/ϕ_2 are disproportionate, then S_B will vary with solids composition. It is not known how, if at all, S_B varies with solids composition. These possibilities are explored further in the next section.

5.3. ANALYSIS OF THE MODEL CHARACTERISTICS

Experimental data for filtrations from deionised water show a minimum in specific resistance as illustrated in Figure 4.24. It is interesting to see how the model derived in Section 5.2 represents the experimental data, in particular the minimum observed in the specific resistance vs. solids composition trend. However, before direct application of the model to the experimental data, the general characteristics of the model are first discussed. The conditions under which minima in specific resistance can be obtained at some intermediate solids composition and the role of specific surface in the model are investigated using various assumptions. The validity of these assumptions is also assessed.

5.3.1. Analysis assuming constant porosity and effective specific surface

Assuming that average cake porosity, and the effective specific surface values of the two solids components (S_1/ϕ_1 and S_2/ϕ_2) remain constant (invariant with respect to solids composition), a minimum or maximum in average specific cake resistance can only be obtained if:

$$\left. \frac{d\alpha_{av}}{dX_D} \right|_{\varepsilon_{av}, \frac{S_i}{\phi_i}} = 0 \quad (5.15)$$

Carrying out the differentiation (presented in detail in Appendix D) leads to:

$$X_D = \frac{1}{S_B - 1} - \frac{2\rho_2}{\rho_1 - \rho_2} \quad (5.16)$$

Utilising the fact that a minimum in specific resistance is to occur when $0 < X_D < 1$ leads to (again, see Appendix D):

$$\frac{2\rho_1}{\rho_1 + \rho_2} < S_B < \frac{\rho_1 + \rho_2}{2\rho_2} \quad (5.17)$$

Equation (5.17) is an interesting result as it outlines the range of S_B , exclusively in terms of the two pure solids densities, within which a minimum or maximum in α_{av} could

occur at some intermediate solids composition; the equation should, in theory, hold for any binary mixture where the average cake porosity and effective specific surface values of the two solids components do not vary with solids composition.

As an example, under the current experimental conditions with fibre/rutile mixtures, a minimum or maximum in α_{av} at some intermediate solids composition will only be obtained if (substituting for fibre and rutile densities):

$$0.47 < S_B < 0.66 \quad (5.18)$$

According to equation (5.13), the expression represented in equation (5.18) is not met experimentally if S_B values are calculated from the pure component filtration data. From the values calculated using data from filtrations with deionised water, S_B was approximately 3.7, 4.6 and 5.5 for filtrations at 150, 450 and 600 kPa, respectively; these values are an order of magnitude above the range specified by equation (5.18). The next step will therefore be to examine the role of variations in porosity.

5.3.2. Analysis assuming constant effective specific surface

The porosity variation with solids composition can be represented by an appropriate model (such as interparticle penetration or the Shirato additive law) to keep the model independent of experimental data for intermediate solids compositions. When no appropriate existing model can be applied, the experimental data may be directly used. It has been previously shown (Section 4.3.4) that the average porosity of cakes resulting from filtrations with deionised water can be adequately represented by Shirato's additive law (equation (4.24)). Substituting equation (4.24) into equation (5.10) results in:

$$\alpha_{av} = \frac{\left(1 - \frac{\left(\frac{\varepsilon_{av,1} X_D}{1 - \varepsilon_{av,1}} + \frac{\varepsilon_{av,2} (1 - X_D)}{1 - \varepsilon_{av,2}} \right)}{\left(\frac{X_D}{1 - \varepsilon_{av,1}} + \frac{1 - X_D}{1 - \varepsilon_{av,2}} \right)} \right)^2 \left(X_D \frac{S_1}{\phi_1} + (1 - X_D) \frac{S_2}{\phi_2} \right)^2}{\left(\frac{\varepsilon_{av,1} X_D}{1 - \varepsilon_{av,1}} + \frac{\varepsilon_{av,2} (1 - X_D)}{1 - \varepsilon_{av,2}} \right)^3 (X_D \rho_1 + (1 - X_D) \rho_2)} \quad (5.19)$$

Assuming that the effective specific surface values of the two solids components remain constant (invariant with respect to solids composition), a minimum or maximum in average specific cake resistance can only be obtained if:

$$\left. \frac{d\alpha_{av}}{dX_D} \right|_{\frac{S_i}{\phi_i}} = 0 \quad (5.20)$$

Carrying out the differentiation (presented in Appendix D) gives:

$$\begin{aligned} & \frac{2}{X_D \frac{S_1}{\phi_1} + (1 - X_D) \frac{S_2}{\phi_2}} \left(\frac{S_1}{\phi_1} - \frac{S_2}{\phi_2} \right) - 3 \frac{\frac{\varepsilon_{av,1}}{1 - \varepsilon_{av,1}} - \frac{\varepsilon_{av,2}}{1 - \varepsilon_{av,2}}}{\frac{\varepsilon_{av,1} X_D}{1 - \varepsilon_{av,1}} + \frac{\varepsilon_{av,2} (1 - X_D)}{1 - \varepsilon_{av,2}}} \\ & - \frac{\rho_1 - \rho_2}{X_D \rho_1 + (1 - X_D) \rho_2} + 2 \frac{\frac{1}{X_D} - \frac{1}{1 - X_D}}{\frac{1}{1 - \varepsilon_{av,1}} - \frac{1}{1 - \varepsilon_{av,2}}} = 0 \end{aligned} \quad (5.21)$$

Utilising the fact that a minimum in specific resistance is to occur when $0 < X_D < 1$ leads to equation (5.22) (the algebraic manipulation is given in Appendix D).

$$\frac{1}{\left(1.5 \frac{\varepsilon_{av,2}}{\varepsilon_{av,1}} - 1 \right) \left(\frac{1 - \varepsilon_{av,1}}{1 - \varepsilon_{av,2}} \right) + 0.5 \frac{\rho_2}{\rho_1}} < S_B < \left(1.5 \frac{\varepsilon_{av,1}}{\varepsilon_{av,2}} - 1 \right) \left(\frac{1 - \varepsilon_{av,2}}{1 - \varepsilon_{av,1}} \right) + 0.5 \frac{\rho_1}{\rho_2} \quad (5.22)$$

Equation (5.22) is another interesting result as it outlines the range of S_B , in terms of the two pure solids densities and pure component ε_{av} , within which a minimum or maximum in α_{av} could occur at some intermediate solids composition. This equation should, in theory, hold for any binary mixture where the effective specific surface values of the two solids components do not vary with solids composition and the ε_{av} vs. solids composition trend can be satisfactorily represented by the Shirato additive law.

As an example, substituting fibre and rutile densities and pure component porosities into equation (5.22), reveals that under the current experimental conditions, a minimum or maximum in α_{av} at some intermediate solids composition will only be obtained if (the data for filtrations from deionised water at 450 kPa was used here as an example, filtrations at other pressures result in similar limits):

$$0.58 < S_B < 1.67 \quad (5.23)$$

In a similar way to the analysis in Section 4.4.2.1., the expression in equation (5.23) is not met experimentally if S_B values are calculated from the pure component suspension data (using equation (5.13)); as noted previously, values for S_B are approximately 3.7, 4.6 and 5.5 for filtrations with deionised water at 150, 450 and 600 kPa, respectively.

It has been shown that accounting for the variation in porosity using the Shirato additive law increases the range of limits for S_B within which a minimum in specific resistance at some intermediate composition is possible. Also, the experimentally obtained values of S_B are closer to the limits set by equation (5.23) than equation (5.18), however, the experimental values of S_B are still outside the range specified by equation (5.23). As a consequence, equation (5.19) will not be able to represent the experimental data for filtrations with deionised water if it is assumed that the effective specific surface of the two solids components remains constant. Furthermore, in the filtration of binary mixtures, the surface area per unit volume of the two solids components in contact with the permeating fluid may vary with solids composition. The next step will therefore be to analyse the role of effective specific surface.

5.3.3. Analysis of the role of effective specific surface in the model

A family of curves were drawn using equation (5.19) with S_B across the range specified by equation (5.23), by varying first S_1/ϕ_1 keeping S_2/ϕ_2 constant (Figure 5.1), and then S_2/ϕ_2 keeping S_1/ϕ_1 constant (Figure 5.2). For the purpose of this illustrative example, the curves in Figure 5.1 were plotted using the value of S_2/ϕ_2 as determined from equation (5.11) with experimental data from a 450 kPa filtration of a pure rutile suspension in deionised water. Values of S_1/ϕ_1 were varied such that S_B ranged from 0.3 to 4.6. Similarly, for the curves in Figure 5.2, S_1/ϕ_1 was determined from equation (5.11) with experimental data from a 450 kPa filtration of a pure fibre suspension in deionised water. Values of S_2/ϕ_2 were varied such that S_B ranged from 0.3 to 4.6. The pure component porosities used were from the 450 kPa pure component filtrations with deionised water. Tables 5.1 and 5.2 summarises the effective specific surface values of the two solids components used in Figures 5.1 and 5.2, respectively.

It is noted that the curves corresponding to $S_B = 4.6$ in Figures 5.1 and 5.2 are identical since for this curve, both S_1/ϕ_1 and S_2/ϕ_2 were calculated from equation (5.11) using data from 450 kPa filtrations of pure fibre and pure rutile suspensions in deionised water, respectively. The modelled curve when $S_B = 4.6$ is therefore meant to correspond to the present work's experimental data if it is assumed that the fibre and rutile effective specific surfaces do not vary with solids composition, and is equal to the value obtained from the pure component filtrations. However, the $S_B = 4.6$ curve (Figures 5.1 and 5.2) shows a gradual increase in α_{av} from pure rutile to pure fibres; no minimum in α_{av} at an intermediate solids composition is obtained. Also, even with the hypothetical curves which show a minimum, the minimum shown is not as pronounced as that obtained experimentally. This apparent discrepancy may not be surprising since, as noticed visually and evidenced by the sedimentation data (where both pure component suspensions do not settle but settling rates are significantly increased for mixtures), the physical nature of the binary suspensions are altered synergistically. An analysis of the behaviour of an interacting binary suspension cannot be made by a simplistic extrapolation from the known behaviour of the two pure component suspensions.

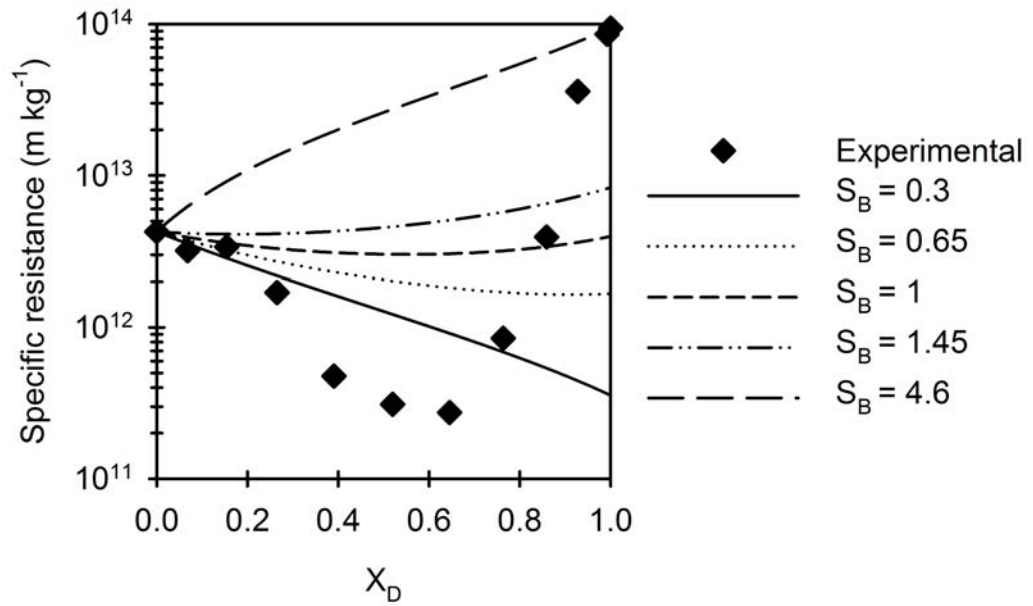


Figure 5.1: Family of curves obtained using equation (5.19), varying S_1/ϕ_1 and keeping S_2/ϕ_2 constant. Experimental data from 450 kPa filtrations with deionised water is included. The parameters used for the curves are summarised in Table 5.1.

Table 5.1: Parameters for the curves plotted in Figure 5.1 at the various S_B .

S_B	S_1/ϕ_1 (m^{-1})	S_2/ϕ_2 (m^{-1})
0.3	1.31×10^7	4.36×10^7
0.65	2.83×10^7	4.36×10^7
1	4.36×10^7	4.36×10^7
1.45	6.32×10^7	4.36×10^7
4.6	2.00×10^8	4.36×10^7

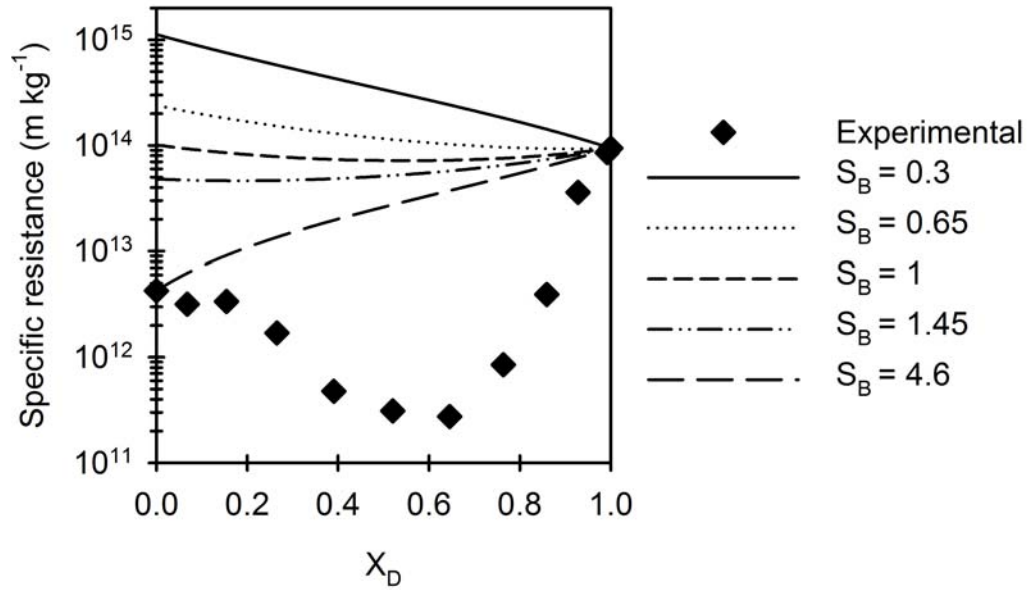


Figure 5.2: Family of curves obtained using equation (5.19), varying S_2/ϕ_2 and keeping S_1/ϕ_1 constant. Experimental data from 450 kPa filtrations with deionised water is included. The parameters used for the curves are summarised in Table 5.2.

Table 5.2: Parameters for the curves plotted in Figure 5.2 at the various S_B .

S_B	S_1/ϕ_1 (m^{-1})	S_2/ϕ_2 (m^{-1})
0.3	2.00×10^8	6.67×10^8
0.65	2.00×10^8	3.08×10^8
1	2.00×10^8	2×10^8
1.45	2.00×10^8	1.38×10^8
4.6	2.00×10^8	4.36×10^7

5.3.3.1. Analysis assuming a constant value of S_B

It is seen from Figures 5.1 and 5.2 that equation (5.19) cannot adequately represent the experimental data and this was attributed to rutile-fibre aggregation resulting in a decreased effective specific surface for both solids. The next step will therefore be to account for variations in effective specific surface across the range of solids composition. In the first instance, it is assumed that S_1/ϕ_1 and S_2/ϕ_2 may vary with solids composition, but vary such that the ratio S_B stays approximately constant.

It may be expected that the greater the extent of aggregation, the lower the effective specific surface; this is generally the motivation behind inducing aggregation during chemical pretreatment of a slurry before filtration. The extent of aggregation is expected to be affected by parameters such as solids composition, solution environment and filtration pressure. However, it is very difficult to experimentally obtain accurate information regarding the effective specific surface of the two solids components in an interacting binary mixture under the various conditions (as required for predictions of specific resistance of cakes consisting of two solids phases). Therefore, a simplifying assumption is used and its validity is subsequently assessed. Essentially, what is investigated is how much S_1/ϕ_1 and S_2/ϕ_2 will have to vary over the range of solids compositions, filtration pressures and solution environments in order to match the experimental filtration data, assuming constant S_B .

Using the Kozeny-Carman model, the relevant equation used to estimate the specific surface of particles forming a single component porous bed from fluid flow data is given as:

$$S_0 = \sqrt{\frac{\alpha_{av} \varepsilon_{av}^3 \rho_s}{5(1 - \varepsilon_{av})^2}} \quad (5.24)$$

To the author's knowledge, a corresponding equation for binary mixture porous beds has not been previously discussed in literature. Considering the derivation outlined in Section (5.2), a framework is hereby presented for estimation of the effective specific surface of the two solids components in a binary mixture porous bed, assuming that the ratio of effective specific surfaces, S_B , remains constant. The validity of this framework

is then assessed, particularly in relation to the assumption of S_B not varying with solids composition.

Rearranging equation (5.14) gives:

$$\frac{S_1}{\phi_1} = \frac{\alpha_{av} \varepsilon_{av}^3 (X_D \rho_1 + (1 - X_D) \rho_2)}{\sqrt{5(1 - \varepsilon_{av}) \left(X_D + (1 - X_D) \frac{1}{S_B} \right)^2}} \quad (5.25)$$

Similarly, the specific surface of the small component (rutile in this thesis) is given by:

$$\frac{S_2}{\phi_2} = \frac{\alpha_{av} \varepsilon_{av}^3 (X_D \rho_1 + (1 - X_D) \rho_2)}{\sqrt{5(1 - \varepsilon_{av}) (X_D S_B + (1 - X_D))^2}} \quad (5.26)$$

It was previously shown in Section 4.3.4 that, for suspensions in deionised water, the relationship between average porosity and solids composition can be represented adequately by the Shirato additive law (equation 4.24). Substituting equation (4.24) into equations (5.25) and (5.26) gives equations (5.27) and (5.28), respectively:

$$\frac{S_1}{\phi_1} = \frac{\alpha_{av} \left(\frac{\varepsilon_{av,1} X_D + \varepsilon_{av,2} (1 - X_D)}{1 - \varepsilon_{av,1} + \frac{1 - \varepsilon_{av,2}}{X_D + (1 - X_D) \frac{1}{S_B}}} \right)^3 (X_D \rho_1 + (1 - X_D) \rho_2)}{\sqrt{5 \left(1 - \frac{\varepsilon_{av,1} X_D + \varepsilon_{av,2} (1 - X_D)}{1 - \varepsilon_{av,1} + \frac{1 - \varepsilon_{av,2}}{X_D + (1 - X_D) \frac{1}{S_B}}} \right)^2}} \quad (5.27)$$

$$\frac{S_2}{\phi_2} = \frac{\alpha_{av} \left(\frac{\frac{\varepsilon_{av,1} X_D + \varepsilon_{av,2} (1 - X_D)}{1 - \varepsilon_{av,1}} + \frac{1 - \varepsilon_{av,2}}{1 - \varepsilon_{av,2}}}{\frac{X_D}{1 - \varepsilon_{av,1}} + \frac{1 - X_D}{1 - \varepsilon_{av,2}}} \right)^3 (X_D \rho_1 + (1 - X_D) \rho_2)}{5 \left(\frac{\frac{\varepsilon_{av,1} X_D + \varepsilon_{av,2} (1 - X_D)}{1 - \varepsilon_{av,1}} + \frac{1 - \varepsilon_{av,2}}{1 - \varepsilon_{av,2}}}{\frac{X_D}{1 - \varepsilon_{av,1}} + \frac{1 - X_D}{1 - \varepsilon_{av,2}}} \right)^2 (X_D S_B + (1 - X_D))^2} \quad (5.28)$$

Equations (5.27) and (5.28) were used to plot the surfaces in Figure 5.3. As seen in Figure 5.3, the ratio of S_1/ϕ_1 to S_2/ϕ_2 (i.e. S_B) remains constant throughout. Also, at the minimum, it is seen that an approximately 10% reduction in effective specific surface for both solids is required to account for the experimental specific resistance data. Although the 10% reduction in effective specific surface appears reasonable, upon closer examination, the assumption of constant S_B does not. Like the rest of Section 5.3, this sub-section and Figure 5.3 are merely presented to serve as an illustrative analysis of the characteristics of the model derived in Section 5.2, using hypothetical scenarios.

Rutile-fibre interaction can be expected to alter the effective specific surface in contact with the permeating fluid. When a rutile particle coats a fibre surface, the total volume of the solids remains constant but the total area in contact with the permeating fluid is reduced. The magnitude of this reduction will depend on the total rutile-fibre contact area. To illustrate this dependence, equations (5.29) and (5.30) are presented:

$$\frac{S_1}{\phi_1} = \frac{n_1 A_1 - A_{cT}}{n_1 V_{av,1}} \quad (5.29)$$

$$\frac{S_2}{\phi_2} = \frac{n_2 A_2 - A_{cT}}{n_2 V_{av,2}} \quad (5.30)$$

where n_1 and n_2 are respectively the number of fibres and rutile particles, A_1 and A_2 are the average surface area (in contact with the permeating fluid) of a fibre and rutile particle assuming no rutile-fibre aggregation. $V_{av,1}$ and $V_{av,2}$ are the average volume of a

fibre and rutile particle, and A_{cT} the total rutile-fibre contact area. The effective specific surface of both fibres and rutile will decrease with increasing contact area (i.e. increasing extent of aggregation). Equations (5.29) and (5.30) are applicable to any interacting binary mixture and for the model developed in Section 5.2 to be physically meaningful in relation to interacting binary mixtures, this loss in effective specific surface will have to be accounted for. In Figure 5.3, this loss in specific surface due to rutile-fibre aggregation is essentially, and perhaps erroneously, accounted for by assuming a constant S_B , and then fitting the model to experimental data.

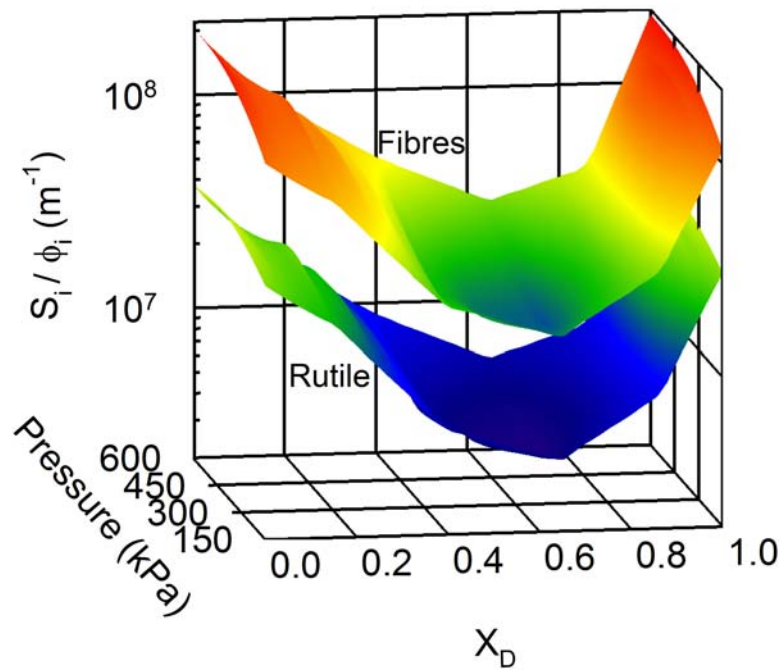


Figure 5.3: Variation in fibre (S_1/ϕ_1) and rutile (S_2/ϕ_2) specific surface area in contact with the permeating fluid (deionised water) as determined from equations (5.27) and (5.28) assuming S_B remains constant with solids composition. The corresponding experimental data for cake average specific resistance is shown in Figure 4.21.

From equations (5.12), (5.29) and (5.30), S_B can be expressed as:

$$S_B = \frac{(n_1 A_1 - A_{cT}) n_2 V_{av,2}}{(n_2 A_2 - A_{cT}) n_1 V_{av,1}} \quad (5.31)$$

Considering that the ratio of the total volumes of the two components can be expressed as:

$$\frac{n_1 V_{av,1}}{n_2 V_{av,2}} = \frac{X_D}{1 - X_D} \quad (5.32)$$

equation (5.31) can be re-written as:

$$S_B = \frac{(n_1 A_1 - A_{cT}) (1 - X_D)}{(n_2 A_2 - A_{cT}) X_D} \quad (5.33)$$

Physical reasoning, sedimentation and filtration data suggest that A_{cT} increases from 0 at $X_D = 0$ up to a maximum value at some intermediate solids composition and then decreases back to 0 at $X_D = 1$. With rutile or fibre rich mixtures, A_{cT} may be limited by the lack of surface area of the more scarce solids component. Furthermore, the values of A_1 and A_2 may vary across the range of solids composition, due to varying packing mechanisms and physico-chemical factors. Due to this highly non-linear relationship, the assumption of constant S_B is expected to be unreasonable. Some further inference can be made from equation (5.33), such as when $X_D \rightarrow 0$ (pure rutile), or when $X_D \rightarrow 1$ (pure fibres), the concept of S_B becomes meaningless. As $X_D \rightarrow 0$, $\frac{(n_1 A_1 - A_{cT})}{(n_2 A_2 - A_{cT})} \rightarrow 0$

and $\frac{1 - X_D}{X_D} \rightarrow \infty$, and as $X_D \rightarrow 1$, $\frac{(n_1 A_1 - A_{cT})}{(n_2 A_2 - A_{cT})} \rightarrow \infty$ and $\frac{1 - X_D}{X_D} \rightarrow 0$. Using this

approach of constant S_B , another concern will be that we do not know at which solids composition the relationship breaks down. Taking equation (5.27) for example, setting $X_D = 1$ results in the Kozeny-Carman equation for pure fibres (equation (5.24) for pure fibres). In other words, the limit for equation (5.27) is correct for when $X_D \rightarrow 1$. However, from equations (5.12) and (5.13), it should be possible to calculate S_2/ϕ_2 from S_1/ϕ_1 , according to:

$$\frac{S_2}{\phi_2} = \frac{S_1}{\phi_1} \sqrt{\frac{\alpha_{av,1} \varepsilon_{av,1}^3 (1 - \varepsilon_{av,2}) \rho_1}{\alpha_{av,2} \varepsilon_{av,2}^3 (1 - \varepsilon_{av,1}) \rho_2}} \quad (5.34)$$

Besides the fact that it makes little physical sense that S_2/ϕ_2 should depend on S_1/ϕ_1 as expressed by equation (5.34), it is seen that the limit for equation (5.34) is wrong for when $X_D \rightarrow 0$. Equation (5.34) does not approach the Kozeny-Carman equation for pure rutile. A similar analysis can be carried out on equation (5.28) which will give the correct limit for pure rutile, but if S_1/ϕ_1 is calculated from S_2/ϕ_2 using equations (5.12) and (5.13) and S_2/ϕ_2 , it is seen that the limit is wrong for when $X_D \rightarrow 1$. These erroneous limits are due to the assumption of constant S_B .

5.3.3.2. Analysis assuming two values of S_B

The initial approach taken to account for varying S_B was the simple case of S_B taking on two distinct values, one for rutile rich cakes and the other for fibre rich cakes. The idea behind this approach was that two separate mechanisms promoted the observed behaviour across the solids composition range; one mechanism was dominant for rutile rich cakes and the other for fibre rich cakes.

It was envisaged that, from the curves in Figure 5.1, further decreasing S_B whilst keeping S_2/ϕ_2 constant may eventually result a curve which represents the experimental data for rutile rich cakes. Similarly, from the curves in Figure 5.2, further increasing S_B and keeping S_1/ϕ_1 constant may eventually result in a curve which represents the experimental data for fibre rich cakes. These two corresponding values of S_B may then provide some insights into the two mechanisms. Figure 5.4 was therefore plotted to see if increasing S_B in Figure 5.2 will eventually result in a curve that represents the experimental data for fibre rich cakes. However, as seen from Figure 5.4 for instance, no matter how much S_B is increased, the experimental data is not represented. This is due to the fact that, as seen in Table 5.2 and equation (5.12), S_B is increased by decreasing S_2/ϕ_2 (rutile effective specific surface) whilst keeping S_1/ϕ_1 (fibre effective specific surface) constant; loss of fibre specific surface is not accounted for with fibre rich cakes. In Figure 5.4 it is seen that the curve reaches a plateau and does not

significantly alter as the rutile effective specific surface is reduced further (even using unrealistically low values of S_2/ϕ_2). This plateau does not represent the experimental data for fibre rich cakes, perhaps illustrating the significance of accounting for loss in fibre specific surface even at larger values of X_D .

It is also interesting that with rutile rich cakes, a better fit to the experimental data can be obtained by using a constant value of S_B (compare Figure 5.1 to Figures 5.2 and 5.4). A potential reason for this is that the pure rutile specific surface is significantly lower than the pure fibre specific surface (as determined from the two pure component filtrations). Further, the decrease in specific resistance from pure fibre cakes (in the range $X_D > 0.8$) is steeper than that from pure rutile cakes (in the range $X_D < 0.3$). In other words, the fibre component can be considered more ‘dominant’ than the rutile component. Nevertheless, as inferred from the fibre rich cakes in particular, it does not

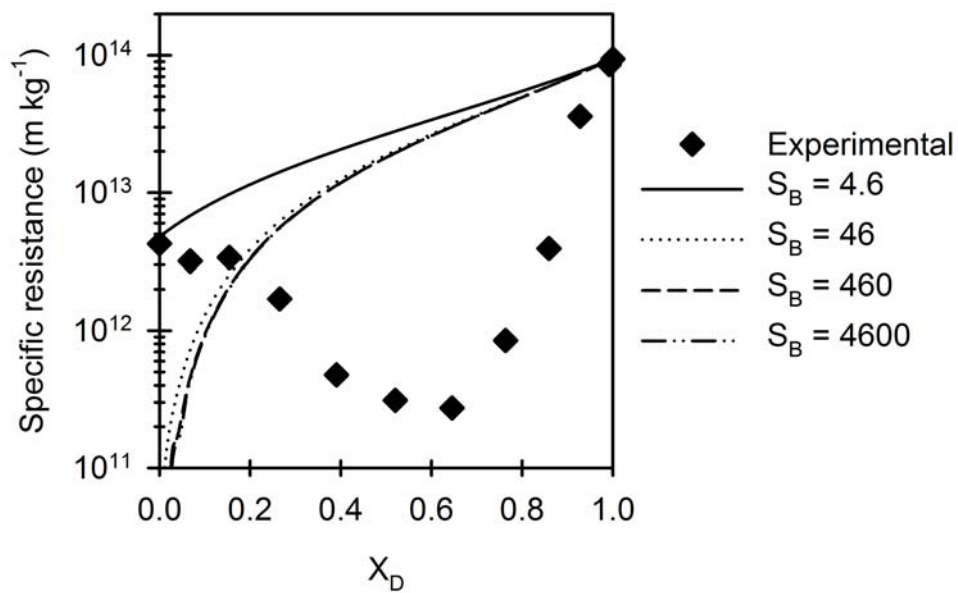


Figure 5.4: Family of curves produced by increasing S_B , keeping the fibre effective specific surface constant. Experimental data from 450 kPa filtrations with deionised water is included.

The parameters used for the curves are summarised in Table 5.3.

Table 5.3: Parameters for the curves plotted in Figure 5.4 at the various S_B .

S_B	S_1/ϕ_1 (m^{-1})	S_2/ϕ_2 (m^{-1})
4.6	2.00×10^8	4.36×10^7
46	2.00×10^8	4.36×10^6
460	2.00×10^8	4.36×10^5
4600	2.00×10^8	4.36×10^4

seem reasonable to represent the experimental data using this method. Also, from a fundamental perspective, it does not seem correct to assume a constant effective specific surface for either component over any solids composition where fibre-rutile aggregation takes place.

5.3.3.3. Significance of S_B

The ratio of effective specific surfaces (S_B) is shown to be a critical parameter in the filtration of aggregating binary mixtures and requires further analysis. The significance of S_B is also seen via equations (5.17) and (5.22), where its range determined some characteristics of the specific resistance vs. solids composition trend. The values of S_B at the different filtration pressures and solution environments are shown in Figure 5.5, as determined from the pure components. It is interesting that S_B varies linearly with filtration pressure, and it is also evident that the values of S_B in the NaCl and CaCl₂ solution environments are similar and much lower than the values of S_B in deionised water. However, it should be noted that the values of S_B shown in Figure 5.5 are merely determined from the two pure components for each case, and are not representative of the ratio of effective specific surfaces of the two solids across the range of solids compositions. Although the effective specific surfaces of the two solids at their pure component packing can be estimated from the corresponding pure

component filtrations, and the ratio of these two specific surface values will give a value of S_B , this value is not likely to correspond to the ratio of fibre to rutile specific surfaces exposed to the permeating fluid at intermediate solids compositions. Not only may the packing characteristics be different, but the proportion of rutile and fibre specific surface lost will vary with solids composition. With binary mixture filtrations, for S_B values to be the basis of a meaningful study, it will have to represent the true ratio of effective specific surfaces at any given solids composition.

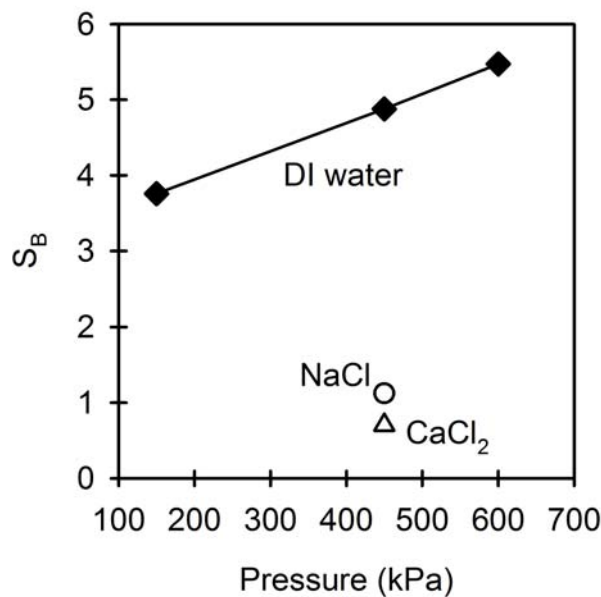


Figure 5.5: Values of S_B calculated from equation (4.40) for the filtrations from deionised water as well as 0.2 M NaCl and 0.1 M CaCl₂ solutions.

S_B is expected to be a function of solids composition (equation (5.33)); the form of this function will depend on the interaction forces and mechanisms, and the resultant packing at that solids composition. In light of the significance of S_B , it is too simplistic to represent the S_B vs. solids composition trend by using one or even two constant values. Also, the values of S_B at the various solids compositions are required in order to calculate the specific surface of one solids component from the other at that respective solids composition. The basis of the presented model (see equation (5.10)) is that it requires the specific surface of the two solids components at the various solids

compositions; this requirement is difficult to satisfy if the values of S_B at the various solids compositions are not known. Perhaps it is therefore unrealistic to attempt to obtain estimates for the specific surface of the two solids components. In the next section, a curve fitting approach is taken to represent the total solids effective specific surface at the various solids compositions.

5.4. APPLICATION OF MODEL TO EXPERIMENTAL DATA

Considering the difficulties involved in estimating the specific surface of the two solids components as required by equation (5.10), the use of equation (5.9) in equation (5.8) is not explored further. Instead, representations of S_0 are experimentally determined by rearranging equation (5.8) to give:

$$S_0 = \sqrt{\frac{\alpha_{av} \varepsilon_{av}^3 (X_D \rho_1 + (1 - X_D) \rho_2)}{5(1 - \varepsilon_{av})}} \quad (5.35)$$

Equation (5.9) gives an ‘additive’ type approach to describing the variation of effective specific surface with solids composition, and may not be appropriate with interacting binary mixtures. Figure 5.6 shows a plot of S_0 vs. solids composition for 450 kPa filtrations with deionised water; the experimental representations of S_0 were determined from equation (5.35) and relevant experimental data. Filtrations with deionised water at 150 kPa and 600 kPa showed similar trends.

Although the total solids specific surface with 450 kPa filtrations are presented in Figure 5.6 as an example, for all filtrations from deionised water, a minimum in S_1/ϕ_1 and S_2/ϕ_2 was seen at $X_D \sim 0.65$. Besides causing the observed α_{av} vs. X_D trend (Figure 4.21), this reduction in specific surface also resulted in the observed initial settling rate vs. X_D trend (Figure 4.7). When a solid body settles in a fluid at a velocity u_s , the drag force, F_D , opposing its motion is expressed by Newton’s law as (Wakeman and Tarleton, 2005):

$$F_D = C_D A_p \frac{\rho_l u_s^2}{2} \quad (5.36)$$

where A_P is the area of the solid projected in the direction of motion, C_D the drag coefficient, and ρ_l the liquid density. For a constant solids volume, a decrease in the specific surface will result in a lower A_P and hence easier settling. However, a more explicit correlation between the total solids specific surface vs. X_D , and initial settling rate vs. X_D trends cannot be easily formulated mainly because at higher fibre concentrations suspensions tend to become structured (thereby altering the settling behaviour) and settling rates will be reduced for loosely networked aggregates (lower effective density difference between the settling solids and suspending liquid).

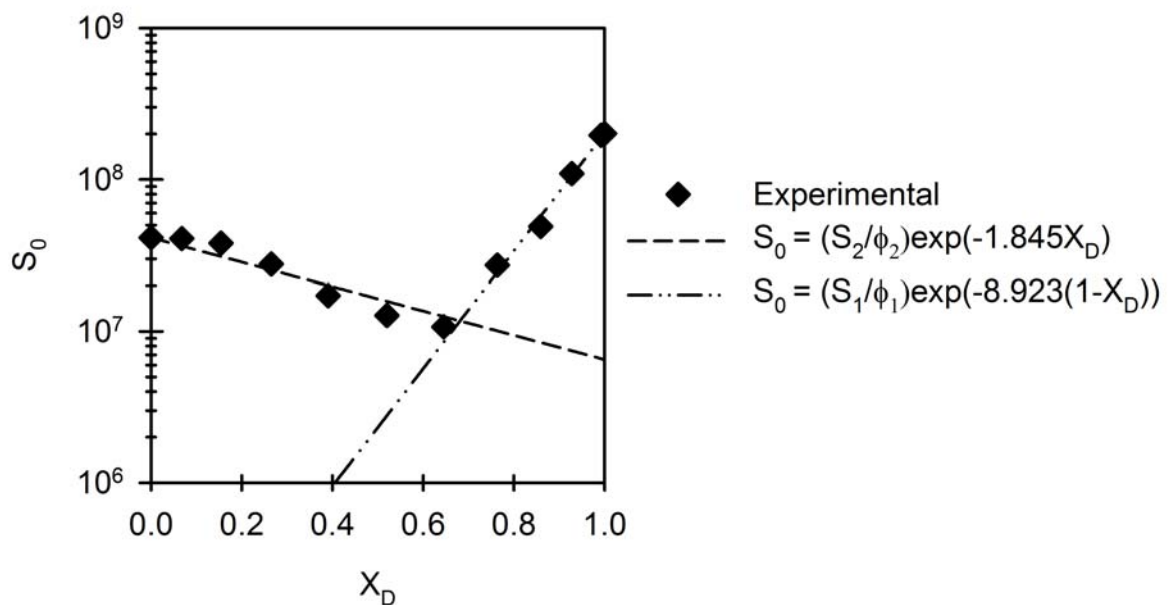


Figure 5.6: Plot of S_0 vs. solids composition, the experimental representations were calculated from equation (5.35) and data from 450 kPa filtrations with deionised water. The pure component specific surface values (S_1/ϕ_1 and S_2/ϕ_2) were calculated from equation (5.11).

From Figure 5.6, it may be inferred that two separate mechanisms promoted the observed behaviour across the solids composition range; one mechanism was dominant for rutile rich cakes (X_D from 0 to 0.65) and the other for fibre rich cakes (X_D from 1 to 0.65). The approach of inferring two separate mechanisms across a solids composition range has been taken by various researchers in the past when analysing binary mixture

packing (McGeary, 1961; Tokumitsu, 1964; Abe and Hirose, 1982; Abe *et al.*, 1993; Dias *et al.*, 2004). Any interaction effects with one packing mechanism may manifest itself on the filtration performance in a different way than with the other. Due to the inherent difficulties in fundamentally accounting for these factors, a curve fitting procedure was carried out and, as seen in Figure 5.6, the two mechanisms apparent in the specific surface-solids composition data are represented well by:

$$S_0 = \frac{S_1}{\phi_1} \exp(-b_{1a}(1 - X_D)) \quad (5.37)$$

$$S_0 = \frac{S_2}{\phi_2} \exp(-b_{2a}X_D) \quad (5.38)$$

where equations (5.37) and (5.38) apply to fibre and rutile rich cakes respectively, and b_{1a} and b_{2a} are experimentally determined coefficients. From equation (5.37) $S_0 = S_1/\phi_1$ when $X_D = 1$. Correspondingly, from equation (5.38), $S_0 = S_2/\phi_2$ when $X_D = 0$. Substituting equations (5.37) and (5.38) into equation (5.8) gives equations (5.39) and (5.40), respectively:

$$\alpha_{av} = \frac{5(1 - \varepsilon_{av})}{\varepsilon_{av}^3(X_D\rho_1 + (1 - X_D)\rho_2)} \left(\frac{S_1}{\phi_1} \exp(-b_{1a}(1 - X_D)) \right)^2 \quad (5.39)$$

$$\alpha_{av} = \frac{5(1 - \varepsilon_{av})}{\varepsilon_{av}^3(X_D\rho_1 + (1 - X_D)\rho_2)} \left(\frac{S_2}{\phi_2} \exp(-b_{2a}X_D) \right)^2 \quad (5.40)$$

where equation (5.39) applies to filter cakes rich in the larger solids component and equation (5.40) to filter cakes rich in the smaller solids component.

The pure component effective specific surface values, S_1/ϕ_1 and S_2/ϕ_2 , are determined from the pure component filtrations. The parameters b_{1a} and b_{2a} are determined by a curve fitting regression analysis. The curve fitting procedure could be carried out using the few experimental points closest to $X_D = 0$ and $X_D = 1$. However, from Figure 5.6, a minimum was noted at an X_D of 0.65, and so for accuracy this was taken to be the transition point. Hence b_{1a} was determined by curve fitting experimental

points that lie between $0.65 \leq X_D \leq 1$ and b_{2a} was determined by curve fitting experimental points that lie between $0 \leq X_D \leq 0.65$.

Data for 450 kPa filtrations with deionised water are used to help provide a descriptive example of how the model is applied to the experimental data. The effective specific surface of pure fibres and rutile were determined from the pure component filtration data according to equation (5.11). Values of S_0 at the different solids compositions were determined from equation (5.35) and relevant experimental values. Curve fitting equation (5.37) to the values of S_0 at $X_D \geq 0.65$, and equation (5.38) to the values of S_0 at $X_D \leq 0.65$, gave b_{1a} and b_{2a} as 8.92 and 1.85, respectively. Linear interpolations were carried out on the experimental porosity vs. solids composition trend, and these values were used in equations (5.39) and (5.40) for the cake average porosity. It is noted that an alternate method for accounting for the experimental porosity trend will be to use an appropriate packing model such as the Shirato additive law or interparticle penetration model (see Section 4.3.4 for further discussions on these models). Appropriately substituting for the average cake porosities (ε_{av}), the pure component densities (ρ_1 and ρ_2) and the effective specific surface values (S_1/ϕ_1 and S_2/ϕ_2), as well as the values of b_{1a} and b_{2a} into equations (5.38) and (5.39), and plotting versus solids composition will result in two curves. The first emanates from the pure rutile data point and the other from the pure fibre data point. These two curves intersect at some intermediate solids composition, and are discontinued at the intersection resulting in one curve as shown in Figure 5.7. The experimental specific resistance data is included in Figure 5.7 for comparison, and it is seen that a relatively good fit is obtained. Relatively good fits are also obtained on the corresponding plots with 150 and 600 kPa filtrations (see Appendix E).

An alternative approach used was to ‘combine’ equations (5.39) and (5.40) to give:

$$\alpha_{av} = \frac{5(1 - \varepsilon_{av})}{\varepsilon_{av}^3 (X_D \rho_1 + (1 - X_D) \rho_2)} \left(X_D \frac{S_1}{\phi_1} \exp(-b_1(1 - X_D)) + (1 - X_D) \frac{S_2}{\phi_2} \exp(-b_2 X_D) \right)^2 \quad (5.41)$$

where b_1 and b_2 are the fitting parameters. The curve fitting process to determine b_1 and b_2 using non-linear regression in SigmaPlot is further described in Appendix E, where an example non-linear regression results file is given. Although b_1 and b_2 carry a different meaning to b_{1a} and b_{2a} , Figure 5.7 shows that similar trends which represent the experimental data can be obtained by using either equations (5.39) and (5.40) or equation (5.41). One noticeable difference may be at the intersection between equations (5.39) and (5.40) (at $X_D \sim 0.64$ in Figure 5.7), where equation (5.41) resulted in a smoother curve. The values of b_1 and b_2 for 450 kPa filtrations with deionised water were 8.41 and 0.76, respectively. Similarly good representations was generally noted with the other trialled filtration pressures and solution environments. Figure 5.8 shows the fits given by equation (5.41) to the deionised water filtration data at 150 kPa and 600 kPa, where smooth curves representative of the data are presented.

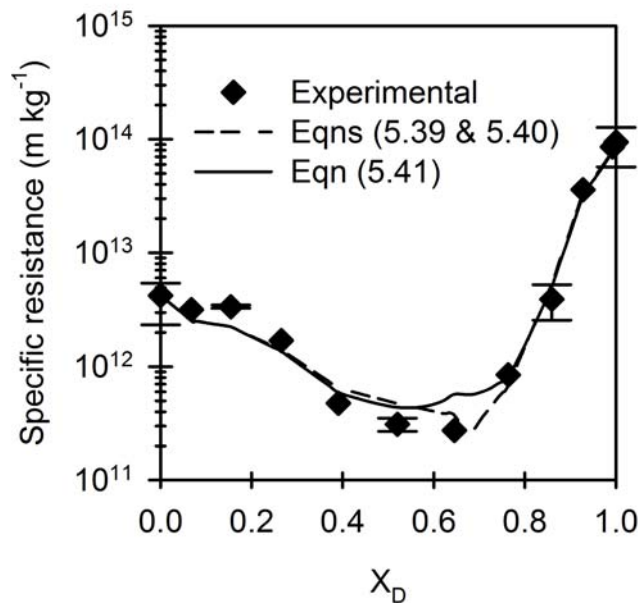


Figure 5.7: Experimental filtration data at 450 kPa with deionised water and the model fit using equations (5.39) and (5.40) as well as equation (5.41).

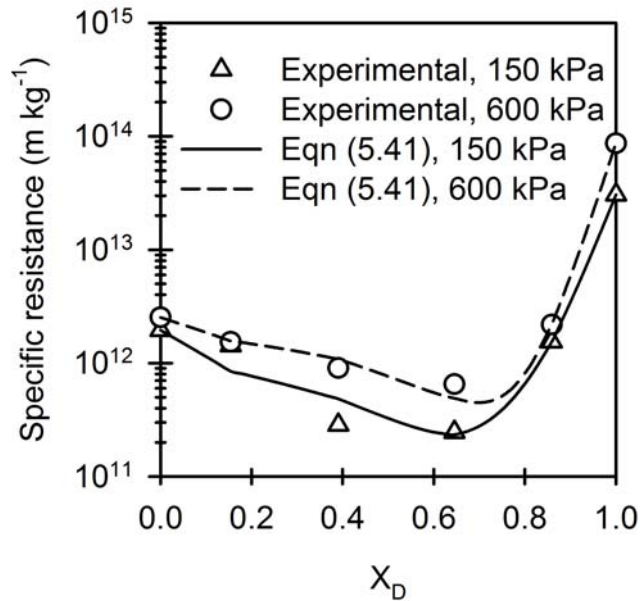


Figure 5.8: Experimental filtration data at 150 kPa and 600 kPa with deionised water and the model fits using equation (5.41).

The model was also fitted to data for 450 kPa filtrations of fibre/rutile mixtures in 0.2 M NaCl and 0.1 M CaCl₂ solutions; the resultant curves are shown in Figure 5.9. For the filtrations with NaCl, the values of b_1 and b_2 were approximately 3.15 and -0.31, respectively; and for the filtrations with CaCl₂, the values of b_1 and b_2 were approximately 8.61 and -0.75, respectively. It is seen that it was possible to fit the model to represent the experimental data not only for filtrations with deionised water but also with the other solution environments tested.

To further trial the model, the filtration data reported by Iritani *et al.* (2002) were used. The suspensions that Iritani *et al.* filtered consisted of mixtures of rutile and silica in deionised water at two different pH values (4.5 and 9.6). The filtrations were at 196 kPa and the pH was adjusted downwards using an HCl solution and upwards using a NaOH solution. At pH 4.5 rutile-silica interactions resulted in a minimum in the specific resistance vs. solids composition trend, and at pH 9.6 the particles were well dispersed (Iritani *et al.*, 2002). Hence, the model could also be tested on a particle-particle binary

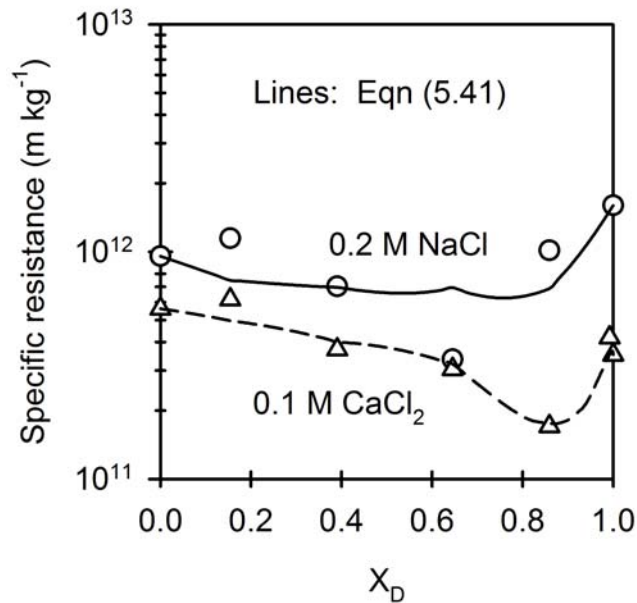


Figure 5.9: Experimental filtration data at 450 kPa with 0.2 M NaCl and 0.1 M CaCl₂ solutions, and the model fits using equation (5.41).

mixture for when aggregation does and does not occur, and the resultant fits are shown in Figure 5.10. For the filtrations at pH 4.5, the values of b_1 and b_2 were approximately 2.90 and 0.67, respectively; and for the filtrations at pH 9.6, the values of b_1 and b_2 were approximately 0.48 and 0.05, respectively. Although equation (5.41) has been used for Figures 5.8 - 5.10, the combined use of equations (5.39) and (5.40) also gave reasonably good fits to the experimental data; these fits are given in Appendix E.

The experimental points presented in Figure 5.10 were recalculated from Iritani *et al.* (2002) as they studied the effects of solids composition in terms of mass fractions. Iritani and co-workers kept the total mass fraction of solids in suspension constant, and varied the mass fraction of rutile, filtering solids ranging from pure rutile to pure silica. Recalculations to obtain the corresponding volume fractions from the various mass fractions were made using the following relationship:

$$\frac{\rho_t}{\rho_s} \left(\frac{1}{\left(\frac{s_t}{s} \right)} - 1 \right) = \frac{X_D}{1 - X_D} \quad (5.42)$$

where (s_t/s) is defined in Iritani *et al.*'s paper as the ratio of mass fraction of rutile to the total mass fraction of solids in suspension, and ρ_t and ρ_s are the pure rutile and silica densities, respectively. As consistent with the rest of this thesis, X_D is defined as the ratio of volume of the larger solids component (silica in the case of Iritani *et al.*'s data) to the total volume of solids in the suspension.

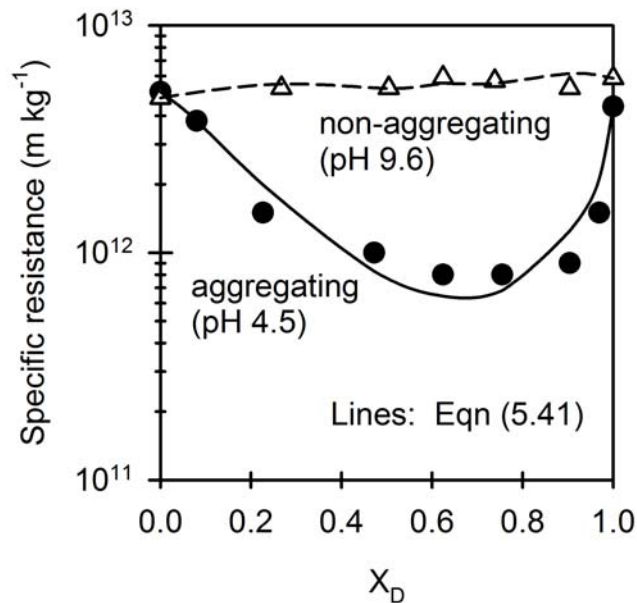


Figure 5.10: Experimental filtration data at 196 kPa with deionised water at pH 4.5 (where rutile-silica aggregation occurred) and pH 9.6 (where no aggregation occurred), and the model fits using equation (5.41). In this figure, an X_D of 0 refers to pure rutile and an X_D of 1 to pure silica. The experimental data points were recalculated from Iritani *et al.* (2002).

Although a potential drawback of Iritani *et al.*'s data is that the solids concentration (by volume) is not constant across the solids composition range, this may not be significant for the purpose of testing the model. The model does not contain nor require any explicit information regarding the initial suspension concentration. Instead,

as is the case with the Kozeny-Carman equation, information regarding solids concentration is implicitly accounted for via the cake average porosity and solids specific surface. Furthermore, two factors that make Iritani *et al.*'s work particularly interesting for trialling the model on experimental data extending beyond those obtained in this thesis are that: (1) they studied a particle-particle system (rutile-silica) as opposed to a fibre-particle system, and (2) they studied one solution environment where rutile-silica aggregation occurred, and another where no apparent aggregation took place and the solids were well dispersed. These two factors provide an interesting test for the model (equation (5.41)).

From Figures 5.7 to 5.10, it is seen that the model represents a wide range of binary suspension filtration data reasonably well using two fitting parameters. The aforementioned data encompass filtrations of fibre/rutile mixtures at various pressures and with different solution environments, as well as filtrations of silica/rutile mixtures at two different pH values (one induced silica/rutile aggregation and the other did not).

Equation (5.9) gives an 'additive' type approach to describing the variation of effective specific surface with solids composition, where it is assumed that no changes in either component's packing mechanism or interactions between the two components take place. Figure 5.11 illustrates a schematic of such a hypothetical scenario, where equation (5.9) may be used to describe the variation of effective solids specific surface with solids composition. Where the two solids are well mixed and of significantly different size distributions and/or shapes, and in particular where interactions between the two solids occur, then equation (5.9) may not be appropriate. Instead, equation (5.43) was used to represent the variation of effective specific surface in the model (equation (5.41)):

$$S_0 = X_D \frac{S_1}{\phi_1} \exp(-b_1(1 - X_D)) + (1 - X_D) \frac{S_2}{\phi_2} \exp(-b_2 X_D) \quad (5.43)$$

Comparing equations (5.43) and (5.9), it is seen that the difference is due to the two exponential terms in equation (5.43).

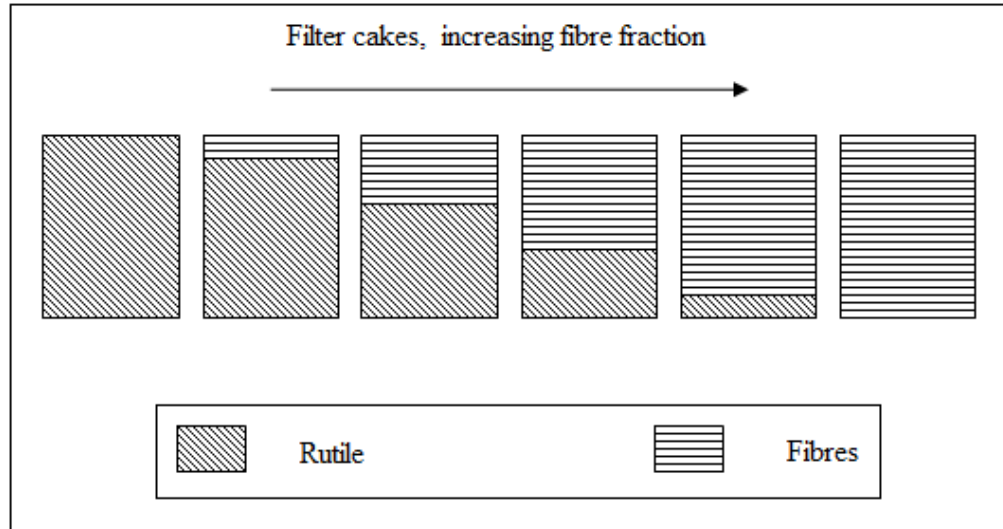


Figure 5.11: A schematic representation of a hypothetical case where equation (5.9) may be used to describe the variation of effective solids specific surface with solids composition. Here no changes in either component's packing (due to the presence of the other component) or interactions between the two components take place.

The use of an exponential type relationship in the model is interesting considering that it appears to fit the data reasonably well. It may be considered that the mechanisms involved across the range of solids compositions effectively account for three separate developments:

- (1) the difference in total solids specific surface brought about by progressively 'removing' a given volume of rutile particles from a pure rutile filter cake and 'replacing' them with fibres of a similar volume, eventually ending with a pure fibre filter cake;
- (2) any change in rutile and fibre specific surface from their pure component values due to varying packing mechanisms;
- (3) any possible loss in rutile and fibre specific surface due to rutile-fibre interactions.

Although the development (1) may be satisfactorily expressed by equation (5.9), this equation says nothing about the packing mechanisms and possible interactions. As discussed in Section 5.3.3, developments (2) and (3) are significant but cannot easily be

described by an equation derived purely from fundamental principles. An example of an equation form which can capture the aforementioned developments appears to be the exponential form, with the fitting parameters b_1 and b_2 giving a quantitative estimate of the effects, especially at both extremes of solids composition, by behaving as ‘lumped coefficients’.

The fitting parameter b_1 is a coefficient for describing the effects of the addition of small solids on the larger solids component’s effective specific surface (due to changes in packing and interactions). Correspondingly, the fitting parameter b_2 is a coefficient for describing the effects of the addition of larger solids on the small solids component’s effective specific surface. For example, as the cake becomes richer in the small solids component (X_D decreases), then the term ‘ $\exp(-b_2X_D)$ ’ in equation (5.43) becomes less significant indicating that the influence of the larger solids component on the effective specific surface of the small solids component becomes less significant. However, the term ‘ $(1-X_D)(S_2/\phi_2)$ ’ becomes greater due to the increasing volume of the small solids component in the cake. Further, the greater the magnitude of b_2 , so the more of an effect the term ‘ $\exp(-b_2X_D)$ ’ will have on the term ‘ $(1-X_D)(S_2/\phi_2)\exp(-b_2X_D)$ ’. The difference between the fitting parameters in equation (5.43) (b_1 and b_2) and those in equations (5.37) and (5.38) (b_{1a} and b_{2a}), is that b_{1a} only has an influence with filter cakes rich in the larger solids component and b_{2a} with filter cakes rich in the smaller solids component (see equations (5.37) and (5.38)), whereas b_1 and b_2 exert their influence over the entire range of solids compositions for binary cakes (with different ‘weightings’). Hence equation (5.43) may be regarded to be more physically meaningful than equations (5.37) and (5.38), and therefore the use of equation (5.41) may be a better approach than the combined use of equations (5.39) and (5.40). The parameters b_1 and b_2 are expected to be unique for a given system.

For rutile-fibre binary mixture filtrations with deionised water, the parameters b_1 and b_2 are plotted against filtration pressure (Figure 5.12). Values of b_1 and b_2 are also tabulated along with values of b_{1a} and b_{2a} and other relevant parameters; this is presented as Table 5.4. From Table 5.4, it is noted that when the effective specific surface of pure rutile was calculated from the data of Iritani *et al.* (2002), the values obtained were close to those calculated from the data obtained in this thesis.

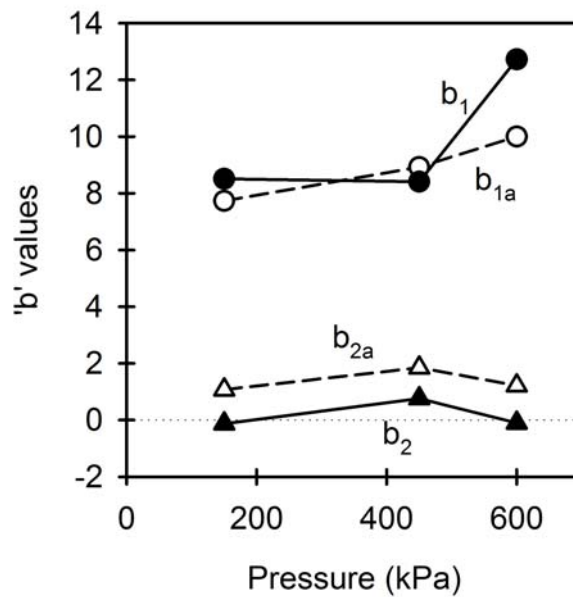


Figure 5.12: Values of b_1 and b_2 (equation (5.41)) for rutile/fibre binary suspension filtrations with deionised water at the different filtration pressures. Corresponding values of b_{1a} and b_{2a} (equations (5.39) and (5.40)) are included for comparison.

From Figure 5.12 and Table 5.4, it is seen that b_1 values were significantly larger than b_2 values for fibre/rutile mixtures, indicating that the effects (on the filtration performance) of adding rutile to a fibre rich suspension were more significant than adding fibres to a rutile rich suspension. The negative values of b_2 perhaps indicate that the presence of fibres increases the rutile effective specific surface for rutile rich cakes. This increase in rutile specific surface may be possible via changes in rutile packing brought about by the presence of fibres; as an example, the rutile primary particles could preferentially deposit onto fibre surfaces instead of forming collections of rutile clusters. Alternatively, since the negative values of b_2 are low in magnitude, it may just be an artefact (experimental and/or fitting) with b_2 actually being ~ 0 .

Table 5.4: Summary of parameters relevant to Figures 5.7 – 5.10.

Solution environment	Filtration pressure (kPa)	S_1/ϕ_1 * (m^{-1})	S_2/ϕ_2 ** (m^{-1})	b_1	b_2	b_{1a}	b_{2a}
Deionised water	150	1.16×10^8	3.08×10^7	8.51	-0.13	7.73	1.07
Deionised water	450	2.01×10^8	4.12×10^7	8.41	0.76	8.92	1.85
Deionised water	600	2.08×10^8	3.81×10^7	12.72	-0.10	10.00	1.22
0.2 M NaCl	450	1.34×10^7	1.91×10^7	3.15	-0.31	3.27	0.79
0.1 M CaCl ₂	450	2.81×10^7	2.50×10^7	8.61	-0.75	2.04	0.85
Deionised water, pH 4.5 (aggregation occurred) ***	196	2.79×10^7 (silica)	4.69×10^7	2.90	0.67	1.48	1.61
Deionised water, pH 9.6 (no aggregation occurred) ***	196	3.10×10^7 (silica)	4.47×10^7	0.48	0.05	-0.13	0.52

* Values for pure fibres unless stated.

** Values for pure rutile.

*** From the data of Iritani *et al.* (2002). Iritani and co-workers carried out experiments such that there was an increase in the number of particle species leading to a variation in total particle volume from one experiment to another.

With the binary mixture filtrations carried out by Iritani *et al.* (2002), values of b_1 and b_2 were more comparable, particularly when no silica-rutile aggregation was reported (pH 9.6). A likely reason for this is that rutile and silica are more comparable in terms of their physical dimensions (size distribution and shape) relative to rutile and fibre. It could be that b_1 and b_2 are material specific parameters which are specific to the solids form in a given solution environment.

Although the potential physical significance in the methods presented for describing the variation of solids specific surface with solids composition (equations (5.37) and (5.38) and equation (5.43)) is discussed for binary mixture filter cakes, it should be noted that the reason for the exponential form was because it fits the data and due to the absence of a more fundamental model. However, considering that equation (5.41) (and equations (5.39) and (5.40)) appear to agree reasonably well with a range of experimental data, the possibility that there may be some underlying fundamental meaning should not be prematurely discarded. More rigorous investigation of this possibility, and indeed other approaches of modelling the experimental data which may hold some fundamental basis, is beyond the scope of this thesis and will be an interesting subject for future work.

5.5. CONCLUSIONS

It was shown that, up to a certain extent, interaction (aggregation) between the two solids components will strongly affect a binary cake's average specific resistance via a decrease in specific surface and/or increase in porosity, with the magnitude of the effects varying with solids composition. Extension of the Kozeny-Carman/Darcy equations resulted in a model whose characteristics were studied under various assumptions. The ratio of the specific surface of the two constituent solids (S_B) was shown to be a critical parameter in the analysis of binary suspension filtrations.

A semi-empirical equation was presented which describes the specific resistance trend with solids composition. This equation was shown to represent a wide range of experimental data reasonably well. The two fitting parameters were b_1 and b_2 . b_1 represented a coefficient for describing the effects of the addition of small solids on the larger solids component's effective specific surface, due to changes in packing and aggregation. Correspondingly, b_2 represented a coefficient for describing the effects of the addition of larger solids on the small solids component's effective specific surface. b_1 and b_2 were more comparable in magnitude when the solids were of similar size and shape, and in particular when no significant aggregation was evident. It is possible that b_1 and b_2 are system specific parameters.

REFERENCES

- Abe E., Hirosue H. and Yokota K. (1979) Pressure drop through a packed bed of binary mixture. *J. Chemical Engineering Japan* **12**, 302-306.
- Abe E. and Hirosue H. (1982) Porosity estimation of a mixed cake in body filtration. *J. Chemical Engineering Japan* **13**, 490-493.
- Abe E., Hirosue H. and Yamada N. (1993) Prediction of the filtration characteristic in body filtration. *Proc. 6th World Filtration Congress*, pp.137-140, Nagoya.
- Dias R., Teixeira J.A., Mota M. and Yelshin A. (2004) Particulate binary mixtures: Dependence of packing porosity on particle size ratio, *Industrial Engineering Chemistry Research* **43**, 7912-7919.
- Donohue T.J. and Wensrich C.M. (2009) Improving permeability prediction for fibrous materials through a numerical investigation into pore size and pore connectivity. *Powder Technology* **195**, 57-62.
- Iritani E., Mukai Y. and Toyoda Y. (2002) Properties of a filter cake formed in dead-end microfiltration of binary particulate mixtures, *J. Chemical Engineering Japan* **35**, 226-233.
- McGeary R.K. (1961) Mechanical packing of spherical particles. *J. American Ceramic Society* **44**, 513-522.
- Tokumitsu Y. (1964) On the packing of granular materials. *J. Material Science Japan* **13**, 752-758.
- Wakeman R.J. and Tarleton E.S. (2005) *Solid/Liquid Separation: Principles of Industrial Filtration*. Elsevier, Oxford.

CHAPTER 6: ANOMALOUS FILTRATION BEHAVIOUR

6.1. INTRODUCTION

In Chapter 4, it was stated that abrupt changes in cake structure were noted part way through some filtrations, resulting in unusual deviations in filtration plots. Various works (Rietema, 1953; Baird and Perry, 1967; Sørensen, 1992; Sørensen *et al.*, 1995; Fathi-Najafi and Theliander, 1995; Tarleton and Morgan, 2001) have previously reported such abrupt changes and have attributed them to various potential causes. These are discussed briefly (in relation to the present data) so as to narrow them down while providing context; the most likely causes are then discussed in further detail using theoretical tools as an aid. This chapter then draws to a close by discussing the potential reasons for the abrupt changes in cake structure noted in the present work.

6.2. PREVIOUS RESEARCH

Rietema (1953) noted transitions in cake structure leading to unexpected reductions in filtrate flow rate during the filtration of polyvinyl chloride particles in water. Although he initially postulated scouring as a potential reason, where fines are entrained by liquid flow through the pores of the cake, he went on to eliminate this hypothesis as scouring should have led to temporary increases in filtrate flow rate. Rietema claimed that the most likely explanation was destabilisation of the cake structure; the higher filtrate flow through the cake toward the start of filtration was deemed to stabilise it prior to a flow transition point at which so called ‘retarded packing compressibility’ (RPC) occurred. A logical inference is that once the stabilising force (due to the filtrate flow) becomes smaller than the compressing force (which increases from the top to the bottom of the cake), then the packing can be significantly rearranged. Whether or not the packing is stabilised therefore depends on the cake thickness and the pore velocity of liquid in the cake.

Fathi-Najafi and Theliander (1995) attributed the abrupt changes in cake structure they observed in the filtration of calcium carbonate, calcium silicate and lime mud⁷, which was accompanied by steep increases in liquid pressure at various heights in the filter cake, to the formation of unobstructed channels within the filter cake. Sørensen *et al.* (1995) noted anomalous filtration behaviour with wastewater solids suspensions and provided a more elaborate discussion on the subject. They postulated wall effects, sedimentation, channelling and the migration of fines as potential reasons. They dismissed wall effects and sedimentation as potential causes, and their arguments are equally valid in the current work. It is perhaps surprising that channelling was ruled out as a possible reason; their rationale for doing so was that the solids pressure in the filter cakes was generally quite large and this closes the channels. They claim that migration of fines/compression mechanism best explains the strange filtration behaviour observed. Sørensen *et al.* suggested that the situation is possible when erosion of previously deposited small size solids results in a temporary reduction in the flow resistance. However, they perhaps failed to recognise that such a mechanism could lead to the formation of preferential flow channels (essentially ‘channelling’). Tarleton and Morgan (2001) acknowledge this last point by suggesting that the changes in cake structure they noted were due to more local variations in cake structure brought about by simultaneous particle fines migration and the subsequent formation of preferential flow channels. They postulated that part(s) of a cake may become sufficiently eroded by the flowing filtrate to generate preferential flow channel(s) that remain ‘open’ for a significant period. Although they noted anomalous filtration behaviour with aggregated zinc sulphide, Tarleton and Morgan found no evidence of RPC or related phenomena during experiments performed with more discrete zinc sulphide particles.

In summary, when the feed particles exhibited a degree of structure, there appears to be an increased tendency for relatively sudden changes in a forming cake to occur. In general, particle networking was a common theme about the cakes that underwent abrupt change. Although Rietema (1953) postulated the RPC mechanism as a potential explanation for abrupt decreases in filtrate flow rate, it may be possible (though intuitively unlikely) that cake collapse due to RPC leads to the temporary increases in filtrate flow rate observed in the present work (see Section 6.3). Also,

⁷ All described as being in a state of agglomeration in suspension.

migration of fines (what Rietema termed scouring) should not be ruled out as a potential reason, as restructuring of the cake in the present work frequently led to temporary increases in filtrate flow rate (unlike in Rietema's). Sørensen *et al.*'s (1995) analysis and postulations regarding migration of fines perhaps substantiates the case for considering this mechanism as a potential reason for restructuring of the filter cake part way through a filtration. The arguments presented by Tarleton and Morgan (2001) relate the effects of fines migration to the formation of preferential flow channels within the cake. This therefore suggests that critical values of filtrate flow rate and cake thickness may occur; these critical values are presented and discussed in the following. A theoretical analysis is also presented and intended to provide estimates of the relative magnitudes involved should the formation of preferential flow channels be the cause of the observed abrupt changes during filtration. The results presented are representative of the dataset obtained during the investigation.

6.3. GENERAL EXPERIMENTAL OBSERVATIONS

The occurrence of abrupt changes to cake structure part way through filtration of a fibre suspension (1.1% v/v) was limited to higher filtration pressures (above ~400 kPa); there was no evidence of RPC or related phenomena during experiments performed at filtration pressures of 300 kPa and below. Figure 6.1 illustrates a phenomenon showing a significant deviation from the 'expected' filtration behaviour (i.e. linear plot of reciprocal filtration rate vs. cumulative filtrate volume) was apparent for the filtration of pure fibre suspensions at a filtration pressure of 450 kPa but not for filtration pressures of 150 and 300 kPa. After approximately $3 \times 10^{-4} \text{ m}^3$ of filtrate had been produced, the cakes formed during the 150 and 300 kPa filtrations undergo cake deliquoring (at approximately point A in Figure 6.1). On the other hand, the cake formed during the 450 kPa filtration showed phenomena related to abrupt changes in cake structure, evidenced by the marked change from the expected behaviour.

Figure 6.2 gives an indication of the reproducibility attainable. Although not all experiments had such a degree of reproducibility, in general the effects of cake restructuring on filtration rates were broadly similar in repeated experiments. Figure 6.3

illustrates the effects of cake restructuring on the instantaneous filtrate flow rate for filtrations of pure fibre suspensions from deionised water at filtration pressures of 450, 550 and 600 kPa. In all cases the changes in cake structure were accompanied by approximately an order of magnitude increase in filtrate flow rate. The filtrate flow rate just before the abrupt transition in cake structure is denoted $(dV/dt)|_{tr}$ and changes to the cake structure increased the filtrate flow rate from $(dV/dt)|_{tr}$ to a maximum peak of $(dV/dt)|_{tr,max}$. At 450 kPa this change was from approximately $1 \times 10^{-7} \text{ m}^3 \text{ s}^{-1}$ to $1.3 \times 10^{-6} \text{ m}^3 \text{ s}^{-1}$, at 550 kPa from approximately $1.1 \times 10^{-7} \text{ m}^3 \text{ s}^{-1}$ to $1.5 \times 10^{-6} \text{ m}^3 \text{ s}^{-1}$, and at 600 kPa from approximately $2.6 \times 10^{-7} \text{ m}^3 \text{ s}^{-1}$ to $1.9 \times 10^{-6} \text{ m}^3 \text{ s}^{-1}$. Generally, when restructuring of the filter cake led to increases in the filtrate flow rate, the maximum peak reached increased with filtration pressure.

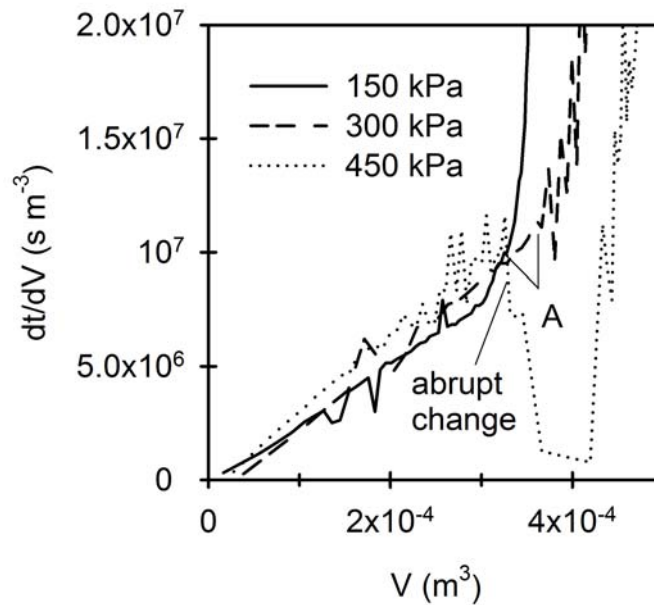


Figure 6.1: Filtration plots for pure fibre suspensions (1.1% v/v) in deionised water at three filtration pressures.

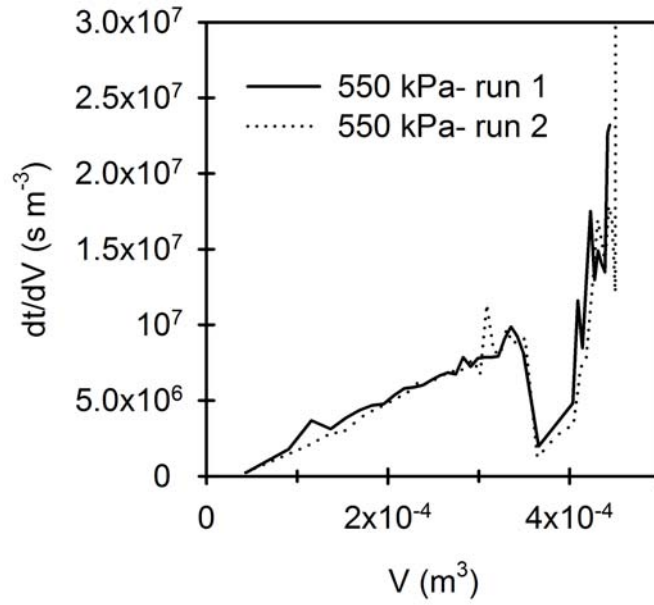


Figure 6.2: Filtration plots for pure fibre suspensions in deionised water at 550 kPa; a repeat experiment is shown to indicate reproducibility.

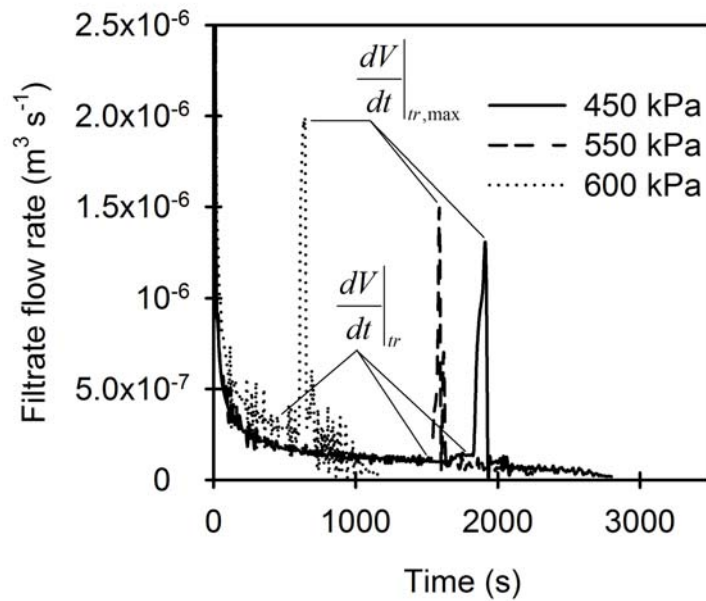


Figure 6.3: Filtrate flow rate profile for pure fibre suspensions (1.1% v/v) in deionised water at three filtration pressures.

The similar gradients of filtrate flow rate vs. filtration time before and after the change in cake structure for all cases in Figure 6.3 may suggest that filtration continues with similar causes of flow resistance before and after the change. The effects of simultaneous sedimentation is ruled out as a possible cause of the observed filtration behaviour as sedimentation effects cannot increase the flow rate as seen in Figure 6.3. Figures 6.4 and 6.5 illustrate the effects of solids composition on cake restructuring for binary suspensions in deionised water. Figure 6.5 again indicates similar gradients of filtrate flow rate vs. filtration time before and after the change in cake structure. Figure 6.4 suggests that the addition of rutile resulted in less pronounced deviations from the ‘expected’ filtration behaviour. This effect of rutile addition is seen by comparing the difference between the inverse of the filtrate flow rates just before the transition, with the corresponding inverse of the maximum filtrate flow rates during the transition, for the three different solids compositions.

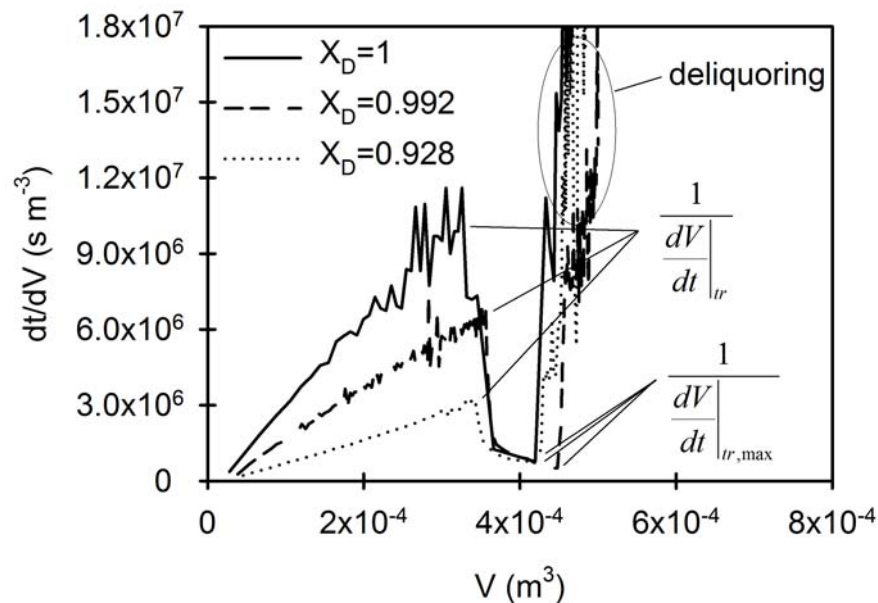


Figure 6.4: Filtration plots for binary suspensions of various solids compositions (fibre rich suspensions of total solids concentration of 1.1% v/v) in deionised water at 450 kPa.

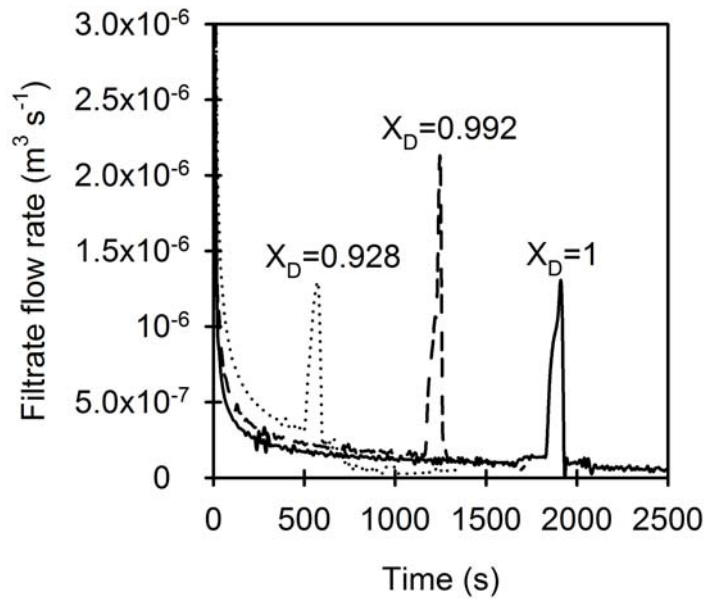


Figure 6.5: Filtrate flow rate profile for binary suspensions of various solids compositions (total solids concentration of 1.1% v/v) in deionised water at 450 kPa.

Addition of more significant amounts of rutile past a critical concentration altered the nature and hence outcomes of cake restructuring altogether, as illustrated by Figure 6.6. By way of example, unlike with suspensions of $X_D \geq 0.928$ (see Figure 6.4), filtration plots for $X_D = 0.859$ and $X_D = 0.764$ exhibit an increase in filtration resistance (upward curvature of the dataset) prior to a relatively short period of increased filtration rate. To further illustrate this, with $X_D = 0.859$, it can be seen from Figure 6.6 that the upward curvature starts at point A. This increase in filtration resistance (reduction in filtration rate) at point A can be seen more clearly in Figure 6.7 which shows the filtrate flow rate profile corresponding to the reciprocal flow rate on Figure 6.6 at $X_D = 0.859$. The regression curve in Figure 6.7 was obtained based on the experimental data points before point A. It is seen that the relatively short period of increased filtration rate takes place from ~ 150 s to point B, and is small in magnitude when compared to, for instance, the suspensions with less rutile in Figure 6.5 ($X_D \geq 0.928$).

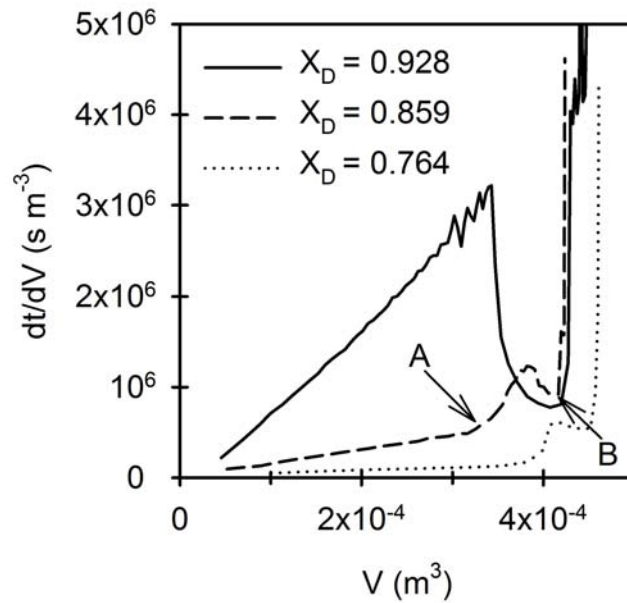


Figure 6.6: Filtration plots for binary suspensions of various solids compositions (from fibre rich to intermediate solids compositions, with total solids concentration of 1.1% v/v) in deionised water at 450 kPa.

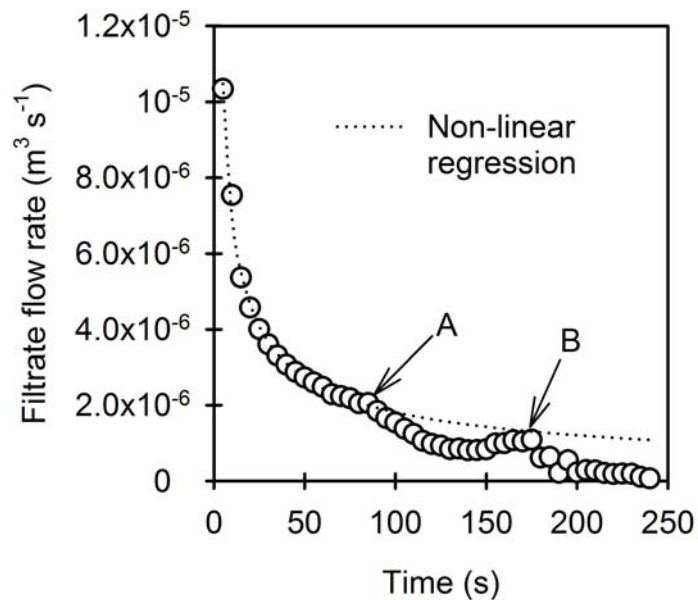


Figure 6.7: Filtrate flow rate profile for an $X_D = 0.859$ suspension in deionised water. The data, and points A and B, correspond with those in Figure 6.6 at $X_D = 0.859$.

Based on intuition alone, the altered nature of cake restructuring below $X_D \sim 0.9$ may have been attributed to the increased proportion of rutile, which has a more isometric shape relative to the fibres. Although this may indeed be a contributing reason, upon closer inspection another factor appears to be the greater filtration rates over the intermediate solids composition range (see the deionised water curve in Figure 4.19 or Figure 4.21 for example); this inference can be substantiated using data from filtrations with 0.1 M CaCl_2 solution. Figure 6.8 shows that with filtrations from 0.1 M CaCl_2 solution, even pure fibre suspension filtrations displayed an increase in filtration resistance (upward curvature of the dataset) prior to a relatively less significant period of increased filtration rate. This behaviour is more akin to the behaviour of, for instance, $X_D = 0.859$ and $X_D = 0.764$ suspensions in deionised water than to the behaviour of more fibre rich suspensions ($1 \geq X_D \geq 0.928$) in deionised water (see, for example, Figures 6.4 and 6.6). It should be noted that the filtration rates were significantly greater for pure fibre suspensions in 0.1 M CaCl_2 solution than deionised water.

Rietema (1953) claimed that it is likely that the onset of transition is due to either the filter cake having achieved a critical height or the pore velocity decreasing below a critical value. He proposed a stabilising effect of the original cake structure originating from the pore velocity of liquid in the filter cake. If his proposal is true, then it may explain the difference in the nature of cake restructuring with cakes containing a significant proportion of rutile (e.g. $X_D = 0.764$) and fibre rich cakes in 0.1 M CaCl_2 solution, and fibre rich cakes in deionised water ($X_D \geq 0.928$). Cakes containing a significant proportion of rutile and fibre rich cakes in 0.1 M CaCl_2 solution generally had greater filtration rates (for example, see Figure 4.19 or 4.23), suggesting greater pore velocities. On the other hand, fibre rich cakes in deionised water resulted in lower filtration rates which suggest lower pore velocities, and hence a lower stabilising effect. Therefore, fibre rich cakes in deionised water had a greater tendency for more significant cake restructuring, and resulted in temporary increases in filtration rate of greater magnitudes.

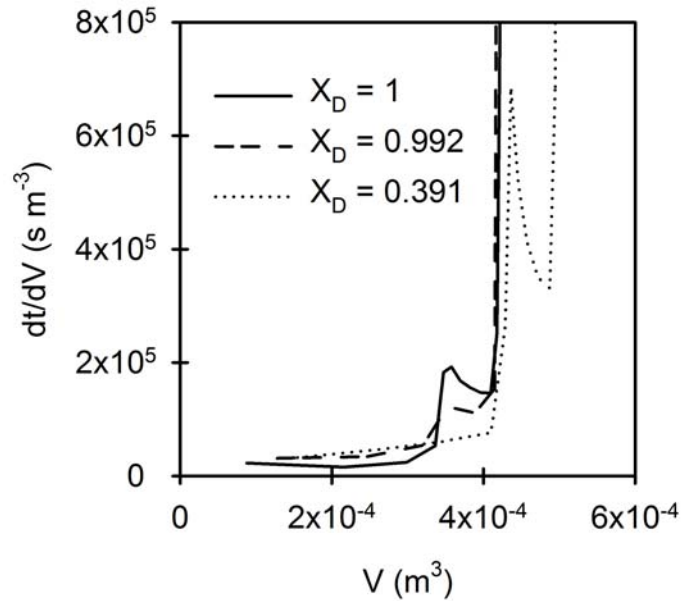


Figure 6.8: Filtration plots for binary suspensions of various solids compositions in 0.1 M CaCl₂ solution at 450 kPa.

Table 6.1 presents some critical parameters just prior to the transition in cake structure for selected filtrations to enable a closer examination. The cake thickness at the transition in structure (h_{tr}) was calculated using equation (6.1):

$$h_{tr} = \frac{V_{tr}}{A} \left(\frac{s(\rho_s(m-1) + \rho_l)}{\rho_s(1-ms)} \right) \quad (6.1)$$

where V_{tr} is the cumulative volume of filtrate at the transition, s the solids mass fraction in the feed, A the filter area, ρ_s and ρ_l are the solids and filtrate density respectively and m the ratio of mass of wet cake to mass of dry cake as measured at the end of an experiment. An assumption made here is that the value of m remains constant throughout the filtration and for the purposes of comparison in this analysis, this assumption is expected to be reasonable. The values of cake thickness reported in Table 6.1 are, in some cases, averaged from up to three experiments with an error of not more than 3%.

Table 6.1: Some parameters of interest during the abrupt transition in cake structure for selected filtrations. The values reported here are representative of the datasets obtained.

X_D	Solution environment	Filtration pressure (kPa)	Cake thickness at the transition, h_{tr} (mm)	h_{tr} , as a percentage of final cake thickness (%)	Filtrate flow rate at the transition, $\left. \frac{dV}{dt} \right _{tr}$ ($\times 10^{-7} \text{ m}^3 \text{ s}^{-1}$)
1	Deionised water	550	1.46	79	1.10
1	Deionised water	600	1.25	67	2.57
1	Deionised water	450	1.24	75	1.47
0.992	Deionised water	450	1.32	71	1.45
0.928	Deionised water	450	1.14	70	3.11
0.859	Deionised water	450	1.20	73	20.5
0.764	Deionised water	450	1.56	77	77.5
1	0.1 M CaCl_2	450	1.40	70	414
0.859	0.1 M CaCl_2	450	1.18	78	233
0.391	0.1 M CaCl_2	450	1.04	83	131
0.154	0.1 M CaCl_2	450	1.31	85	65.9

It can be seen from Table 6.1 that the abrupt changes to cake structure appear to occur once a cake reaches a similar thickness. The cake thicknesses where such transitions occur were all within 1.3 ± 0.3 mm and, similar to the results of Sørensen *et al.* (1995) and Tarleton and Morgan (2001), alterations in cake structure were noted toward the later stages of filtration. It may also be inferred from Table 6.1 along with Figures 6.6 and 6.8 that the nature of the abrupt transitions to cake structure is altered from one which causes a pronounced increase in filtration rate when $(dV/dt)|_{tr}$ is in the region of $10^{-7} \text{ m}^3 \text{ s}^{-1}$ to one that causes a decrease in filtration rate followed by a relatively less significant period of increased filtration rate when $(dV/dt)|_{tr}$ is in the region of $10^{-6} \text{ m}^3 \text{ s}^{-1}$ or greater, and this, as mentioned, could be due to stabilising effects. Also, the introduction of rutile into fibre suspensions does not only affect the nature of alterations in cake structure but also the magnitudes. The behaviour exhibited by $X_D = 0.391$ in Figure 6.8 is an example of the effects of even further introduction of rutile which resulted in a more significant decrease in filtration rate at the onset of transition. This is an example of cake restructuring with a greater proportion of particles of more isometric shape and with a lower stabilising effect since $(dV/dt)|_{tr}$ was greater for $X_D = 1$ than it was for $X_D = 0.391$ (see Figure 6.8 and Table 6.1).

The shear stress experienced by the walls of pores in the filter cake at the point of cake restructuring is likely to be important, depending on the mechanism causing the abrupt change, and is inferred through values of $(dV/dt)|_{tr}$. $(dV/dt)|_{tr}$ does not seem to vary much with filtration pressure for pure fibre suspensions but does so with solution environment and solids composition. Figure 6.9 illustrates the variation of $(dV/dt)|_{tr}$ with fibre fraction. Although abrupt transitions in filter cake structure apparently occurred during all experiments performed with suspensions in 0.1 M CaCl_2 solution, there was no evidence of RPC or related phenomena with suspensions in deionised water containing less than $\sim 15\%$ v/v of fibres. This is in keeping with the observation made by Tarleton and Morgan (2001) that all reports of abrupt changes in cake structure have occurred during the filtration of suspensions containing networked solids, since fibre rich and intermediate composition suspensions in deionised water appeared to be networked (for example, see Section 4.2), and in 0.1 M CaCl_2 solution even pure rutile suspensions seemed to flocculate. Rutile rich suspensions in deionised water seemed less structured, and with these suspensions no abrupt restructuring of the filter cake

occurred, presumably since there was less scope for constituent solids and liquid movements within the cake. The trend seen in Figure 6.9 is comparable to that in Figure 4.19; in general, greater filtration rates resulted in a larger value of $(dV/dt)|_{tr}$. Also, as discussed, the nature of cake restructuring and magnitude of the resultant increase and/or decrease in filtrate flow rates varied with solution environment and solids composition, and hence $(dV/dt)|_{tr}$.

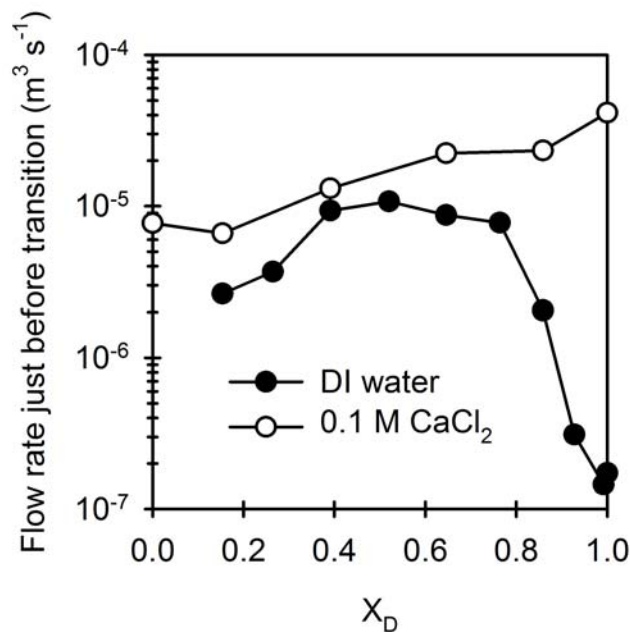


Figure 6.9: Filtrate flow rate just prior to the transition vs. solids composition for experiments performed with deionised water and 0.1 M $CaCl_2$ solution.

Rietema (1953) and Baird and Perry (1967) exclusively noted cakes that collapsed during filtration with the consequence of reduced filtration rates (increased resistance) while later work by Sørensen *et al.* (1995) and Tarleton and Morgan (2001) exclusively noted changes in cake structure with the consequence of increased filtration rates (reduced resistance). It is, perhaps interestingly, shown in this work that not only can the changes in cake structure be relatively reproducible, but also the nature of the change can be altered by changes in solids composition and/or solution environment. This degree of control of the alterations in filter cake structure is likely to be due to the control over filtration rate (via changes in filtration pressure, solids composition and

solution environment) and also solids form. It was discussed that various factors potentially had some effect on the nature of the abrupt change and magnitude of the consequent increase and/or decrease in filtrate flow rate. Considering all these parameters and the inherent complexity, it is difficult to accurately quantify the effects of each factor separately, particularly since the specifics of the contributing mechanism(s) are unclear. However, in the following section, a quantitative analysis is carried out based on some simplifying assumptions to assess the likelihood of contributing mechanisms postulated by past researchers (see Section 6.2).

6.4. ANALYSIS OF CAKE STRUCTURE CHANGES

Considering the almost exclusive reliance on qualitative rather than quantitative assessments when it comes to analysis of abrupt changes to cake structure part way through a filtration, a theoretical framework is presented here to obtain estimates of the magnitudes involved if it is assumed that the formation of channels, change in channel radius and/or changes in cake porosity is the cause of the transitions to cake structure, and the pores in the filter cake can be interpreted as straight circular tubes normal to the cake surface. Of particular interest in this analysis are the filter cakes obtained from the filtration of fibre rich suspensions in deionised water where anomalous filtration behaviour occurred, since: (1) the magnitudes of increase in filtration rates were most significant with the fibre rich filter cakes, and (2) analysis of intermediate solids compositions and other solution environments bring about extra variables (e.g. solids form and physico-chemical interactions). For laminar flow through a straight circular channel:

$$\frac{Q}{A_{ch}} = \frac{R^2 \Delta P}{8\mu L} \quad (6.2)$$

where Q is the channel volumetric flow rate, A_{ch} the average channel cross-sectional area, R the average channel hydraulic radius, ΔP the pressure difference across the channel, μ the viscosity and L the channel length. Considering N to be the number of channels within the filter cake and Q_T to be the total volumetric flow rate through these channels:

$$Q_T = N \frac{A_{ch} R^2 \Delta P}{8 \mu L} \quad (6.3)$$

Taking a to be the fraction of flow channels present at a given time that can alter during a filtration and b to be the remaining fraction of channels, then $a + b = 1$ and:

$$Q_T = N \frac{\pi (aR_a^2 + bR_b^2) (aR_a + bR_b)^2 \Delta P}{8 \mu L} \quad (6.4)$$

where R_a is the average hydraulic radius of the flow channels that can alter their size and R_b the average hydraulic radius of the remaining channels. Taking A to be the filtration area and ϵ_{av} to be the average porosity within the filter cake:

$$NA_{ch} = N\pi (aR_a^2 + bR_b^2) = A\epsilon_{av} \quad (6.5)$$

Considering the assumption of straight channels, L is taken to be the cake thickness (h) and calculated using:

$$L = h = \frac{V}{A} \left(\frac{s(\rho_s(m-1) + \rho_l)}{\rho_s(1-ms)} \right) \quad (6.6)$$

where V is the cumulative filtrate volume at a given time. Similarly, Q_T is taken to be the instantaneous filtrate flow rate.

The fundamental basis of this framework may be questioned with regards to unaccounted for parameters such as tortuosity and varying pore radius. However, considering the complex structure of binary filter cakes and that quantification of the magnitudes involved with absolute accuracy is not practically feasible at present, the framework outlined above is considered to be useful. Based on the equations derived above and the relevant assumptions, two scenarios are investigated to study the observed filtration behaviour. The first scenario, discussed in Section 6.4.1, considers changes in channel radius and number of channels to account for the observed filtration behaviour, with the cake average porosity remaining constant. The second scenario, discussed in Section 6.4.2, considers changes in cake porosity and channel radius to account for the observed filtration behaviour, with the number of channels remaining constant. In both scenarios, the degree of how ‘localised’ changes within the filter cake

can be controlled by changing the parameters a and b is investigated. For example, if $a = 0.05$ and $b = 0.95$, then the changes in channel radius take place in a region containing 5% of the cake's total channels.

6.4.1. Changing channel radius and number of channels

Substituting equation (6.5) into equation (6.4) and rearranging gives:

$$R_a = \frac{1}{a} \left(\sqrt{\frac{8\mu h Q_T}{\Delta P A \varepsilon_{av}}} - b R_b \right) \quad (6.7)$$

and from equation (6.5), the number of channels is given by:

$$N = \frac{A \varepsilon_{av}}{\pi (a R_a^2 + b R_b^2)} \quad (6.8)$$

Solving equations (6.7) and (6.8) gives values for channel radius of the channels that can alter in size, and the number of channels (unique combination). Here, the porosity is assumed constant and any changes in filtrate flow rate during a filtration are attributed to expansions and contractions of some or all of the hypothetical channels. The assumption of equation (6.6) holding throughout is expected to be reasonable. Although compression may take place during a filtration and the cake may 'collapse' reducing h at a certain time during a filtration, all cakes in this investigation were relatively thin and trial calculations shows that minor changes in cake length do not cause significant variation in the results obtained (see Appendix F).

Solving equations (6.7) and (6.8) gives a unique solution for channel radius and number of channels which corresponds to the instantaneous filtration rate, in accordance with the aforementioned assumptions. Essentially, what is being investigated here is the range of magnitudes involved if the deviations in expected filtrate flow rate can be explained by changing pore size (interpreted via channel diameter), with the average cake porosity kept constant. Further, if an unexpected increase in filtrate flow rate is attributed to the expansion of a proportion of channels within a cake, with the average cake porosity kept constant, then some channels will have to 'close' ('loss of pores'). In

reality the ‘loss of pores’ could correspond to: (1) the ingress of freshly filtered solids, or migration of fines (fibre fines and/or rutile) followed by deposition in constricted regions of a channel within a cake, and/or (2) ‘collapsed’ solids from the already formed cake.

Figure 6.10 illustrates how the average channel radius would need to vary to account for the filtrate flow rate profiles shown in Figure 6.3 for the hypothetical case where $a = 1$ (when all the channels present at a given time expand and contract uniformly). Figure 6.11 shows the corresponding plot of number of channels vs. time. It is seen that to solely account for the marked increases in filtration rate shown by Figure 6.3, the average channel radius has to increase by approximately three times its original value, and the number of channels reduce by approximately an order of magnitude. Using the Kozeny-Carman and Happel models, Tarleton and Morgan (2001) showed that unrealistically large macroscopic changes (increases) in average porosity are required to promote the flow increases observed after the change in cake structure. Similar calculations were carried out in this investigation and led to a similar conclusion (see, for example, Appendix F). However, the results illustrated by Figures 6.10 and 6.11 suggest that the formation of large channels within the cake can account for the increases in filtration rate, though the ‘number of open pores’ may correspondingly reduce keeping the porosity essentially constant.

It may be unrealistic to assume that all the pores present in the cake at a given time can expand. As pointed out by Sørensen *et al.* (1995), the effective pressure in filter cakes tends to be quite large and the formation of channels will have to (in a sense) open up ‘against’ this effective pressure. Sørensen *et al.* go on to suggest that locally increasing liquid pressure gradients in some sections of the cake can cause an erosion of previously deposited small-scale solids. It may be possible that this could result in a more localised channel formation. It may also be possible that compression in certain regions leads to interconnection of two previously ‘closed’ pores, leading to the formation of a preferential channel. The idea of more localised cake restructuring has been promoted by previous workers (Rietema, 1953; Sørensen *et al.*, 1995; Tarleton and Morgan, 2001).

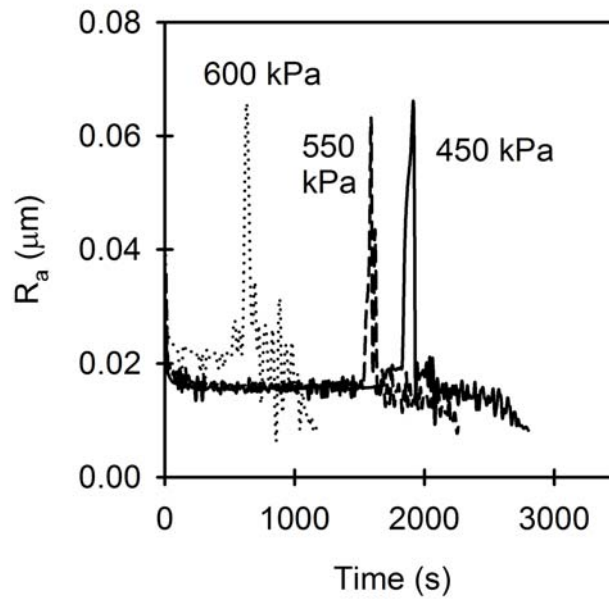


Figure 6.10: Average channel radius vs. filtration time for filtrations of pure fibre suspensions from deionised water at three filtration pressures when $a = 1$. The corresponding flow rate profiles are given in Figure 6.3.

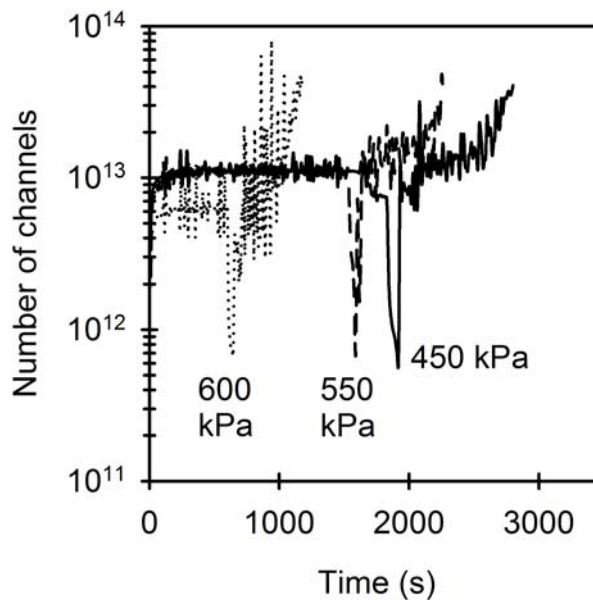


Figure 6.11: Number of channels vs. filtration time for filtrations of pure fibre suspensions from deionised water at three filtration pressures when $a = 1$. The corresponding flow rate profiles are given in Figure 6.3.

Figures 6.12 and 6.13 illustrate the effects of changing a on plots of R_a vs. filtration time and corresponding number of channels vs. filtration time during the period of increased filtration rate in the 450 kPa filtration of a pure fibre suspension from deionised water. For instance, a value of a of 0.05 indicates that only 5% of the pores within the cake (interpreted as channels in this model) can alter in size, and this may be more physically realistic, if indeed the change is more localised. R_a (the average hydraulic radius of pores that can alter size) was calculated using equation (6.7), with the value of R_b set to equal the quasi-steady state value (prior to the onset of transition) of R_a for the case when $a = 1$. For example, from Figure 6.10 the quasi-steady state values of R_a were 0.015 μm , 0.016 μm , and 0.021 μm for filtrations at 450 kPa, 550 kPa and 600 kPa, respectively. These values were then substituted into equation (6.7) as R_b (a constant for a given filtration) to enable calculation of R_a at various times during filtration at the specified pressure.

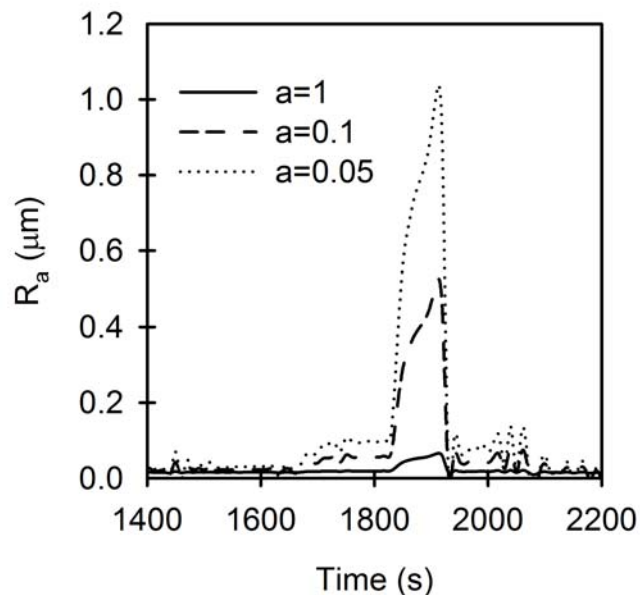


Figure 6.12: Effect of varying a on the increase in R_a during the period of increased filtration rate for the filtration of pure fibre suspension from deionised water at 450 kPa.

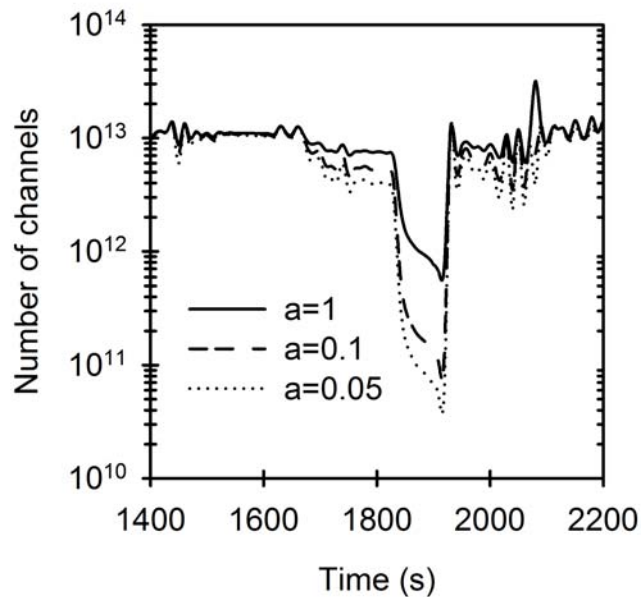


Figure 6.13: Effect of varying a on the number of channels during the period of increased filtration rate for the filtration of pure fibre suspension from deionised water at 450 kPa.

Although Figure 6.10 shows that when all the channels within the cake can expand, an increase in average channel radius to a maximum of $\sim 0.065 \mu\text{m}$ is required to promote the observed flow increase; Figure 6.12 illustrates a perhaps more likely case when only 5% of the channels can expand ($a = 0.05$) where an increase in average channel radius to a maximum of approximately $1 \mu\text{m}$ is required. Also, from Figure 6.13, it is seen that if only 5% of the channels can expand, then to account for the observed flow increase while keeping the porosity constant, the number of pores will have to decrease from approximately 1×10^{13} to a minimum of 5×10^{10} . In this theoretical scenario with $a = 0.05$, just prior to the transition there were approximately 1×10^{13} channels of $\sim 0.02 \mu\text{m}$ radius within the cake, and at the maximum measured filtration rate there were approximately 2.5×10^9 (5% of 5×10^{10}) channels of $\sim 1 \mu\text{m}$ radius and 4.75×10^{10} (95% of 5×10^{10}) channels of $\sim 0.02 \mu\text{m}$ radius. It is obvious that with more localised changes so the greater the magnitude of the change will have to be.

Potential reasons for the ‘loss of pores’ was earlier suggested to be ingress of solids, cake ‘collapse’ and/or formation of preferential flow channels rendering neighbouring channels essentially ‘ineffective’ in relation to liquid flow. However, arguments could also be made against the ‘loss of pores’ hypothesis since this hypothesis probably implies that the pores ‘reappear’ after a temporary increased filtration rate (see Figures 6.11 and 6.13 for example).

Since the exact extent of local changes in cake structure is unknown, the remainder of this section assumes only 5% of the channels present within the cake at any given time can expand or contract ($a = 0.05$). Figures 6.14 and 6.15 illustrate how R_a and N will have to change with filtration time in order to account for the observed flow increases in the filtration of fibre suspensions at 450, 550 and 600 kPa when $a = 0.05$. From Figure 6.14 it is seen that R_a will have to increase from the region of 0.02 μm to $\sim 1 \mu\text{m}$ in all cases, and from Figure 6.15 it is seen that N will have to decrease by approximately two orders of magnitude in all cases.

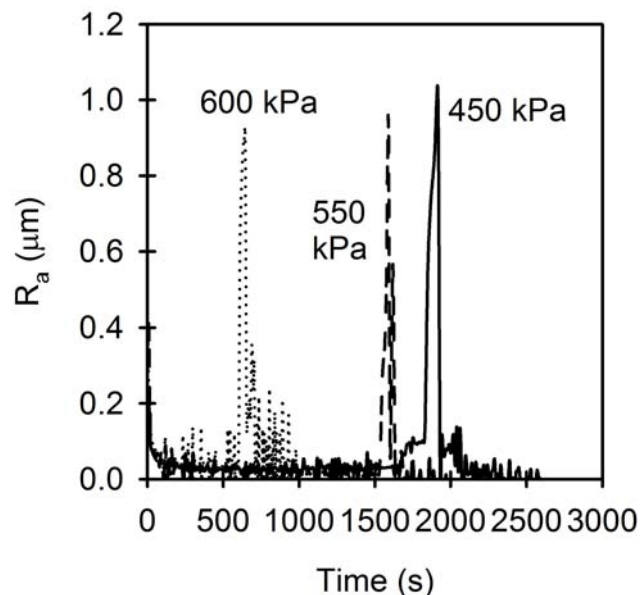


Figure 6.14: R_a profile for filtrations of pure fibre suspensions from deionised water at three filtration pressures when $a = 0.05$.

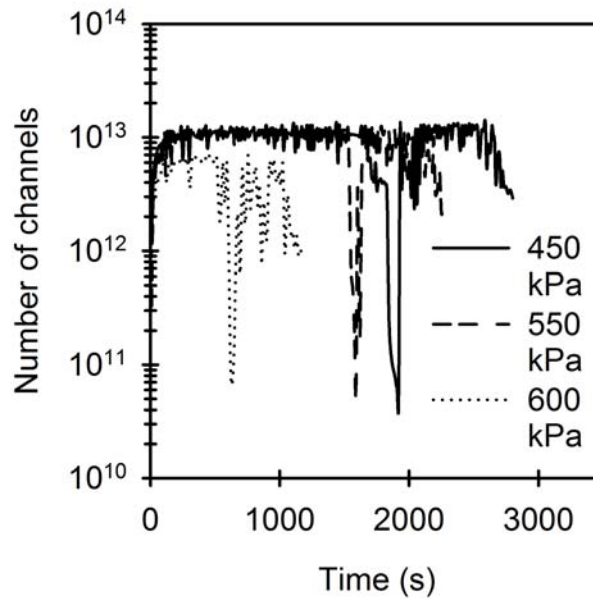


Figure 6.15: Number of channels vs. filtration time for filtrations of pure fibre suspensions from deionised water at three filtration pressures when $a = 0.05$.

Figures 6.16 and 6.17 illustrate how R_a and N will have to change with filtration time in order to account for the observed flow increases in the 450 kPa filtrations of binary suspensions when $a = 0.05$, the corresponding filtration rate profiles are illustrated in Figure 6.5. It is seen that the channel radius will have to increase from the region of $0.02 \mu\text{m}$ to the region of $1 \mu\text{m}$. In this theoretical scenario, taking $X_D = 0.992$ by way of example, just prior to the transition there were approximately 7.5×10^{12} channels of $\sim 0.02 \mu\text{m}$ radius within the cake, and at the maximum measured filtration rate there were approximately 1.9×10^9 (5% of 3.7×10^{10}) channels of $\sim 1.3 \mu\text{m}$ radius and 3.52×10^{10} (95% of 3.7×10^{10}) channels of $\sim 0.02 \mu\text{m}$ radius.

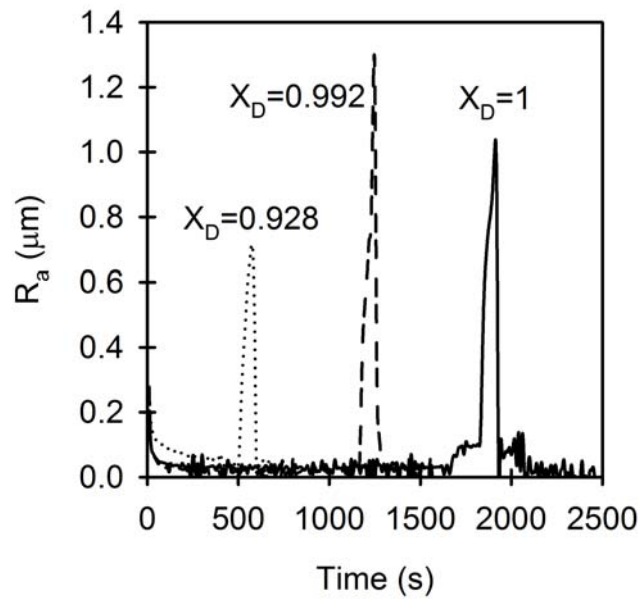


Figure 6.16: R_a profile for filtrations of binary suspensions of various solids composition from deionised water at 450 kPa when $a = 0.05$. The corresponding flow rate profiles are given in Figure 6.5.

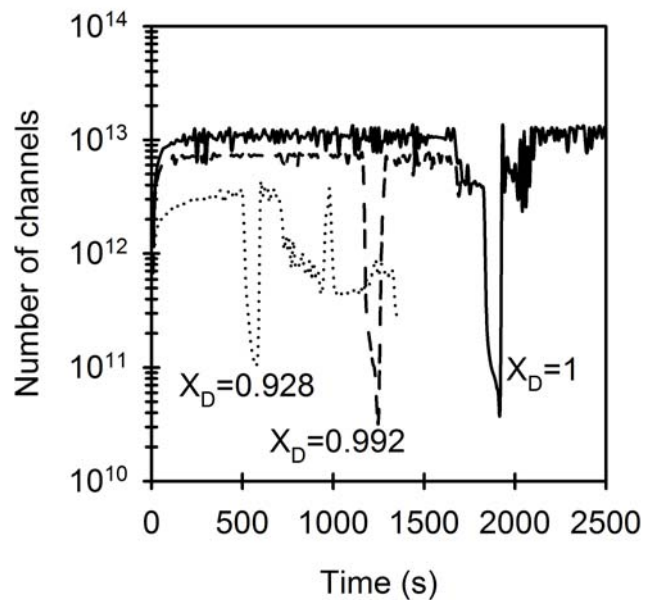


Figure 6.17: Number of channels vs. filtration time for filtrations of binary suspensions of various solids composition from deionised water at 450 kPa when $a = 0.05$. The corresponding flow rate profiles are given in Figure 6.5.

6.4.2. Changing channel radius and cake porosity

Rearranging equation (6.4) gives:

$$(aR_a^2 + bR_b^2)(aR_a + bR_b)^2 = \frac{8\mu h Q_T}{N\pi\Delta P} \quad (6.9)$$

and rearranging equation (6.5) gives:

$$\varepsilon_{av} = \frac{N\pi(aR_a^2 + bR_b^2)}{A} \quad (6.10)$$

Solving equations (6.9) and (6.10) gives values which represent the average channel radius of the channels that can alter in size and the filter cake average porosity, respectively. Here the number of channels (N) is assumed constant and any changes in filtrate flow rate during a filtration are attributed to expansions or contractions of some or all of the hypothetical channels, resulting in an increase or decrease in cake average porosity. The value of N in equations (6.9) and (6.10) is constant and was set to equal the quasi-steady state value (prior to the onset of transition). For example, from Figure 6.11, the quasi-steady state values of N are 1×10^{13} for filtrations at 450 kPa and 550 kPa and 6×10^{12} for filtrations at 600 kPa; these values were inserted into equations (6.9) and (6.10) to obtain R_a and average cake porosity. However, solving equation (6.9) was still not as straightforward as solving equation (6.7) since equation (6.9) is a fourth order equation and so has four roots. Equation (6.9) was solved using Maple and it was found that it only had one physically meaningful solution for R_a at all the filtration pressures and times trialled and at the different values of a . All the other three roots were negative and/or involved the imaginary number (I). For sample calculations of equation (6.9) for R_a using Maple, see Appendix F. This one physically meaningful value of R_a was used in equation (6.10) to calculate filter cake average porosity at various filtration times and pressures.

Figure 6.18 illustrates the profile of the model's representation of filter cake average porosity for a 550 kPa filtration of a pure fibre suspension in deionised water. During the transition in cake structure, the representation of average porosity rises

above 1, but it is obvious that the true porosity cannot rise above 1 as the volume of voids within a cake can never be greater than the total volume of the cake! However, Figure 6.18 is meant to serve as an illustrative example to suggest the likelihood of the mechanism inferred by this variation of the model (equations (6.9) and (6.10)). The porosity values prior to the transition are reasonable, considering that the average porosity as calculated after the experiment was 0.75.

With $a = 1$ and 0.05, the maximum porosity as determined from equation (6.10) was 2.7 and 4.9, respectively. Though it is not suggested that either of these values accurately represent the true porosity values at the transition, it does suggest that when the transition is due to a more localised change in pore diameter(s), so the greater the change in average porosity will be. However, physical reasoning and previous researchers (for example, see Tarleton and Morgan, 2001) suggest that it is unlikely that the changes in pore diameters occur macroscopically throughout the cake.

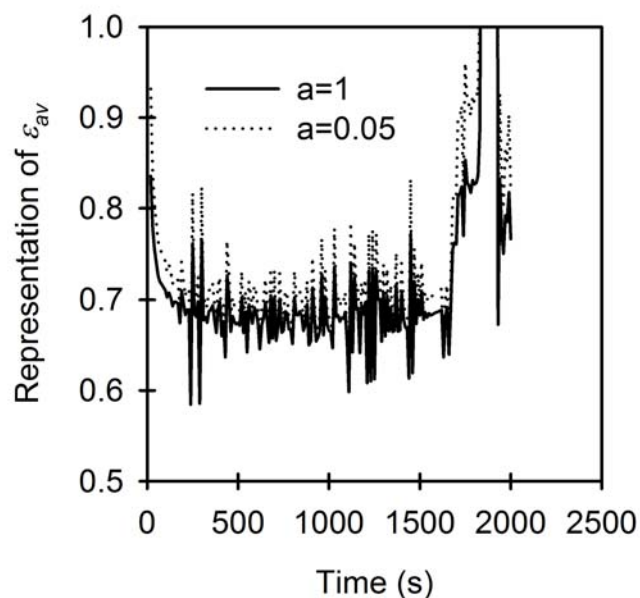


Figure 6.18: Variation of the model representation of filter cake average porosity with filtration time for a 550 kPa filtration of a pure fibre suspension in deionised water.

Considering the unexpected increases in filtration rate as evident with pure fibre suspensions at higher pressures, the results from this analysis suggest that it is unlikely that changes in porosity alone (via changes in channel diameter) can promote the observed behaviour. In the author's opinion, it is likely that the more dominant factor in this case would be the formation of sufficiently large preferential flow channels, even if this is at the expense of neighbouring channels either 'closing' or becoming essentially 'inactive'. However, an accompanying increase in porosity may potentially be a contributing mechanism, and will mean that the increases in R_a and decreases in N will not have to be as significant as suggested in Figures 6.10 – 6.15.

6.5. DISCUSSION AND IMPLICATIONS

Although a definite description of the mechanism(s) that caused the transitions in cake structure cannot be given, potential reasons that are largely consistent with the observed phenomena have been presented. With pure fibre suspensions, no abrupt changes were noted with filtration pressures below 400 kPa. At higher pore filtrate velocities, although there may be a greater stabilising force (if indeed the cake is initially flow stabilised) there will also be a greater shear stress at the pore walls resulting in a greater tendency for the erosion of fines from the walls of channels forming the porous structure in the filter cake, especially for cakes consisting of networked solids. As the transitions in cake structure were all noted once the cake reached a similar thickness, it could be that a sufficiently large local gradient of compressive force resulted in a 'critically' high hydraulic pressure gradient locally which in turn resulted in an increased detaching shear force. The erosion of fines may then have resulted in preferential flow channels which would have caused an increase in filtration rate. A theoretical investigation assuming straight circular channels showed the changes in channel diameter required to promote the observed flow increases, even without the need for changes in cake average porosity.

The region surrounding that involved in this channel formation is also significant. The formation of preferential channels is more likely when the surrounding region is made up of structured or loosely networked solids. With regions of this nature,

it is possible that pores in the vicinity could ‘close’ due to ingress of the eroded solids, or ‘collapse’ of that local region of the cake. It was shown that to promote the unexpected increases in filtration rate as encountered with fibre rich cakes, it is likely that there will be some ‘loss’ of pores, as inferred from the model which suggests that if the number of pores remain roughly the same and a proportion of pores increase in size to promote the increased flow, then this would imply an unrealistically large cake average porosity. However, it may be that if the pore velocity in the surrounding region during a transition in cake structure is sufficiently high, then the cake is adequately stabilised and less likely to experience formation of preferential channels with the accompanying ‘loss’ of pores. This dependence of the nature of transition on pore velocity is illustrated by the fact that when the filtrate flow rate just prior to the change is in the region of $10^{-7} \text{ m}^3 \text{ s}^{-1}$ then the change in cake structure results in a marked decrease in resistance and when the filtrate flow rate just prior to the change is in the region of $10^{-6} \text{ m}^3 \text{ s}^{-1}$ or greater then the change in cake structure results in a relatively less pronounced increase in resistance generally followed by a less significant period of decreased resistance (see, for example, Figures 6.6 and 6.8, and Table 6.1).

Figure 6.19 shows the liquid pressure profiles at various heights within a cake forming during the 450 kPa filtration of a $X_D = 0.154$ suspension from 0.1 M CaCl_2 solution, and Figure 6.20 the corresponding filtration plot. Just prior to point A, a significant decrease in hydraulic pressure may have developed close to the medium, which led to a localised increase in hydraulic pressure gradient. It is possible that this increase in hydraulic pressure gradient resulted in erosion of some fines, which, due to the sufficiently high filtrate flow rate stabilising the surrounding region, did not result in the formation of preferential flow channels (since this may need the closing of other pores in the vicinity) but instead in the blinding of channels within the cake. This erosion-blinding mechanism correspondingly resulted in an increase in filtration resistance (as seen in Figure 6.20) as well as an increase in the compressive solids pressure. The increase in compressive pressure is seen in Figure 6.19 manifested as a drop in liquid pressure close to the medium at point A, and the increased compressive force may have resulted in a return to ‘no cake’ condition (liquid pressure equal to the filtration pressure) 1 mm above the medium. In principle, this mechanism is similar to that proposed by Sørensen *et al.* (1995), with one difference being that the temporary

increase in filtrate flow that they reported was accompanied by a sudden increase in the filtrate turbidity whereas the filtrate remained visually clear at all times in the present work. At point B, the liquid pressure throughout the cake returned to the filtration pressure until filtration ceased.

Figure 6.21 shows liquid pressure profile at various heights within a cake forming during the 600 kPa filtration of an $X_D = 0.391$ suspension from deionised water and Figure 6.22 the corresponding filtration plot. The solids composition, solution environment and filtration pressure for the filtrations represented by Figures 6.21 and 6.22 are different to that represented by Figures 6.19 and 6.20, and so it is likely that the mechanisms involved in the cake structure alterations are also dissimilar. Figure 6.21 shows that just before 28 s into the filtration, a more noticeable liquid pressure gradient built up close to the top of the cake, again resulting in an erosion-blinding mechanism which increased the filtration resistance (Figure 6.22). Just before 38 s, the migration of

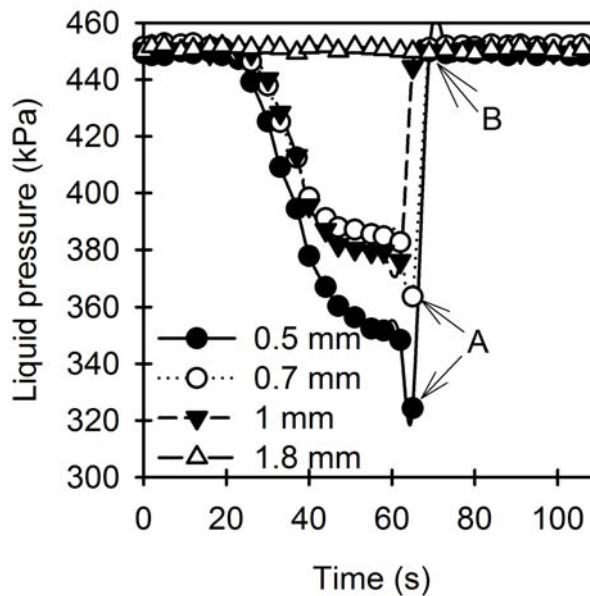


Figure 6.19: Liquid pressure profile at various heights (from the medium) within a cake forming during the 450 kPa filtration of a $X_D = 0.154$ suspension from 0.1 M CaCl_2 solution. The corresponding filtration plot is shown in Figure 6.20.

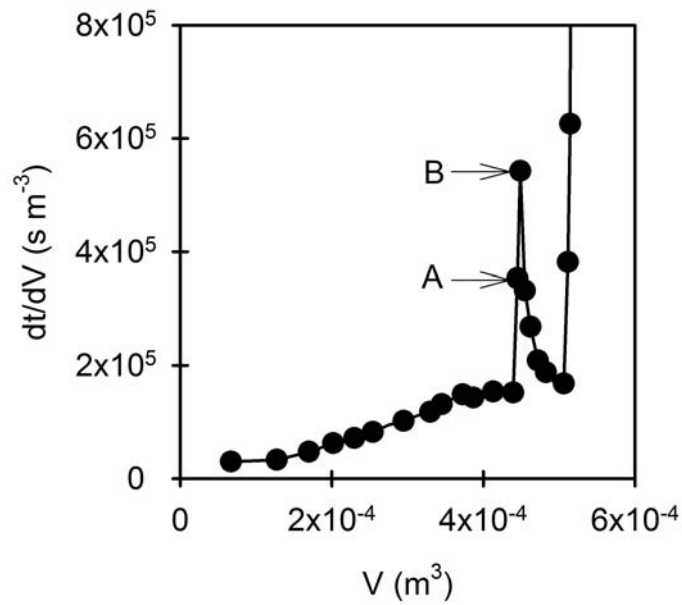


Figure 6.20: Filtration plot for a $X_D = 0.154$ suspension in 0.1 M CaCl₂ solution at a filtration pressure of 450 kPa. The corresponding liquid pressure profile is given as Figure 6.19.

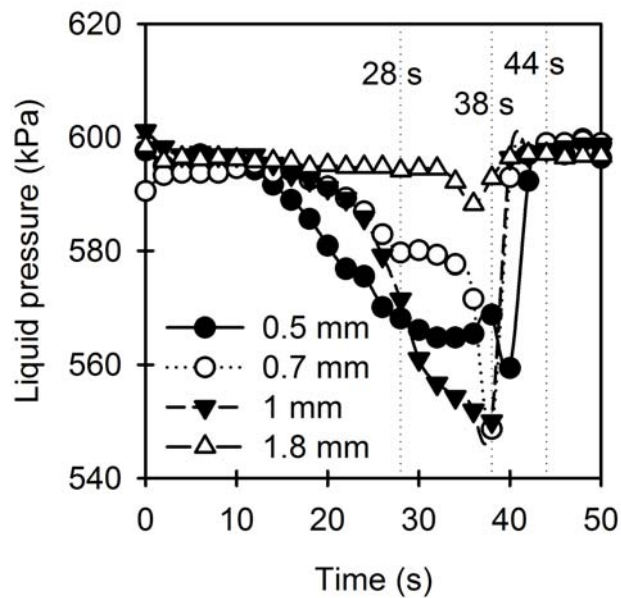


Figure 6.21: Liquid pressure profile at various heights (from the medium) within a cake forming during the 600 kPa filtration of a $X_D = 0.391$ suspension from deionised water. The corresponding filtration plot is shown in Figure 6.22.

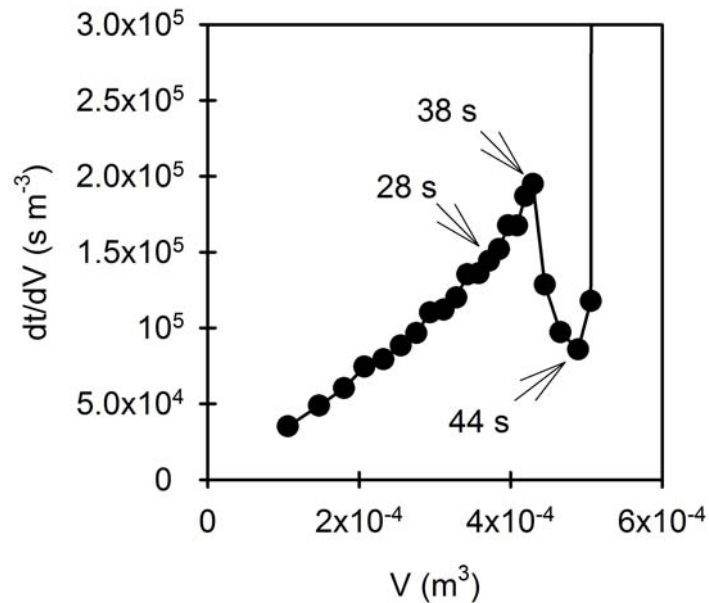


Figure 6.22: Filtration plot for a $X_D = 0.391$ suspension in deionised water at a filtration pressure of 600 kPa. The corresponding liquid pressure profile is given as Figure 6.21.

fibre fines and/or rutile towards the medium may have been the cause of the more noticeable liquid pressure gradient which appeared closer to the medium, and at 38 s the transducer closest to the medium showed a sudden drop in liquid pressure. At this point the drop in liquid pressure close to the medium was accompanied by an unexpected increase in filtrate flow. The instantaneous filtration rate reached a peak 44 s into the filtration, when all the transducers within the cake had returned to the filtration pressure until filtration ceased.

Although the liquid pressure values may not be absolute in their accuracy (see Appendix B), they were useful for the purpose of comparing the behaviour at one cake height and time to another. Further, the liquid pressure profiles do not seem to contradict the postulated mechanisms. However, even with the liquid pressure profiles, it was difficult to ascertain the definite mechanism(s) that resulted in the anomalous filtration behaviour.

6.6. CONCLUSIONS

Abrupt changes to cake structure part way through a filtration appear to be affected by parameters such as filtration pressure and filtrate pore velocity. These transitions appear to occur at a given cake thickness. Previous workers who have noted broadly similar phenomena have generally observed the consequences sporadically (without much control over when it occurs) and exclusively reported either a resultant increase or decrease in filtration rate. It is, perhaps interestingly, shown in this work that not only are the changes in cake structure relatively reproducible, but also the nature of the change can be altered by changes in filtration pressure, solids composition and/or solution environment (some transitions in cake structure result in an increased filtration rate while others in a decreased filtration rate). A postulated mechanism that appeared largely consistent with the observations was that erosion of fines yields an increased filtration rate in some cases via the formation of preferential flow channels, and a decreased filtration rate in others via blinding of channels within the cake. Which of these two cases occur during a filtration appeared to be dependent on the degree of structure exhibited by the cake and the filtrate flow rate just prior to the transition. A theoretical investigation using straight circular channels to represent the pores in a filter cake suggested that the changes in pore size needed to promote the observed flow increases were sufficiently large that it would require the 'loss' of some surrounding pores, otherwise it would imply an unrealistically large value of average cake porosity. Potential mechanisms that would have resulted in this 'loss' of pores were discussed, and are more likely to occur if the surrounding regions exhibited a degree of structure.

REFERENCES

- Baird R.L. and Perry M.G. (1967) The distribution of porosity in filter cakes. *Filtration and Separation* **4**, 471-476.
- Fathi-Najafi M. and Theliander H. (1995) Determination of local filtration properties at constant pressure. *Separation Technology* **5**, 165-178.

Rietema K. (1953) Stabilizing effects in compressible filter cakes. *Chemical Engineering Science* **2**, 88-94.

Sørensen P.B. (1992) *Unified Modelling of Filtration and Expression of Biological Sludge*, Ph.D. Thesis, Aalborg University.

Sørensen P.B., Christensen J.R. and Bruus J.H. (1995) Effect of small scale solids migration in filter cakes during filtration of waste water solids suspension. *Water Environmental Research* **67**, 25-32.

Tarleton E.S. and Morgan S.A. (2001) An experimental study of abrupt changes in cake structure during dead-end pressure filtration. *Filtration* **1**(4), 93-100.

CHAPTER 7: OVERALL CONCLUSIONS AND FUTURE WORK

7.1. OVERALL CONCLUSIONS

Reproducible and accurate filtration data have been obtained through the use of a well controlled automated pressure filtration apparatus, and the constant pressure filtration results of both pure component and binary suspensions were discussed in relation to cake properties such as average porosity and specific resistance. Sedimentation experiments aided the interpretation of filtration results. The effects of solids composition, filtration pressure and solution environment were investigated. The significance of physico-chemical factors was highlighted and the effects of rutile-fibre interactions discussed. Packing models were applied to binary filter cakes and a permeability model was investigated and further developed to advance understanding of interacting fibre/particle mixtures. Deviations from expected filtration behaviour were noted with some filtrations and this was attributed to abrupt transition in cake structure.

The average porosities of filter cakes formed from pure rutile and fibre suspensions in deionised water were approximately 0.6 and 0.75, respectively, and a steady and progressive increase in porosity with fibre fraction was generally observed. Packing models describing the concepts of interparticle penetration and additive porosity were presented and compared to illustrate the fibre/rutile packing characteristics. The additive porosity concept represented the data better, and this was attributed to the limited freedom of rutile particles to migrate within the cake, due to interaction with fibre surfaces. The concept of ‘equivalent packing diameter’ was also discussed in relation to the non-spherical fibrous solids.

With filtrations at 450 kPa, the average specific cake resistances for pure fibre and rutile in deionised water were approximately 9.4×10^{13} and 4.2×10^{12} m kg⁻¹ respectively, with the variation of specific resistance with solids composition showing a minimum. Similar trends were observed at filtration pressures of 150 and 600 kPa. No minimum in specific resistance was observed with 450 kPa filtrations of suspensions

made using 0.2 M NaCl and 0.1 M CaCl₂ solutions. Filtration data presented indicated the significance of physico-chemical interactions as the most likely cause of minima in the trend of average specific cake resistance with solids composition for feeds in deionised water. In general, the relationship between specific resistance and solids composition corresponded with the sedimentation data, where the trend of initial settling rate with solids composition experienced a maximum at a fibre fraction of ~50% v/v. This is not surprising as the initial settling rates were also largely influenced by the degree of aggregation.

Relative to the influence of solids composition and solution environment, the influence of filtration pressure on specific resistance was less significant. The influence of solids composition was most pronounced in the absence of NaCl and CaCl₂ and the influence of solution environment was most pronounced at the extremes of solids composition (i.e. rutile rich and fibre rich). With rutile rich cakes, the reduction in specific resistance due to the 0.2 M NaCl and 0.1 M CaCl₂ solution environments were most likely due to suppression of the rutile electrical double layer resulting in a larger effective rutile size; this was supported by size distribution measurements and an increase in settling rate and average cake porosity. The influence of the 0.1 M CaCl₂ solution was relatively more substantial, and this could have been due to a greater ionic strength and/or Ca²⁺ ions physically adsorbing onto the solids surfaces whereas Na⁺ ions behaved as an indifferent electrolyte. For fibre rich cakes, although definitive reasons for the reduction in specific resistance due to NaCl and CaCl₂ addition were not apparent, several hypotheses were postulated and the most likely reason was suggested to be the aggregation of fibre fines.

The functional dependence of a filter cake's average specific resistance on porosity and the solids effective specific surface has been illustrated by extending the Kozeny-Carman equation for binary mixtures, and the effects of aggregation on these parameters highlighted. Extension of the Kozeny-Carman/Darcy equations resulted in a model whose characteristics were investigated under various assumptions. The ratio of the specific surface of the two constituent solids was shown to be a critical parameter in determining the trend of specific resistance with solids composition for binary mixture filtrations. The difficulties in describing the variation in solids effective specific surface

of the two solids components with solids composition were due to the complexities arising from varying packing mechanisms and aggregation.

A semi-empirical equation was proposed to represent the average specific resistance trend with solids composition. This equation contains two exponential terms and fitting parameters. The model was trialled on fibre/rutile mixtures in various solution environments and at different filtration pressures, as well as on aggregating and non-aggregating silica/rutile mixtures. The model was shown to represent a wide range of experimental data reasonably well. The two fitting parameters were b_1 and b_2 . b_1 represented a coefficient for describing the effects of the addition of small solids on the larger solids component's effective specific surface, due to changes in packing and aggregation. Correspondingly, b_2 represented a coefficient for describing the effects of the addition of larger solids on the small solids component's effective specific surface. b_1 and b_2 were more comparable in magnitude when the solids were of similar size and shape, and in particular when no significant aggregation was evident. It is possible that b_1 and b_2 are system specific parameters. b_1 and b_2 were analysed and may be practically useful for characterisation purposes and/or to serve as a good platform on which to build on in order to increase fundamental understanding of the filtration of binary mixtures.

Abrupt changes to cake structure were evident part way through some filtrations, and resulted in unexpected filtrate flow behaviour. The alterations in cake structure were affected by parameters such as solids form, filtration pressure and filtrate pore velocity, and seemed to occur at a given cake thickness. It was shown that not only are the changes in cake structure relatively reproducible, but also the nature of the change can be altered by changes in filtration pressure, solids composition and/or solution environment (some transitions in cake structure resulted in an increased filtration rate while others in a decreased filtration rate). The nature of the transition in cake structure appeared to be dependent on the degree of structure exhibited by the cake and the filtrate flow rate just prior to the transition. For example, the nature of cake restructuring is altered from one which causes a pronounced increase in filtration rate when the filtrate flow rate just before the transition is in the region of $10^{-7} \text{ m}^3 \text{ s}^{-1}$, to one that causes a decrease in filtration rate followed by a relatively less significant period of

increased filtration rate when the filtrate flow rate just before the transition is in the region of $10^{-6} \text{ m}^3 \text{ s}^{-1}$ or greater.

A mechanism was postulated that appeared consistent with the experimental observations, which suggested that erosion of fines (fibre fines and/or rutile) from the walls of a pore in the cake results an increased filtration rate in some cases (due to the formation of preferential flow channels), and a decreased filtration rate in others (due to blinding of surrounding channels). A theoretical investigation using straight circular channels to represent the pores in a filter cake suggested that the changes in pore size needed to promote the observed flow increases were sufficiently large that it would require the ‘loss’ of some surrounding pores, otherwise it would imply an unrealistically large value of average cake porosity. It is more likely for a ‘loss’ of pores to occur with a cake consisting of more structured solids. Potential mechanisms that would have resulted in this ‘loss’ of pores were suggested to be: (1) the ingress of solids blinding channels, and/or (2) ‘collapsed’ regions of a formed cake.

7.2. FUTURE WORK

Investigations into constant pressure cake filtration of binary suspensions are sparse. It would be useful to obtain a substantial body of data, including data for filtrations of mixtures of particles of varying sizes (but of a sufficiently large size ratio) and mixtures of fibres and particles. This data collection exercise may be time consuming and should not be done randomly but in a systematic manner. It is quite likely that if an appropriate apparatus is used, liquid pressure profiles within a forming binary cake could be measured (especially for mixtures of particles). These profiles should provide interesting insights. An experimental matrix could be drawn to isolate variables in binary suspension filtration such as particle size ratio of the two solids and shape combinations. Elucidating the effects of such a matrix of variables could prove significant for, as an example, the drilling fluids industry, where it is common to try to control the filtration performance of drilling fluids by manipulating the solids properties.

A reasonable system to start off with could be two industrially relevant and common minerals whose sizes differ by roughly an order of magnitude. In order to look at the effects of solids shapes and solids composition on cake filtration performance, an experimental matrix could be developed on 3-4 differently shaped solids, for example fibrous, cylindrical, spherical and flaky. For example, a fibre/bentonite system will be interesting since bentonite cakes are generally more compressible than rutile cakes and particles are less isometric in shape. Also, a fibre/bentonite system will be relevant to the paper and pulp industry since bentonite is a common filler. A plot of 'compressibility index' vs. solids composition will be quite novel and interesting when accompanied by a modelling analysis, particularly if the surface properties of the solids could be controlled to induce aggregation. For instance, the surface properties of the solids could be altered by changing the pH or solution environment. It is noted that surface forces have the greatest influence when the particles are smaller than a few microns. Another, more long term, option will be rigorous experimentation with ternary systems.

The current work resulted in abrupt changes to cake structure part way through some filtrations, which could be controlled to a reasonable extent. This is an interesting phenomenon that should be further investigated. It is also likely that with filtration experimentation with other binary (and perhaps ternary) suspensions, abrupt changes in cake structure are noted and occur in a manner that can be well controlled by changes in filtration pressure, solution environment and/or suspension composition. If better control and accuracy could be exerted on such phenomena, and with a broader matrix of variables designed specifically to elucidate the cause mechanisms, this could potentially lead to great fundamental insight into cake filtration in general and not just when such transitions occur.

Considering that all anomalous filtration behaviour induced by abrupt transitions in cake structure has occurred during the filtration of suspensions containing networked solids, polymeric flocculants could be introduced into suspension. However, this may result in further complications by introducing a third phase and so careful thought will have to be put into what effects the polymers themselves would have on the filtration performance. The extents of aggregation could again be assessed by sedimentation

experimentation. The effect of flocculant concentration on binary suspension filtration performance will then be another fascinating variable for investigation, and may result in an interesting interpretation of ‘optimum’ flocculant concentration.

Binary filtration experiments could be coupled with spectroscopy methods such as X-rays, small angle neutron scattering and/or NMR or optical methods like confocal laser scanning microscopy to get a better picture of localised behaviour within the cake. For example, Antelmi *et al.* (2001) used small-angle neutron scattering as well as void volume fraction and flux measurements to analyse latex filter cakes which extensively collapsed at all tested filtration pressures (20-400 kPa) to investigate the relative motions of the particles. Further, La Heij *et al.* (1996) used NMR imaging to determine porosity profiles during filtration of sewage sludge and claimed that the potential applications of the technique are, for example, checking the constitutive parameters or boundary conditions. To add on to their claim, it is suggested that further insight could be obtained on the internal mechanisms during transitions in cake structure, and binary suspension filtration in general, using NMR imaging either independently or to complement another measurement technique.

The generation and collation of aforementioned data will be a useful addition to those available in the filtration literature, and may present interesting insights into some of the mechanisms involved in the industrial filtration of some complex, heterogeneous suspensions. To complement the data, the packing models presented and discussed in Section 4.3.4.1 and Appendix C of this thesis could be employed and eventually developed further. Also, the concept of ‘equivalent packing diameter’ as developed by Yu and Standish (1993) and Yu *et al.* (1993), which was shown to be a useful concept in relating non-spherical packing to spherical packing (see, for example, Appendix C), may prove useful when investigating the effects of particle shape. The permeability model discussed and developed in Chapter 5 could be further developed in terms of its sophistication and/or physical significance. If somehow in the future the effective specific surface values corresponding to the two solids species of a binary cake could be determined, then the ratio of these two values should be analysed in light of the discussions presented in Chapter 5. Otherwise, the potential physical significance of the

fitting parameters b_1 and b_2 should be interesting and useful, or perhaps the development of a more fundamental model which represents the data.

A model was developed in Chapter 6 to obtain estimates of the magnitudes potentially involved during abrupt transitions in filter cake structure. Based on the equations derived and the relevant assumptions, two scenarios were investigated in this thesis to study the observed filtration behaviour. The first considered changes in channel radius and number of channels to account for the observed filtration behaviour, with the cake average porosity remaining constant, and the second considered changes in cake porosity and channel radius to account for the observed filtration behaviour, with the number of channels remaining constant. It would be useful if the model could be increased in sophistication, based on the theoretical framework, and if a scenario could be investigated where simultaneous variation in all three parameters (channel radius, number of channels and porosity) could be meaningfully analysed.

REFERENCES

Antelmi D., Cabane B., Meireles M. and Aimar P. (2001) Cake collapse in pressure filtration. *Langmuir* **17**, 7137-7144.

La Heij E.J., Kerkhof P.J.A.M., Kopinga K. and Pel L. (1996) Determining porosity profiles during filtration and expression of sewage sludge by NMR imaging. *American Institute of Chemical Engineers J.* **42**, 953-959.

Yu A.B. and Standish N. (1993) Characterisation of non-spherical particles from their packing behaviour. *Powder Technology* **74**, 205-213.

Yu A.B., Standish N. and McLean A. (1993) Porosity calculation of binary mixtures of nonspherical particles. *J. American Ceramic Society* **76**, 2813-2816.

LIST OF NOTATION

A	filtration area (m^2)
A_{ch}	average cross-sectional area of a channel (m^2)
A_{cT}	total contact area between two interacting solids species in a binary mixture (m^2)
A_i	average surface area (in contact with the permeating fluid) of a solids species in a binary mixture, assuming no aggregation (m^2)
A_P	the area of a solid projected in the direction of motion during sedimentation (m^2)
a	fraction of channels that can expand and contract during filtration (-)
b	fraction of channels that cannot expand and contract during filtration (-)
b_1	fitting parameter defined by equation (5.41) (-)
b_{1a}	fitting parameter defined by equation (5.37) (-)
b_2	fitting parameter defined by equation (5.41) (-)
b_{2a}	fitting parameter defined by equation (5.38) (-)
C_D	drag coefficient (-)
C_V	concentration of solids component in feed by volume (%)
c	mass of solids per unit volume of feed liquid (kg m^{-3})
F_D	drag force opposing the motion of a solid body during sedimentation (N)
h	cake thickness (m)
L	final cake thickness (m)
l_f	fibre length (m)
M	mass of solids in suspension (kg)
M_{dc}	mass of dry cake (kg)
M_{wc}	mass of wet cake (kg)
m	ratio of mass of wet cake to mass of dry cake (-)
N	number of hypothetical channels present in a filter cake (-)
n	compressibility index, or number of particles or fibres (-)
Q	channel volumetric flow rate
R	average channel hydraulic radius (m)
R_c	resistance to fluid flow through a filter cake (m^{-1})

S_B	ratio of the larger component's specific surface to the smaller component's specific surface in a binary mixture (-)
S_0	specific surface of solids in binary mixture ($\text{m}^3 \text{m}^{-2}$)
S_i/ϕ_i	specific surface of the larger ($i = 1$) or smaller ($i = 2$) solids component in contact with the permeating fluid with binary mixtures ($\text{m}^3 \text{m}^{-2}$)
s	mass fraction of solids in suspension (-)
t	cake formation time (s)
u	filtrate superficial velocity ($\text{m}^3 \text{m}^{-1} \text{s}^{-1}$)
u_s	sedimentation velocity of a solid body (m s^{-1})
V	cumulative filtrate volume (m^3)
V_1	volume of fibres (m^3)
V_2	volume of rutile (m^3)
V_{feed}	volume of feed (m^3)
V_{fin}	final filtrate volume (m^3)
v	true volume (excluding voids) of filter cake per unit filtration area ($\text{m}^3 \text{m}^{-2}$)
w	mass of dry solids deposited per unit area (kg m^{-2})
X_D	ratio of volume of fibres to the total volume of solids in the binary suspensions (-)
X_M	ratio of mass of fibres to the total mass of solids in the binary suspension (-)
x	particle size (width for fibres) (m)
x_p	equivalent packing diameter (m)

Greek letters

α_{av}	average specific resistance of a filter cake (m kg^{-1})
α_0	average specific resistance at unit applied pressure ($\text{m kg}^{-1} \text{Pa}^{-n}$)
ΔP	filtration pressure (Pa)
μ	liquid viscosity (Pa s)
ε_{av}	average filter cake porosity (-)
ρ	pure component solids true density (kg m^{-3})
ρ_l	liquid density (kg m^{-3})
ρ_s	effective solids density for binary mixtures (kg m^{-3})
ψ	sphericity (-)

Subscripts

<i>a</i>	channels that can alter in size during cake restructuring (Chapter 6)
<i>b</i>	channels that cannot alter in size during cake restructuring (Chapter 6)
<i>l</i>	referring to liquid phase
<i>s</i>	referring to solids phase
<i>tr</i>	value just before an abrupt transition in cake structure (Chapter 6)
1	referring to the (larger) solids component 1 (fibres in this work)
2	referring to the (smaller) solids component 2 (rutile in this work)

APPENDIX A: SELECTED FILTRATION DATASHEETS

In this Appendix, data sheets for selected filtration experiments discussed in Chapter 4 are presented with some relevant experimental parameters given. X_D was defined in the thesis to be the ratio of the volume of fibres to the total volume of solids in the mixture. The temperature was measured using a thermometer prior to an experiment. Filter cake parameters such as average specific cake resistance, average cake porosity and final cake height were calculated after a filtration experiment, as described in Chapter 4. To ensure consistency, the values of total solids concentration and feed volume given were as calculated after an experiment.

Datasheet 1

Experimental Parameters	Data
Solids (total solids concentration, % v/v)	fibres (1.2)
X_D	1
Solution environment	deionised water
Feed volume ($\times 10^{-4} \text{ m}^3$)	5.03
Pressure (kPa)	450
Temperature ($^{\circ}\text{C}$)	21
Average specific cake resistance (m kg^{-1})	1.28×10^{14}
Average cake porosity	0.72
Final cake height (mm)	1.81

Datasheet 2

Experimental Parameters	Data
Solids (total solids concentration, % v/v)	fibres (1.3)
X_D	1
Solution environment	deionised water
Feed volume ($\times 10^{-4} \text{ m}^3$)	5.4
Pressure (kPa)	550
Temperature ($^{\circ}\text{C}$)	21
Average specific cake resistance (m kg^{-1})	1.05×10^{14}
Average cake porosity	0.75
Final cake height (mm)	2.30

Datasheet 3

Experimental Parameters	Data
Solids (total solids concentration, % v/v)	fibres and rutile (1.1)
X_D	0.992
Solution environment	deionised water
Feed volume ($\times 10^{-4} \text{ m}^3$)	5.2
Pressure (kPa)	450
Temperature ($^{\circ}\text{C}$)	22
Average specific cake resistance (m kg^{-1})	8.57×10^{13}
Average cake porosity	0.75
Final cake height (mm)	1.85

Datasheet 4

Experimental Parameters	Data
Solids (total solids concentration, % v/v)	fibres and rutile (1.2)
X_D	0.928
Solution environment	deionised water
Feed volume ($\times 10^{-4} \text{ m}^3$)	5.1
Pressure (kPa)	450
Temperature ($^{\circ}\text{C}$)	21
Average specific cake resistance (m kg^{-1})	3.59×10^{13}
Average cake porosity	0.70
Final cake height (mm)	1.62

Datasheet 5

Experimental Parameters	Data
Solids (total solids concentration, % v/v)	fibres and rutile (1.2)
X_D	0.928
Solution environment	deionised water
Feed volume ($\times 10^{-4} \text{ m}^3$)	4.9
Pressure (kPa)	550
Temperature ($^{\circ}\text{C}$)	22
Average specific cake resistance (m kg^{-1})	2.99×10^{13}
Average cake porosity	0.77
Final cake height (mm)	2.11

Datasheet 6

Experimental Parameters	Data
Solids (total solids concentration, % v/v)	rutile (1.2)
X_D	0
Solution environment	deionised water
Feed volume ($\times 10^{-4} \text{ m}^3$)	4.4
Pressure (kPa)	450
Temperature ($^{\circ}\text{C}$)	22
Average specific cake resistance (m kg^{-1})	5.45×10^{12}
Average cake porosity	0.59
Final cake height (mm)	1.09

Datasheet 7

Experimental Parameters	Data
Solids (total solids concentration, % v/v)	fibres and rutile (1.1)
X_D	0.068
Solution environment,	deionised water
Feed volume ($\times 10^{-4} \text{ m}^3$)	4.7
Pressure (kPa)	450
Temperature ($^{\circ}\text{C}$)	23
Average specific cake resistance (m kg^{-1})	3.19×10^{12}
Average cake porosity	0.62
Final cake height (mm)	1.12

Datasheet 8

Experimental Parameters	Data
Solids (total solids concentration, % v/v)	fibres and rutile (1.0)
X_D	0.154
Solution environment	deionised water
Feed volume ($\times 10^{-4} \text{ m}^3$)	5.1
Pressure (kPa)	450
Temperature ($^{\circ}\text{C}$)	23
Average specific cake resistance (m kg^{-1})	3.50×10^{12}
Average cake porosity	0.61
Final cake height (mm)	1.04

Datasheet 9

Experimental Parameters	Data
Solids (total solids concentration, % v/v)	fibres and rutile (1.0)
X_D	0.265
Solution environment	deionised water
Feed volume ($\times 10^{-4} \text{ m}^3$)	5.2
Pressure (kPa)	450
Temperature ($^{\circ}\text{C}$)	23
Average specific cake resistance (m kg^{-1})	1.70×10^{12}
Average cake porosity	0.63
Final cake height (mm)	1.16

Datasheet 10

Experimental Parameters	Data
Solids (total solids concentration, % v/v)	fibres and rutile (1.1)
X_D	0.391
Solution environment	deionised water
Feed volume ($\times 10^{-4} \text{ m}^3$)	5.1
Pressure (kPa)	450
Temperature ($^{\circ}\text{C}$)	23
Average specific cake resistance (m kg^{-1})	4.77×10^{11}
Average cake porosity	0.68
Final cake height (mm)	1.45

Datasheet 11

Experimental Parameters	Data
Solids (total solids concentration, % v/v)	1.2
X_D	0.520
Solution environment	deionised water
Feed volume ($\times 10^{-4} \text{ m}^3$)	4.7
Pressure (kPa)	450
Temperature ($^{\circ}\text{C}$)	22
Average specific cake resistance (m kg^{-1})	2.69×10^{11}
Average cake porosity	0.68
Final cake height (mm)	1.45

Datasheet 12

Experimental Parameters	Data
Solids (total solids concentration, % v/v)	fibres and rutile (1.0)
X_D	0.646
Solution environment	deionised water
Feed volume ($\times 10^{-4}$ m ³)	5.5
Pressure (kPa)	450
Temperature (°C)	22
Average specific cake resistance (m kg ⁻¹)	2.74×10^{11}
Average cake porosity	0.67
Final cake height (mm)	1.41

Datasheet 13

Experimental Parameters	Data
Solids (total solids concentration, % v/v)	fibres and rutile (1.1)
X_D	0.764
Solution environment	deionised water
Feed volume ($\times 10^{-4}$ m ³)	4.9
Pressure (kPa)	450
Temperature (°C)	22
Average specific cake resistance (m kg ⁻¹)	8.50×10^{11}
Average cake porosity	0.78
Final cake height (mm)	2.03

Datasheet 14

Experimental Parameters	Data
Solids (total solids concentration, % v/v)	fibres and rutile (1.1)
X_D	0.859
Solution environment	deionised water
Feed volume ($\times 10^{-4} \text{ m}^3$)	4.5
Pressure (kPa)	450
Temperature ($^{\circ}\text{C}$)	21
Average specific cake resistance (m kg^{-1})	5.28×10^{12}
Average cake porosity	0.76
Final cake height (mm)	1.64

Datasheet 15 (repeat experiment)

Experimental Parameters	Data
Solids (total solids concentration, % v/v)	fibres (1.1)
X_D	1
Solution environment	deionised water
Feed volume ($\times 10^{-4} \text{ m}^3$)	4.0
Pressure (kPa)	450
Temperature ($^{\circ}\text{C}$)	20
Average specific cake resistance (m kg^{-1})	9.80×10^{13}
Average cake porosity	0.77
Final cake height (mm)	1.65

Datasheet 16 (repeat experiment)

Experimental Parameters	Data
Solids (total solids concentration, % v/v)	rutile (1.0)
X_D	0
Solution environment	deionised water
Feed volume ($\times 10^{-4} \text{ m}^3$)	4.7
Pressure (kPa)	450
Temperature ($^{\circ}\text{C}$)	21
Average specific cake resistance (m kg^{-1})	4.96×10^{12}
Average cake porosity	0.57
Final cake height (mm)	0.92

Datasheet 17 (repeat experiment)

Experimental Parameters	Data
Solids (total solids concentration, % v/v)	fibres and rutile (1.1)
X_D	0.520
Solution environment	deionised water
Feed volume ($\times 10^{-4} \text{ m}^3$)	5.0
Pressure (kPa)	450
Temperature ($^{\circ}\text{C}$)	22
Average specific cake resistance (m kg^{-1})	3.52×10^{11}
Average cake porosity	0.68
Final cake height (mm)	1.46

Datasheet 18 (repeat experiment)

Experimental Parameters	Data
Solids (total solids concentration, % v/v)	1.1
X_D	0.154
Solution environment	deionised water
Feed volume ($\times 10^{-4} \text{ m}^3$)	5.2
Pressure (kPa)	450
Temperature ($^{\circ}\text{C}$)	23
Average specific cake resistance (m kg^{-1})	3.27×10^{12}
Average cake porosity	0.61
Final cake height (mm)	1.20

Datasheet 19

Experimental Parameters	Data
Solids (total solids concentration, % v/v)	fibres and rutile (0.9)
X_D	0.391
Solution environment	0.1 M CaCl_2
Feed volume ($\times 10^{-4} \text{ m}^3$)	5.1
Pressure (kPa)	450
Temperature ($^{\circ}\text{C}$)	21
Average specific cake resistance (m kg^{-1})	3.71×10^{11}
Average cake porosity	0.68
Final cake height (mm)	1.25

Datasheet 20

Experimental Parameters	Data
Solids (total solids concentration, % v/v)	rutile (0.9)
X_D	0
Solution environment	0.1 M CaCl ₂
Feed volume (x10 ⁻⁴ m ³)	5.5
Pressure (kPa)	450
Temperature (°C)	21
Average specific cake resistance (m kg ⁻¹)	5.61x10 ¹¹
Average cake porosity	0.65
Final cake height (mm)	1.16

Datasheet 21

Experimental Parameters	Data
Solids (total solids concentration, % v/v)	fibres and rutile (1.2)
X_D	0.154
Solution environment	0.1 M CaCl ₂
Feed volume (x10 ⁻⁴ m ³)	5.4
Pressure (kPa)	450
Temperature (°C)	21
Average specific cake resistance (m kg ⁻¹)	6.16x10 ¹¹
Average cake porosity	0.66
Final cake height (mm)	1.54

Datasheet 22

Experimental Parameters	Data
Solids (total solids concentration, % v/v)	fibres and rutile (1.2)
X_D	0.646
Solution environment	0.1 M CaCl ₂
Feed volume (x10 ⁻⁴ m ³)	4.9
Pressure (kPa)	450
Temperature (°C)	21
Average specific cake resistance (m kg ⁻¹)	3.04x10 ¹¹
Average cake porosity	0.66
Final cake height (mm)	1.51

Datasheet 23

Experimental Parameters	Data
Solids (total solids concentration, % v/v)	fibres and rutile (1.2)
X_D	0.859
Solution environment	0.1 M CaCl ₂
Feed volume (x10 ⁻⁴ m ³)	4.3
Pressure (kPa)	450
Temperature (°C)	22
Average specific cake resistance (m kg ⁻¹)	1.70x10 ¹¹
Average cake porosity	0.71
Final cake height (mm)	1.52

Datasheet 24

Experimental Parameters	Data
Solids (total solids concentration, % v/v)	fibres and rutile (1.2)
X_D	0.992
Solution environment	0.1 M CaCl ₂
Feed volume (x10 ⁻⁴ m ³)	4.4
Pressure (kPa)	450
Temperature (°C)	20
Average specific cake resistance (m kg ⁻¹)	4.19x10 ¹¹
Average cake porosity	0.75
Final cake height (mm)	1.83

Datasheet 25

Experimental Parameters	Data
Solids (total solids concentration, % v/v)	fibres (1.2)
X_D	1
Solution environment	0.1 M CaCl ₂
Feed volume (x10 ⁻⁴ m ³)	4.5
Pressure (kPa)	450
Temperature (°C)	20
Average specific cake resistance (m kg ⁻¹)	3.52x10 ¹¹
Average cake porosity	0.77
Final cake height (mm)	1.98

Datasheet 26

Experimental Parameters	Data
Solids (total solids concentration, % v/v)	fibres (1.3)
X_D	1
Solution environment	deionised water
Feed volume ($\times 10^{-4} \text{ m}^3$)	3.8
Pressure (kPa)	150
Temperature ($^{\circ}\text{C}$)	21
Average specific cake resistance (m kg^{-1})	3.19×10^{13}
Average cake porosity	0.73
Final cake height (mm)	1.58

Datasheet 27

Experimental Parameters	Data
Solids (total solids concentration, % v/v)	fibres and rutile (1.3)
X_D	0.646
Solution environment	deionised water
Feed volume ($\times 10^{-4} \text{ m}^3$)	4.4
Pressure (kPa)	150
Temperature ($^{\circ}\text{C}$)	21
Average specific cake resistance (m kg^{-1})	2.47×10^{11}
Average cake porosity	0.78
Final cake height (mm)	2.27

Datasheet 28

Experimental Parameters	Data
Solids (total solids concentration, % v/v)	rutile (1.1)
X_D	0
Solution environment	deionised water
Feed volume ($\times 10^{-4} \text{ m}^3$)	4.7
Pressure (kPa)	150
Temperature ($^{\circ}\text{C}$)	21
Average specific cake resistance (m kg^{-1})	1.95×10^{12}
Average cake porosity	0.61
Final cake height (mm)	1.07

Datasheet 29

Experimental Parameters	Data
Solids (total solids concentration, % v/v)	fibres and rutile (0.9)
X_D	0.391
Solution environment	deionised water
Feed volume ($\times 10^{-4} \text{ m}^3$)	4.5
Pressure (kPa)	150
Temperature ($^{\circ}\text{C}$)	22
Average specific cake resistance (m kg^{-1})	2.85×10^{11}
Average cake porosity	0.72
Final cake height (mm)	1.18

Datasheet 30

Experimental Parameters	Data
Solids (total solids concentration, % v/v)	fibres and rutile (1.3)
X_D	0.154
Solution environment	deionised water
Feed volume ($\times 10^{-4}$ m ³)	4.6
Pressure (kPa)	150
Temperature (°C)	23
Average specific cake resistance (m kg ⁻¹)	1.43×10^{12}
Average cake porosity	0.70
Final cake height (mm)	1.64

Datasheet 31

Experimental Parameters	Data
Solids (total solids concentration, % v/v)	fibres and rutile (1.3)
X_D	0.859
Solution environment	deionised water
Feed volume ($\times 10^{-4}$ m ³)	4.1
Pressure (kPa)	150
Temperature (°C)	22
Average specific cake resistance (m kg ⁻¹)	1.55×10^{12}
Average cake porosity	0.79
Final cake height (mm)	2.13

Datasheet 32 (repeat experiment)

Experimental Parameters	Data
Solids (total solids concentration, % v/v)	fibres (1.3)
X_D	1
Solution environment	deionised water
Feed volume ($\times 10^{-4} \text{ m}^3$)	4.2
Pressure (kPa)	150
Temperature ($^{\circ}\text{C}$)	24
Average specific cake resistance (m kg^{-1})	3.00×10^{13}
Average cake porosity	0.77
Final cake height (mm)	1.91

Datasheet 33

Experimental Parameters	Data
Solids (total solids concentration, % v/v)	fibres (1.0)
X_D	1
Solution environment	deionised water
Feed volume ($\times 10^{-4} \text{ m}^3$)	5.0
Pressure (kPa)	600
Temperature ($^{\circ}\text{C}$)	22
Average specific cake resistance (m kg^{-1})	8.66×10^{13}
Average cake porosity	0.77
Final cake height (mm)	1.87

Datasheet 34

Experimental Parameters	Data
Solids (total solids concentration, % v/v)	rutile (1.1)
X_D	0
Solution environment	deionised water
Feed volume ($\times 10^{-4} \text{ m}^3$)	4.6
Pressure (kPa)	600
Temperature ($^{\circ}\text{C}$)	22
Average specific cake resistance (m kg^{-1})	2.07×10^{12}
Average cake porosity	0.64
Final cake height (mm)	1.14

Datasheet 35 (repeat experiment)

Experimental Parameters	Data
Solids (total solids concentration, % v/v)	rutile (1.1)
X_D	0
Solution environment	deionised water
Feed volume ($\times 10^{-4} \text{ m}^3$)	4.8
Pressure (kPa)	450
Temperature ($^{\circ}\text{C}$)	21
Average specific cake resistance (m kg^{-1})	2.34×10^{12}
Average cake porosity	0.59
Final cake height (mm)	1.05

Datasheet 36 (repeat experiment)

Experimental Parameters	Data
Solids (total solids concentration, % v/v)	rutile (0.9)
X_D	0
Solution environment	deionised water
Feed volume ($\times 10^{-4} \text{ m}^3$)	4.7
Pressure (kPa)	600
Temperature ($^{\circ}\text{C}$)	21
Average specific cake resistance (m kg^{-1})	2.98×10^{12}
Average cake porosity	0.62
Final cake height (mm)	0.93

Datasheet 37 (repeat experiment)

Experimental Parameters	Data
Solids (total solids concentration, % v/v)	fibres (1.1)
X_D	1
Solution environment	deionised water
Feed volume ($\times 10^{-4} \text{ m}^3$)	5.0
Pressure (kPa)	450
Temperature ($^{\circ}\text{C}$)	21
Average specific cake resistance (m kg^{-1})	5.70×10^{13}
Average cake porosity	0.76
Final cake height (mm)	1.84

Datasheet 38

Experimental Parameters	Data
Solids (total solids concentration, % v/v)	fibres and rutile (1.2)
X_D	0.154
Solution environment	deionised water
Feed volume ($\times 10^{-4} \text{ m}^3$)	5.4
Pressure (kPa)	600
Temperature ($^{\circ}\text{C}$)	22
Average specific cake resistance (m kg^{-1})	1.54×10^{12}
Average cake porosity	0.67
Final cake height (mm)	1.60

Datasheet 39

Experimental Parameters	Data
Solids (total solids concentration, % v/v)	fibres and rutile (1.1)
X_D	0.646
Solution environment	deionised water
Feed volume ($\times 10^{-4} \text{ m}^3$)	4.9
Pressure (kPa)	600
Temperature ($^{\circ}\text{C}$)	21
Average specific cake resistance (m kg^{-1})	6.51×10^{11}
Average cake porosity	0.70
Final cake height (mm)	1.54

Datasheet 40

Experimental Parameters	Data
Solids (total solids concentration, % v/v)	fibres and rutile (1.2)
X_D	0.391
Solution environment	deionised water
Feed volume ($\times 10^{-4} \text{ m}^3$)	5.3
Pressure (kPa)	600
Temperature ($^{\circ}\text{C}$)	21
Average specific cake resistance (m kg^{-1})	9.02×10^{11}
Average cake porosity	0.67
Final cake height (mm)	1.53

Datasheet 41

Experimental Parameters	Data
Solids (total solids concentration, % v/v)	fibres and rutile (1.2)
X_D	0.859
Solution environment	deionised water
Feed volume ($\times 10^{-4} \text{ m}^3$)	4.5
Pressure (kPa)	600
Temperature ($^{\circ}\text{C}$)	21
Average specific cake resistance (m kg^{-1})	1.90×10^{12}
Average cake porosity	0.75
Final cake height (mm)	1.86

Datasheet 42 (repeat experiment)

Experimental Parameters	Data
Solids (total solids concentration, % v/v)	fibres and rutile (1.2)
X_D	0.859
Solution environment	deionised water
Feed volume ($\times 10^{-4} \text{ m}^3$)	4.5
Pressure (kPa)	450
Temperature ($^{\circ}\text{C}$)	21
Average specific cake resistance (m kg^{-1})	2.57×10^{12}
Average cake porosity	0.76
Final cake height (mm)	1.81

Datasheet 43 (repeat experiment)

Experimental Parameters	Data
Solids (total solids concentration, % v/v)	fibres and rutile (1.2)
X_D	0.859
Solution environment	deionised water
Feed volume ($\times 10^{-4} \text{ m}^3$)	4.8
Pressure (kPa)	600
Temperature ($^{\circ}\text{C}$)	20
Average specific cake resistance (m kg^{-1})	2.47×10^{12}
Average cake porosity	0.75
Final cake height (mm)	1.95

Datasheet 44

Experimental Parameters	Data
Solids (total solids concentration, % v/v)	rutile (1.0)
X_D	0
Solution environment	0.2 M NaCl
Feed volume ($\times 10^{-4}$ m ³)	5.1
Pressure (kPa)	450
Temperature (°C)	24
Average specific cake resistance (m kg ⁻¹)	9.55×10^{11}
Average cake porosity	0.65
Final cake height (mm)	1.17

Datasheet 45

Experimental Parameters	Data
Solids (total solids concentration, % v/v)	fibres and rutile (1.2)
X_D	0.646
Solution environment	0.2 M NaCl
Feed volume ($\times 10^{-4}$ m ³)	5.1
Pressure (kPa)	450
Temperature (°C)	23
Average specific cake resistance (m kg ⁻¹)	3.36×10^{11}
Average cake porosity	0.66
Final cake height (mm)	1.52

Datasheet 46

Experimental Parameters	Data
Solids (total solids concentration, % v/v)	fibres (1.2)
X_D	1
Solution environment	0.2 M NaCl
Feed volume ($\times 10^{-4} \text{ m}^3$)	4.4
Pressure (kPa)	450
Temperature ($^{\circ}\text{C}$)	23
Average specific cake resistance (m kg^{-1})	1.60×10^{12}
Average cake porosity	0.77
Final cake height (mm)	1.89

Datasheet 47

Experimental Parameters	Data
Solids (total solids concentration, % v/v)	fibres and rutile (1.2)
X_D	0.391
Solution environment	0.2 M NaCl
Feed volume ($\times 10^{-4} \text{ m}^3$)	5.4
Pressure (kPa)	450
Temperature ($^{\circ}\text{C}$)	24
Average specific cake resistance (m kg^{-1})	7.04×10^{11}
Average cake porosity	0.66
Final cake height (mm)	1.56

Datasheet 48

Experimental Parameters	Data
Solids (total solids concentration, % v/v)	fibres and rutile (1.2)
X_D	0.154
Solution environment	0.2 M NaCl
Feed volume ($\times 10^{-4}$ m ³)	5.1
Pressure (kPa)	450
Temperature (°C)	23
Average specific cake resistance (m kg ⁻¹)	1.15×10^{12}
Average cake porosity	0.67
Final cake height (mm)	1.59

Datasheet 49

Experimental Parameters	Data
Solids (total solids concentration, % v/v)	fibres and rutile (1.2)
X_D	0.859
Solution environment	0.2 M NaCl
Feed volume ($\times 10^{-4}$ m ³)	4.4
Pressure (kPa)	450
Temperature (°C)	22
Average specific cake resistance (m kg ⁻¹)	1.01×10^{12}
Average cake porosity	0.75
Final cake height (mm)	1.83

APPENDIX B: RECORDED LIQUID PRESSURE PROFILES

Although liquid pressure profiles were successfully recorded by the micro-pressure transducers in the validation experiments, the majority of pressure profiles in this investigation could not be reliably measured due to the nature of the binary cakes, particularly the fibre rich ones. Although it is difficult to know exactly why this happened, a potential reason is the relatively low solids concentrations tested. For example, the recorded liquid pressure profiles appeared more reliable and were more consistent with rutile rich cakes of higher total solids concentration. Further, due to the greater solids presence, filter cakes generally form at a greater rate with suspensions of higher total solids concentrations, and there is less time and space for solids to ‘rearrange’ themselves in the vicinity of a micro-pressure transducer. Another potential reason is the fibre shapes, and how these fibres align themselves and pack in the vicinity of a micro-pressure transducer. An alternative, more simple, explanation is that the filter cakes are too open.

As an example, the recorded liquid pressure profiles during filtrations of an $X_D = 0.859$ suspension in deionised water at three filtration pressures are shown in Figure B1, where it is seen that the measured liquid pressure at various heights within the cake unexpectedly (and perhaps erroneously) remained almost constant at the applied filtration pressure throughout. Therefore, no further reference to recorded liquid pressure profiles is made in Chapters 4 and 5. However, with a few filtration experiments, the liquid pressure profiles do show some variation with time, and were analysed (where appropriate) to provide some insight into specific filtration behaviour as discussed in Chapter 6. Although these values may not be absolute in their accuracy, they were useful for the purpose of comparing the behaviour at one cake height relative to another. Further, with the experiments where the liquid pressure profiles do show variation with time, transitions in cake structure generally corresponded with abrupt changes in liquid pressure as recorded by one or more transducers.

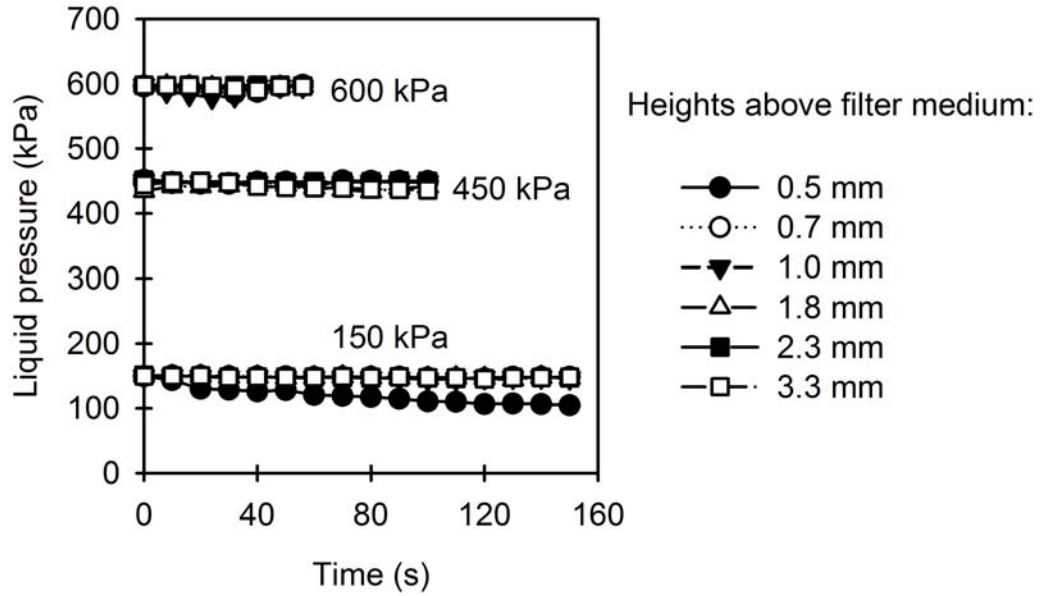


Figure B1: Recorded liquid pressure profiles at various heights above the filter medium during filtrations of an $X_D = 0.859$ suspension in deionised water at three filtration pressures

APPENDIX C: FURTHER DISCUSSION ON THE PACKING MODELS

In Section 4.3.4.1, the Tokumitsu model was used to describe the variation of porosity with fibre fraction, using the concept of interparticle penetration. Although there have been various interparticle penetration models developed, the Tokumitsu model was taken as a representative example. To illustrate the fact that it is indeed representative in the context of this thesis, for comparison purposes the equations presented by Dias *et al.* (2004) were used as an alternative to the Tokumitsu model. After presenting a system of equations, Dias and co-workers reduced them to the two equations, one for a packed bed rich in small particles:

$$\varepsilon_{av} = \varepsilon_{av,2} \left(\frac{1 - X_D}{1 - X_D \varepsilon_{av,2}} \right) \quad (C1)$$

and another for a packed bed rich in large particles:

$$\varepsilon_{av} = 1 - \frac{1 - \varepsilon_{av,1}}{X_D} \quad (C2)$$

where $\varepsilon_{av,1}$ is the average porosity of a bed of large particles (fibres in this case) and $\varepsilon_{av,2}$ the average porosity of a bed of small particles (rutile in this case). Similar to the Tokumitsu model, plots of equation (C1) and (C2) vs. solids composition, with equation (C1) emanating from the pure small component and equation (C2) emanating from the pure large component, will result in two curves which intersect at some intermediate solids composition. This point of intersection is generally taken to be representative of a minimum porosity and indicates a transition from one dominant mechanism to another. Discontinuation of these two curves beyond the intersection point results in one smooth curve which attempts to describe the variation of porosity with solids composition. Equations (C1) and (C2) correspond to the classic linear mixing model, which has been developed in some previous works (Yu and Standish, 1991; Yu *et al.*, 1996; Dias *et al.*, 2004).

Predictions of ε_{av} given by equations (C1) and (C2) for cakes formed from suspensions in deionised water at 450 kPa has been plotted in Figure C1 along with the experimental data for the purposes of comparison with another interparticle penetration model, the Tokumitsu model (equations (4.20) and (4.21)). Predictions given by the Shirato equation for additive porosity (equation (4.24)) were also included in this figure. It is seen that, in general, equations (C1) and (C2) produced a trend similar to that obtained using the Tokumitsu model where a minimum in porosity ($\varepsilon_{av,\min} < 0.5$) was obtained at an $X_D \sim 0.4$. Hence, the use of the Tokumitsu model as being representative of the interparticle penetration mechanism in Section 4.3.4.1 is justified. It is also seen that the concept of additive porosity is apparently more representative of the experimental data than the two interparticle penetration models used (the Tokumitsu model and equations (C1) and (C2)).

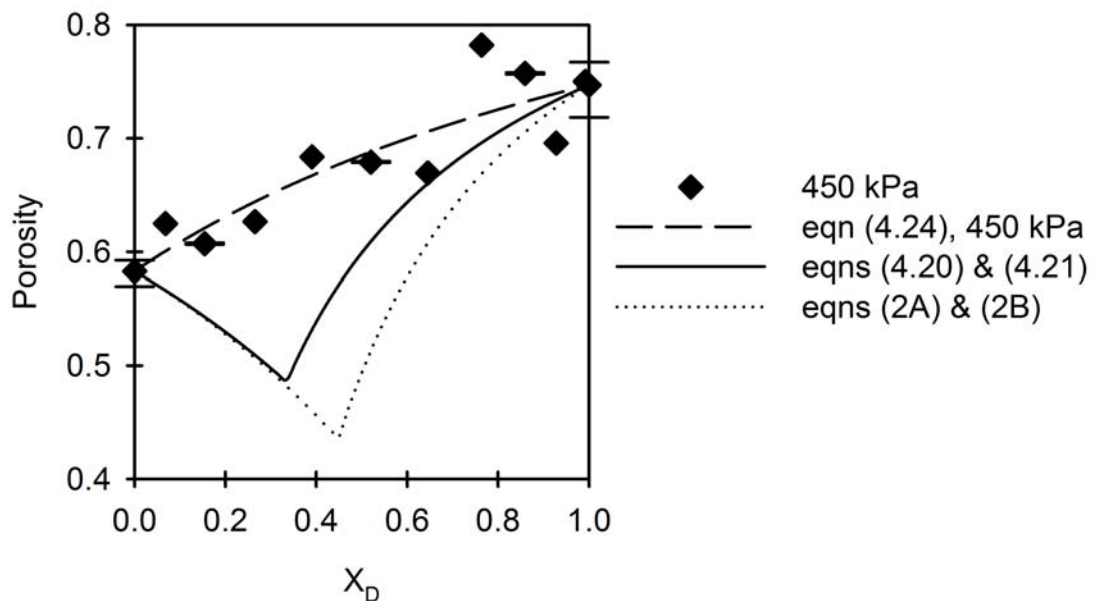


Figure C1: Effects of solids composition on ε_{av} for filtrations from deionised water at 450 kPa.

The predictions given by equation (4.24) (Shirato model), equations (4.20) and (4.21) (Tokumitsu model), and equations (C1) and (C2) (Dias, *et al.*, 2004) are included along with the experimental data.

It is seen that, with fibre rich cakes, the Tokumitsu model predicts a greater porosity than equation (C2), and this could be due to the fibre ‘size’ (x_1) used in the Tokumitsu model. A convenience in the use of equations (C1) and (C2) is that these equations do not require a particle size, since ‘size’ becomes difficult to define, particularly with fibrous type solids. In Section 4.3.4.1, it has been mentioned that the Tokumitsu model showed similar trends (in general) when an ‘equivalent packing diameter’ was used in place of the fibre diameter. Assuming the fibre to be cylindrical, the fibre sphericity is given by equation (4.23) with the ‘equivalent packing diameter’ calculated using equation (4.22). However, as discussed in Section 3.5.2, the fibres were not perfectly cylindrical but had more angular edges. The sphericity of a fibre assumed to take on the shape illustrated in Figure C2 is derived below.

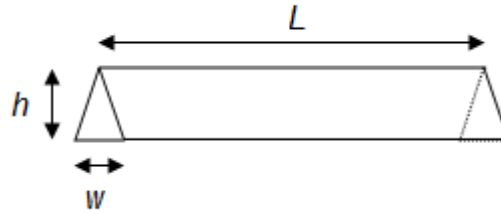


Figure C2: A hypothetical fibre with annotated dimensions.

The surface area of the fibre in Figure C2, S_{A1} , is given by:

$$S_{A1} = w(h + L) + 2hL \quad (C3)$$

The volume of the fibre, V_{A1} , is given by:

$$V_{A1} = \frac{1}{2}whL \quad (C4)$$

If x_v is defined as an equivalent volume diameter, or the diameter of a sphere having the same volume as the fibre, then the following relationship holds:

$$\frac{1}{2}whL = \frac{1}{6}\pi x_v^3 \quad (C5)$$

Rearranging equation (C5) gives an expression for the equivalent volume diameter:

$$x_v = \left(\frac{3}{\pi} whL \right)^{\frac{1}{3}} \quad (C6)$$

The surface area (S_{A2}) of this sphere having the same volume as the fibre is then given by:

$$S_{A2} = \pi x_v^2 = 3.048(whL)^{\frac{2}{3}} \quad (C7)$$

The fibre sphericity (ψ), which is defined as the ratio of the surface area of a sphere (with the same volume as the fibre) to the surface area of the fibre, is then obtained as S_{A2}/S_{A1} , and can be determined by dividing equation (C7) by equation (C3) to give:

$$\psi = \frac{3.048(whL)^{\frac{2}{3}}}{w(h+L) + 2hL} \quad (C8)$$

Yu and Standish (1993) empirically derived the following equation relating the equivalent packing diameter, x_{p1} , to the equivalent volume diameter, x_v , and the solids sphericity:

$$\frac{x_{p1}}{x_v} = \left(3.1781 - 3.6821 \frac{1}{\psi} + 1.5040 \frac{1}{\psi^2} \right) \quad (C9)$$

It can be seen from equation (C9) that for spherical particles $\psi = 1$ and $x_{p1} = x_v$. For a cylindrical shaped fibre, the equivalent volume diameter is given by:

$$x_v = \left(1.145 \left(\frac{l_1}{x_1} \right)^{\frac{1}{3}} x_1 \right) \quad (C10)$$

and sphericity by:

$$\psi = 2.621 \frac{\left(\frac{l_1}{x_1}\right)^{2/3}}{1 + 2\left(\frac{l_1}{x_1}\right)} \quad (\text{C11})$$

Substituting equations (C10) and (C11) into equation (C9) and rearranging gives:

$$x_{p1} = \left(3.1781 - 1.4048 \frac{1 + 2\left(\frac{l_1}{x_1}\right)}{\left(\frac{l_1}{x_1}\right)^{2/3}} + 0.2189 \left(\frac{1 + 2\left(\frac{l_1}{x_1}\right)}{\left(\frac{l_1}{x_1}\right)^{2/3}} \right)^2 \right) \left(1.145 \left(\frac{l_1}{x_1}\right)^{1/3} x_1 \right) \quad (\text{C12})$$

which is the equivalent packing diameter of a cylindrical fibre. Similarly, for a fibre with the dimensions illustrated by Figure C2, substituting equations (C6) and (C8) into equation (C9) and rearranging gives the corresponding equivalent packing diameter as:

$$x_{p1} = \left(3.1781 - 1.2080 \frac{w(h+L) + 2hL}{(whL)^{2/3}} + 0.1619 \left(\frac{w(h+L) + 2hL}{(whL)^{2/3}} \right)^2 \right) \left(\frac{3}{\pi} whL \right)^{1/3} \quad (\text{C13})$$

In Section 3.5.2, the fibres were shown to have a median width of $\sim 15 \mu\text{m}$ and an aspect ratio in the region of 100, and this was used to provide estimates of the parameters in equations (C12) and (C13). x_1 , w and h were assigned a value of $15 \mu\text{m}$, and l_1 and L were assigned a value of 1.5 mm . In an attempt to analyse the sensitivity of the Tokumitsu model to the input fibre ‘size’, three cases were studied:

- Case 1: the fibre width of $15 \mu\text{m}$ was used to represent the fibre ‘size’ as required by the Tokumitsu model;
- Case 2: the fibre ‘size’ as required by the Tokumitsu model was calculated using equation (C12), assuming cylindrical fibres;

- Case 3: the fibre ‘size’ as required by the Tokumitsu model was calculated using equation (C13), assuming fibres shaped as illustrated in Figure 2B.

The plots corresponding to Cases 1-3 (based on the Tokumitsu model) are illustrated in Figure C3, along with equations (C1) and (C2) (as an alternate interparticle penetration model), the Shirato model (concept of additive porosity), and the experimental data for 450 kPa filtrations from deionised water.

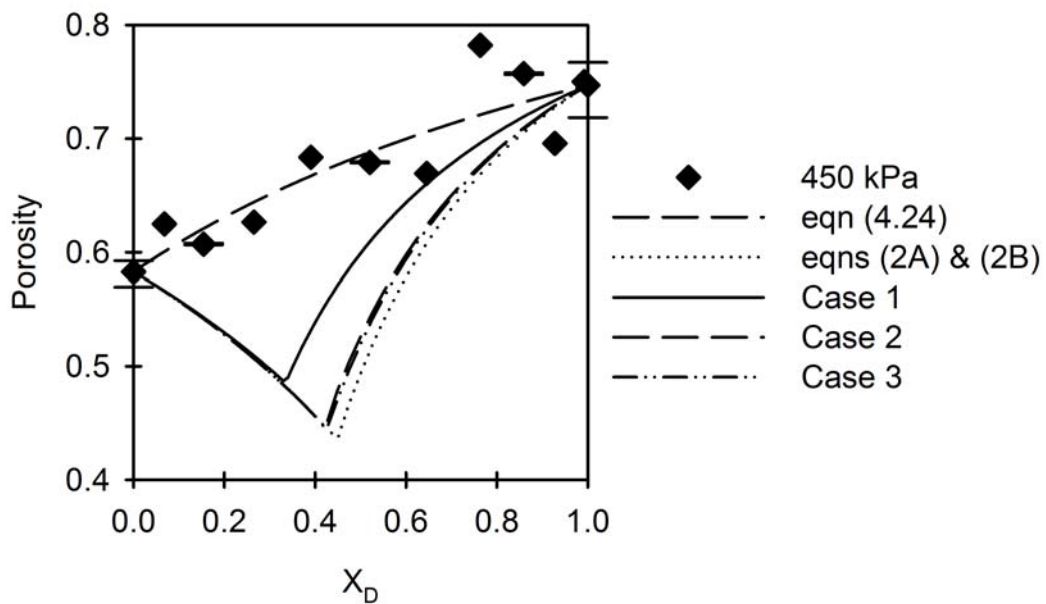


Figure C3: Effects of solids composition on ε_{av} for filtrations from deionised water at 450 kPa. The predictions given by equation (4.24) (Shirato model), equations (2A) and (2B) (Dias *et al.*, 2004), and Cases 1-3 (Tokumitsu model) as described above, are included along with the experimental data.

It is evident that in Cases 2 and 3, the Tokumitsu model approaches the model (equations (C1) and (C2)) presented in the paper published by Dias *et al.* (2004) for spherical particles, substantiating the claims made by Yu and Standish (1993) and Yu *et al.* (1993) that the equivalent packing diameter is a useful concept in relating non-spherical packing to spherical packing. Moving from (physically meaningless) ‘spherical fibres’ (Case 1) to cylindrical ones (Case 2) resulted in a decrease in the

predicted porosity for fibre rich cakes, and a shift in the solids composition at which a minimum in porosity is observed (to cakes richer in fibres). Moving from cylindrical fibres (Case 2) to ones with angular edges as schematically illustrated Figure C2 (Case 3) did not bring about much change in the porosity vs. solids composition trend.

This appendix is presented to complement the discussions made in Section 4.3.4.1. In conclusion, the use of the Tokumitsu model to represent the interparticle penetration mechanism has been justified by comparison with another, widely used, interparticle penetration model. It is seen that a complication with the Tokumitsu model is that a fibre ‘size’ input is required. This input affects the predictions, and using the fibre width as a single parameter to represent its ‘size’ may not be the best approach. The concept of ‘equivalent packing diameter’, as developed by Yu and Standish (1993) and Yu *et al.* (1993), is shown to be a useful concept in relating non-spherical packing to spherical packing. However, whichever fibre ‘size’ used, it is clear that Shirato’s concept of additive porosity represented the experimental data better than the interparticle penetration models, which all showed similar general trends, in particular a minimum porosity at some intermediate fibre fraction.

References:

- Yu A.B., and Standish N. (1991) Estimation of the porosity of particle mixtures by a linear-mixture packing model. *Industrial Engineering Chemistry Research* **30**, 1372-1385.
- Yu A.B., Zou R.P., and Standish N. (1996) Modifying the linear packing model for predicting the porosity of nonspherical particle mixtures. *Industrial Engineering Chemistry Research* **35**, 3730-3741.
- Dias R., Teixeira J.A., Mota M. and Yelshin A. (2004) Particulate binary mixtures: Dependence of packing porosity on particle size ratio, *Industrial Engineering Chemistry Research* **43**, 7912-7919.

APPENDIX D: ADDITIONAL DETAILS OF PERMEABILITY MODEL

This appendix gives further details and discussion on the permeability model presented in Chapter 5. It is a supplement to Section 5.3, and provides further details on the differentiation and relevant manipulation of equations (5.15) and (5.20). Further checks on the methods and results presented here have been made, including checks with Maple.

SUPPLEMENT TO SECTION 5.3

Differentiation and manipulation of equation (5.15)

Equation (5.10) was written as:

$$\alpha_{av} = \frac{5(1 - \varepsilon_{av})}{\varepsilon_{av}^3 (X_D \rho_1 + (1 - X_D) \rho_2)} \left(\frac{X_D S_1}{\phi_1} + \frac{(1 - X_D) S_2}{\phi_2} \right)^2 \quad (D1)$$

Assuming a constant solids effective specific surface and cake average porosity across the range of solids composition, a minimum or maximum in α_{av} can be obtained when:

$$\left. \frac{d\alpha_{av}}{dX_D} \right|_{\varepsilon_{av}, \frac{S_i}{\phi_i}} = 0 \quad (D2)$$

Substituting for the specific resistance in equation (D2) gives:

$$\frac{d}{dX_D} \left(\frac{5(1 - \varepsilon_{av})}{\varepsilon_{av}^3 (X_D \rho_1 + (1 - X_D) \rho_2)} \left(\frac{X_D S_1}{\phi_1} + \frac{(1 - X_D) S_2}{\phi_2} \right)^2 \right) = 0 \quad (D3)$$

Removing the constants from the term in brackets to be differentiated gives:

$$\frac{5(1-\varepsilon_{av})}{\varepsilon_{av}^3} \frac{d}{dX_D} \left(\frac{1}{X_D \rho_1 + (1-X_D) \rho_2} \left(X_D \left(\frac{S_1}{\phi_1} - \frac{S_2}{\phi_2} \right) + \frac{S_2}{\phi_2} \right)^2 \right) = 0 \quad (D4)$$

and carrying out the differentiation in equation (D4) gives:

$$\frac{5(1-\varepsilon_{av})}{\varepsilon_{av}^3} \left(\left(\frac{2}{X_D \rho_1 + (1-X_D) \rho_2} \right) \left(\frac{X_D S_1}{\phi_1} + \frac{(1-X_D) S_2}{\phi_2} \right) \left(\frac{S_1}{\phi_1} - \frac{S_2}{\phi_2} \right) - \left(\frac{X_D S_1}{\phi_1} + \frac{(1-X_D) S_2}{\phi_2} \right)^2 \left(\frac{\rho_1 - \rho_2}{(X_D \rho_1 + (1-X_D) \rho_2)^2} \right) \right) = 0 \quad (D5)$$

Equation (D5) can be rearranged to give:

$$\frac{\rho_1 - \rho_2}{X_D \rho_1 + (1-X_D) \rho_2} \left(\frac{X_D S_1}{\phi_1} + \frac{(1-X_D) S_2}{\phi_2} \right) = 2 \left(\frac{S_1}{\phi_1} - \frac{S_2}{\phi_2} \right) \quad (D6)$$

Manipulating the left hand side term gives equations (D7) and (D8):

$$\frac{\rho_1 - \rho_2}{X_D \rho_1 + (1-X_D) \rho_2} \left(\frac{X_D S_1}{\phi_1} - \frac{X_D S_2}{\phi_2} + \frac{S_2}{\phi_2} \right) = 2 \left(\frac{S_1}{\phi_1} - \frac{S_2}{\phi_2} \right) \quad (D7)$$

$$\frac{1}{X_D + \left(\frac{\rho_2}{\rho_1 - \rho_2} \right)} \left(X_D \left(\frac{S_1}{\phi_1} - \frac{S_2}{\phi_2} \right) + \frac{S_2}{\phi_2} \right) = 2 \left(\frac{S_1}{\phi_1} - \frac{S_2}{\phi_2} \right) \quad (D8)$$

Rearranging equation (D8) gives equations (D9) and (D10):

$$X_D \left(\frac{S_1}{\phi_1} - \frac{S_2}{\phi_2} \right) + \frac{S_2}{\phi_2} = 2X_D \left(\frac{S_1}{\phi_1} - \frac{S_2}{\phi_2} \right) + 2 \left(\frac{S_1}{\phi_1} - \frac{S_2}{\phi_2} \right) \left(\frac{\rho_2}{\rho_1 - \rho_2} \right) \quad (D9)$$

$$X_D \left(\frac{S_1}{\phi_1} - \frac{S_2}{\phi_2} \right) = \frac{S_2}{\phi_2} - 2 \left(\frac{S_1}{\phi_1} - \frac{S_2}{\phi_2} \right) \left(\frac{\rho_2}{\rho_1 - \rho_2} \right) \quad (D10)$$

Manipulating to obtain X_D as the subject expressed in the most convenient manner results in equations (D11):

$$X_D = \frac{1}{\frac{S_1\phi_2}{S_2\phi_1} - 1} - \frac{2\rho_2}{\rho_1 - \rho_2} \quad (\text{D11})$$

Since X_D is defined as the fibre fraction, it ranges from 0 to 1 and so a minimum in specific resistance at an intermediate solids composition can only occur at $0 < X_D < 1$.

From equation (D11), using the constraint $X_D > 0$ gives:

$$\frac{1}{\frac{S_1\phi_2}{S_2\phi_1} - 1} > \frac{2\rho_2}{\rho_1 - \rho_2} \quad (\text{D12})$$

From equation (D11), using the constraint $X_D < 1$ gives:

$$\frac{1}{\frac{S_1\phi_2}{S_2\phi_1} - 1} - \frac{2\rho_2}{\rho_1 - \rho_2} < 1 \quad (\text{D13})$$

From equations (D12) and (D13), using the definition of S_B leads to (i.e. a minimum is observed if):

$$\frac{2\rho_1}{\rho_1 + \rho_2} < S_B < \frac{\rho_1 + \rho_2}{2\rho_2} \quad (\text{D14})$$

Equation (D14) gives the limits of S_B within which a minimum in specific cake resistance can be obtained at some intermediate solids composition, in terms of the solids densities. Equation (D14) highlights the significance of the ratio of solids effective specific surfaces (S_B).

Differentiation and manipulation of equation (5.20)

Unlike equation (5.15) which assumes a constant porosity, in equation (5.20) the variation in cake porosity with solids composition is accounted for via the Shirato model (equation (4.24)). The corresponding form of equation (D1) accounting for varying porosity is given as:

$$\alpha_{av} = \frac{\left(5 \left[1 - \frac{\left(\frac{\varepsilon_{av,1} X_D + \varepsilon_{av,2} (1 - X_D)}{1 - \varepsilon_{av,1}} + \frac{1 - \varepsilon_{av,2}}{1 - \varepsilon_{av,2}} \right)}{\frac{X_D}{1 - \varepsilon_{av,1}} + \frac{1 - X_D}{1 - \varepsilon_{av,2}}} \right] \right)}{\left(\frac{\varepsilon_{av,1} X_D + \varepsilon_{av,2} (1 - X_D)}{1 - \varepsilon_{av,1}} + \frac{1 - \varepsilon_{av,2}}{1 - \varepsilon_{av,2}} \right)^3} \left(X_D \frac{S_1}{\phi_1} + (1 - X_D) \frac{S_2}{\phi_2} \right)^2 \quad (D15)$$

$$\left(X_D \rho_1 + (1 - X_D) \rho_2 \right)$$

Assuming a constant solids effective specific surface across the range of solids composition, a minimum or maximum in α_{av} can be obtained when:

$$\left. \frac{d\alpha_{av}}{dX_D} \right|_{\frac{S_i}{\phi_i}} = 0 \quad (D16)$$

If, for convenience we define terms P , Q , T and U as:

$$P = \frac{X_D}{1 - \varepsilon_{av,1}} + \frac{1 - X_D}{1 - \varepsilon_{av,2}} \quad (D17)$$

$$Q = \frac{\varepsilon_{av,1} X_D}{1 - \varepsilon_{av,1}} + \frac{\varepsilon_{av,2} (1 - X_D)}{1 - \varepsilon_{av,2}} \quad (D18)$$

$$T = X_D \frac{S_1}{\phi_1} + (1 - X_D) \frac{S_2}{\phi_2} \quad (D19)$$

$$U = X_D \rho_1 + (1 - X_D) \rho_2 \quad (\text{D20})$$

Then it follows that:

$$\frac{dP}{dX_D} = \frac{1}{1 - \varepsilon_{av,1}} - \frac{1}{1 - \varepsilon_{av,2}} = V \quad (\text{D21})$$

and

$$\frac{dQ}{dX_D} = \frac{\varepsilon_{av,1}}{1 - \varepsilon_{av,1}} - \frac{\varepsilon_{av,2}}{1 - \varepsilon_{av,2}} = W \quad (\text{D22})$$

Now equation (D15) can be written as:

$$\alpha_{av} = 5 \frac{P^2 T^2}{Q^3 U} \quad (\text{D23})$$

$$\text{since } \varepsilon_{av} = \frac{Q}{P} \text{ and } 1 - \varepsilon_{av} = \frac{P - Q}{P} = \frac{1}{P} \quad (\text{since } P - Q = 1)$$

Differentiating equation (D23) with respect to solids composition gives:

$$\frac{d\alpha_{av}}{dX_D} = 5 \left(\frac{T^2}{Q^3 U} 2P \frac{dP}{dX_D} + \frac{P^2}{Q^3 U} 2T \frac{dT}{dX_D} - \frac{P^2 T^2}{U} \frac{3}{Q^4} \frac{dQ}{dX_D} - \frac{P^2 T^2}{Q^3} \frac{1}{U^2} \frac{dU}{dX_D} \right) \quad (\text{D24})$$

Removing the like terms on the right hand side of equation (D24) gives:

$$\frac{d\alpha_{av}}{dX_D} = 5 \frac{PT}{Q^3 U} \left(2T \frac{dP}{dX_D} + 2P \frac{dT}{dX_D} - \frac{3PT}{Q} \frac{dQ}{dX_D} - \frac{PT}{U} \frac{dU}{dX_D} \right) \quad (\text{D25})$$

$$\frac{d\alpha_{av}}{dX_D} = 5 \frac{PT}{Q^3 U} \left(2TV + 2P \left(\frac{S_1}{\phi_1} - \frac{S_2}{\phi_2} \right) - \frac{3PTW}{Q} - \frac{PT}{U} (\rho_1 - \rho_2) \right) \quad (\text{D26})$$

Checks on equation (D26) were made using Maple and Excel.

At the minimum, $\frac{d\alpha_{av}}{dX_D} = 0$ and so equation (D26) is set to 0, also it is noted that

$5\frac{PT}{Q^3U}$ cannot equal 0. So, setting equation (D26) to 0 and rearranging gives:

$$2TV + 2P\left(\frac{S_1}{\phi_1} - \frac{S_2}{\phi_2}\right) = 3\frac{PTW}{Q} + \frac{PT}{U}(\rho_1 - \rho_2) \quad (D27)$$

Rearranging equation (D27) gives the following equations:

$$\frac{2}{T}\left(\frac{S_1}{\phi_1} - \frac{S_2}{\phi_2}\right) = 3\frac{W}{Q} + \frac{(\rho_1 - \rho_2)}{U} - 2\frac{V}{P} \quad (D28)$$

Since X_D is defined as the fibre fraction, it ranges from 0 to 1 and so a minimum in specific resistance at an intermediate solids composition can only occur at $0 < X_D < 1$.

Using the limit $X_D = 0$ to simplify the terms P , Q , T , U , V and W from equations (D17-D22) gives the following equations:

$$P = \frac{1}{1 - \varepsilon_{av,2}} \quad (D29)$$

$$Q = \frac{\varepsilon_{av,2}}{1 - \varepsilon_{av,2}} \quad (D30)$$

$$T = \frac{S_2}{\phi_2} \quad (D31)$$

$$U = \rho_2 \quad (D32)$$

$$V = \frac{1}{1 - \varepsilon_{av,1}} - \frac{1}{1 - \varepsilon_{av,2}} \quad (D33)$$

$$W = \frac{\varepsilon_{av,1}}{1 - \varepsilon_{av,1}} - \frac{\varepsilon_{av,2}}{1 - \varepsilon_{av,2}} \quad (D34)$$

Substituting equations (D29-D34) into equation (D28) for when $X_D = 0$ gives:

$$\begin{aligned} \frac{2}{\left(\frac{S_2}{\phi_2}\right)} \left(\frac{S_1}{\phi_1} - \frac{S_2}{\phi_2}\right) = \\ 3 \left(\frac{\varepsilon_{av,1}}{1 - \varepsilon_{av,1}} - \frac{\varepsilon_{av,2}}{1 - \varepsilon_{av,2}}\right) \left(\frac{1 - \varepsilon_{av,2}}{\varepsilon_{av,2}}\right) + \frac{\rho_1 - \rho_2}{\rho_2} - 2 \left(\frac{1}{1 - \varepsilon_{av,1}} - \frac{1}{1 - \varepsilon_{av,2}}\right) (1 - \varepsilon_{av,2}) \end{aligned} \quad (D35)$$

Rearranging equation (D35) gives the following equations:

$$\frac{2}{\left(\frac{S_2}{\phi_2}\right)} \left(\frac{S_1}{\phi_1} - \frac{S_2}{\phi_2}\right) = 3 \left(\frac{\varepsilon_1(1 - \varepsilon_2)}{(1 - \varepsilon_1)\varepsilon_2} - 1\right) + \left(\frac{\rho_1}{\rho_2} - 1\right) - 2 \left(\frac{1 - \varepsilon_2}{1 - \varepsilon_1} - 1\right) \quad (D36)$$

$$2 \left(\frac{\left(\frac{S_1}{\phi_1}\right)}{\left(\frac{S_2}{\phi_2}\right)} - 1 \right) = 3 \frac{\varepsilon_1}{\varepsilon_2} \frac{1 - \varepsilon_2}{1 - \varepsilon_1} - 2 \frac{1 - \varepsilon_2}{1 - \varepsilon_1} + \frac{\rho_1}{\rho_2} - 2 \quad (D37)$$

$$\frac{\left(\frac{S_1}{\phi_1}\right)}{\left(\frac{S_2}{\phi_2}\right)} = 1.5 \frac{\varepsilon_1}{\varepsilon_2} \frac{1 - \varepsilon_2}{1 - \varepsilon_1} - \frac{1 - \varepsilon_2}{1 - \varepsilon_1} + 0.5 \frac{\rho_1}{\rho_2} \quad (D38)$$

Finally, put in the simplest form:

$$\frac{\left(\frac{S_1}{\phi_1}\right)}{\left(\frac{S_2}{\phi_2}\right)} = \left(1.5 \frac{\varepsilon_1}{\varepsilon_2} - 1\right) \left(\frac{1 - \varepsilon_2}{1 - \varepsilon_1}\right) + 0.5 \frac{\rho_1}{\rho_2} \quad (D39)$$

Using the limit $X_D = 1$ to simplify the terms P , Q , T , U , V and W from equations (D17-D22) gives the following equations:

$$P = \frac{1}{1 - \varepsilon_{av,1}} \quad (D40)$$

$$Q = \frac{\varepsilon_{av,1}}{1 - \varepsilon_{av,1}} \quad (D41)$$

$$T = \frac{S_1}{\phi_1} \quad (D42)$$

$$U = \rho_1 \quad (D43)$$

$$V = \frac{1}{1 - \varepsilon_{av,1}} - \frac{1}{1 - \varepsilon_{av,2}} \quad (D44)$$

$$W = \frac{\varepsilon_{av,1}}{1 - \varepsilon_{av,1}} - \frac{\varepsilon_{av,2}}{1 - \varepsilon_{av,2}} \quad (D45)$$

Substituting equations (D40-D45) into equation (D26) for when $X_D = 1$ gives:

$$\begin{aligned} \frac{2}{T} \left(\frac{S_1}{\phi_1} - \frac{S_2}{\phi_2} \right) = \\ 3 \left(\frac{\varepsilon_{av,1}}{1 - \varepsilon_{av,1}} - \frac{\varepsilon_{av,2}}{1 - \varepsilon_{av,2}} \right) \left(\frac{1 - \varepsilon_{av,1}}{\varepsilon_{av,1}} \right) + \frac{\rho_1 - \rho_2}{\rho_1} - 2 \left(\frac{1}{1 - \varepsilon_{av,1}} - \frac{1}{1 - \varepsilon_{av,2}} \right) (1 - \varepsilon_{av,1}) \end{aligned} \quad (D46)$$

Rearranging equation (D46) gives the following equations:

$$\frac{2}{\left(\frac{S_1}{\phi_1} \right)} \left(\frac{S_1}{\phi_1} - \frac{S_2}{\phi_2} \right) = 3 \left(1 - \frac{\varepsilon_{av,2}}{\varepsilon_{av,1}} \frac{1 - \varepsilon_{av,1}}{1 - \varepsilon_{av,2}} \right) + \left(1 - \frac{\rho_2}{\rho_1} \right) - 2 \left(1 - \frac{1 - \varepsilon_{av,1}}{1 - \varepsilon_{av,2}} \right) \quad (D47)$$

$$\frac{2}{\left(\frac{S_1}{\phi_1}\right)} \left(\frac{S_1}{\phi_1} - \frac{S_2}{\phi_2} \right) = -3 \frac{\varepsilon_{av,2}}{\varepsilon_{av,1}} \frac{1 - \varepsilon_{av,1}}{1 - \varepsilon_{av,2}} + 2 \frac{1 - \varepsilon_{av,1}}{1 - \varepsilon_{av,2}} - \frac{\rho_2}{\rho_1} + 2 \quad (\text{D48})$$

$$2 - 2 \frac{\left(\frac{S_2}{\phi_2}\right)}{\left(\frac{S_1}{\phi_1}\right)} = -3 \frac{\varepsilon_{av,2}}{\varepsilon_{av,1}} \frac{1 - \varepsilon_{av,1}}{1 - \varepsilon_{av,2}} + 2 \frac{1 - \varepsilon_{av,1}}{1 - \varepsilon_{av,2}} - \frac{\rho_2}{\rho_1} + 2 \quad (\text{D49})$$

$$-2 \frac{\left(\frac{S_2}{\phi_2}\right)}{\left(\frac{S_1}{\phi_1}\right)} = -3 \frac{\varepsilon_{av,2}}{\varepsilon_{av,1}} \frac{1 - \varepsilon_{av,1}}{1 - \varepsilon_{av,2}} + 2 \frac{1 - \varepsilon_{av,1}}{1 - \varepsilon_{av,2}} - \frac{\rho_2}{\rho_1} \quad (\text{D50})$$

Finally, put in the simplest form:

$$\frac{\left(\frac{S_1}{\phi_1}\right)}{\left(\frac{S_2}{\phi_2}\right)} = \frac{1}{1.5 \frac{\varepsilon_{av,2}}{\varepsilon_{av,1}} \frac{1 - \varepsilon_{av,1}}{1 - \varepsilon_{av,2}} + 1 \frac{1 - \varepsilon_{av,1}}{1 - \varepsilon_{av,2}} - 0.5 \frac{\rho_2}{\rho_1}} \quad (\text{D51})$$

From equations (D39) and (D51), considering a minimum is to occur at $0 < X_D < 1$ and using the definition of S_B :

$$\frac{1}{\left(1.5 \frac{\varepsilon_2}{\varepsilon_1} - 1\right) \left(\frac{1 - \varepsilon_1}{1 - \varepsilon_2}\right) + 0.5 \frac{\rho_2}{\rho_1}} < S_B < \left(1.5 \frac{\varepsilon_1}{\varepsilon_2} - 1\right) \left(\frac{1 - \varepsilon_2}{1 - \varepsilon_1}\right) + 0.5 \frac{\rho_1}{\rho_2} \quad (\text{D52})$$

Assuming the solids specific surface remains constant at the various solids compositions, than a minimum in specific cake resistance at some intermediate solids composition can only occur if equation (D52) is satisfied.

APPENDIX E: SUPPLEMENT TO PERMEABILITY MODEL FITTING

Equation (5.41) was chosen over the combined use of equations (5.39) and (5.40) for Figures 5.8 - 5.10 because: (1) it results in a smoother curve, and (2) equation (5.41) seems to be more physically meaningful. Although further discussion is given in Section 5.4, one reason why equation (5.41) is perhaps more meaningful is due to the difference between the fitting parameters in equation (5.41) (b_1 and b_2) and those in equations (5.39) and (5.40) (b_{1a} and b_{2a}); which is that b_{1a} only has an influence with filter cakes rich in the larger solids component and b_{2a} with filter cakes rich in the smaller solids component (see equations (5.37) and (5.38)), whereas b_1 and b_2 exert their influence over the entire range of solids compositions for binary cakes (with different ‘weightings’). However, the combined use of equations (5.39) and (5.40) also gave acceptable fits to the experimental data, as illustrated in Figures E1 – E4.

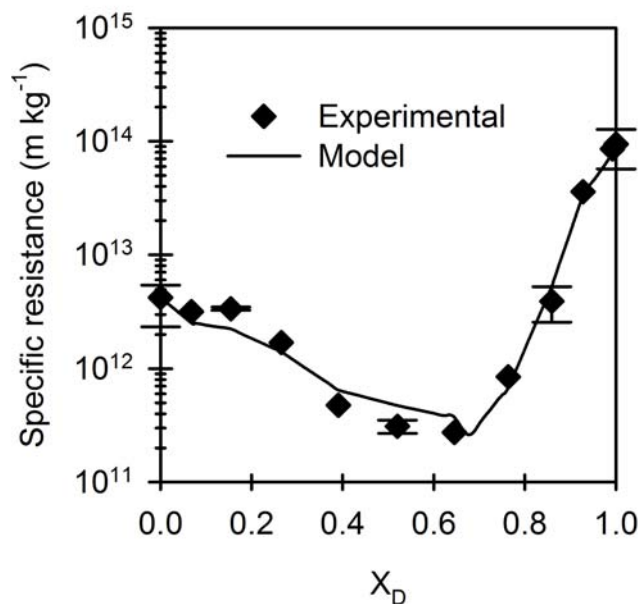


Figure E1: Experimental filtration data for a fibre/rutile system in deionised water at 450 kPa, and the model fit using equations (5.39) and (5.40).

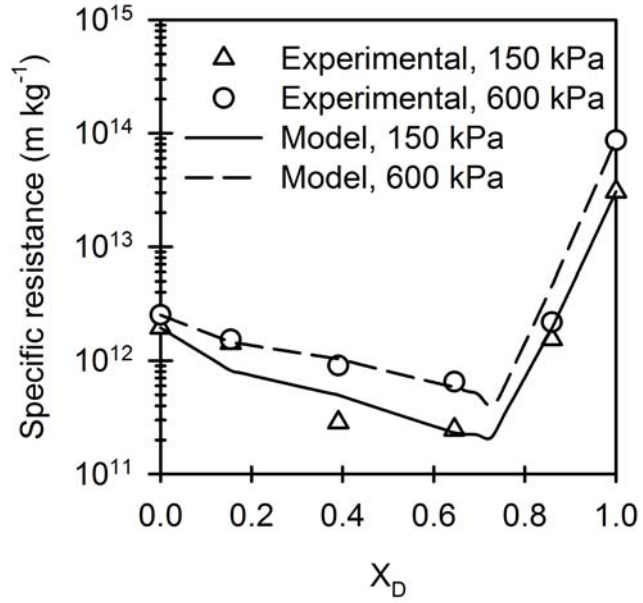


Figure E2: Experimental filtration data for a fibre/rutile system in deionised water at 150 and 600 kPa, and the model fits using equations (5.39) and (5.40).

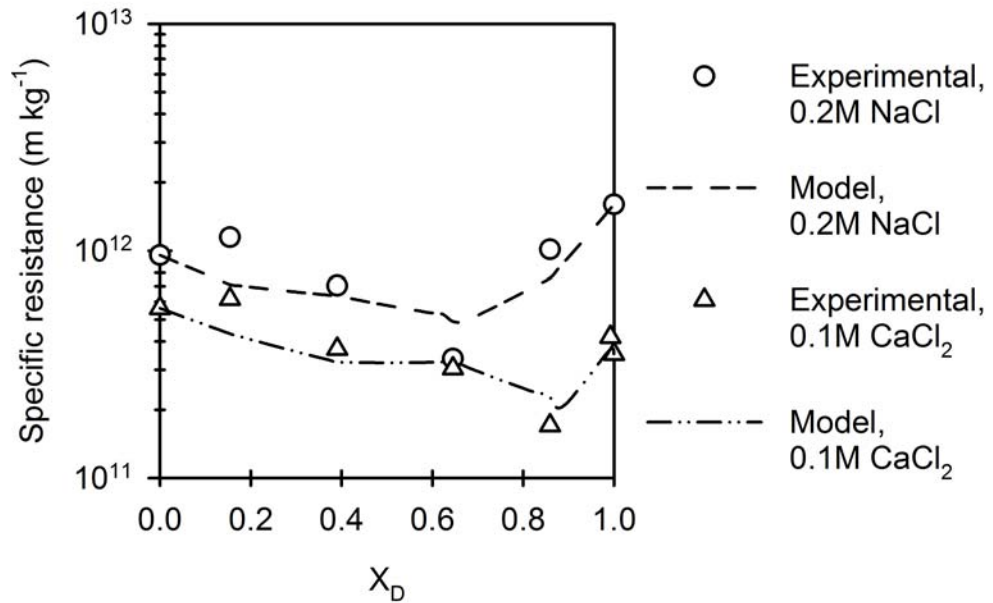


Figure E3: Experimental filtration data for a fibre/rutile system in two solution environments at 450 kPa, and the model fits using equations (5.39) and (5.40).

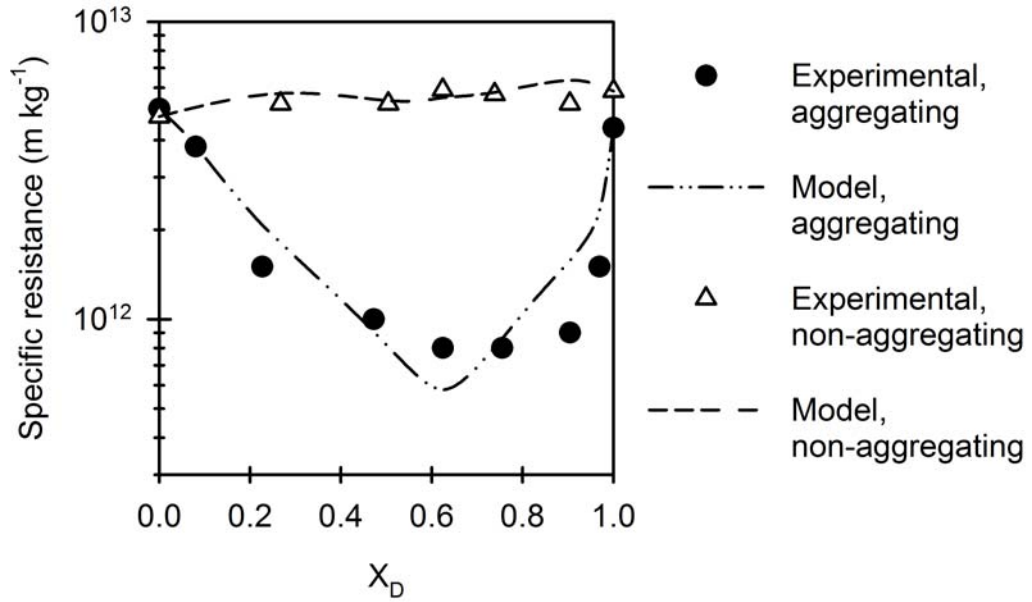


Figure E4: Experimental filtration data at 196 kPa with deionised water at pH 4.5 (where rutile-silica aggregation occurs) and at pH 9.6 (where no aggregation took place), and the model fits using equations (5.39) and (5.40). In this figure, an X_D of 0 refers to pure rutile and an X_D of 1 refers to pure silica. The experimental data points were recalculated from that reported by Iritani *et al.* (2002).

It is seen that the combined use of equations (5.39) and (5.40) also gave reasonably good fits to a wide range of experimental data. A descriptive example of how the combined use of equations (5.39) and (5.40) is applied to the experimental data has been given in Section 5.4. A similar procedure was used for equation (5.41), where equation (E1) was curve fitted to the experimentally determined representation of total solids specific surface trend with solids composition, to determine the values of b_1 and b_2 .

$$S_0 = X_D \frac{S_1}{\phi_1} \exp(-b_1(1 - X_D)) + (1 - X_D) \frac{S_2}{\phi_2} \exp(-b_2 X_D) \quad (\text{E1})$$

The experimentally determined representations of total solids specific surface were calculated from equation (5.35).

Once values of b_1 and b_2 were determined, they were used in equation (5.41) to represent the variation of specific cake resistance with solids composition. Fitting equation (E1) to the calculated total solids specific surface vs. solids composition trend was done using non-linear regression in SigmaPlot. It should be noted that the equation was coded into SigmaPlot (user defined) and in the code, a represented the specific surface of pure fibres (S_1/ϕ_1) and c the specific surface of pure rutile (S_2/ϕ_2). a and c were determined from the two pure component filtrations and since these were known for a given set of conditions (binary mixture, solution environment and filtration pressure), they were input as constraints. Also, in the code, b represented the fitting parameter b_1 , and d represented the fitting parameter b_2 . An example SigmaPlot non-linear regression results file with fibre/rutile mixtures in deionised water at a filtration pressure of 450 kPa is given as Table E1. An example plot generated using SigmaPlot, for the non-linear regression shown in Table E1 (fibre/rutile in deionised water at 450 kPa), is presented as Figure E5; this plot shows the fit of equation (E1) to the calculated specific surface data.

Table E1: Example SigmaPlot non-linear regression results file.

Nonlinear Regression **Fibre/rutile in deionised water, 450 kPa**

Data Source: 150 kPa in f(S) vs Xd 2
Equation: User-Defined, Kuhan
 $f=x*a*\exp(-b*(1-x))+(1-x)*c*\exp(-d*x)$

Data Source: 450 kPa in f(S) vs Xd 2
Equation: User-Defined, Kuhan
 $f=x*a*\exp(-b*(1-x))+(1-x)*c*\exp(-d*x)$

R	Rsqr	Adj Rsqr	Standard Error of Estimate		
0.997	0.994	0.992	5940310.459		
		Coefficient	Std. Error	t	P
a	200821320.944	4466833.190		44.958	<0.0001
b	8.411	0.615		13.683	<0.0001
c	41166647.955	4521351.789		9.105	<0.0001
d	0.758	0.567		1.337	0.2180

Analysis of Variance:

Analysis of Variance:

	DF	SS	MS
Regression	4	9.962E+016	2.491E+016
Residual	8	2.823E+014	3.529E+013
Total	12	9.990E+016	8.325E+015

Corrected for the mean of the observations:

	DF	SS	MS	F	P
Regression	3	5.014E+016	1.671E+016	473.653	<0.0001
Residual	8	2.823E+014	3.529E+013		
Total	11	5.042E+016	4.584E+015		

Statistical Tests:

Normality Test (Shapiro-Wilk) Passed (P = 0.9754)

W Statistic= 0.9782 Significance Level = 0.0500

Constant Variance Test Passed (P = 0.5877)

Fit Equation Description:

```
[Variables]
x = col(3)
y = col(8)
reciprocal_y=1/abs(y)
reciprocal_ysquare=1/y^2
'Automatic Initial Parameter Estimate Functions
xnear0(q)=max(abs(q))-abs(q)
yatxnear0(q,r)=xatymax(q,xnear0(r))
[Parameters]
a = yatxnear0(y,x)/2 "Auto {{previous: 2.00821e+008}}
b = if(x50(x,y)-min(x)=0, 1, -ln(.5)/(0.5*(x50(x,y)-min(x)))) "Auto {{previous: 8.41123}}
c = yatxnear0(y,x)/2 "Auto {{previous: 4.11666e+007}}
d = if(x50(x,y)-min(x)=0, .5, -ln(.5)/(1.5*(x50(x,y)-min(x)))) "Auto {{previous: 0.758021}}
[Equation]
f=x*a*exp(-b*(1-x))+(1-x)*c*exp(-d*x)
fit f to y
"fit f to y with weight reciprocal_y
"fit f to y with weight reciprocal_ysquare
[Constraints]
a=200821321
c=41166648
[Options]
tolerance=1e-010
stepsize=1
iterations=200
```

Number of Iterations Performed = 8

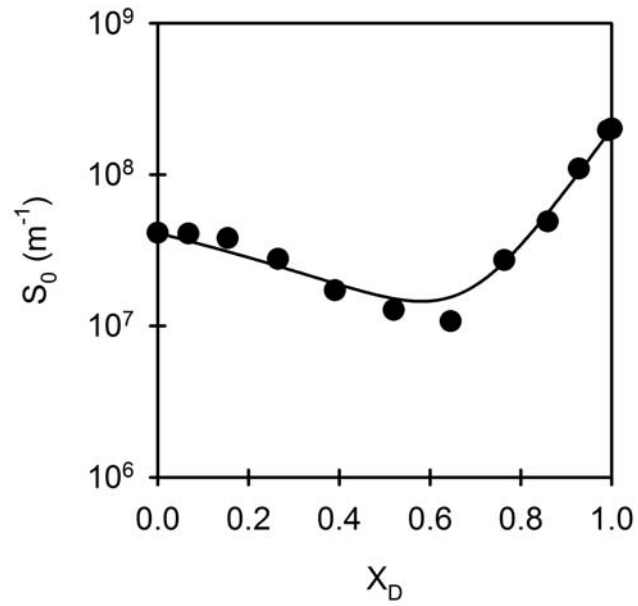


Figure E5: Plot of S_0 vs. solids composition. The line corresponds to equation (E1). The data points were calculated from 450 kPa filtrations with deionised water using equation (5.35), and the pure component effective specific surface values (S_1/ϕ_1 and S_2/ϕ_2) from equation (5.11) and the pure component filtration data.

APPENDIX F: SUPPLEMENT TO SECTION 6.4

This appendix discusses three points relevant to Section 6.4 by means of examples and sample calculations. These points are:

1. the sensitivity of parameters such as average channel radius and number of channels as determined from equations (6.7) and (6.8) to the cake height (h) value used in these equations;
2. the use of the Kozeny-Carman model to get a ‘feel’ for the macroscopic changes (increases) in cake average porosity required to promote the flow increases observed after a change in cake structure;
3. the solution of equation (6.9) to determine the value of R_a using Maple.

1. Sensitivity to cake height

This part discusses the sensitivity of the model presented in Section 6.4 to the cake height, which is the parameter h in the model. Using equation (6.6) to obtain values of h , and substituting into equations (6.7) and (6.8) to solve for average channel radius and number of channels, resulted in the plots illustrated by Figures 6.10 and 6.11 (respectively) for pure fibre suspensions in deionised water at three filtration pressures with $a = 1$. Here, the 550 kPa filtration of a pure fibre suspension in deionised water, with $a = 1$, has been used as an example to illustrate the sensitivity of the model to the parameter h . Figure F1 illustrates the cake height profile, as calculated from equation (6.6). It is unlikely that the true cake height profile is represented by Figure F1, particularly when restructuring of the cake occurs (~ 1500 s), and this makes it all the more important to determine the sensitivity of the model to cake height.

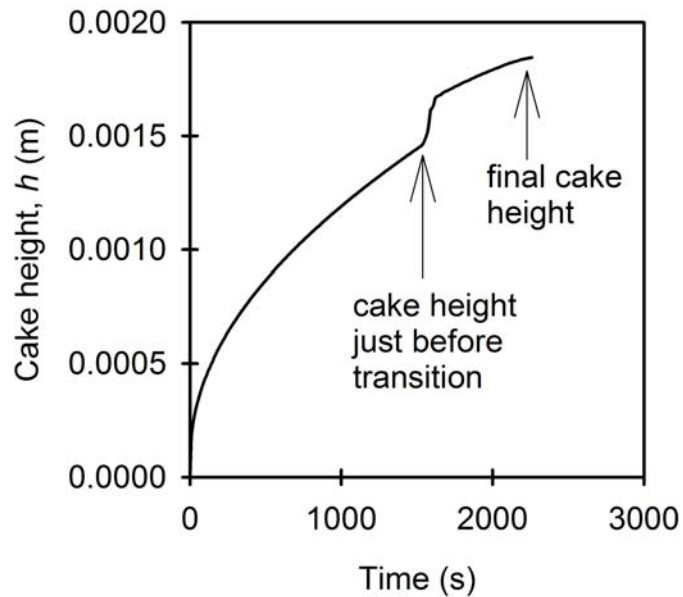


Figure F1: Cake height profile for a 550 kPa filtration of a pure fibre suspension in deionised water as determined from equation (6.6).

To investigate the sensitivity of equations (6.7) and (6.8) on cake height, two cases were compared to the one presented in Section 6.4.1, which assumes a cake height profile as illustrated in Figure F1. Case 1 assumes that, from a filtration time of 1000 s, the cake height remains constant at the value just before the transition in cake structure of 1.46 mm (see Figure F1). Case 2 assumes that, from a filtration time of 1000 s, the cake height remains constant at the final cake height value of 1.85 m (Figure F1). The results of these two cases have been plotted alongside the data presented in Figures 6.10 and 6.11 for the channel radius and number of channels, respectively; these plots have been presented as Figures F2 and F3.

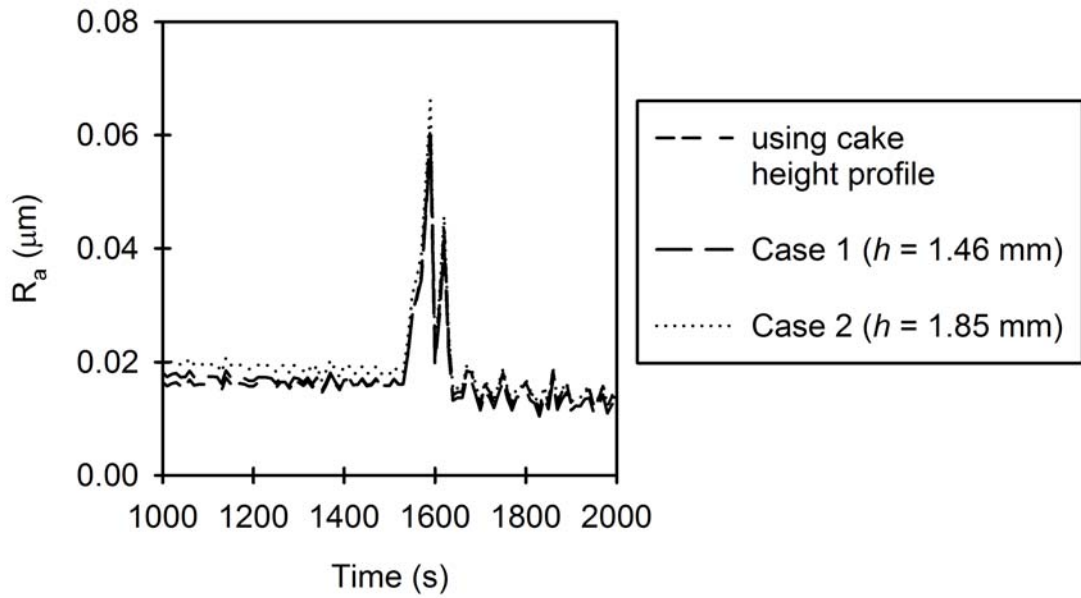


Figure F2: Illustration of the sensitivity of average channel radius as determined from equation (6.7) to the value of cake height (h) used.

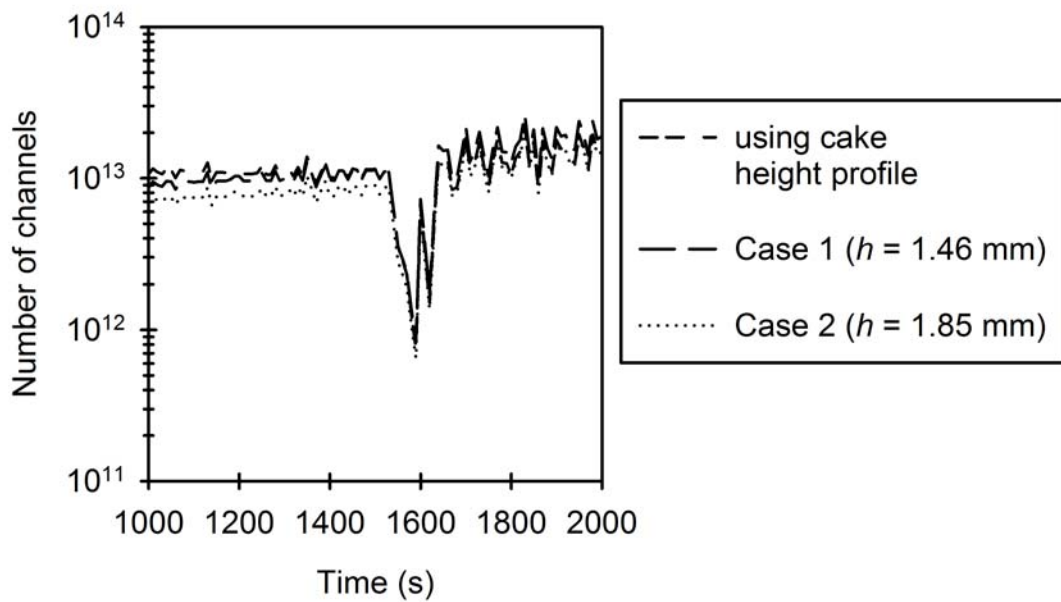


Figure F3: Illustration of the sensitivity of number of channels as determined from equation (6.8) to the value of cake height (h) used.

It is seen that the lines in Figures F2 and F3 are similar regardless of whether the cake height profile (equation (6.6)), or two different (constant) values of cake height were used in equations (6.7) and (6.8). In conclusion, although compression may take place during a filtration and the cake may ‘collapse’ reducing h at a certain time during a filtration, all cakes in this investigation were relatively thin and trial calculations (an example has been shown here for a 550 kPa filtration of pure fibres in deionised water) shows that minor changes in cake height do not cause significant variation in the results obtained. Hence the use of equation (6.6) in the model in Section 6.4 is validated.

2. Calculations using Kozeny-Carman for change in porosity

The Kozeny-Carman equation can be written as:

$$k_{av} = \frac{\varepsilon_{av}^3}{5S_0^2(1 - \varepsilon_{av})^2} \quad (F1)$$

where S_0^2 is the solids specific area in contact with the permeating fluid. The average cake permeability, k_{av} , is related to the liquid flow rate and filter cake thickness according to Darcy’s Law:

$$\frac{1}{A} \frac{dV}{dt} = \frac{-k_{av}}{\mu} \frac{dP}{dx} \quad (F2)$$

where dP is the pressure difference across thickness dx of filter cake of permeability k_{av} . Substituting equation (F1) into equation (F2) and rearranging gives:

$$\frac{dV}{dt} = \frac{A\varepsilon_{av}^3}{5S_0^2\mu(1 - \varepsilon_{av})^2} \frac{dP}{dx} \quad (F3)$$

It is assumed that the variation in cake thickness is negligible, and the specific surface remains approximately constant over this short period. By way of example, equation (F3) is applied to the data for a 550 kPa filtration of a fibre suspension in deionised water. It is noted that the final filter cake average porosity was approximately 0.75 for

this filtration. Further, there was an approximately 8 times increase in liquid flow after the change in cake structure. To account for this measured increase, the average cake porosity needs to change over the range 0.75 to 0.89 if it is assumed that 0.75 is the average cake porosity just before the transition, or 0.55 to 0.75 if it is assumed that 0.75 is the average cake porosity at the maximum filtrate flow rate. These ranges are purely to serve as an example to obtain a ‘feel’ for the magnitudes involved, and both show that a relatively large, and probably unrealistic, macroscopic changes in average porosity are required to promote the observed flow increases. Further discussions on how porosity may have influenced the measured filtrate flow behaviour are presented in Section 6.4.2.

3. Sample Maple calculations for the solution of equation (6.9)

Equation (6.9) is a fourth order equation and so has four roots. This equation was solved using Maple and it was found that it only had one physically meaningful solution for R_a at all the filtration pressures and times trialed and at the different values of a ; the other three roots were negative and/or involved the imaginary number (I). For example, the following Maple solution scheme is for a 550 kPa filtration of a pure fibre suspension in deionised water:

> `solve(equation, variable);`

> $f := x \rightarrow (0.05 \cdot x^2 + 0.95 \cdot (1.6 \cdot 10^{-8})^2) \cdot (0.05 \cdot x + 0.95 \cdot 1.6 \cdot 10^{-8})^2 - 1.0971 \cdot 10^{-30};$

$$f := x \rightarrow \left(0.05 x^2 + 0.95 \cdot 1.6^2 \left(\frac{1}{100000000} \right)^2 \right) \left(0.05 x + 0.95 \cdot 1.6 \frac{1}{100000000} \right)^2 + (-1) \cdot 1.0971 \frac{1}{10000000000000000000000000000000000}$$

> `solve(f(x) = 0, x);`

$$1.80393578410^{-7}, -1.48003723410^{-7} + 2.68041181510^{-7} I, \\ -4.92386131610^{-7}, -1.48003723410^{-7} - 2.68041181510^{-7} I$$

>

With the above, $a = 0.05$, $b = 0.95$, $R_b = 1.6 \times 10^{-8}$ m, and the right hand side of equation (6.9) given by:

$$\frac{8\mu h Q_T}{N\pi\Delta P} = 1.0971 \times 10^{-30}$$

It is seen from the Maple solution scheme above that only one physically meaningful value for R_a was obtained, the other three roots were either negative and/or involved the imaginary number (I). This one value for R_a was then inserted into equation (6.10) to calculate the filter cake average porosity.

APPENDIX G: PAPERS ARISING FROM THE RESEARCH

This appendix gives the academic papers arising from the research, which have either been published or submitted for publication. These include:

Refereed Journals:

1. Chellappah K., Tarleton E.S. and Wakeman R.J. (2009) Filtration and sedimentation behaviour of fibre/particle binary suspensions. *FILTRATION* **9**(4), 286-294.
2. Chellappah K., Tarleton E.S. and Wakeman R.J. (2010) The porosity, permeability and restructuring of heterogeneous filter cakes. *Chemical Engineering and Technology* (In Press).
3. Chellappah K., Tarleton E.S. and Wakeman R.J. (2010) Aggregation effects in the cake filtration of interacting binary mixtures (submitted to *Chemical Engineering Science*).

Conference Contributions- refereed:

1. Chellappah K., Tarleton E.S. and Wakeman R.J. (2009) Cake filtration of fibre/particle mixtures. *Proceedings of FILTECH 2009*, Vol. 1, pp. 260-267, Wiesbaden, Germany.

Others (not given here):

1. Chellappah K., Tarleton E.S. and Wakeman R.J. (2009) Cake filtration and sedimentation of fibre/particle mixtures. Poster session presented at: 10th UK Particle Technology Forum, 2009 Jul 1-2; Birmingham, UK (won 2nd place in poster competition).
2. Chellappah K., Tarleton E.S. and Wakeman R.J. (2009) Cake filtration of fibre/particle binary suspensions. Poster session presented at: IChemE Particles (of all shapes and sizes) into liquids, 2009 Sept 23; GSK Stevenage, UK.
3. Chellappah K., Tarleton E.S. and Wakeman R.J. (2009) Cake filtration of fibre/particle mixtures. Oral presentation at: *IChemE What's New in Fluid Separations*, 4th June, Sunbury, UK.

